2010

Characterization of Rock/Fluids Interactions at Reservoir Conditions

Dayanand Saini
Louisiana State University and Agricultural and Mechanical College, dayanand2001@gmail.com

CHARACTERIZATION OF ROCK/FLUIDS INTERACTIONS AT RESERVOIR CONDITIONS

A Dissertation

Submitted to the graduate faculty of the
Louisiana State University and
Agricultural and Mechanical College
in partial fulfillment of
the requirements for the degree of
Doctor of Philosophy
in

The Department of Petroleum Engineering

by

Dayanand Saini
B.Sc. in Mathematics, CCS University, Meerut, India, 1996
B.E. in Chemical Engineering, CCS University, Meerut, India, 2000
May 2011

DEDICATION

This work is dedicated to my beloved wife, Rekha; daughter, Lalima; my father; my in-laws; and all of my family members and friends.

ACKNOWLEDGEMENTS

I am thankful to my advisor Dr. Dandina N. Rao for giving me an opportunity to fulfill my dream of pursuing the Doctor of Philosophy degree in petroleum engineering and for his able guidance, suggestions, motivation, and continuous encouragement throughout this research work. I thank and express my deepest appreciation to Dr. Stephen O. Sears, Dr. Jeffrey S. Hanor, Dr. Richard Hughes, and Dr. Seung I. Kam for graciously agreeing to serve on my examination committee and providing valuable suggestions during my dissertation. I thank Dr. Hughes from the bottom of my heart for his time to review this dissertation and valuable comments given to improve its quality.

Financial support from Louisiana Board of Regents research grant (LEQSF 2006-09-RD-B-03), summer student support (2007) from ConocoPhillips, and various agencies including Marathon Oil Company for equipping the L.C. Soileau, III Rock-Fluids Interactions Laboratory is gratefully acknowledged. The donation from Louis C. and Denise R. Soileau, IV for the renovation of the L.C. Soileau, III Rock-Fluids Interactions Laboratory is gratefully acknowledged. Financial support in the form of an economic development assistantship (EDA) awarded by the Louisiana Board of Regents and Louisiana State University and the SPE Nico van Wingen memorial graduate fellowship in petroleum engineering awarded by the SPE Foundation is greatly appreciated. I am thankful to Mr. Frank H. Lim and Mr. Nikhil Joshi of Anadarko Petroleum Corporation, and Mr. David Zornes and Mr. Dan Maloney of ConocoPhillips for their support and encouragement. The support of Mr. Paul Rodriguez (LSU Chemical Engineering), Mr. Rick Young (LSU Geology), and Mr. Gerry Masterman (LSU Petroleum Engineering) with experimental procedures is highly appreciated.

I would like to express my sincere thanks to my former lab mate, Daryl Sequeira, for his help during my initial days in explaining different lab equipment which I later used in my research. My special thank goes to Mauricio Toscano of LSU Department of Petroleum Engineering for his

immense help with lab equipment, inventory, and for conducting reservoir condition experiments in the case of the T reservoir. I am also thankful to my fellow graduate students, Ruiz W. Paidin and Yu Zheng for their valuable feedback and frequent technical discussions. Special thanks go to Yu Zheng for her help with ambient condition tests for the B oil field and constant encouragement throughout my stay at LSU. The diligent support of Mr. Fenelon Nunes of the LSU Department of Petroleum Engineering is gratefully acknowledged. I sincerely express my gratitude to all the faculty members and fellow graduate students in the Department of Petroleum Engineering for their help and encouragement. A final word of gratitude is reserved for my friends and family members for their love and support.

The copyrights of the Society of Petroleum Engineers (SPE paper no.113321-PA) and BRILL (Chapter 7 of Contact Angle, Wettability and Adhesion, Vol-6) are duly acknowledged as a part of my previously reported work in the above mentioned publications and have been included in this study. The copyrights of the publishers of various technical publications (for the various figures and excerpts (<200 words)) are also duly acknowledged.

TABLE OF CONTENTS

LIST OF TABLES

LIST OF FIGURES

ABSTRACT

In this study, interfacial phenomena of spreading, wettability, and rock/oil adhesion interactions in complex rock/oil/water systems were characterized at reservoir conditions of elevated pressures and temperatures. Capabilities of both ambient and reservoir condition optical cells were used for measuring the oil/water interfacial tension and dynamic (the water-receding and the water-advancing) contact angles for various complex rock/oil/water systems. Well known sessile oil drop volume alteration method was successfully used in this study for evaluating the applicability of the modified Young's equation for characterizing the line tension in complex rock/oil/water systems at reservoir conditions.

This appears to be first time when rock/fluids interactions in complex rock/oil/water systems of petroleum engineering interest have been characterized in terms of the measured oil/water interfacial tension (IFT), wettability, line tension, and the work of adhesion at elevated pressures (up to 14,000 psi) and temperatures (up to 250°F) using representative reservoir fluids and common reservoir rock minerals surfaces (glass, quartz, dolomite or calcite). Different oil (recombined live oil and stock-tank oil) and aqueous (deionized water, synthetic reservoir brines, synthetic sea water, and 35,000 ppm NaCl solution) phases were used to study the effects of fluids composition and experimental conditions on the oil/water IFT and the wetting characteristics of complex rock/oil/water systems of petroleum engineering interest. The effect of rock mineralogy was investigated by conducting the experiments with different mineral surfaces (quartz and calcite).

A new equation was developed using the concepts of the line tension and the work of adhesion to estimate the adhesion energy per unit volume correlatable to maximum disjoining pressure in complex rock/oil/water systems. This equation uses the measured data of the oil/water interfacial tension (IFT) and dynamic contact angles, and an assumed thickness of the aqueous wetting films. The experimentally estimated adhesion energy per unit volume values for two

glass/recombined live oil/synthetic reservoir brine systems using this new equation were compared with the maximum disjoining pressure values derived from the published reservoir condition disjoining pressure isotherms for the glass/Yates crude oil/Yates brine systems. The experimentally estimated values were found to be one order of magnitude higher than the theoretical values.

1. INTRODUCTION

1.1 Problem Statement

1.1.1 Background

Rock/fluids interactions (spreading, wettability, and rock/oil adhesion) play a crucial role in determining ultimate oil recovery in petroleum reservoirs. On one hand, precise knowledge of the initial wettability state of any reservoir does help in designing optimum exploitation strategies; on the other hand, wettability alteration (overcoming the strong rock/oil adhesion interactions) may play a key role in the implementation and success of any enhanced oil recovery (EOR) process for maximizing oil recovery after primary depletion or secondary oil recovery phase.

The influence of reservoir wettability on oil recovery is widely recognized, however the reservoir specific nature of wetting characteristics prohibits any generalization of reservoir wettability itself. The reservoir specific wetting characteristics are a delicate interplay of several effects such as pore size distribution, pore shape especially the pore wall curvature, rock mineralogy, structural position, fluids composition, and the interfacial interactions between different phases at prevailing reservoir conditions of elevated pressures and temperatures. All these factors play a major role in determining the wetting characteristics of a reservoir that ultimately determines oil recovery in it.

1.1.2 Problem Identification

A thorough description of interfacial phenomena of spreading, wettability, and rock/oil adhesion interactions in petroleum reservoirs is necessary for fundamental understanding of the wetting characteristics and oil trapping mechanisms at the pore level. Oil trapping in water-wet reservoirs is normally attributed to capillary trapping however the presence of strong rock/oil adhesion interactions in oil-wet reservoirs may cause significantly low recovery in them. Also, rock/oil adhesion forces can be several folds stronger than capillary forces. Hence a proper

depiction of rock/oil adhesion aspects of the reservoir wettability, especially the extent of rock/oil adhesion interactions in complex rock/oil/water systems at reservoir conditions is essential. The extent of rock/oil adhesion interactions can be defined as the magnitude of different intermolecular surface forces that arise due to the interactions between molecules of different phases (oil, water, and solid rock surface) in and around the three-phase contact region. The magnitude of these intermolecular surface forces is found to be significantly large when the thickness of aqueous wetting films squeezed between the bulk oil phase and reservoir rock surface becomes significantly small.

Conventionally, intermolecular surface forces in complex rock/oil/water systems of petroleum engineering interest are studied by generating force-distance profile versus aqueous wetting film thickness curves using different surface forces measurement techniques such as atomic force microscopy (AFM) or surface force apparatus (SFA). The observed relationship between the experimentally measured surface force-distance profile and the aqueous wetting film thickness is used to determine the extent of rock/oil adhesion interactions in rock/oil/water systems. For this, the experimentally measured magnitude of surface forces in the form of adhesion energy per unit area is compared with either theoretically determined disjoining pressure using DLVO (Derjaguin, Landau, Verwey, and Overbeek) theory or using the concept of work of adhesion that relies on the theoretical determination of the equilibrium (Young's) contact angle and its comparison with experimentally measured values of the equilibrium (Young's) contact angle. An agreement between the experimental measurements and the theoretically determined surface force-distance profile versus film thickness curves is sought for the development of accurate mathematical models to describe the wettability of complex rock/oil/water systems at the pore level. However, the experiential determination of surface force versus film thickness relationship using atomic force microscopy (AFM) or surface force apparatus (SFA) has only been reported at ambient conditions. The use of stock-tank oil or pure hydrocarbons as the oil phase in these types of experiments also

limits the use of such measurements in determining the extent of rock/oil adhesion interactions in petroleum reservoirs, especially at reservoir conditions.

The use of the line tension-based modified Young's equation in determining the extent of rock/oil adhesion interactions at reservoir conditions seems to be promising to overcome the experimental limitations associated with the above mentioned experimental techniques. Because it involves the use of the measured data of dynamic contact angles and oil/water interfacial tension. These data can be generated at prevailing reservoir conditions using representative reservoir fluids and common reservoir rock mineral surfaces by using three available experimental techniques: the pendant drop method, the sessile oil drop volume alteration method, and the dual-drop dual crystal (DDDC) contact angle technique.

1.1.3 Scope of This Study

It is clear from this discussion that there exists a need to explore the applicability of this knowledge of surface force measurements for quantifying rock/oil adhesion interactions in complex rock/oil/water systems at reservoir conditions using representative reservoir fluids and common reservoir rock mineral surfaces. This important aspect of the rock/fluids interactions and its implication to oil trapping remain to be investigated at prevailing reservoir conditions using representative reservoir fluids and common reservoir rock mineral surfaces have defined the scope of this study. Such quantification of rock/oil adhesion interactions is expected to provide a better understanding of the wetting characteristics of complex rock/oil/water systems at the pore level.

This study aims to characterize the rock/fluids interactions of the oil/water interfacial tension (IFT), spreading, wettability, and the rock/oil adhesion at prevailing reservoir conditions of elevated reservoir pressures and temperatures. It also proposes to investigate the applicability of the line tension-based modified Young's equation in complex rock/oil/water systems to describe the commonly observed phenomenon of contact angle hysteresis or a pinning of the contact line in extreme cases. In the present study, the development of a new work of

adhesion-based equation to estimate the magnitude of intermolecular surface forces in terms of the adhesion energy per unit volume (correlatable to maximum disjoining pressure) is proposed. This new equation utilizes the experimentally determined adhesion energy per unit area estimated using the line tension-based modification of the conventional equation of the work of adhesion (The Young's-Dupré equation) and an assumed thickness of the aqueous wetting films to estimate the magnitude of the adhesion energy per unit volume in complex rock/oil/water systems. This reservoir condition characterization of rock/fluids interactions in terms of the adhesion energy per unit volume along with the measured oil/water interfacial tension and dynamic contact angle values is expected to provide a better understanding of the role of the extent of rock/oil adhesion interactions on oil trapping, residual oil saturation, and mobilization of oil in pore spaces.

1.2 Objectives

The specific objectives of this study are:

(1) To determine the wettability of different rock/oil/water systems at ambient conditions by measuring the water-advancing contact angle using the dual-drop dual-crystal (DDDC) technique. This involves the use of stock-tank oil samples obtained from different reservoirs (two onshore and two offshore), respective synthetic reservoir brines, and representative reservoir rock mineral surfaces (glass, quartz, dolomite or calcite);

(2) To determine the wettability of different rock/oil/water systems at prevailing reservoir conditions (pressures up to 12,000 psi and temperatures up to 238°F) by measuring the water-advancing contact angle using the DDDC technique. This involves the use of recombined live oil samples from different reservoirs (two onshore and two offshore), respective synthetic reservoir brines, and representative reservoir rock mineral surfaces (glass, quartz, dolomite or calcite);

(3) To measure the oil/water interfacial tension (IFT) using the pendant drop method at both ambient and reservoir conditions (pressures up to 14,000 psi and temperatures up to 250°F) using the reservoir fluids mentioned in objectives (1) and (2);

(4) To evaluate the applicability of the line tension-based modified Young's equation to quantify the extent of rock/fluids interactions in different rock/oil/water systems at both ambient and reservoir conditions by evaluating drop size dependence of the water-advancing contact angle using the sessile oil drop volume alteration method;

(5) To investigate the presence and the stability of the thin aqueous wetting films in different rock/oil/water systems using the line tension-based modified Young's equation and the concept of the work of adhesion;

(6) To determine the magnitude of maximum disjoining pressure in terms of the adhesion energy per unit volume using a line tension-based modification of the conventional equation of the work of adhesion (the Young-Dupré equation);

(7) To compare the values of maximum disjoining pressure derived from the published reservoir condition disjoining pressure isotherms for the glass/Yates crude oil/Yates brine systems with the magnitude of the adhesion energy per unit volume for the glass/crude oil/brine systems estimated by using the new equation developed in this study;

(8) To study the effect of fluids composition, rock mineralogy and pressure and temperature conditions on rock/fluids interactions.

1.3 Methodology

To achieve the objectives of this study, both stock-tank oil and recombined live oil samples from four different oil reservoirs were selected. These reservoirs include two onshore reservoirs, B oil field in Louisiana; the other is in Texas (Y oil Field). A Gulf of Mexico (GOM) deepwater offshore oil field with two producing reservoirs (F and T) was also included in this study to characterize rock/fluids interactions at offshore reservoir conditions.

The composition of actual reservoir brines for each of the reservoir included in this study was supplied by the operating company of the field. Accordingly, synthetic reservoir brines were prepared by adding the calculated amounts of various salts to deionized water (DIW) to match the actual brine compositions in order to represent the actual brine composition in the experiments. Flat and carefully polished surfaces of quartz, glass, dolomite or calcite minerals were used to represent the dominant rock minerals present in the respective reservoir rocks.

Characterization of rock/fluid interactions at reservoir conditions in terms of measurable quantities of the oil/water interfacial tension (IFT) and dynamic contact angles require the use of such experimental techniques that can confidently measure these quantities. Available experimental techniques include the pendant drop method, the dual-drop dual-crystal (DDDC) contact angle technique, and the conventional sessile drop volume alteration method. The pendant drop technique is a reliable method to measure the oil/water IFT at elevated pressures and temperatures. The DDDC technique is a reliable technique that provides an accurate and reproducible measurement of the water-water advancing contact angle (a measure of the reservoir wettability) at actual reservoir conditions of elevated pressures and temperatures using representative reservoir fluids. The conventional sessile drop volume alteration method was used to study the drop size dependence of the water-advancing contact angle to explore the applicability of the modified Young's equation for quantifying the extent of rock/oil adhesion interactions in complex rock/oil/water systems. All three of the above mentioned experimental techniques are assisted with two sophisticated drop shape image analysis softwares, namely Axisymmetric Drop Shape Analysis (ADSA) software and commercial Drop Shape Analysis (DSA) software. These softwares are used for analyzing the captured images of the pendant and the sessile oil drops for accurate contact angle values and oil/water IFT measurements, respectively.

In this study, applicability of the line tension-based, modified Young's equation was evaluated for characterizing rock/fluids interactions at both ambient and reservoir conditions.

The line tension-based, modified Young's equation provides a relationship between the water-advancing contact angle (θ_a) and the equilibrium contact (Young's) contact angle (θ_∞) to accommodate the imbalance of different intermolecular forces experienced by molecules in and around the three-phase confluence zone on the Young's contact angle. The slope of the cosine of the water-advancing contact angle ($Cos\theta_a$) versus reciprocal of contact radius ($1/r$) relationship described by the modified Young's equation was used to compute the magnitude of the line tension in various rock/oil/water systems. The experimentally determined line tension values were then correlated with the adhesion number to quantify the extent of rock/oil adhesion interactions in terms of the line tension.

In this study, the extent of rock/oil adhesion interactions was also estimated after incorporating the effect of the line tension on the work of adhesion. The conventional Young-Dupré equation of work of adhesion describes the extent of rock/oil adhesion interactions in terms of measured Young's equilibrium contact angle (θ_∞). However, this equation holds for water-wet systems in which the measured water-receding contact angle (θ_r) subtended by the sessile oil drop to the rock surface in the presence of an aqueous phase corresponds to θ_∞. For oil-wet systems, where the measured water-advancing contact angle (θ_a) corresponds to θ_∞, a new line-tension based modification to the Young-Dupré equation was proposed to estimate the work of adhesion in such systems. This modification to the conventional Young-Dupré equation was sought to explain the effect of rock/oil adhesion interactions on the regularly observed phenomenon of contact angle hysteresis or a pinning of the contact line in complex rock/oil/water systems.

The line tension-based modified Young's equation and the line tension-based modification to the conventional work of adhesion equation were used to compute the work of adhesion (adhesion energy per unit area). The experimental observations were interpreted in terms of the presence and the stability of the thin aqueous wetting films using existing theory and a new equation was proposed for estimating the magnitude of the adhesion energy per unit volume at prevailing

reservoir conditions. The maximum change in the estimated adhesion energy per unit area and an assumed thickness of the aqueous wetting films at which the effect of intermolecular forces is significantly felt by the system were used to estimate the magnitude of the adhesion energy per unit volume.

2. LITERATURE REVIEW

2.1 Domestic Oil Resources in the United States

According to a recently published study (report prepared by Advanced Resources International of Arlington, VA for the U.S. Department of Energy (DOE), 2007), the United States has 582 billion barrels of discovered original oil in place (OOIP) resources. Out of 582 billion barrels of discovered OIIP, 208 billion barrels have already been produced or proved, leaving behind 374 billion barrels. The largest portion of this huge amount of left behind oil resources is in the form of immobile or residual oil (bypassed oil) after primary depletion and secondary oil recovery processes. Out of this, 110 billion barrels may be technically recovered by using appropriate enhanced oil recovery (EOR) technologies. Several technological and economical risks are associated with the process of converting these technically recoverable resources into economically recoverable reserves.

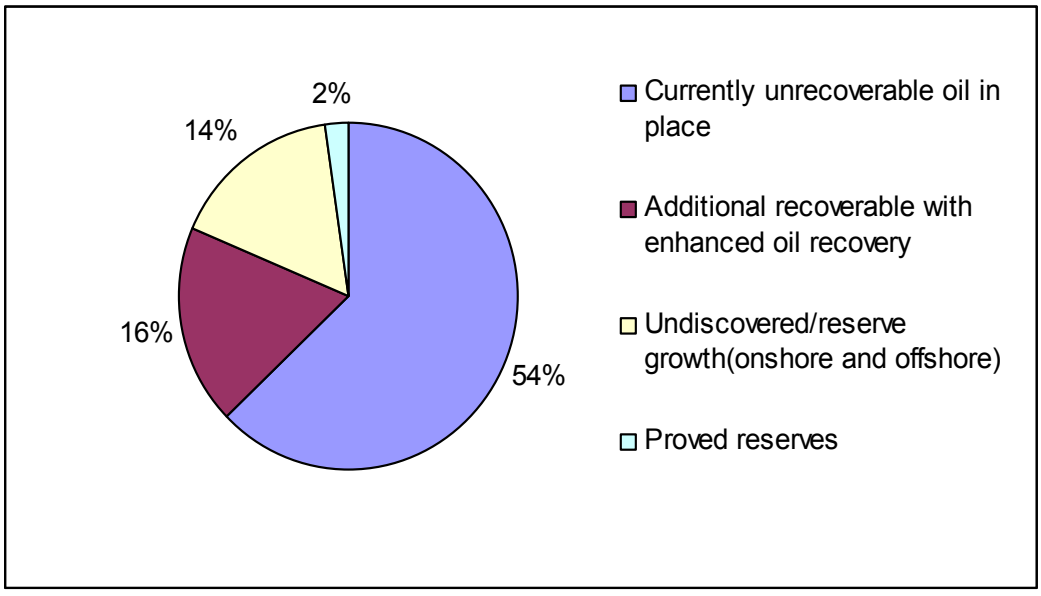

Figure 2.1: Stranded oil resources in the USA (Report prepared by Advanced Resources of Arlington, VA for DOE, 2007)

Recently, oil exploration and production (E&P) companies have begun to develop deeper, hotter and higher-pressure reservoirs, especially in offshore environments such as the outer

continental shelf (OCS), Gulf of Mexico (GOM).With the development of deepwater (water depth of >1,000 ft) and ultra-deepwater (water depth of >5,000 ft) offshore reservoirs in the GOM region, typical well depths have increased from 15,000 ft (true vertical depth, TVD) to greater that 31,000 ft (TVD) since 1990 (Richardson et al., OCS report MMS 2008-13), and pressure and temperature conditions have followed suit (temperature >200°F and pressure >10,000 psi). These ultra-deep wells are very expensive to drill and complete with costs exceeding $300 million. The cost of developing a single offshore reservoir can exceed $1 billion, with costs likely to increase as operations are conducted in even deeper waters (Sarian and Gibson, 2005).

It is worth mentioning here that in onshore environment, we may afford to have an EOR process late in the life of a reservoir but it may not be economically feasible to introduce any secondary or tertiary EOR process in an offshore environment, especially in the deepwater offshore reservoir, such as those in the GOM. Due to huge investments associated with the development of offshore reservoirs, operating companies may have no other option than to leave significant portions of original oil in place (OIIP) as bypassed oil in the reservoir.

An accurate evaluation of spreading behavior, reservoir wettability, and the extent of rock/fluids interactions in early stage of the production cycle, especially in case of offshore reservoirs, can play a decisive role in devising suitable means to recover bypassed oil. Also, due to the high cost associated with the development of offshore reservoirs, an accurate description of rock/fluids interactions at representative reservoir conditions would help to understand their implications to oil recovery for devising efficient and economically viable exploitation strategies in such cases.

2.2 Reservoir Wettability and Its Implications to Oil Recovery

Wettability is a widely used term in petroleum engineering. It can be defined as the tendency of one fluid to spread on or adhere to a solid surface in the presence of other immiscible fluids (Craig, 1971). Tiab and Donaldson (1996) describe wettability as the relative adhesion of two

fluids to a solid surface. In the early stages of reservoir engineering, it was generally considered that all formations were preferentially wet with water (Craig, 1971). This seemed to be valid in the case of sandstone reservoirs as they were deposited in an aqueous environment and the oil migrated late into these formations. However, a few sandstone formations have been reported to have oil-wet nature also, such as Tensleep (Nutting, 1934) and Wilcox (Katz, 1942). Many carbonate reservoirs exhibit oil-wet tendencies (Treiber et al., 1972).

Based on the results of numerous experimental studies and field examples, reservoir wettability is broadly classified into five main categories: 1) Water-wet; 2) Neutral or intermediately-wet; 3) Oil-wet; 4) Mixed wet; and 5) Fractionally-wet. The terms water-wet, neutral-wet, and oil-wet represent uniform states of wettability, whereas the term mixed-wet and fractionally-wet are generally used to represent heterogeneous state of the wettability, where different sections of the porous flow paths exhibit different wettability states. The wettability state of reservoir rocks significantly influences the relative distribution of reservoir fluids and their displacement behavior in the porous space of reservoir rock, and thus governs the success of any oil recovery mechanism.

Among early studies on the effect of wettability on oil recoveries, Amott (1959) has described a test consisting of four displacement operations for evaluating the wettability of the porous rock as a function of the displacement properties of rock/oil/water systems. He attempted to correlate the wettability and waterflood oil recovery using the developed procedure by conducting core flooding experiments for outcrop (Ohio sandstone) and Alundum. He concluded that there was no single correlation of wettability with waterflood recovery for different porous mediums despite the use of one standard set of conditions during experiments. He attributed these observed differences in the relationship between wettability and waterflood oil recovery to the variation in pore geometry from one core to another.

Donaldson et al. (1969) have developed a quantitative method named the USBM (U. S. Bureau of Mines) method using capillary pressure curves determined with a centrifuge for the evaluation

of wettability of porous media containing brine and crude oils. They examined the effect of wettability on oil recovery by conducting waterflood tests after altering the core wettability by chemical treatment. They concluded that change in wettability greatly affected the capillary pressure, relative permeability and recovery efficiency of waterflooding and recommended that wettability of the system should be known for proper understanding of the test data.

Treiber et al. (1972) have evaluated the wettability of fifty oil-producing reservoirs using contact angle tests, and the results were compared with available laboratory flow tests data. In the majority (82%) of reservoirs where contact angle data and relative permeability data were available for wettability comparison, good agreement was obtained between wettability determined by contact angle tests and inferred wettability from flow test data. Also, their study indicated that the wettability of different reservoirs could cover a broad spectrum from strongly water-wet to strongly oil-wet. According to them, if cores with representative wettability characteristics are available for testing, then flow tests on these cores may provide all the data needed for a given application, making unnecessary the actual definition of reservoir wettability.

Salathiel (1973) postulated a mechanism defined as "mixed wettability" to explain a very efficient water/oil displacement attained in an East Texas reservoir emphasizing the role of the wettability state of the reservoir on oil recovery. In mixed wettability, the fine pores and grain contacts would be preferentially water-wet and the surfaces of the larger pores would be strongly oil-wet. If oil-wet paths were continuous through the rock, water could displace oil from the larger pores and little or no oil would be held by capillary forces in small pores or at grain contacts. This condition of mixed wettability is different from fractionally-wet condition in which distinct completely oil-wet or water-wet regions exist in porous media. He concluded that both pore structure and the mineral composition of porous rocks appeared to affect the surface drainage of oil from mixed-wettability laboratory cores. Also, this type of surface drainage of oil through continuous oil films is greatly dependant on the composition of reservoir fluids and rock properties.

Depending on the favorable conditions for the development of mixed wettability in a specific reservoir, gravity drainage would also assist in attaining low residual oil saturation if depletion times are long enough.

In his six part wettability literature survey, Anderson (1986, 1987) summarized the effect of wettability on different reservoir parameters such as capillary pressure, relative permeability, waterflood behavior, dispersion and electrical properties. One of his conclusions was that the most accurate results are obtained when native or restored-state core are run with native crude oil and brine at reservoir temperature and pressure. According to Anderson, the wettability of originally water-wet reservoir rock can be altered by the adsorption of polar compounds and/or the deposition of organic material present originally in oil. The degree of alteration is determined by the interactions of the oil constituents, the mineral surface and its brine chemistry.

Morrow (1990) has discussed the effect of wettability on oil recovery and factors affecting wettability. This study concluded that oil recovery was found to be optimum at neutral wettability. He stressed the proper understanding of the relationship between wettability, capillary pressure, and the distribution of oil and water in pore spaces to quantify wettability and its relation to oil recovery. He concluded that the complex pore structure and mineralogy of reservoir rocks and the effects of adsorbed organic components from the crude oil makes it difficult to characterize wettability using methods based on capillary pressure curves.

Rao et al. (1992) evaluated the effect of initial core wettability on waterflood oil recovery by conducting several corefloods involving water-wet, intermediate-wet and oil-wet reservoir systems. Their study showed that an intermediate-wet system yielded the highest waterflood oil recoveries and a water-wet system was next. An oil-wet system yielded the least oil recovery during waterflooding. Reservoir wettability affected the miscible flood oil recovery significantly with a trend of increasing oil recovery with increasing oil-wetness. They also reported that miscible gas

flooding led to the possible development of a mixed-wettability condition in some cases that resulted in increased waterflood oil recovery in successive cycles.

Vizika and Lombard (1996) conducted core flooding experiments to evaluate the effect of wettability on oil recovery in tertiary air injection processes with gravity drainage. Results showed that highest oil recoveries were obtained in water-wet or fractionally-wet conditions because hydraulic conductivity was maintained by means of spreading oil films. Lowest recovery was obtained in oil-wet media, due to strong capillary retention in spite of the formation of continuous wetting films of oil.

Christensen et al. (2001) published a comprehensive review of WAG field experience from approximately 60 fields including both onshore and offshore projects. The study showed that miscible WAG injection in carbonate formations yielded the highest improved oil recovery, and dolomites had higher predicted recoveries than the average for sandstones. These findings were similar as reported by other studies such as Rao et al. (1992). Higher recoveries in oil-wet cases can be attributed to lower water shielding of oil from the injected gas and some favorable wettability alterations.

In a recent study, Agbalaka et al. (2008) reviewed the reported results of secondary and tertiary oil recovery processes to deduce the effect of wettability on oil recovery. The study concluded that mixed-wet reservoirs yielded the best waterflood oil recoveries and oil-wet reservoirs showed best gas flood oil recovery for tertiary recovery processes (i.e. at waterflood oil saturation). The mixed-wet and water-wet systems yielded the higher oil recoveries in case of secondary gas floods.

As evident from the above discussion, the role of reservoir wettability in determining the ultimate recovery from any oil recovery process is widely recognized. An inference about the wettability state of porous media can be made from displacement experiments using different methods such as the Amott method and the USBM method. Core flooding experiments have been

proven an excellent source for studying the effect of wettability on the displacement of reservoir fluids in pore space and its implication to oil recovery.

Here, a fundamental question of interest arises: how do the rock surface and reservoir fluids in petroleum reservoirs interact with each other at a standard set of conditions (i.e. pressure, temperature, fluids composition, and rock mineralogy) that ultimately influences oil recovery? To answer this question, a realistic depiction of interactions between reservoir fluids and the rock surface at representative reservoir conditions is necessary. To investigate the rock/fluids interactions of spreading, wettability, and rock/oil adhesion, displacement tests may not be very helpful as other factors such because complex pore structure; fluid/fluid interactions (interfacial tension); fluid saturations, and aging time also affect their results.

2.3 Concept of Contact Angle and the Young's Equation

In 1805, Young introduced the concept of contact angle (the Young's equation) to describe the equilibrium relationship between surface free energies of three phases (solid, liquid and vapor) at contact line where all three phases meet to each other. An ideal and perfectly flat, solid surface, and a constant drop volume are the necessary conditions for obtaining an equilibrium relationship described by the Young's equation. For solid/liquid/vapor (S/L/V) systems, the Young's equation is given by:

$$\gamma_{LV} \cos\theta_{\infty} = \gamma_{SV} - \gamma_{SL} \quad \text{..... (1)}$$

where θ_{∞} is the equilibrium contact angle or the Young's contact angle, and γ_{LV}, γ_{SV}, and γ_{SL} are the surface tensions of the liquid/vapor interface, the solid/vapor interface, and the solid/liquid interface, respectively. The Young's equation is widely used to describe the wettability of solid surfaces with liquids in the presence of a vapor phase in terms of easily measurable quantity, the equilibrium or the Young's contact angle (θ_{∞}).

According to the Young's equation, for a given wettability state, only a unique equilibrium (Young's) contact angle is possible. However, for any solid/fluid/fluid system, prediction of its wetting behavior may not be possible until the equilibrium relationship described by the Young's equation is disturbed. Hence, dynamic behavior of the system in terms of dynamic contact angles is studied to gain insights into the wetting of solid surfaces by fluids.

For S/L/V systems, this dynamic behavior (deviation from equilibrium condition) is studied by using different sessile drop techniques such as the drop volume expansion and contraction, lateral shift of the base of the sessile drop resting on the solid surface while anchoring the tip of the drop to the needle used for drop placement, and tilting of the solid surface. The dynamic contact angles (measured in the denser phase) obtained by these techniques are denoted as the advancing and the receding contact angles depending on the direction of the movement of the liquid/vapor interface on a solid surface. For S/L/V systems, a common assumption is made that if the liquid spreads on the surface, it must also adhere to it. Any observed contact angle hysteresis (deviation of the advancing contact angle from the initial receding contact angle) in S/L/V systems is generally attributed to surface heterogeneity and roughness (Wenzel, 1949; Bobek et al., 1958).

Neumann and Good (1972) have provided the theoretical treatment of the effect of surface heterogeneity on contact angles hysteresis in S/L/V systems. This study concluded that for a patch-wise heterogeneous surface with patches smaller that about 0.1 μm, surface heterogeneity should make a negligible contribution to hysteresis.

In the case of solid/liquid/liquid (S/L/L) systems, contact angle is defined in a different manner compared to S/L/V systems. A schematic representation of contact angle in S/L/V and S/L/L (rock/oil/water) systems is shown in Figure 2.2. Rao (2003) has provided a detailed discussion on the differences of the manner in which the concept of contact angle is measured in S/L/V and S/L/L systems.

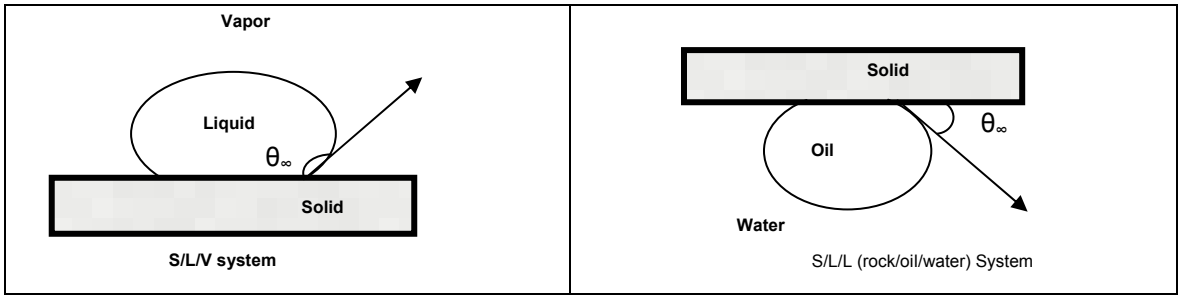

Figure 2.2: Concept of contact angle in S/L/V and S/L/L systems

The applicability of the Young's equation has been extended to understand the wettability phenomenon in the S/L/L systems. According to Morrow (1990), contact angle is the most universal measure of the wettability of the surfaces. For S/L/L (rock/oil/water) systems of petroleum engineering interest, the Young's equation is given as:

$$\gamma_{ow} Cos\theta_{\infty} = \gamma_{so} - \gamma_{sw} \quad \text{..... (2)}$$

Where θ_{∞} is the equilibrium contact angle or the Young's contact angle and γ_{ow}, γ_{so}, and γ_{sw} are the interfacial tensions of the oil/water interface, the solid/oil interface, and the solid/water interface.

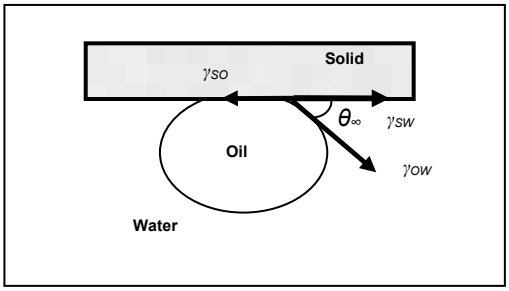

Figure 2.3: Depiction of the equilibrium (Young's) contact angle in rock/oil/water systems

The two-century old Young's equation has been widely used in petroleum engineering to depict the reservoir wettability in terms of contact angle, which describes the mechanical

equilibrium relationship between interfacial tensions of all three phases (i.e. rock, oil, and water) at contact line (Figure 2.3). This equilibrium relationship can easily be described in terms of easily measurable variables (i.e. oil/water IFT and contact angle).

In the early days of use the contact angle concept for evaluating reservoir wettability, Wagner and Leach (1956) conducted contact angle experiments to study the factors responsible the reservoir wettability and possible improvement in oil displacement efficiency in water flooding. These experiments were conducted at moderate pressures (around 500 psi) and at reservoir temperatures (95 to 135°F) using reservoir fluids and the dominant reservoir rock mineral (quartz). They evaluated different rock/oil/water systems in terms of the water-advancing contact angle i.e. limiting contact angle obtained after the water has been advanced over solid surface just previously covered by oil. This procedure was devised to overcome the problem of long aging time (months) for attaining adsorption equilibrium between interfaces. A sessile oil drop was held between two flat and smooth quartz crystals, and the lower crystal was moved so that water could advance over oil/solid surfaces which had already reached adsorption equilibrium. A detailed description of the method is given by Leach et al. (1962).

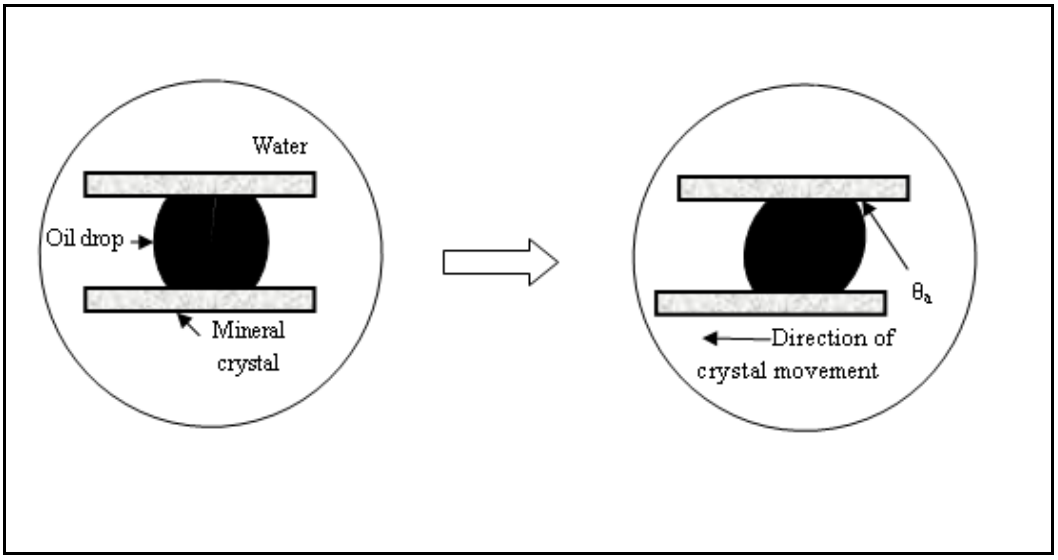

Figure 2.4: Schematic depiction of the contact angle method used by Wagner and Leach (1956)

Figure 2.4 shows the schematic diagram of the contact method used by Wagner and Leach. The study concluded that the presence of natural surface-active components in the reservoir fluids along with other factors (surface roughness and heterogeneity) were responsible for the preferential wetting behavior exhibited by many reservoirs. They stressed the need to bring solid surface into surface equilibrium with the reservoir fluids to reproducible wettability in laboratory core tests. In their study, addition of simple inexpensive chemicals (acids, bases, or salts) was reported to be effective in changing the reservoir wettability.

Treiber et al. (1972) evaluated the wettability of fifty oil-producing reservoirs by both conducting flow tests in the laboratory and using the contact angle measurement procedure reported by Wagner and Leach (1956). They concluded that the equilibrium water-advancing contact angle correlates well with other wettability indicators while the water-receding contact angle does not. In their study, contact angle experiments were conducted up to a pressure of 5 psig and at temperatures up to 212°F. The bubble-point pressure of the crude oil samples used was reduced to a low value by passing laboratory-grade nitrogen through the crude oil sample before using it. An excellent agreement was observed between contact angle and flow test results for determining wettability in the majority of reservoirs (82%) for which both types of data were available. Also, the majority of the reservoir crude oil/water/mineral systems for which data was reported were indicated to be moderately oil-wet. The preferential wetting behavior of a particular system was attributed to the presence (oil-wet) or absence (water-wet) of adsorbable surfactants in the crude oil. They also warned against the practice of making an assumption of near zero degree water advancing contact angle in most schemes to obtain water saturations from capillary pressure curves as a non-zero (small) water advancing contact angle was shown by the system in which adsorbable components were either virtually absent or neutralized in crude oil. Their study concluded that wettability characteristics are reservoir specific as no general correlation was observed between reservoir temperature or API gravity of crude oil and wettability.

McCaffery (1972) reported the development of a custom built high-pressure optical cell capable of measuring interfacial tension and contact angles up to 10,000 psia and 320°F. Single drop contact angle experiments were conducted for pure liquid n-alkane/water pairs with polished quartz crystal. The water-advancing contact angle for different quartz/hydrocarbon/brine systems were also measured at 300 psia and various temperatures. A decrease in the contact angle value was observed on an increase in temperature.

Hjelmelend (1984) reported the use of a high pressure optical cell to conduct contact angle measurements using two parallel crystals. In this optical cell, both the upper and lower crystals could be moved sideways and vertically respectively with the provision of a needle to place oil drops between the crystals. His method also claimed that the simultaneous measurement of the water-receding and advancing contact angles can be obtained in a single test by moving the upper crystal horizontally.

Hjelmelend and Larrando (1986) reported the measurement of the water-receding and advancing contact angles using a sessile oil drop volume alteration method to quantify the wetting behavior of rock/oil systems with calcium carbonate crystals. Both stock-tank oil and oil recombined to the original bubble point were utilized at varying temperature and pressure conditions during contact angle experiments. They reported the formation of rigid interfacial films during IFT and contact angle experiments with stock-tank oil. Their study showed that, apart from the aging time, temperature has a profound effect on the ability of oil to make a hydrophilic solid surface hydrophobic. They recommended conducting contact angle experiments at reservoir temperature and pressure with the most representative reservoir fluids (e.g. live oil as opposed to stock-tank oil) to avoid results that might lead to serious misinterpretation.

Teeters et al. (1988) demonstrated the use of the dynamic Wilhelmy plate technique to evaluate wettability of crude oils. The behavior of the solid/oil/water three-phase contact line is monitored by recording the difference between interfacial forces and buoyancy forces experienced by a solid

plate when it is moved back and forth several times through oil/water interface. Force (adhesion tension)-distance loop is calculated for the indicated advancing and receding contact angles. Pinning of the contact line was observed in certain oil/water systems that resulted in an increase in the magnitude of force experienced by the plate during the wetting (immersion-emersion) cycle.

Wang and Gupta (1995) studied the effect of temperature and pressure on contact angle at pressures ranging from 200 to 3,000 psi and temperature from room temperature to 200°F for crude oil-brine-quartz/calcite systems using a modified pedant drop method. The measured contact angle showed an increase with pressure and decrease with temperature for the quartz surface, whereas a decrease in the measured contact angle with temperature was observed in the case of the calcite surface.

As evident from the above discussion, successful use of the concept of contact angle using different contact angle measurement techniques to evaluate the wetting behavior of rock/oil/water systems of petroleum engineering interest is widely reported in the existing literature. However, conventional contact angle measurement techniques have some inherent problems. A detailed discussion on this issue can be found elsewhere (Rao and Girard, 1996)

A new contact angle measurement technique called "dual-drop dual-crystal (DDDC) technique" was developed and reported by Rao and Girard (1996) to overcome the problems associated with other contact angle experimental techniques. As the name suggests, in this technique, two separate crude oil drops are placed on two parallel crystal surfaces held by horizontal and vertical arms of an optical cell. The water film between the crude oil sessile drops and the crystal surfaces is drained with the help of the buoyancy forces to attain adhesion equilibrium before measuring the advancing and the receding contact angles with respect to aging time. By turning the lower crystal upside down and mingling the two oil drops, the advancing and the receding contact angles can be measured by shifting the lower crystal laterally. A schematic diagram of the DDDC technique is shown in Figure 2.5.

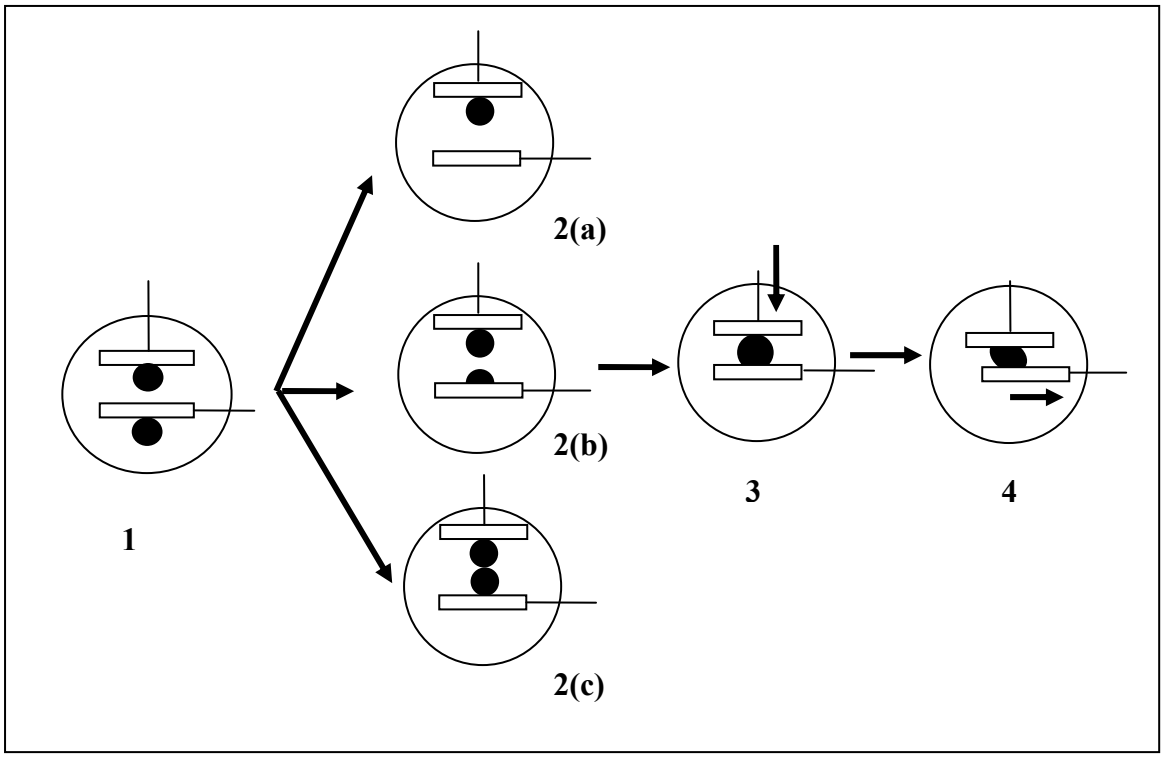

Figure 2.5: Schematic depiction of the dual-drop dual-crystal (DDDC) technique (Rao, 2001)

Rao (1997) compared the wettability derived from oil-water relative permeability curves and the DDDC contact angles with each other for seven different rock/oil/water systems at their respective reservoir conditions. For five of the seven systems studied, the wettability from both methods (corefloods and the DDDC contact angle measurements) appeared to correlate with each other. For the two remaining cases in which both methods did not agree, core-scale heterogeneities and the level of pore interconnectivity were attributed to the observed discrepancies in the results from both methods.

In the DDDC technique, movement of contact line in terms of normalized three phase contact line (TPCL) movement is observed without any ambiguity. Such monitoring of contact line movement ensures the accuracy of the measured water-advancing contact angle in the DDDC technique. Contact line movement can be reproduced by moving the oil drop back to the original position. Rao (2001) and Rao and Karyampudi (2002) discussed the method of monitoring the

contact line movement in the DDDC technique in detail. A schematic depiction of the method of the monitoring the contact line movement in the DDDC test is shown in Figure 2.6.

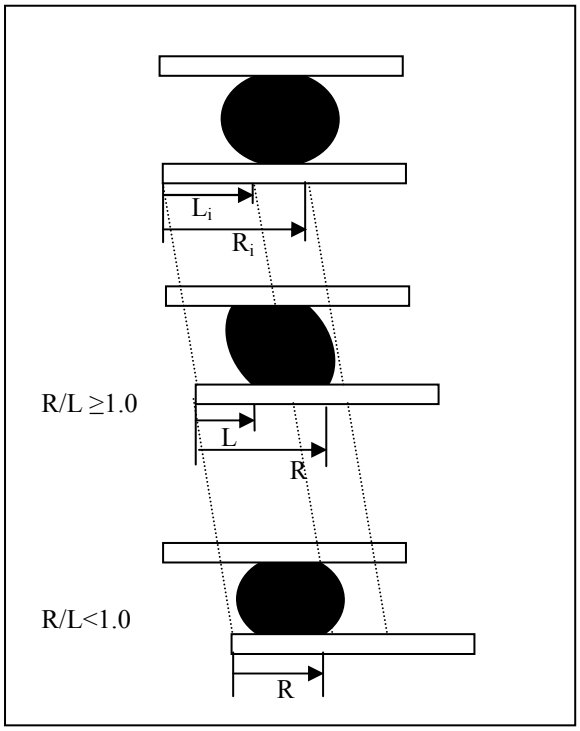

Figure 2.6: Method of monitoring the movement of the three phase contact line (TPCL) in the DDDC technique (Rao, 2001)

The successfully use of the DDDC technique was reported by Rao (2001) to determine the wettability of complex rock/oil/water systems at reservoir conditions of elevated pressure and temperature by measuring the water-advancing contact angles in a reproducible manner. He reported the measured water-advancing contact angles (θ_a) in the DDDC tests conducted at 3,600 psi and 205°F for two rock/live oil/brine systems, namely the quartz/Beaverhill recombined live oil/Beaverhill synthetic reservoir brine and the calcite/Beaverhill recombined live oil/Beaverhill synthetic reservoir brine systems. The quartz/Beaverhill recombined live oil/Beaverhill synthetic reservoir brine system exhibited water-wet tendency (θ_a=50°) whereas the calcite/Beaverhill recombined live oil/Beaverhill synthetic reservoir brine systems showed an oil-wet behavior (θ_a=147°).

Xu et al. (2006) used the DDDC technique for studying the compositional (fluids composition and rock mineralogy) effects on the water-receding and the water advancing contact angle for different rock/oil/water systems at reservoir conditions. The dolomite/Yates live oil/Yates synthetic reservoir brine system showed an intermediate-wet behavior (θ_a=95°) in the DDDC test conducted at 2,785 psi and 82°F. The quartz/Yates live oil/Yates synthetic reservoir brine system showed weakly water-wet behavior (θ_a=60°) in the DDDC test conducted at 2,495 psi and 82°F. However, both systems showed limited spreading behavior by exhibiting lower water-receding contact angles (20-24°) irrespective of a large variation in the water-advancing contact angle values at elevated pressures and reservoir temperature. It was also concluded that the removal of light gaseous ends due to depressurization or addition of extra light ends such as n-pentane to the crude oil could results in more oil-wetting behavior due to precipitation of insolubles in the oil.

As mentioned earlier, to avoid the difficulty in obtaining a unique equilibrium contact angle to measure the reservoir wettability, use of two distinct dynamic contact angles was adopted by the industry. Later, with the development of reliable contact angle measurement techniques such as the DDDC technique, it became possible to measure reservoir wettability in a reproducible manner at reservoir conditions of elevated pressures and temperatures using representative reservoir fluids and common reservoir rock mineral crystals. However, the implications of rock/fluids interactions, especially the effect of the strength or the extent of rock/fluids interactions on residual oil saturation in the porous space remain be investigated at elevated pressures and temperatures using representative reservoir fluids. These issues are discussed in the next section.

2.4 Rock/fluids Interactions

For more than two centuries, the concept of contact angles is has been used to describe the wetting behavior of solid/fluids systems. In the case of S/L/V (solid/liquid/vapor) systems, when a sessile drop of liquid is formed on the solid surface in presence of a vapor phase, a higher density

fluid displaces the lower density fluid and the corresponding measured contact angle represents the wetting condition of the system. Both spreading and adhesion of a liquid drop on a solid surface in the presence of vapor phase have the same meaning because if liquid spreads on the liquid surface it will adhere also or vice-versa. But spreading and adhesion of oil on a rock surface in the presence of water are two different phenomena in complex rock/oil/water systems of petroleum engineering interest. This situation is explained in more detail in the next few paragraphs.

In the case of S/L/L (rock/oil/water) systems, when a sessile drop of oil is formed, a higher density fluid (water) is displaced by the lower density fluid (oil) and the corresponding contact angle subtended measured contact angle by the oil/water interface with the rock surface represents the spreading behavior of the system, and is defined as the water-receding contact angle. This situation is similar to the "pristine drainage" process in which oil had initially migrated to the previously water filled pores of reservoir rocks over geological time. Depending on the geological features of the systems such as pore geometry, structural position, pore connectivity, and the fluid properties such as fluid/fluid (oil/water) interactions (interfacial tension) and rock/fluids interactions, the distribution of oil in previously water filled pores is decided by a combined effect of all these parameters. Hence, the water-receding contact angle as explained in the previous paragraph provides information about the relative distribution of reservoir fluids (spreading behavior) in pore space.

During this pristine process, a combined effect of all these parameters may lead to a situation (the thickness of one of the fluid (aqueous) phases becomes significantly small due to imposed capillary pressure) in which the system may feel a significant effect of different intermolecular surface forces present in the system. These intermolecular surface forces may be strong enough to permanently alter the wetting behavior of the system. Also, the equilibrium between the rock surface and reservoir fluids (oil and water) attained over a long geological time is only disturbed when oil is produced from the reservoir. Once this equilibrium is disturbed, the

strength of rock/fluids interactions or the extent of rock/oil adhesion interactions and its impact on the dynamic behavior of rock/oil/water interface in pore space determine the extent of oil recovery.

Buckley et al. (1998) discussed several categories of rock/fluids interactions by which crude oils can alter the wetting of high energy oxide surfaces (glass) by observing the contact angles between pure fluids on flat surface after exposure to crude oil. Experimentally observed contact angle hysteresis (θ_a-θ_r) in different rock/fluids systems was correlated with the mechanisms of rock/fluids interactions that were responsible for the observed wetting changes. These mechanisms of rock/fluids interactions include polar interactions, surface precipitation, acid/base interactions, and ion bonding or specific interactions. The mechanism of polar interactions was indentified as the main mechanism for wetting change in the cases where water film was absent between oil and solid. In this case, exhibited contact angle hysteresis was found to be moderate. Surface precipitation was found to be dependent on the solvent properties of crude oil with respect to the asphaltene. In this case, contact angle hysteresis was low. Acid/base interactions between ionized acidic and basic sites were dominant mechanisms of rock/fluids interactions in the cases where the brine was a monovalent salt solution at low concentration. In these cases, pH was found to be the main variable and observed contact hysteresis was high. Another mechanism of rock/fluids interactions was identified as ion bonding. In this, divalent and multivalent ions can bind at both oil and solid/water interfaces. Observed contact hysteresis was found to be high in case of ion bonding and this mechanism of rock/fluids interactions depend on oil and brine compositions.

2.4.1 Strength of Rock/fluids Interactions

The terms “strength of rock/fluids interactions” and “the extent of rock/oil adhesion interactions” are often used interchangeably in the literature to describe the interactions between reservoir fluids and rock surface that ultimately determine the wettability state of petroleum reservoirs. The majority of experimental studies involving the measurements of dynamic contact

angles (by means of disturbing the initial equilibrium) (section 2.4) regularly report the significant deviation in the water-advancing contact angle value from the initial water-receding contact angle, a phenomenon that is generally referred as contact angles hysteresis or in extreme situations, a pinning of the contact line, while studying the wetting characteristics of rock/oil/water systems. Adsorption of certain surface-active chemicals from the bulk oil phase on a rock surface in the presence of water as well as some other reasons (surface roughness and surface heterogeneity) are attributed to this regularly observed phenomenon in rock/oil/water systems. It is to be noted that the use of fairly or sometime molecularly smooth surfaces of a single rock mineral such as glass, quartz or calcite in contact angle experiments reduces the possible impact of surface roughness and heterogeneity on contact angles significantly. The phenomenon of contact angle hysteresis or pinning of the contact line is seen as the manifestation of the strength of rock/oil adhesion interactions. Attempts have been made and reported in the literature to understand this regularly observed phenomenon of contact angle hysteresis (or a pinning of the contact line) in terms of the presence and the stability of the thin aqueous wetting films for better understanding of the underlying mechanisms and realistic depiction of rock/fluids interactions in complex rock/oil/water systems.

To experimentally investigate the strength of rock/fluids interactions in rock/oil/water systems, two different approaches have been reported in the literature. These experimental approaches are:

a) Adhesion Test Approach:

This approach includes the use of conventional adhesion tests in various forms (Buckley et al., 1989; Buckley and Morrow, 1990; Valat et al., 1993; Rao and Maini, 1993) and the sessile oil drop volume alteration method (Hjelmeland and Larrando, 1986; Liu and Buckley, 1997). The observed behavior of contact angle hysteresis or a pinning of the contact line is explained in terms of the presence and the stability of the thin aqueous wetting films. Such tests are also used to investigate the role of different factors such as

fluids composition, rock mineralogy, pressure, and temperature on the extent of rock/oil adhesion interactions in complex rock/oil/water systems.

b) Measurement of Intermolecular Surface Forces Approach:

This approach relies on the measurement of intermolecular surface force across the thin liquid films sandwiched between two planar surfaces. Different experimental techniques such as atomic force microscopy (AFM) (Basu and Sharma, 1996), surface force apparatus (SFA) (Drummond and Israelachvili, 2002), and interference imaging of thin film method (Ward et al., 1999) have been reported in the literature to estimate the magnitude of intermolecular surface forces in rock/oil/water systems. The measurement of intermolecular forces using these techniques has proved to be very useful in studying the effect of rock/fluids interactions on the wetting characteristics of rock/oil/water systems.

A detailed discussion on both approaches is provided next.

2.4.1.1 Adhesion Test Approach

Use of adhesion tests in different configurations have been reported in the literature to study and qualitatively characterize the extent of rock/oil adhesion interactions responsible for wetting behavior in complex rock/oil/water systems. Two different configurations of such adhesion tests reported in the literature are depicted in Figures 2.7 and 2.8, respectively.

2.4.1.1.1 Conventional Adhesion Tests

In the conventional adhesion test described in Figure 2.7, an oil drop is brought into contact with mineral surface in the presence of water. After a brief contact time, the oil drop is withdrawn back into the injector tube. Depending on the extent of rock/oil adhesion interactions, the oil drop may be detached cleanly from the mineral surface (non adhesion) or it may partially or completely adhere to the mineral surface forming a large water-advancing contact angle which signifies the presence of strong rock/oil adhesion interactions. Further withdrawal of the oil drop may result

in the oil drop breaking from injector tube tip and leaving a fraction of oil drop on the mineral surface.

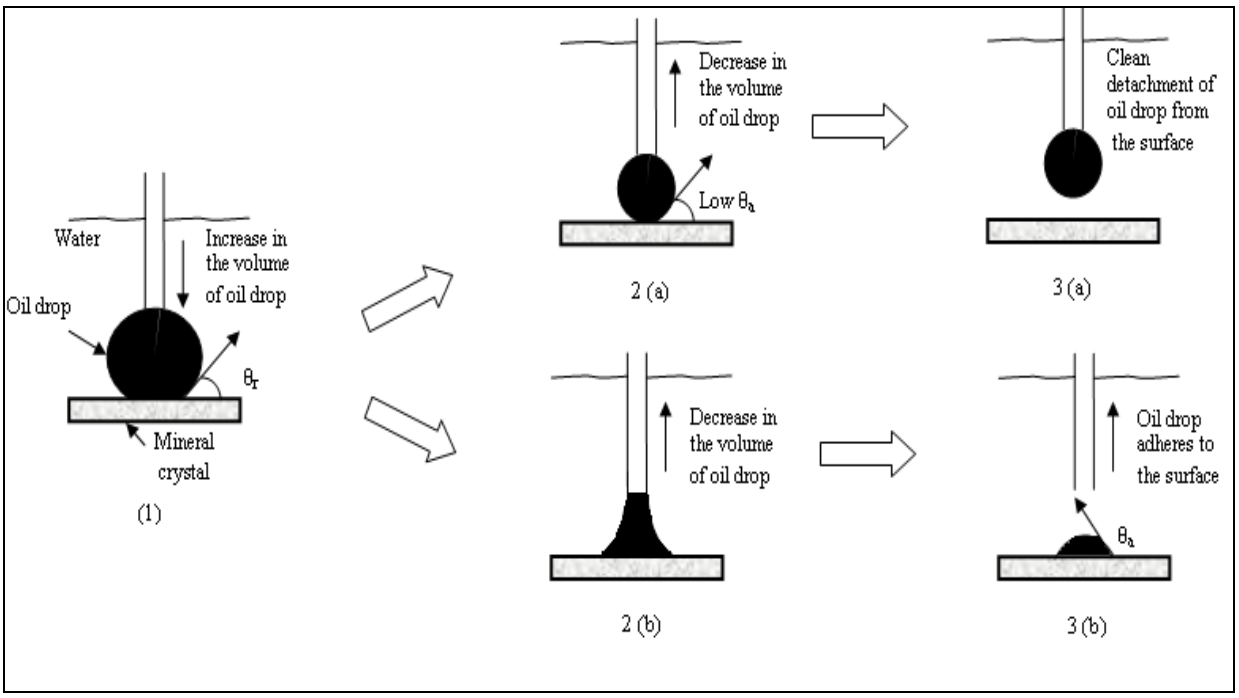

Figure 2.7: Schematic depiction of conventional adhesion test for rock/oil/water systems

Buckley et al. (1989) have studied the conditions under which oil adheres to a particular solid surface by examining the behavior of several crude oil samples using the adhesion test by forming a captive bubble of oil in water as described in Figure 2.8. The crude oil samples used in the study had asphaltene content (pentane insoluble) in them ranging from 2.52 wt% to 8.14 wt%. Their study investigated the effect of pH and ionic strength on the conditions under which adhesion occurs. Results showed that lack of adhesion signified the presence of a stable aqueous film that resulted from double-layer repulsion forces between the crude oil and the solid surface. These experiments were performed at ambient conditions using stock-tank oil.

Buckley and Morrow (1990) reported the use of qualitative adhesion tests at ambient pressure and elevated temperatures (95 to 122°F) to characterize crude oils with respect to their interactions

with brine and solids. They repeated the test for a range of brine concentrations and pH. In their study, adhesion maps were generated to differentiate the regions of adhesive and non-adhesive behavior over an intermediate range of pH from 4 to 8 and sodium chloride concentrations from 0.01 to 1.0 M. Most of the crude oils investigated in the study exhibited strongly pH-dependent adhesion behavior. Also, a change in oil composition showed a large effect on adhesion. Asphaltene removal by precipitation with hexane made Moutray crude oil non-adhesive over the range of brine compositions studied. The adhesion tests conducted with dissolved asphaltene showed some adhesive tendency, but did not duplicate the map of the original oil sample. The study demonstrated the use of adhesion tests as a rapid, semi-quantitative means for characterizing rock/oil adhesion interactions. They correlated the large contact angle hysteresis to adhesion in the system. The outcome of adhesion tests was explained in terms of the stability of the water film present between the solid and the oil drop. They concluded that if the water films are unstable, crude oil has access to rock surface and adsorption of polar compounds in the contacted area may permanently alter the wetting properties of the system.

Valat et al. (1993) studied the adhesion behavior of a crude oil on a mineral substrate as a function of brine pH and salinity using qualitative adhesion tests conducted at ambient conditions. Results showed that adhesion occurred only at pH below 5.8 for a given mineral substrate.

Rao and Maini (1993) reported the development of rock/oil adhesion during reservoir condition adhesion tests although the measured water-advancing contact angle was smaller than 40° (presence of thin water wetting films on the crystal surface). These observations confirmed that rock/oil adhesion could occur even in the presence of the thin films of water. Their study stressed on the need to develop means of quantifying the adhesion aspect of wettability for better understanding of the effect of rock/oil adhesion interactions on reservoir wettability and oil recovery.

Liu and Buckley (1997) have used the adhesion test in another configuration, where a water drop was formed on a pre-oil-wetted glass surface submersed in decane in a rectangular cuvette. This configuration was used to assess the wettability alteration in terms of contact angles after removing of the bulk oil phase. The influences of aging time, temperature and fluids composition on the adsorption and desorption behaviors of oil components were studied by increasing (the water-advancing contact angle) and decreasing (the water-receding contact angle) the volume of the water drop, respectively. Results showed that the adsorption of crude oil components onto dry glass surfaces was not strongly time-dependent. However, for the pre-wetted glass surface, a highly time-dependent adsorption was observed. At higher temperatures, an increased adsorption rate was observed for adhering oil/brine systems. Desorption of crude oil components was found to be dependent on both brine composition and temperature. The observed behavior was explained in terms of the stability of the thin aqueous wetting films. If the aqueous wetting film thins, the polar or ionized oil species may directly interact with ionized or polar sites on a solid surface. The crude oil samples used in their study had asphaltene content (pentane insoluble) in them ranging from 1.5 wt% to 10.9 wt%. These experiments were performed at ambient conditions using stock-tank oil.

2.4.1.1.2 The Sessile Oil Drop Volume Alteration Method

Another form of adhesion test is the sessile oil drop volume alteration (increase/decrease) method. A schematic diagram of the sessile oil drop volume alteration method is shown in Figure 2.8. In this method, an oil drop is brought into contact with the mineral surface in the presence of water, and drop volume is increased with the help of an injector capillary tube to remove the bulk water phase away from the rock surface (Figure 2.8, step 1). In this step, observed contact angle measured in water phase corresponds to the water-receding contact angle. After a sufficient equilibrium time (usually 24 hours), the volume of the oil drop is reduced in steps by

withdrawing oil back into the injector tube (Figure 2.8, step 2), and movement of the contact line (reduction in contact radius) is monitored. This technique can easily be adapted to reservoir conditions of elevated pressures and temperatures thereby facilitating the use of live oil in such experiments.

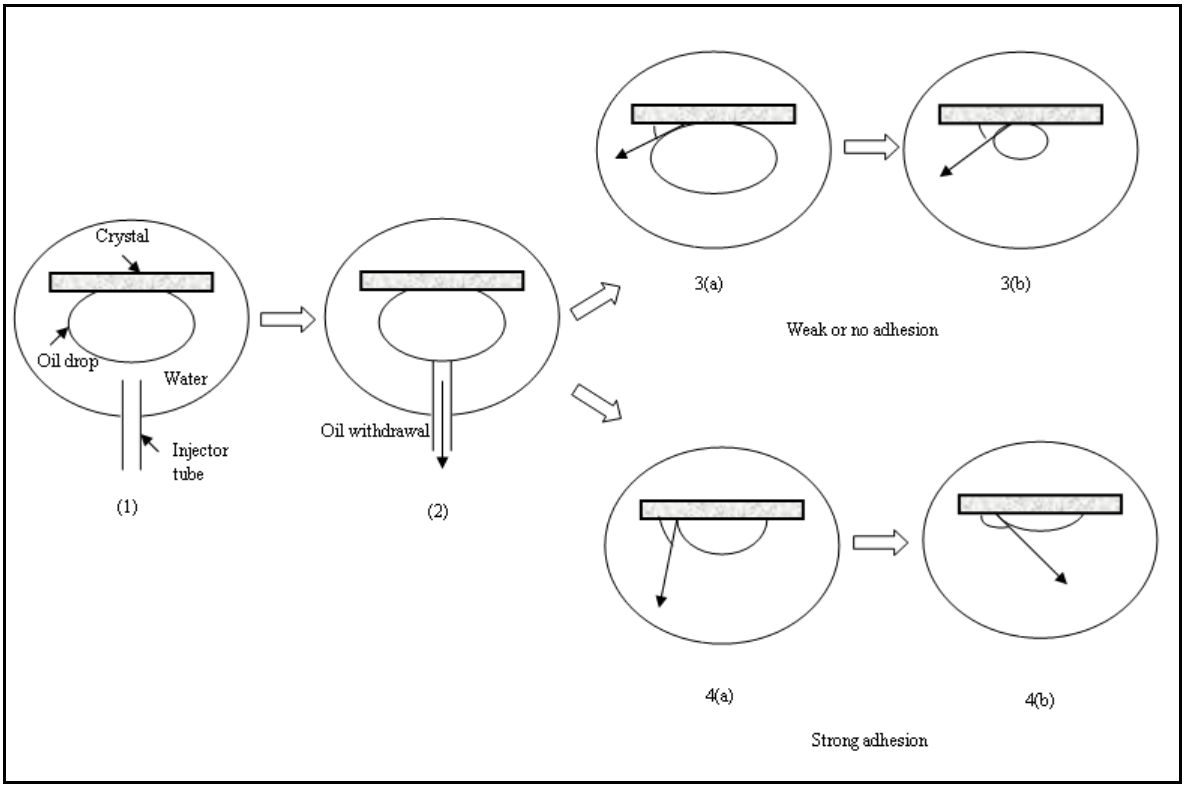

Figure 2.8: Schematic depiction of the sessile oil drop volume alteration method

Depending on the extent of rock/oil adhesion interactions, either the oil drop contact radius may be reduced without observing any significant change in the measured contact angle (Figure 2.8, steps 3(a) and 3(b)) in water phase (the water-advancing contact angle) or a pinning of the contact line may be observed that results in a monotonic increase in the contact angle value up to 180° (Figure 2.8, steps 4(a) and 4(b)). In the case of a pinning of the contact line, the measured contact angle does not satisfy the definition of the water-advancing contact angle.

Hjelmeland and Larrondo (1986) reported the strong wetting (adhesion) of the solid surface by stock-tank oil in the presence of brine at 104°F and 3,800 psi while conducting contact angle experiments using this method. They concluded that the temperature dependent adsorption and desorption of surface active material were the mechanisms responsible for the observed contact angle behavior in such experiments.

Rao (2003) has reported the pinning of the contact line while reporting the results of ambient condition drop volume reduction experiment for the quartz/Gilwood stock-tank oil/deionized water system (Figure 2.9[1]).

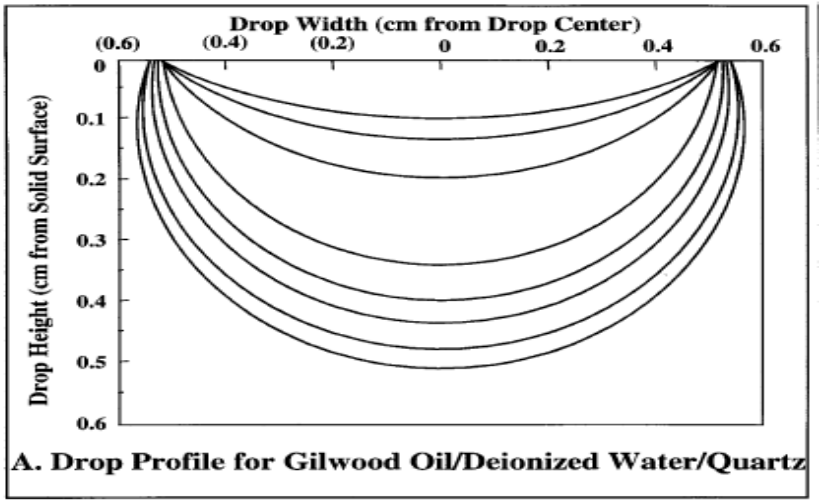

Figure 2.9: A pinning of the contact line in the ambient condition sessile oil drop volume reduction experiment (Rao, 2003)

This observed behavior of a pinning of the contact line was attributed to the presence of strong rock/oil adhesion interactions in the system. To explain the physical significance of rock/oil adhesion interactions in rock/oil/water systems, using the definition of adhesion forces in S/L/V systems, Rao (2003) defined a simplified adhesion number ($Cos\theta_r$-$Cos\theta_a$) for rock/oil/water systems, as the ratio of the adhesion forces to the capillary forces in. The term ($Cos\theta_r$-$Cos\theta_a$),

[1] © VSP 2003, reproduced with permission

which is generally referred to contact angle hysteresis while evaluating the flow behavior of reservoir fluids in pore space, was used to quantify the extent of rock/oil adhesion interactions in the system. Both the water-receding and the water-advancing contact angles used to compute the adhesion number in the study were measured using the DDDC technique. In the study, the computed adhesion number was also correlated with the wettability of the system that was determined by the measured water-advancing contact angle using the DDDC technique. Water-wet system showed lowest adhesion number while highest adhesion number was exhibited by oil-wet system. The study concluded that the observed contact angle hysteresis could indeed be due, partly or entirely, to the adhesion phenomenon at the rock/oil/water interface.

As evident from the discussion, different types of adhesion tests provide a qualitative estimate of the extent of rock/oil adhesion interactions in rock/oil/water systems. The observed behavior is explained in terms of the presence and the stability of the thin aqueous wetting films squeezed between the rock surface and the bulk oil phase. However, rupture of the thin aqueous wetting films may not be the necessary condition for the development of adhesion between the rock surface and the oil phase even in a water-wet system (Rao and Maini, 1993).

2.4.1.2 Measurement of Intermolecular Surface Forces Approach

This approach is based on the theoretical treatment of the thin liquid films. Theoretically, the stability and the thickness of the thin liquid wetting films sandwiched between the two surfaces are studied as a function of disjoining pressure computed from the classical DLVO (Derjaguin, Landau, Verwey and Overbeek) theory (Derjaguin and Landau, 1941; Verwey and Overbeek, 1948). Experimentally, the presence and the stability of the thin liquid films is studied by measuring the magnitude of different intermolecular surface forces across the thin liquid films squeezed between two interacting surfaces using different experimental techniques. Three main experimental techniques are 1) Atomic force microscopy (AFM) technique, 2) Surface force apparatus (SFA), and 3) Interference imaging of thin film and Newton's ring method.

2.4.1.2.1 Atomic Force Microscopy (AFM) Technique

Theoretically, the magnitude of intermolecular surface forces across the thin liquid films squeezed between two interacting surfaces is estimated in terms of disjoining pressure. Disjoining pressure is the integral effect of primary intermolecular forces (London-van der Waals dispersion forces and double layers electrostatic interactions) when one dimension of a fluid phase becomes sufficiently small (thin liquid film). Disjoining pressure components of these primary intermolecular forces are computed using classical DLVO theory. At a distance of a few molecular diameters between two approaching surfaces, the classical DLVO theory based on two primary intermolecular forces fails to describe the interactions between different phases (Israelachvili, 2006). In this situation, the effect of other short range forces such as solvation, structural, and hydration forces become dominant (Derjaguin and Churaev, 1974) and the effect of these short range forces should be suitably incorporated in the theoretical models for computing the disjoining pressure in such cases.

Basu and Sharma (1996) have reported the use of AFM technique to measure the force between a crude oil-coated tip and a mineral surface in brine In the AFM experimental setup (Figure 2.10[2]) used by them, one of the solid surfaces, a small glass microsphere coated with a thin layer of solid hydrocarbon phase (octadecane, which is solid at room temperature), was glued to the cantilever tip as a colloid particle. The other solid surface, mica substrate was positioned on a piezoelectric stage which could be moved vertically toward the colloidal particle (hydrocarbon coated glass microsphere). Deflection of cantilever tip versus vertical position was measured using AFM to measure the magnitude of forces across the brine film squeezed between the glass microsphere and the mica substrate. Different configurations were also used for measuring surface forces with different substrates.

[2] © ELSEVIER 1996, reproduced with permission

The measured force was then converted into *F/R* value where *F* is the force measured using AFM and *R* is the radius of sphere. This *F/R* value is directly proportional to the potential energy of interaction (*W*) using Derjaguin approximation (Derjaguin, 1934) for interactions between interacting sphere and plate surfaces as given by Eq.3.

$$\frac{F}{R} = 2\pi W \quad \ldots\ldots (3)$$

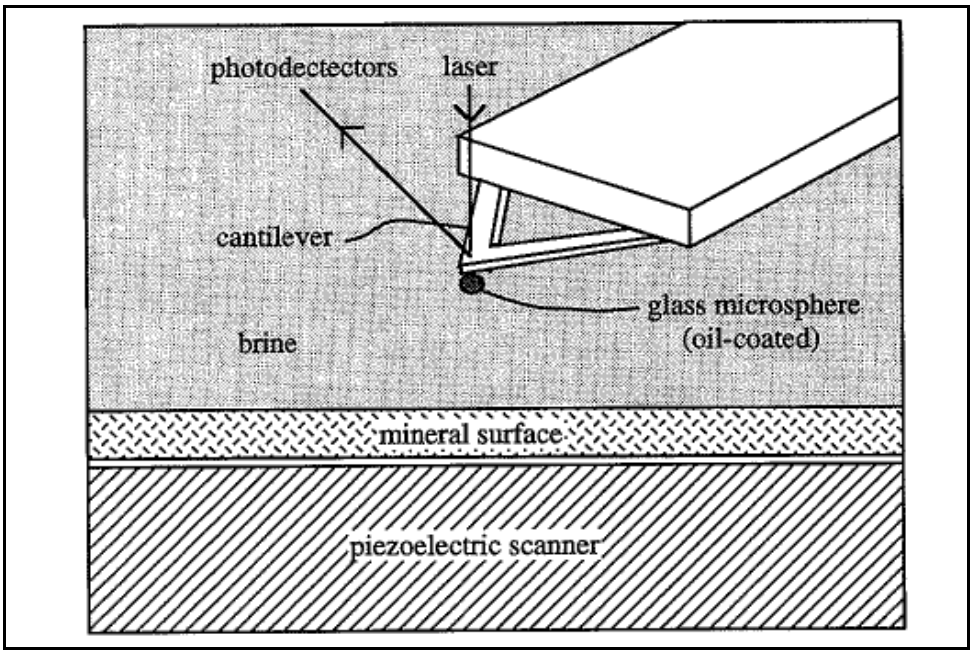

Figure 2.10: AFM experimental setup (Basu and Sharma, 1996)

Theoretically computed disjoining pressure between two planar surfaces using DLVO theory was converted to potential energy of interaction/area between the two interacting surfaces (sphere and plate) using the Derjaguin approximation. The relationship between potential energy of interactions per unit area and disjoining pressure is given by Eq.4. Theoretically computed potential energy of interaction per unit area (Eq.4) was compared with experimental measured *F/R* values (Figure 2.11[3]) obtained from AFM measurements.

[3] © ELSEVIER 2002, reproduced with permission

$$\frac{F}{R} = 2\pi W = 2\pi(-\int_{h}^{\infty} \Pi dh) \quad \text{.....} \quad (4)$$

The study concluded that the de-wetting of a solid surface could be quantified by observing hysteretic effects on the force versus distance curves. Stable or completely wetting films showed no hysteresis while meta-stable or unstable films showed large hysteresis in the measured force versus distance curves, when the imposed disjoining pressure (i.e. imposed capillary pressure) exceeded the critical disjoining pressure (Π_{crit}).

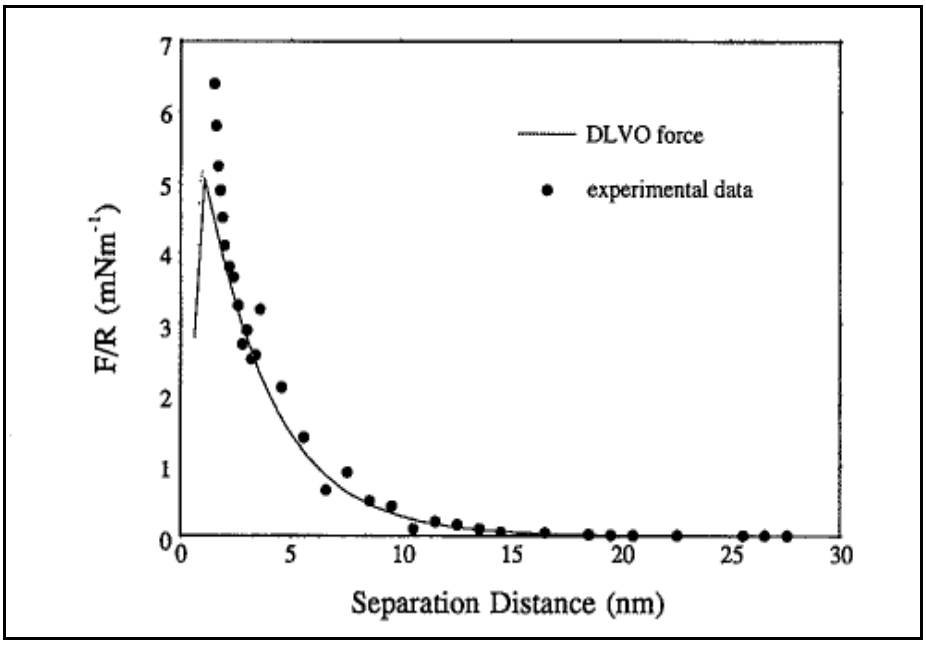

Figure 2.11: Experimental and theoretical surface forces versus distance profiles (Basu and Sharma, 1996)

Values of critical disjoining pressure were computed by converting measured *F/R* data to disjoining pressure curves. The study investigated the effect of pH, salinity and surface characteristics on the wetting behavior of solid surfaces. Also, higher salt concentration and pH of the aqueous film resulted in a more stable aqueous film on the mineral surface. Use of real crude oil (stock-tank oil) resulted in a more stable aqueous film compared to the use of octadecane in the

experiments. Also, at high salt concentration and pH, a poor agreement was observed between the DLVO theory and the measured data. Good match was found after including very short-range repulsive "hydration forces" in theoretical disjoining curves. These experiments were conducted at ambient conditions using octadecane or stock-tank oil.

2.4.1.2.2 Surface Force Apparatus (SFA) Technique

Use of SFA to measure the force and viscosity of crude oil thin films (Christenson and Israelachvili, 1987) has been reported in the literature. Drummond and Israelachvili (2002) used SFA technique to measure the force of interaction between two molecularly smooth mica surfaces confining thin films of crude oil in brine at different conditions of pH and salinity. In the study, interaction between two 'asymmetric' mica surfaces (Figure 2.12[4]) in a brine environment was studied by measuring force-distance curves using SFA.

For this, one of the mica surfaces was modified by allowing the crude oil to preadsorb on the surface. After 12 hours of asphaltene adsorption, the surface was rinsed with toluene and n-hexane to remove the non adsorbed fractions of the crude oil from the mineral surface.

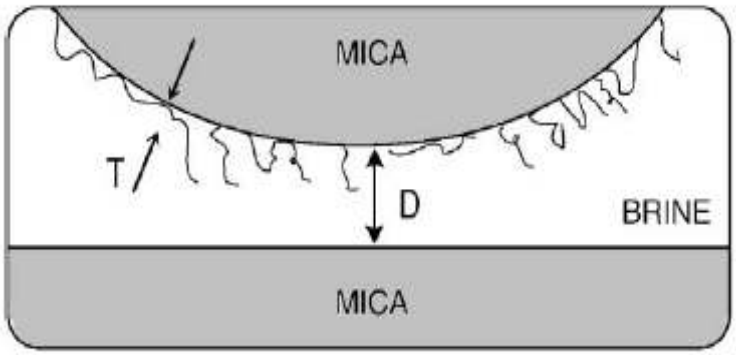

Figure 2.12: Geometry of the 'asymmetric' mica surfaces (Drummond and Israelachvili, 2002)

[4] © ELSEVIER 2002, reproduced with permission

An absorbed layer of asphaltene remains having a uniform thickness was observed as determined by AFM. Results of multiple beam interferometry (MBI), AFM and contact angle experiments suggested that the adsorption process was irreversible and the rinsing process did not seem to affect the thickness or other properties of the adsorbed layer. However, this adsorbed layer did come off when brought into contact with certain brine solutions. This uniformly asphaltene-coated surface was assumed to be a good representative of the crude oil surface.

The measured surface forces in terms of *F/R* value (Figure 2.13[5]) were related to the interaction energy per unit area (*W*) between two interaction flat surfaces using the Derjaguin approximation. The adhesion energy per unit area between two flat surfaces can be calculated from the adhesion or pull-off force, *F* (force required to separate the surface from adhesive contact, Christenson and Israelachvili, 1987), from Eq.5:

$$W = \frac{F}{2\pi R} \quad \text{..... (5)}$$

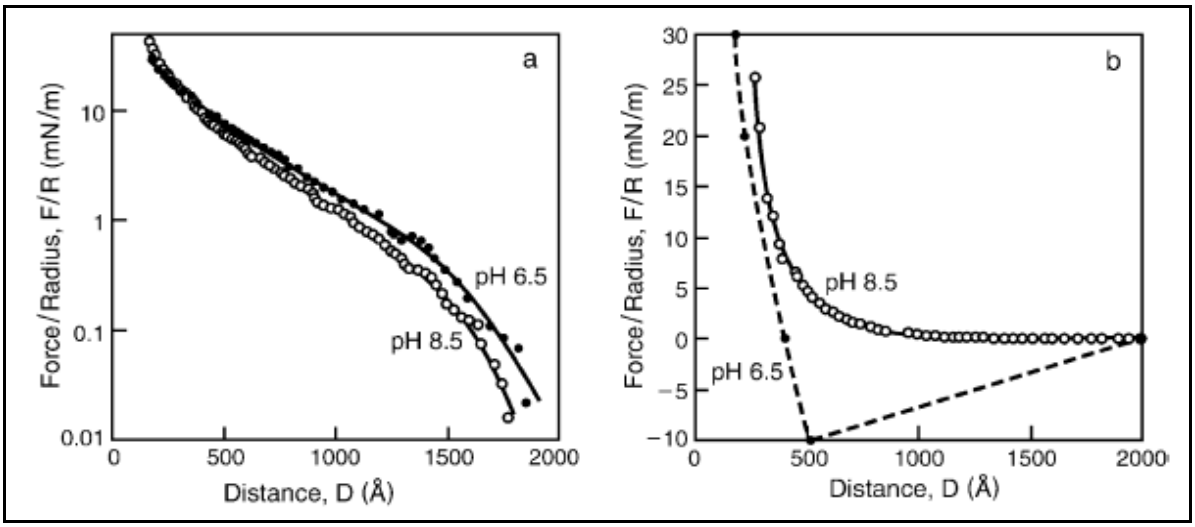

Figure 2.13: Measured surface forces between asymmetric mica surfaces (Drummond and Israelachvili, 2002)

[5] © ELSEVIER 2002, reproduced with permission

Adhesion energy per unit area for rock/oil/water systems can also be computed using the conventional Young-Dupré equation of the work of adhesion. For, rock/oil/water system, the Young-Dupré equation is written as:

$$W_{sow} = \gamma_{ow}(1 - Cos\theta_{\infty}) \quad \text{..... (6)}$$

Where W_{sow} is the work of adhesion or "adhesion energy per unit area" of the oil phase interacting with the solid surface in water, and θ_{∞} is the Young's contact angle (Eq.1). In the study, the adhesion energy per unit area computed from SFA measurement (Eq.5) was correlated with the results of adsorption and wettability (dynamic contact angle) experiments using the concept of work of adhesion (Eq.6). The wettability experiments were conducted under the same conditions of salinity and pH.

For computing W_{sow}, the water-advancing, the water-receding, and the static contact angles were measured using sessile drop technique, while the oil/water IFT was measured using a spinning drop tensiometer. A good agreement was found in the results obtained from both approaches. Typical measured values for the adhesion energy per unit area (W), as determined using Eq.5, were around 5 mJ/m^2 and corresponding value of the water receding contact angle (θ_r) or static contact angle (Young's contact angle, θ_{∞}) obtained using Eq.6 was found to be 35°, which was close to measured $\theta_r = \theta_{\infty} = 42°$. Measured adhesion energy per unit area was found to be dependent on the rate of approach and separation of the surfaces as well as on the time the surfaces are kept in contact.

It is noted here that SFA experiments can only measure complete water wetting (presence of stable aqueous wetting films) i.e. $\theta_{\infty}= 0°$. Results indicated that the wettability of a rock/oil/water system was dependent on the conditions of pH, brine salinity, and on the nature of the rock surface. The same rock/oil system exhibited different wetting state on changing brine composition. Their study emphasized the need to specify the conditions of whole system while evaluating the

wettability. All measurements were performed at ambient conditions using stock-tank oil that had 0.7 wt% of asphaltene content in it.

2.4.1.2.3 Interference Imaging of Thin Film and Newton's Ring Method

Use of a third technique (i.e. interference imaging of thin film method) has been reported by Ward et al. (1999). They used it to investigate the stability of the thin aqueous wetting film that separates a hydrocarbon droplet from a quartz plate immersed in a electrolyte solution under various conditions. Interference microscopy aided by digital image analysis techniques was used to measure the thickness of water films. Experiments were conducted at ambient pressure and 77°F. A schematic diagram of experimental setup used by Ward et al. is shown in Figure 2.14[6].

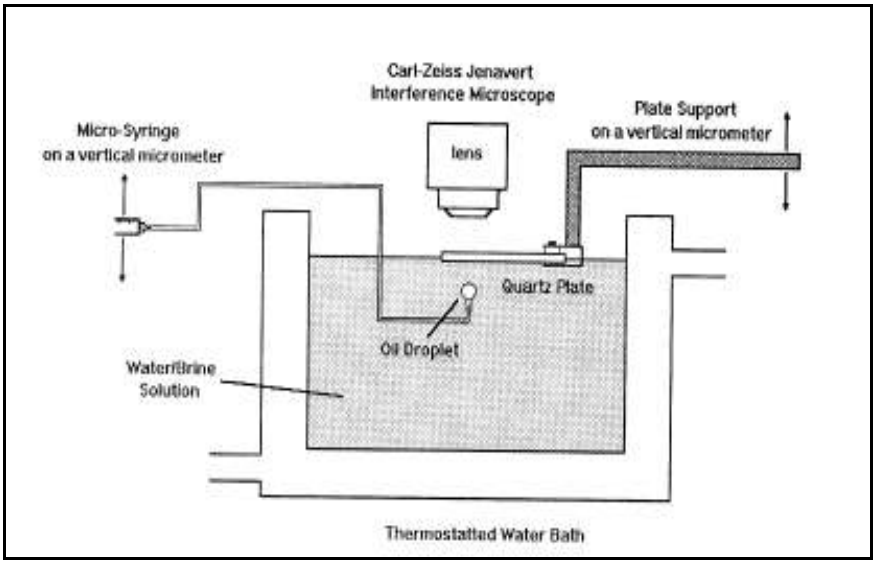

Figure 2.14: Experimental setup for studying the thickness of thin films (Ward et al., 1999)

In first step of this study, a pendant drop of dodecane was formed using an injector tip and was kept for 60 min to attain equilibrium with aqueous phase. Then, the pendant drop was moved carefully towards the quartz plate using a vertical micrometer until a small circular film was observed. The apparatus was designed in such manner that the oil droplet was almost at the water

[6] © ELSEVIER 1999, reproduced with permission

surface to keep the hydrostatic effects minimal on the capillary pressure exerted by oil drop on the thin aqueous film present between oil droplet and quartz plate. The images of the circular film and Newton's ring patterns (Figure 2.15[7]) were digitally recorded and analyzed by translating them into a radial averaged intensity profile to compute the water film thickness and curvature of the droplet as it approached the quartz plate.

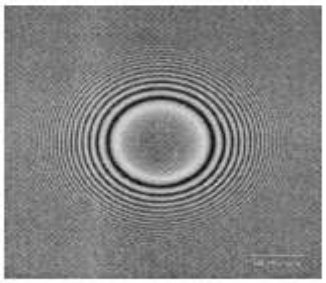

Figure 2.15: Interference image of a thin film and Newton's rings (Ward et al., 1999)

The computed radius of curvature was used to calculate capillary pressure. The variation in water film thickness between dodecane and quartz was plotted as a function of capillary pressure as shown in Figure 2.16[8].

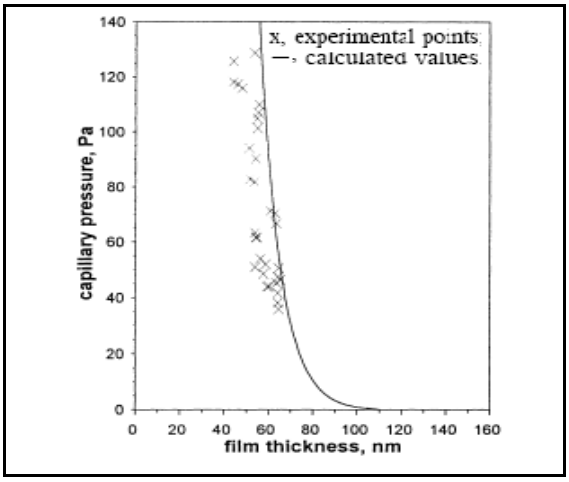

Figure 2.16: Variation of film thickness as a function of capillary pressure (Ward et al., 1999)

[7,8] © ELSEVIER 1999, reproduced with permission

Capillary pressure was altered by changing the oil drop size. Collapse of thin aqueous film was recognized as optically black film in average intensity profile. Two crude oil samples with varying asphaltene contents were also tested to characterize the film thickness as a function of pH. One crude oil sample had little or no asphaltene and the second crude oil sample contained 6 wt% of asphaltene. The results are shown in Figure 2.17[9].

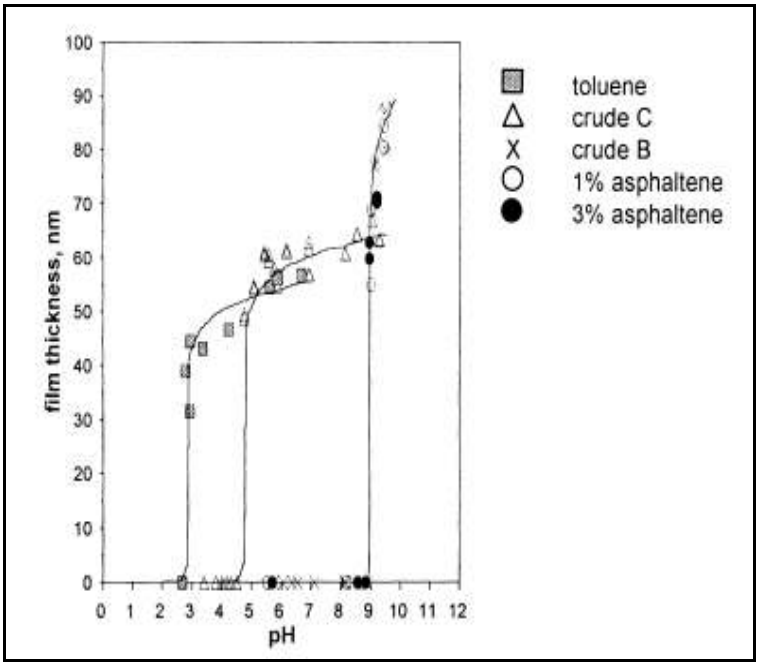

Figure 2.17: Variation of film thickness with different oil types (Ward et al., 1999)

To assess if the collapse of the aqueous film in certain pH ranges was solely due to the asphaltene component, experiments were conducted with 1% and 3% asphaltene dissolved in toluene. The results were similar that of crude oil. A solution of 6% asphaltene in toluene was found to give no stable film from pH 5 to pH 10. The study concluded that the variation of the simple properties of the bulk aqueous phase, such as pH and ionic strength, has been shown to alter the film thickness and stability in different crude oil/quartz systems. These changes in the equilibrium film thickness can be described in terms of interaction pressure by consideration of DLVO theory using electrostatic forces calculated from the linear superposition approximation

[9] © ELSEVIER 1999, reproduced with permission

(LSA) model proposed by Gregory (1981). The results indicated that the collapse of thin aqueous film did not imply a change in the wettability conditions in case of simple hydrocarbon systems investigated in the study. It was observed that the crude oil drops remained attached to the plate surface after collapse of water film, and an oily residue was observed to coat the plate. This indicated that the presence of asphaltene in oil phase resulted in irreversible change in wettability due to adsorption of asphaltic material onto the plate surface.

As evident from the above discussion, the extent of rock/oil adhesion interactions in rock/oil/water systems is often explained in terms of the presence and the stability of the thin aqueous wetting films which are greatly affected by a change in the composition of the fluids (oil and water). On one hand, the adhesion test approach is purely an experimental tool to asses the extent of rock/oil adhesion interactions. On the other hand, the theoretical considerations of the thin liquid films by either computing the disjoining pressure components of different intermolecular surface forces or computing the adhesion energy per unit area using the concept of work of adhesion and their experimental validation by different surface force measurement techniques provide a quantitative estimate of the extent of rock/oil adhesion interactions in complex rock/oil/water systems.

All three of the above mentioned experimental approaches have proven to be very valuable quantifying the extent of rock/oil adhesion interactions and in gaining a fundamental understanding of its role in determining the wetting behavior of complex rock/oil/water systems. However, all of the reported experimental measurements of intermolecular surface forces and thickness of aqueous wetting films were conducted at ambient conditions of pressure and temperature using simple hydrocarbons and stock-tank oil. Also, majority of the experiments conducted using these techniques were limited to the measurement of intermolecular forces in preferentially water-wet systems. It was normally observed that the systems having the stable thin aqueous wetting films (preferentially water-wet) exhibit a smaller contact angle hysteresis on none at all compared to the

systems (preferentially oil-wet) with collapsed thin wetting aqueous films (large contact angle hysteresis or a pinning of the contact line).

The presence and the stability of the thin aqueous wetting films are seen as a physical explanation for the observed phenomenon of contact angle hysteresis in rock/oil/water systems. In the next sub-section, the interrelationship between the dynamic contact angles and the presence and stability of thin aqueous films is discussed on both theoretical and experimental bases.

2.4.2 Interrelation of Equilibrium Contact Angle and the Stability of the Thin Aqueous Wetting Films

The presence and the stability of the thin aqueous wetting films are used for describing the wetting behavior of rock/oil/water systems by knowing the fact, that, initially water filled porous space of reservoir rock was invaded by migrating oil during pristine drainage process, indicating that this process left thin aqueous wetting films squeezed between the rock surface and bulk phase. Mohanty et al. (1981) discussed the interplay of geometric quantities (such as meniscus curvature) and physical properties (such as film thickness and apparent contact angle) on the fluid behavior in porous media. They discussed the equilibrium of thin-films with bulk fluid behind menisci in slots, tubes, and porous media. This equilibrium is described next.

First, the curvature of a meniscus in a pore is determined by both the pore radius (R_p) and the contact angle (θ) that the meniscus makes with the pore wall. The curvature of the meniscus set by the R_p and θ then sets the capillary pressure (P_c). P_c is the difference in pressure between wetting and non-wetting phases. The imposed P_c determines the thickness of the wetting films (h) separating the non-wetting phase and the solid phase. When the dimension of a fluid phase becomes sufficiently small (~0.1 μm), the presence of strong intermolecular forces causes an excess pressure across the thin film (Derjaguin and Landau, 1941; Verwey and Overbeek, 1948). This excess pressure felt across the thin film is denoted as the disjoining pressure (Π), which is a function of film thickness, h.

According to Hirasaki (1991), the change in energy per unit area with change in distance as the pair of interfaces is brought from a large separation to a finite thickness is expressed as disjoining pressure. The disjoining pressure, Π, is a force per unit area that tends to separate two interfaces when it is positive and tends to attract two interfaces when it is negative (Hirasaki, 1991). If the imposed capillary pressure, P_c, exceeds the net forces due to disjoining pressure and surface curvature, the wetting films reduced spontaneously thin to molecularly adsorbed films (Radke et al., 1992). A relationship between P_c and Π is given by the augmented Laplace-Young equation. The augmented Laplace-Young equation is written as:

$$P_c = \Pi + 2\gamma_{ow} J \quad \text{..... (7)}$$

Where, J is the surface curvature, which is negative for convex surfaces, positive for concave surfaces, and is equal to zero in the case of flat surfaces.

Radke et al. (1992) presented a pore-level scenario for the development of mixed wettability in oil reservoirs by incorporating the thin wetting aqueous film forces into a collection of capillary tube model to describe the geological development of so-called mixed wettability in reservoir rock. In the absence of measured disjoining pressure isotherms in rock/oil/water systems, they assumed a contact angle of 20° for the molecular aqueous films and a contact angle value of 0° while computing the critical capillary pressure in a single pore using the augmented Young-Laplace equation (Eq.7) in the presence of pore wall curvature. The study concluded that non-axisymmetric pore shapes and thin films are necessary to understand the wettability at fundamental level.

Melrose (1982) examined the limits under which stable thin wetting aqueous films can exist. He showed that the occurrence of thin aqueous wetting films is limited by the pore size which depends on the salinity of the brine. He stressed that the physico-chemical analysis of the aqueous wetting film stability should be applied only within the context of a general geological model for a particular reservoir.

To understand the delicate interplay of contact angle and the thickness of the aqueous wetting films in determining the wettability, the surface curvature, *J*, can be eliminated from Eq.7 by considering the surface curvature equal to zero (flat surface). For rock/oil/water systems, a relationship between the contact angle, θ, subtended by a sessile oil drop with a flat solid surface (Figure 2.18[10]) in the presence of the thin aqueous wetting film of thickness, *h*, and the disjoining pressure, Π, can be derived using the augmented Laplace-Young equation (Eq.7) and the Young's equation (Eq.1), if the film is represented as a single Gibbs dividing surface (Martynov and Derjaguin, 1962).

This relationship is written as:

$$Cos\theta = 1 + \frac{1}{\gamma_{ow}} \int_0^{P_C} h\, d\prod \quad \text{..... (8)}$$

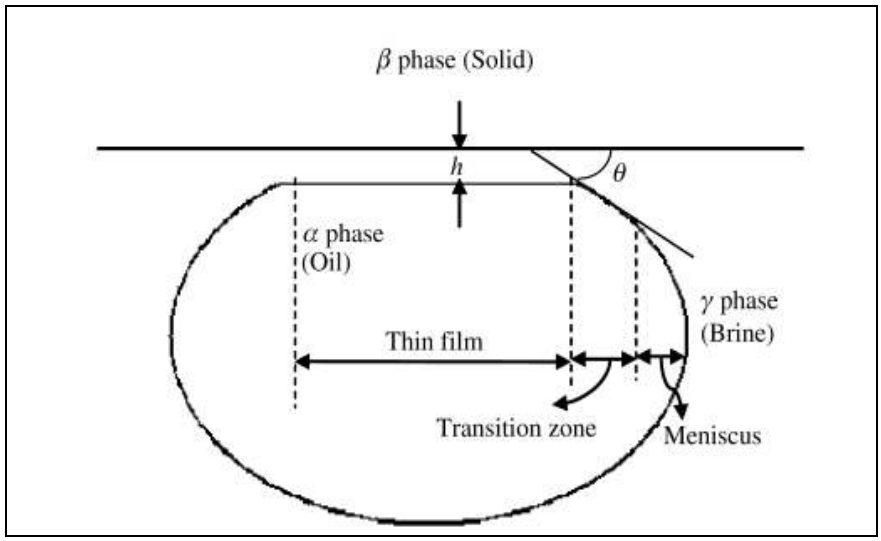

Figure 2.18: Description of sessile oil drop in rock/oil/water system (Busireddy and Rao, 2007)

A detailed derivation of Eq.8 can be found elsewhere (Basu and Sharma, 1996). A good discussion on the inclusion of disjoining pressure in Eq.8 is given by Hirasaki (1991). Equation 8

[10] © ELSEVIER 2007, reproduced with permission

shows that the disjoining pressure, Π, is directly related to the contact angle, θ. It is noted here that the contact angle, θ, mentioned in Eq.8 is actually the static or the Young's contact angle, θ_∞, given by the Young's equation (Eq.1).

Equation 8 can also be rearranged as:

$$\gamma_{ow}(1 - Cos\,\theta_\infty) = -\int_0^{P_C} h\ d\Pi \quad \text{..............} \quad (9)$$

A careful comparison of Eq.9 with Eq.6 reveals that the integral term containing disjoining pressure is equivalent to the work of adhesion (adhesion energy per unit area), W_{sow}.

Busireddy and Rao (2007) developed a computational model for thin-film stability and spreading in solid/liquid/liquid (S/L/L) systems. Theoretical disjoining pressure isotherms were generated for different S/L/L systems by modeling the intermolecular surface forces using the classical DLVO theory and modifications to it. The computed disjoining pressure curves for the glass/Yates crude oil/Yates brine system at reservoir conditions (700 psi, 82°F) are shown in Figure 2.19[11].

The relationship between the equilibrium (Young's) contact angle (θ_∞) and the disjoining pressure (Eq.9) was used to compute θ_∞. The computed θ_∞ were compared with the experimentally measured θ_∞ exhibited by a sessile crude oil (Yates) drop resting with the solid (glass or Berea sandstone substrate) surface in a brine (Yates) filled optical cell kept at reservoir conditions of pressure (700 psi) and temperature (82°F). The experimentally measured θ_∞ for glass/Yates crude oil/Yates brine system (pH=7.5) at reservoir conditions was 22° whereas computed θ_∞ was found to be 7°. The difference between the calculated and measured equilibrium contact angles was attributed to the difficulty in measuring small contact angles in the HPHT optical cell. It is important to note that the calculated contact angle obtained for the glass/Yates live oil/Yates

[11] © ELSEVIER 2007, reproduced with permission

reservoir brine system indicated that system was strongly water-wet, which agreed well with the experimental measurements mentioned in the study. Authors specifically mentioned that the computation of equilibrium contact angle by using theoretical disjoining pressure isotherms was applicable to water-wet systems only. It is worth mentioning here that for strongly water-wet systems, both the water-receding (θ_r) and the water advancing contact angle (θ_a) correspond well to θ_∞. However, in other rock/oil/water systems, a large deviation between θ_r and θ_a (i.e. contact angle hysteresis) is regularly observed. The extent of deviation depends upon the extent of rock/oil adhesion interactions present in the system.

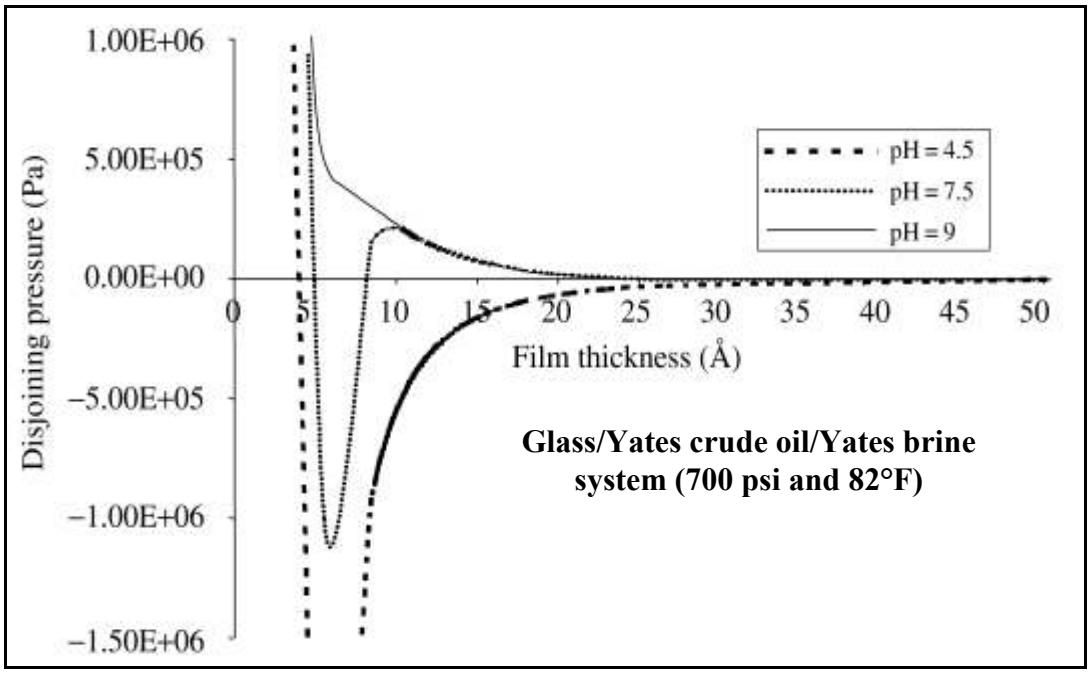

Figure 2.19: Reservoir condition theoretical disjoining pressure isotherms (Busireddy and Rao, 2007)

The reported experimental results (Drummond and Israelachvili, 2002; Busireddy and Rao, 2007; and Freer et al., 2003) confirm that the measured equilibrium contact angle for a sessile oil drop resting with a solid surface kept in a water filled optical cell agrees well with the computed θ_∞ either by using the concept of the work of adhesion (Eq.6) or considering the relationship between θ_∞ and the disjoining pressure in the presence of stable aqueous wetting films (Eq.9).

In all three of the above mentioned studies, the investigated S/L/L systems exhibited strongly water-wet nature in the region of stable thin aqueous wetting films.

As evident from the results of reported studies discussed in sub-sections 2.4.1.2 and 2.4.2, the experimentally measured θ_∞ and the theoretically computed θ_∞ in the presence of the stable thin aqueous wetting films (strongly water-wet systems) are found to be in good agreement. Due to the presence of the stable thin aqueous wetting films, negligible contact angle hysteresis or none at all is observed in the preferentially strong water-wet systems. The question to be asked then is, could this knowledge (Eq.6 and Eq.9) be applied in the case of other S/L/L (rock/oil/water) systems as well, which generally exhibit significant contact angle hysteresis?

2.4.3 Modified Young's Equation

The observed wetting behavior of S/L/V and S/L/L (rock/oil/water) systems is explained in terms of the presence and the stability of the thin wetting aqueous films. In certain systems, the presence of stronger intermolecular surface forces leads to reduction in the thickness of the aqueous wetting films up to such extent (molecularly thin) that a wetting alteration (preferentially water-wet to preferentially oil-wet) or a large contact angle hysteresis is exhibited by the system. In this scenario, the Young's equation fails to take an account of these strong intermolecular surface forces and the system does not exhibit a unique value of contact angle which could adequately describe the wetting state of the system.

To overcome this inadequacy of the Young's equation particularly in S/L/V systems, the Young's equation has been modified in the recent literature to include a line tension term. This modification was sought to accommodate the imbalance of different intermolecular forces experienced by molecules located in and around the three-phase confluence zone (Amirfazli and Neumann, 2004). These intermolecular forces include van der Waals forces, electrostatic forces, solvation (hydration) and steric forces. However it is not necessary that all types of intermolecular forces are present in all systems.

Gibbs (1961) was the first to mention line tension in his theory of capillarity. For S/L/V systems, line tension is defined as the reversible work which is necessary to expend isothermally the unit length of contact line, a line common to all three phases (Toshev et al., 1988). In other words, the excess energy of the three phase system per unit length of the triple junction is attributed to line tension (Drelich and Miller, 1996).

Boruvka and Neumann (1977), in their general theory of capillarity, provided a clear definition of line tension as a thermodynamic property by including the three-phase confluence zone in their analysis and derived a generalized Young's equation as:

$$\gamma_{SV} - \gamma_{SL} = \gamma_{LV} Cos\theta + \gamma_{SLV} \kappa_{gs} \quad \text{..... (10)}$$

Where γ_{SV}, γ_{SL}, γ_{LV} and γ_{SLV} are the surface tensions of the solid/vapor interface, the solid/liquid interface; the liquid/vapor interface; and the solid/liquid/vapor interface, respectively; θ is the contact angle; and κ_{gs} is the local curvature of the three-phase contact line in the plane of solid phase. For a circular three-phase contact line, κ_{gs} is replaced with the reciprocal of the radius of the contact circle, *1/r*.

The line tension-based modified Young's equation as derived by Boruvka and Neumann (1977) and used by Li and Neumann (1990) is written as:

$$Cos\theta = Cos\theta_{\infty} - \frac{\sigma}{\gamma_{LV}}(1/r) \quad \text{..... (11)}$$

where γ_{LV} is the surface tensions of the liquid/vapor interface; σ is the line tension; θ is the contact angle subtended by the Axisymmetric sessile liquid drop of finite and small contact radius placed on the solid surface surrounded by a vapor phase; θ_{∞} is the contact angle when $r \rightarrow \infty$; and r is the radius of the three-phase contact circle, respectively. Equation 11 shows that the contact angle varies with drop size (i.e., contact radius, r). Hence it should be possible to determine the line tension by measuring the dependence of contact angle on the radius of the three-phase contact circle (Li and Neumann, 1990). However, Marmur (1997) suggested that the contact angle versus

drop size relationship may not be due to the line tension effect, especially in the systems that exhibit high value of line tension. A detailed state of the art literature review of the status of the three-phase line tension is provided in the recent literature (Amirfazli and Neumann, 2004). Line tension is one of the parameters that affects the contact angle and is of practical importance in wetting of surfaces in different processes, such as froth flotation and stability of emulsions (Amirfazli and Neumann, 2004).

The line tension approach to incorporate the imbalance of molecules in and around three phase contact region on contact angle in the case of S/L/V systems seems to be equivalent to the approach of disjoining pressure in the case of S/L/L systems. Could the modified Young's equation derived for S/L/V systems by replacing the solid/vapor surface tension and contact angle in the liquid phase with the liquid/liquid interfacial tension (IFT) and the water-advancing contact angle be used for S/L/L (rock/oil/water) systems? If the answer is yes, then a plot of $Cos\theta_a$ against *1/r* should be linear with a slope equal to the ratio of the line tension to the oil/water IFT (σ/γ_{ow}) (Rao et al., 1995). Then, the line tension-based modified Young's equation for rock/oil/water systems can be written in a manner similar to S/L/V systems (Rao et al., 1995):

$$Cos\theta_a = Cos\theta_\infty - \frac{\sigma}{\gamma_{ow}}(1/r) \quad \text{..... (12)}$$

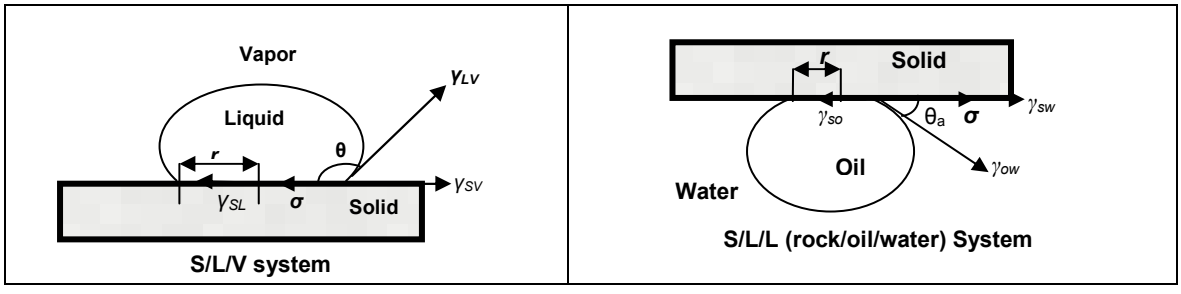

Figure 2.20: Concept of the line tension for S/L/V and S/L/L Systems

A schematic representation of the concept of the line tension in both S/L/V and S/L/L systems is shown in Figure 2.20. For S/L/L systems, the line tension can be defined as the work which is necessary to reduce isothermally the unit length of contact line (Saini and Rao, 2009).

As evident from the recent literature review of the status of three-phase line tension presented by Amirfazli and Neumann (2004), much of the research effort in studying the effect of line tension has been reported for S/L/V systems. Drelich and Miller (1992) reported the experimentally measured value of line tension for two different S/L/L (quartz A/kerosene/water and quartz B/heptane/water) systems. It appears that these studies were conducted at ambient conditions. Considering the possible effect of surface roughness and heterogeneity, he used a term "pseudo-line tension" in place of line tension while reporting the experimental results in S/L/L systems.

Rao et al. (1995) studied the drop size dependence of the sessile oil drop contact angle for three widely differing S/L/L (rock/oil/deionized water) systems at ambient conditions and suggested that the modified Young's equation can be used to explain rock/oil adhesion interactions present in rock/oil/water systems of petroleum engineering interest.

The concept of the line tension as described by the modified Young's equation seems to be a promising experimental means to estimate the magnitude of intermolecular surface forces i.e. the extent of rock/oil adhesion interactions in terms of the measured oil/water interfacial tension and dynamic contact angles. The applicability of the line tension-based modified Young's equation for characterizing rock/fluids interactions in rock/oil/water systems at reservoir conditions needs to be further investigated.

Thus, from the detailed literature and discussion cited above on the experimental and theoretical aspects of the characterization of rock/fluids interactions in rock/oil/water systems, it is clearly evident that the use of available experimental approaches for measuring the magnitude of intermolecular surface forces in rock/oil/water systems are limited to making such measurements at

ambient conditions. The magnitude of intermolecular forces or the extent of rock/oil adhesion interactions in complex rock/oil/water systems at representative reservoir conditions is essential for devising means to overcome these strong forces. Such characterization of rock/fluids interactions remains to be investigated at prevailing reservoir conditions using representative reservoir fluids and common reservoir rock mineral surfaces and has defined the scope of this study.

2.5 Fluid/fluid Interactions

As discussed in previous sections, along with the measured dynamic contact angles, measured oil/water IFT data is also needed to quantitatively estimate the extent of rock/oil adhesion interactions in complex rock/oil/water systems (Eq.6, 9, and 12). Although the role of oil/water IFT in reservoir dynamics is very well recognized by the petroleum industry, very few efforts have been made to measure this important parameter at elevated pressures and temperatures using actual reservoir fluids. Though IFT measurements for pure fluid pairs and simple hydrocarbons/water systems have been reported up to 15,000 psi and 350°F, most of the published data involving representative reservoir fluids (live oil and reservoir brine) have been measured at pressures only up to 5,000 psi and temperatures up to 200°F

Hocott (1939) studied the IFT between water and subsurface samples of three different reservoir crude-oils as a function of pressures (atmospheric pressure to 3,800 psi) at respective reservoir temperatures (130 to 178°F). Results showed that oil/water IFT increased with pressure until the saturation pressure is reached, and then slowly decreased with pressure.

Jennings (1967) reported the measurement of interfacial tension of Benzene-water and n-Decane-water systems at reservoir conditions of temperatures (74 to 350°F) and pressures (14.7 to 12,000 psia). A significant decrease in IFT was observed with an increase in temperature. Pressure also affected the IFT but the effect of temperature was much greater than that of pressure.

Jennings and Newman (1972) also reported the measurement of interfacial tension of water against an ideal “live-oil (methane-decane mixture)” system at reservoir conditions of temperatures

(74 to 350°F) and pressures (14.7 to 12,000 psia). A decrease in IFT with temperature and an increase in IFT with pressure at given temperature were observed.

McCaffery (1972) investigated the effect of pressure and temperature on the IFT for n-dodecane/water and n-octane/water systems at elevated pressures up to 6,000 psia and at elevated temperatures up to 300°F using pendant drop method. Both systems showed a decrease in measured IFT with an increase in temperature at a given pressure. A slight increase in IFT was observed with increased pressure at a given temperature. The effect of temperature on oil/water IFT was found to be significantly higher compared to the effect of pressure.

Hjelmeland and Larrondo (1986) studied the IFT between crude-oils (stock-tank and live) and brine at various temperatures (72 to 140°F) and pressures (29 and 3,800 psi). Results showed that stock-tank oil and live reservoir oil from the same reservoir and similar experimental conditions exhibited different IFT. They also reported a significant decrease in oil/water IFT with time at a given temperature and pressure.

Wang and Gupta (1995) investigated the interfacial tension for one mineral oil/distilled water and two crude oil/brine systems at elevated pressures and temperatures. IFT experiments were conducted at pressures up to 10,000 psi and temperatures up to 200°F. Measured IFT was found to increase with pressure. However no definite trend was observed with temperature. Depending on the composition of the system, IFT values, either increased or decreased with temperature.

Amin and Smith (1998) studied IFT between water and recombined reservoir oil sample at reservoir conditions of elevated pressures (up to 3,500 psi) and temperature (180°F). The study showed an increase in oil/water IFT with increasing pressure at given temperature.

Rao (2001) has reported the measured IFT values for n-octane/water system at elevated pressures and temperatures using both sessile and pendant drop techniques. These measurements were made at pressures up to 10,152 psi and temperatures up to 338°F. An increase in IFT with increasing pressure and decrease in IFT with increasing temperature were observed.

Buckley and Fan (2005) reported the measured IFT values for 41 well characterized stock-tank crude oil samples against water. The effect of different variables such as salinity, pH, time (transient IFT), viscosity, and amount of asphaltenes was studied. The study demonstrated that IFT of crude oils varied predictably with pH and composition of the aqueous phase and increased with increasing amount of asphaltenes. The relationship between oil-water IFT and other variables appears to be investigated at ambient conditions.

Xu et al. (2008) investigated the pressure, temperature, oil and brine composition and time dependence of oil/water IFT while studying the effect of surfactants on interfacial interactions at reservoir conditions (pressures up to 3,000 psi and 138°F). They reported a linear increase in first-contact and equilibrium IFT for the live oil/synthetic reservoir brine system at reservoir temperature. The oil/water IFT was found to be largely influenced by the oil and brine compositions. They also concluded that asphaltenes were the critical components responsible for the dynamic behavior of IFT, while overall composition of oil decided the first contact IFT (zero time).

Saini and Rao (2009) reported the measured oil/water IFT values at elevated pressure (1,500 psi) and 238°F for crude oil (live and stock-tank oil)/water (synthetic reservoir brine/deionized water) systems. The measured oil/water IFT was found to sensitive to the experimental conditions of pressure and temperatures and the composition of reservoir fluids (oil and brine).

As evident from the above mentioned experimental studies that there is scarcity of crude oil/water IFT data published in the petroleum industry at elevated pressure and temperature conditions using representative fluids. Shafer and Fate (2007) highlighted the need for measured crude-oil/water IFT at high-pressure high-temperature (HPHT) conditions. According to them, the uncertainty in the IFT of any live reservoir oil at HPHT conditions may be nearly an order of magnitude. According to them a linear extrapolation of IFT data from Hocott (1939) from 4,000 psi

to 20,000 psi resulted in a decrease in IFT from about 30 dyne/cm to 10 dyne/cm. Any such extrapolation of low pressure IFT data to very high pressures may result in significant errors in quantifying original oil in place (OOIP) on the basis of primary drainage capillary pressure curve derived using laboratory capillary pressure data (Shafer and Fate, 2007). As evident from the above cited literature that majority of the oil/water IFT measurements at pressures beyond 10,000 psi are made, either for pure hydrocarbons or stock-tank oil. Also, the measured oil/water IFT data in an input parameter for determining the line tension using the modified Young's equation (Eq.12). All of these issues make it necessary to measure the oil/water IFT at reservoir conditions of elevated pressures and temperatures using representative reservoir fluids. Hence, the measurement of oil/water IFT and the study of the effects of different variables on it at elevated pressures (up to 14,000 psi) and temperatures up to 250°F is one of the main objectives of this study.

3. EXPERIMENTAL APPARATUSES AND PROCEDURES

A precise measurement of the dynamic contact angles, the oil/water interfacial tension, and the drop-size dependence of sessile oil drop dynamic contact angles is needed to experimentally characterize rock/fluids interactions in complex rock/oil/water systems at both ambient and reservoir conditions.

Both the ambient and reservoir-condition optical cells were used, with stock-tank and recombined live oil, respectively, to measure the water-receding and the water-advancing contact angles for determining the system's wettability using the dual-drop dual-crystal (DDDC) contact angle measurement technique. The capabilities of both the optical cells were used for making oil/water interfacial tension measurements using the pendant drop method. The drop-size dependence of sessile oil drop dynamic contact angle subtended by the oil/water interface to the surface of rock mineral crystal was studied using the sessile oil drop volume alteration method for studying the applicability of modified Young's equation in rock/oil/water systems.

The equipment and the experimental techniques used in this study are discussed next.

3.1 Experimental Apparatuses

3.1.1 Ambient Condition Dual-Drop Dual-Crystal (DDDC) Optical Cell Apparatus

An ambient condition DDDC optical cell apparatus was used to characterize rock/fluids interactions at ambient conditions using stock-tank oil. The ambient condition DDDC optical cell and its associated components are shown in Figure 3.1. Two crystal holders (upper and lower) are available in for making dynamic contact angle measurements. The upper crystal holder moves in the vertical direction, while the lower one moves horizontally. In addition, the lower horizontal holder can be rotated around its horizontal axis as well. The DDDC tests and the sessile oil drop volume alteration experiments at ambient conditions were also conducted using it. It was used for making the oil/water interfacial tension measurements using the pendant drop method.

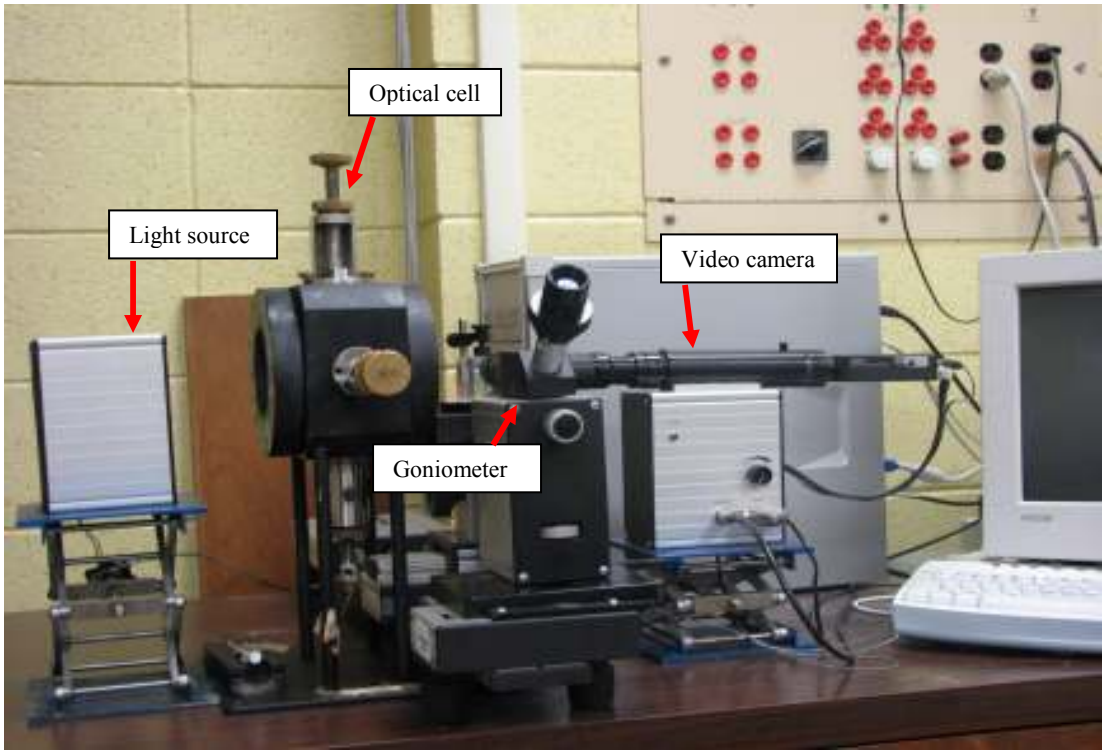

Figure 3.1: Ambient condition DDDC optical cell apparatus

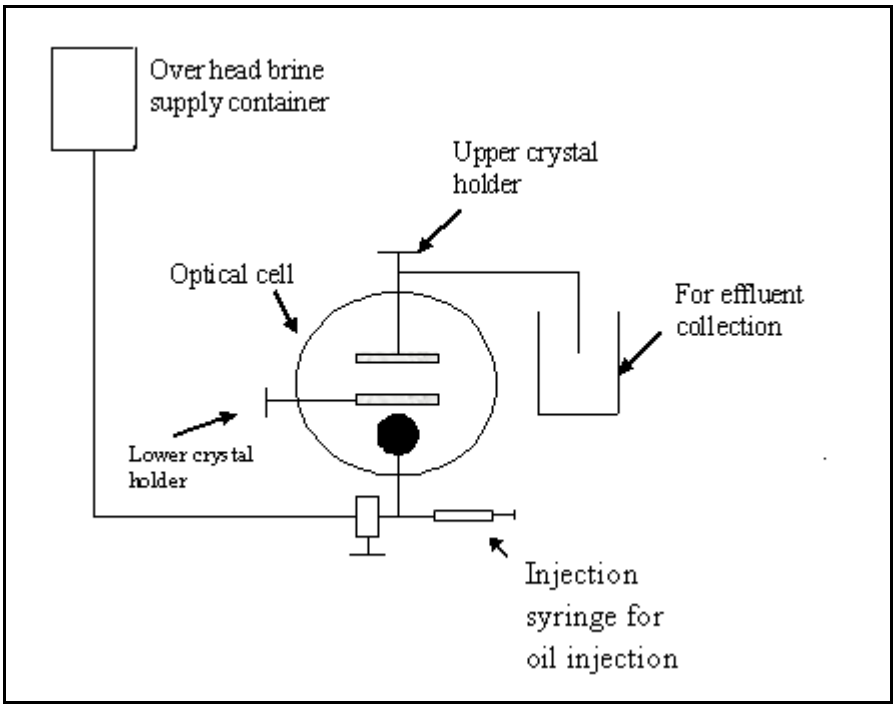

Figure 3.2: Schematic diagram of the ambient condition experimental setup

A metal (HC 276) capillary tube is available at the bottom of the cell for forming a pendant oil drop in the aqueous phase. Stock-tank oil is injected by a syringe which is connected to the capillary injection tubing. An inlet and an outlet valve available at the bottom and the top of the optical cell control the influent and effluent, respectively. A schematic diagram of the ambient condition experimental setup is shown in Figure 3.2. The accessories include a digital video camera, a computer equipped with a commercial image capturing and drop shape analysis software package, namely DSA software.

3.1.1.1 Cleaning of the Ambient Condition Optical Cell Apparatus

The ambient condition DDDC optical cell was first cleaned with deionized water. After each experiment, the inlet valve was opened to let some deionized water or brine in so that the oil floating at the top could be drained out from the outlet valve, aiming to avoid the floating oil falling down to touch and contaminate the cell's Teflon interior. Afterwards, the cell and its accessories were cleaned by toluene to dissolve all the crude oil, followed by acetone to dissolve all the toluene. Occasionally, isopropyl alcohol was also used to eliminate the possibility of any contamination. Finally deionized water was used to remove any traces of acetone. After the cleaning process, nitrogen was used to dry the cell and its accessories.

3.1.2 High-Pressure High-Temperature (HPHT) DDDC Optical Cell Apparatus

The HPHT DDDC optical cell apparatus was used to measure the oil/water IFT, the dynamic contact angles, and the drop size dependence of the dynamic contact angles in complex rock/oil/water systems at reservoir conditions. The main part of this apparatus is an optical cell which is comprised of four adjustable arms. These four arms make this cell unique. The top arm and a side arm are used to hold crystals; the other side arm is used to hold a calibration ball, and the bottom arm has a needle tip which is used to introduce the oil drop to form a pendant drop of oil in the aqueous phase and to place the oil drops on the crystal surfaces either in the sessile drop or in

the DDDC test. All these arms can rotate and move back and fourth enabling the use of this optical cell for a variety of experiments. It has a design rating of 20,000 psi at 400ºF. The HPHT DDDC optical cell apparatus and the schematic diagram of the HPHT experimental setup are shown in Figures 3.3 and 3.4, respectively.

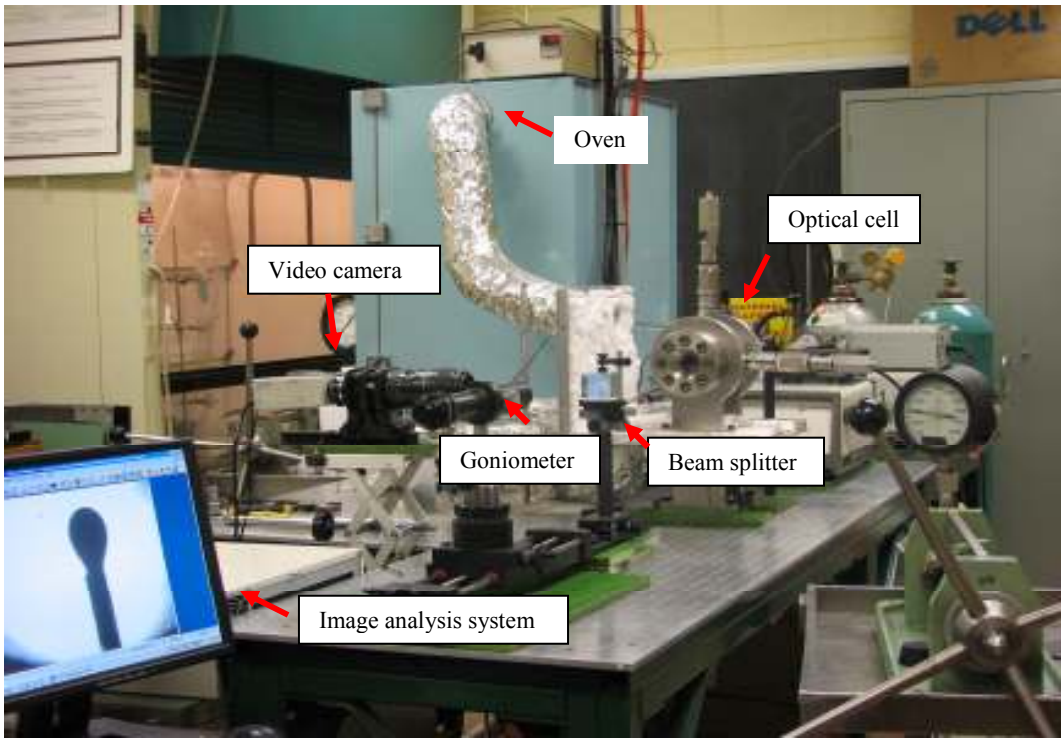

Figure 3.3: High-pressure high-temperature (HPHT) DDDC optical cell apparatus

The other accessories include an oven which is used to adjust temperature, high-pressure/high-temperature floating piston transfer vessels and valves to hold and transport fluids, and an image capturing and analysis system. The image capturing and analysis system includes a high-quality digital video camera, a computer equipped with image analysis software, monitor, video recorder and a light source. A goniometer is also available for manual measurement of contact angles. All of the wetted metal part of the optical cell and it accessories such as valves, connection tubing and fittings, and floating piston transfer vessels are made of highly corrosion resistant HC-276 metal.

3.1.2.1 Cleaning of the HPHT DDDC Optical Cell Apparatus

First, all the wetted parts of the HPHT DDDC optical cell, tubing, fittings, valves, and transfer vessels were flushed by a large amount of deionized water. Toluene was used to dissolve any oil traces present in the system followed by acetone to remove the toluene. Occasionally, isopropyl alcohol was also used to eliminate the possibility of any contamination. After the cleaning process high pressure nitrogen was used to dry the system.

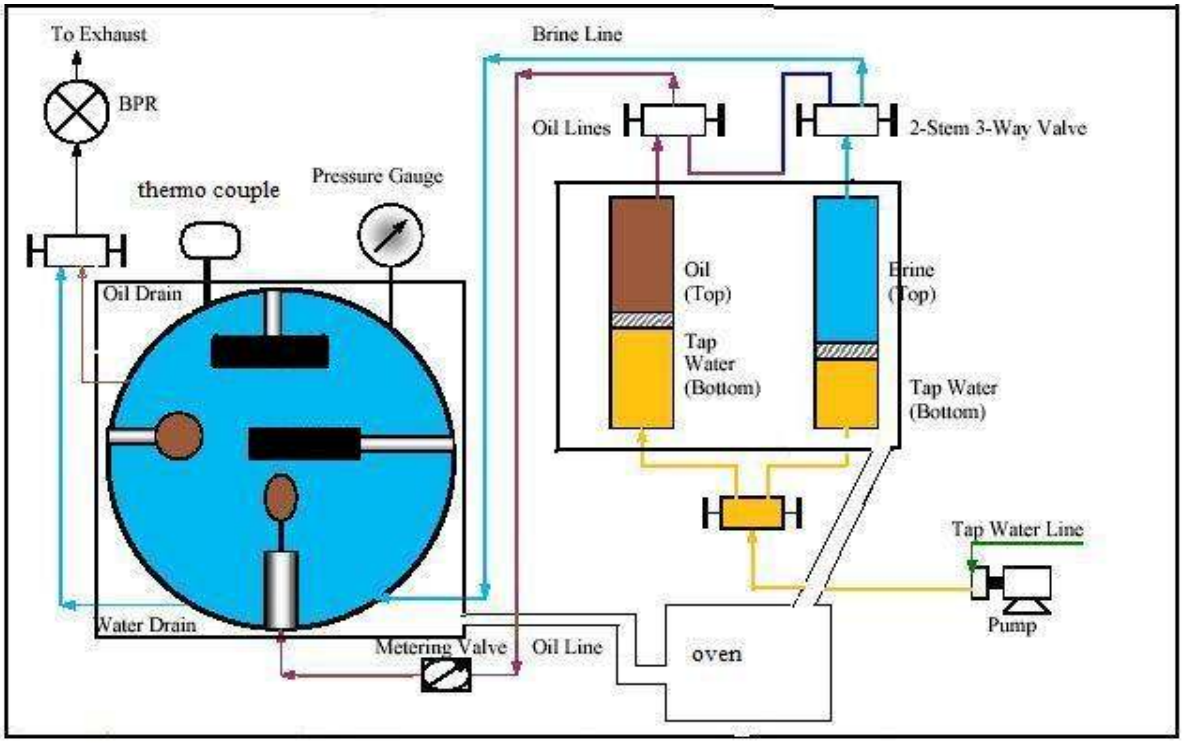

Figure 3.4: Schematic diagram of the HPHT experimental setup

3.2 Experimental Techniques

To achieve the specific research objectives outlined in sub-section 1.2, the following experimental techniques were used.

- Determination of system wettability using the dual-drop dual-crystal (DDDC) contact angle technique
- Determination of drop size dependence of sessile oil drop dynamic contact angle using the sessile oil drop volume alteration method
- Measurement of oil/water interfacial tension (IFT) using the pendant drop method

Each experimental technique used in this study is briefly discussed next.

3.2.1 The Dual-Drop Dual-Crystal (DDDC) Contact Angle Technique

In this study, the DDDC technique was used for evaluating the wettability state of various rock/oil/water systems at both ambient and reservoir conditions. As the name suggests, in this technique, two separate crude oil (stock-tank oil or recombined live oil) drops are placed on two parallel mineral crystal surfaces held by horizontal and vertical arms of an optical cell. The water film between the crude oil sessile drops and mineral crystal surfaces is drained with the help of the buoyancy forces to attain adhesion equilibrium before measuring the water-advancing and the water-receding contact angles with respect to aging time. By turning the lower crystal upside down and mingling the two oil drops, the advancing and receding contact angles can be measured by shifting the lower crystal laterally. In this technique, movement of contact line is observed without any ambiguity. The movement of contact line can be reproduced by moving the oil drop back to the original position. A schematic diagram of the DDDC technique is shown in Figure 2.5 (Section 2.3).

3.2.2 The Sessile Oil Drop Volume Alteration Method

A schematic diagram of the sessile drop volume alteration method is shown in Figure 2.8 of sub-section 2.4.1.1.2. In this method, an oil drop is brought into contact with a mineral crystal surface in the presence of water, and drop volume is increased gradually with the help of an injector capillary tube to remove bulk water phase away from the rock surface (Figure 2.8, step 1).

The volume of the oil drop was increased until the contact diameter exceeded the drop height to attain a limiting capillary pressure imposed on the thin aqueous film squeezed between the crystal surface and bulk oil phase. The observed contact angle measured in water phase at this step corresponds to θ_r.

After a sufficient equilibrium time (usually 24 hours), volume of oil drop is reduced in steps by withdrawing oil back into the injector tube (Figure 2.8, step 2). The movement of the contact line (reduction in contact radius) is monitored, and corresponding change in dynamic contact angle (i.e. the water-advancing contact angle, θ_a) is recorded. This technique can easily be adapted to reservoir conditions of elevated pressures and temperatures, thus facilitating the use of live oil in such experiments.

3.2.3 The Pendant Drop Method

The pendant drop technique is a reliable and accurate experimental technique to measure the oil/water IFT at elevated pressures and temperatures. In this, a drop of crude oil is introduced through a capillary tube the optical cell filled with an aqueous phase and is kept hanging at the tip of the capillary tube to attain the equilibrium between oil and aqueous phases. When buoyancy exceeds the interfacial tension between oil and water, drop does tend to leave the tip and image captured at this time is used to measure the oil/water interfacial tension by analyzing the image using commercial drop shape analysis (DSA) software

3.3 Oil Reservoirs Included in This Study

In this study, four different oil reservoir (two onshore and two offshore) were included for characterization of rock/fluids interactions in a wide range of pressure (atmospheric pressure to 14,000 psi) and temperature (72 to 250°F). These oil reservoirs are:

- B oil field (Louisiana)
- Y oil field (Texas)

- A Gulf of Mexico (GOM) deep water offshore oil field with two producing reservoirs (F and T)

A brief description of each oil reservoir is provided in the next sub-section.

3.3.1 B Oil Field (Louisiana)

The first onshore reservoir studied included in this study is the B oil field situated in Louisiana. This sandstone reservoir has an area of 480 acres with an average reservoir thickness of about 13 feet. The average porosity values for this reservoir range from 11.8% to 25% and permeability varies from 6 md to 1708 md. The reservoir simulation based estimates of initial oil in place for this oil field are about 7.1 million stock tank barrels. This oil field was under waterflooding for almost six years after a brief primary depletion period of two years. The waterflooding was stopped in the year 1972. This left behind around 5.4 million stock tank barrels of oil in the reservoir. The field has been shut in since 1972. The initial reservoir pressure in this field was 4,050 psi at a reservoir temperature of 238°F with initial bubble point pressure of 1,267 psi. The current reservoir pressure is around 1,100 psi.

3.3.1.1 B Reservoir Fluids

3.3.1.1.1 Stock-tank Oil (B-STO) and Recombined Live Oil (B-RLO)

Stock-tank oil samples obtained from this depleted reservoir were used to prepare the recombined live oil representative to initial reservoir conditions of pressure and temperatures. A detailed procedure to prepare recombined live oil is provided by Sequeira (2006). The composition of recombined live oil (B-RLO) is given in Table 3.1. Both the stock-tank oil (B-STO) and recombined live oil (B-RLO) were used to conduct the experiments at reservoir conditions of 1,500 psi (above the bubble point pressure of 1,267 psi) and 238°F. Ambient condition experiments were conducted using stock-tank oil (B-STO) at atmospheric pressure and 72°F.

Table 3.1: Composition of recombined live oil (B-RLO)

Component	Live oil mole fraction
C_1	0.240
C_{6+}	0.760
Total	1.000

3.3.1.1.2 Aqueous Phases

Synthetic reservoir brine (B-SRB) was prepared by adding the calculated amount of various salts in deaerated deionized water (DIW) to match the actual reservoir brine of the B oil field (provided by the operating company). The composition of the actual reservoir brine is given in Table 3.2. Apart from synthetic reservoir brine (B-SRB), deionized water (DIW) was also used as another aqueous phase in the experiments.

Table 3.2: Composition of synthetic reservoir brine (B-SRB)

Salt	Chemical Name	Concentration (gm/liter)
Sodium Chloride	NaCl	133.26
Potassium Chloride	KCl	0.82
Calcium Chloride Dihydrate	$CaCl_2.2H_2O$	40.35
Magnesium Chloride Hexahydrate	$MgCl_2.6H_2O$	5.19
Sodium Sulfate Decahydrate	$Na_2SO_4.10H_2O$	0.54
Sodium Bicarbonate	$NaHCO_3$	0.03

Table 3.3: Rock/fluids systems studied at reservoir conditions (B oil field)

Reservoir conditions experiments, B oil field (P =1500 psi, T= 238°F)		
Oil/water IFT experiment (4 systems)	**Wettability (DDDC) test (3 systems)**	**Drop volume alternation experiment (12 systems)**
B-RLO/B-SRB	Quartz/B-RLO/B-SRB	Quartz/B-RLO/B-SRB
B-RLO/DIW	Dolomite/B-RLO/B-SRB	Dolomite/B-RLO/B-SRB
B-STO/B-SRB	Calcite/B-RLO/B-SRB	Calcite/B-RLO/B-SRB
B-STO/B-DIW		Quartz/B-RLO/DIW
		Dolomite/B-RLO/DIW
		Calcite/B-RLO/DIW
		Quartz/B-STO/B-SRB
		Dolomite/B-STO/B-SRB
		Calcite/B-STO/B-SRB
		Quartz/B-STO/DIW
		Dolomite/B-STO/DIW
		Calcite/B-STO/DIW

B-RLO- Recombined live oil (B oil field), B-STO- Stock-tank oil (B oil field),
B-SRB- Synthetic reservoir brine (B oil field), DIW- Deionized water

Table 3.4: Rock/fluids systems studied at ambient conditions (B oil field)

Ambient conditions experiments, B oil field (Atmospheric pressure, T=72°F)		
Oil/water IFT experiment (2 systems)	**Wettability (DDDC) test (None)**	**Drop volume alternation experiment (6 systems)**
B-STO/B-SRB	-	Quartz/B-STO/B-SRB
B-STO/DIW	-	Dolomite/B-STO/B-SRB
	-	Calcite/B-STO/B-SRB
		Quartz/B-STO/DIW
		Dolomite/B-STO/DIW
		Calcite/B-STO/DIW

B-

STO- Stock-tank oil (B oil field), B-SRB- Synthetic reservoir brine (B oil field),
DIW- Deionized water

3.3.1.1.3 Rock Mineral Surfaces

Three different mineral crystals, namely quartz, dolomite, and calcite were used as the solid phase to investigate the effect of rock mineralogy on the extent of rock/fluids interactions in the B oil field.

3.3.1.2 Details of Rock/fluids Systems Investigated in This Study (B Oil Field)

Different combinations of the reservoir fluids and selected mineral crystals were chosen for conducting the oil/water IFT, the DDDC tests, and the sessile oil drop volume alteration experiments for characterizing rock/fluids interactions in the B oil field. The details of rock/fluid systems investigated in this study are given in Tables 3.3 and 3.4.

3.3.2 Y Oil Field (Texas)

The second oil field studied in this study is the Y oil field situated in Texas. The stock-tank oil provided by the operating company was used to prepare the Y recombined live oil (Y-RLO). The composition of Y-RLO is given in Table 3.5. The Y synthetic reservoir brine (Y-SRB) was

prepared using composition of actual reservoir brine supplied by the operating company. The composition of Y-SRB is given in Table 3.6. Quartz glass slides were used as the solid surface to conduct the drop volume alteration experiments for glass/Y-RLO system with two different pH (7.6 and 4.58) synthetic brines (Y-SRB). Certain properties of prepared Y-SRB such as TDS, salinity and pH were also measured at lab conditions and are given in Table 3.7 along with their comparison to the actual Y reservoir brine properties.

The sessile oil drop volume alteration experiments for the glass/Y-RLO/Y-SRB (pH=7.6) and the glass/Y-RLO/Y-SRB (pH=4.58) systems along with the pendant drop experiments for the Y-RLO/Y-SRB (pH=7.6) and the Y-RLO/Y-SRB (pH=4.58) systems were conducted at reservoir conditions of 700 psi and 82°F for characterizing rock/oil adhesion interactions in terms of the line tension (Eq.12).

Table 3.5: Composition of Y recombined live oil (Y-RLO)

Component	Live oil mole fraction
N_2	0.012013
CO_2	0.053261
C_1	0.092727
C_2	0.035863
C_3	0.021439
C_4	0.035741
C_5	0.027104
C_{6+}	0.721846
Total	1.000000

Table 3.6: Composition of Y synthetic brine (Y-SRB)

Salt	Chemical Name	Salt weight g/3 liters (for DIW density of 0.9977 gm/cc)
NaCl	Sodium Chloride	18.2526 (9.4926+8.76)*
KCl	Potassium Chloride	0.2882
$CaCl_2.2H_2O$	Calcium Chloride Dihydrate	4.6661
$MgCl_2.6H_2O$	Magnesium Chloride Hexahydrate	5.6082
$Na_2SO4.10H_2O$	Sodium Sulfate Decahydrate	6.6262
$NaHCO_3$	Sodium Bicarbonate	3.2967
TOTAL		38.7379

*Include the additional amount that was added to match up the TDS with actual reservoir brine

Table 3.7: Measured properties of Y-SRB and actual reservoir brine

Property	Actual Res. Brine (Data provided by the operating company)	Syn. Res. Brine (Y-SRB) (before TDS adjustment)	Syn. Res. Brine (Y-SRB) (after TDS adjustment)
Density(gm/cc)	-	1.004	1.004
TDS(mg/l)	9,200	6,280	9,130
Conductivity (mS/cm)	-	10.27	14.56
Resistivity (Ohm-m)	-	0.973	0.687
Salinity (ppm)	-	6,500	9,500
pH	7.39	7.70	7.61
Remarks	Additional NaCl was added to match up the TDS of Y-SRB with actual reservoir brine		

3.3.3 Gulf of Mexico (GOM) Deepwater Offshore Oil Field

The offshore oil field included in this study is a large Gulf of Mexico (GOM) deepwater offshore oil field. It comprises two main oil producing reservoirs, namely F and T reservoirs. These reservoirs are Miocene age turbidite sheet deposits located subsalt below 25,000 feet SSTVD.

The initial reservoir pressures are in the range from 12,800 psia to 15,800 psia with reservoir temperatures ranging from 180 to 220°F and bubble point pressures ranging from 2,420 psia to 4,000 psia @ 208°F. The current reservoir pressures in both the producing zones are in the range of 8,000 psia. The reservoir oils of both the producing zones are characterized as medium to high asphaltene oil with low to medium gas oil ratios (600 scf/bbl to 900 scf/bbl). The average permeability is 700 md ranging from a few hundred to 1,500 md and the porosity is in the range from 22% to 26% with an average porosity of 23%. The lack any substantial natural drive recovery mechanisms in both the reservoirs make it necessary to characterize rock/fluids interactions to aid in the design and implementation of EOR processes in these reservoirs.

3.3.3.1 Reservoir Fluids (F and T Reservoirs)

3.3.3.1.1 Stock-tank Oils

One gallon of F stock-tank oil (F-STO) and T stock-tank oil (T-STO) were supplied by the operating company of the field. The typical physical properties of both stock-tank oil (STO) samples are given in Table 3.8.

Table 3.8: Properties of F and T stock-tank oils

Property	F-STO	T-STO
API Gravity (°API)	23.7	26.6
nC_5 insoluble Asphaltene Content (wt%)	16.5	7.3
Paraffin content (%)	3.6	6
Wax App. Temp (°F)	76	89
Total Acid No.(mgKOH/g)	0.12	0.2
Total Sulfur (%)	3.73	2.22
Viscosity, cP (75°F)	663.63	47.84
Mol. Wt.(g/mol)	287.44	269.65

Both stock-tank oil samples are medium gravity crude oils (API gravity ranging from 23.9° to 26.6°) with significant amount of asphaltene content. F-STO contains 16.5 wt% of pentane insoluble asphaltene whereas, T-STO has 7.3 wt% of pentane insoluble asphaltene content in it.

3.3.3.1.2 Live Oils

The recombined live oil samples for the F and T reservoirs i.e. F recombined live oil (F- RLO) and T recombined live oil (T-RLO) used in this study were prepared and supplied by a major service company on behalf of the operating company. The detailed compositions of F-RLO and T-RLO are given in Table 3.9 and 3.10, respectively.

3.3.3.1.3 Aqueous Phases

The aqueous phases used in this study include deionized water (DIW), commercially (Cole-Parmer) available synthetic sea water (SSW), 35,000 ppm NaCl solution, and synthetic reservoir brines (i.e., F-SRB and F-SRB) representative of actual reservoir brines of both producing reservoirs F and T, respectively.

The DIW used was obtained from the LSU water quality lab. Both Synthetic brines were prepared in the lab using the brine compositions supplied by the operating company. Synthetic sea water (SSW) was also included in this study to investigate the rock/fluids interactions in the presence of possible injection water source (sea water). A comparison of the composition of SSW and actual sea water in the vicinity of GOM deepwater offshore oil field included in this study is given in Table 3.11. As evident from the data given in Table 3.11, SSW is a good representative of actual sea water in the vicinity of the oil field.

3.3.3.1.3.1 Preparation of Synthetic Reservoir Brines (F-SRB and T-SRB)

Calculated amounts of various salts were added to DIW for representing each of the ions having a concentration greater than 5 mg/kg in the actual F reservoir brine and 7 mg/kg in the actual T reservoir brine.

Table 3.9: Composition of F recombined live oil (F-RLO)

Component	MW	Monophasic Fluid	
	(g/mole)	wt%	Mole%
Carbon Dioxide	44.01	0.07	0.21
Hydrogen Sulfide	34.08	0.00	0.00
Nitrogen	28.01	0.07	0.32
Methane	16.04	4.44	34.11
Ethane	30.07	1.94	7.97
Propane	44.10	2.40	6.72
I - Butane	58.12	0.49	1.05
N - Butane	58.12	1.59	3.38
I - Pentane	72.15	1.14	1.95
N - Pentane	72.15	0.97	1.65
C6	84.00	2.39	3.50
M-C-Pentane	84.16	0.27	0.39
Benzene	78.11	0.04	0.06
Cyclohexane	84.16	0.20	0.30
C7	96.00	2.31	2.97
M-C-Hexane	98.19	0.45	0.56
Toluene	92.14	0.19	0.25
C8	107.00	2.56	2.95
E-Benzene	106.17	0.09	0.11
M/P-Xylene	106.17	0.20	0.23
O-Xylene	106.17	0.15	0.17
C9	121.00	2.57	2.62
C10	134.00	2.94	2.70
C11	147.00	2.81	2.35
C12	161.00	2.59	1.98
C13	175.00	2.63	1.85
C14	190.00	2.54	1.65
C15	206.00	2.42	1.45
C16	222.00	2.24	1.24
C17	237.00	2.11	1.10
C18	251.00	2.03	1.00
C19	263.00	1.96	0.92
C20	275.00	1.77	0.79
C21	291.00	1.72	0.73
C22	300.00	1.56	0.64
C23	312.00	1.51	0.60
C24	324.00	1.39	0.53
C25	337.00	1.45	0.53
C26	349.00	1.10	0.39
C27	360.00	1.27	0.44
C28	372.00	1.20	0.40
C29	382.00	1.15	0.37
C30+	665.06	37.06	6.87
Total		100.00	100.00
MW			123.29

Table 3.10: Composition of T recombined live oil (T-RLO)

Component	MW	Monophasic Fluid	
	(g/mole)	wt%	Mole%
Carbon Dioxide	44.01	0.04	0.09
Hydrogen Sulfide	34.08	0.00	0.00
Nitrogen	28.01	0.05	0.19
Methane	16.04	6.98	45.84
Ethane	30.07	1.58	5.53
Propane	44.10	2.19	5.24
I - Butane	58.12	0.49	0.89
N - Butane	58.12	1.59	2.88
I - Pentane	72.15	0.84	1.22
N - Pentane	72.15	1.08	1.57
C6	84.00	2.03	2.54
M-C-Pentane	84.16	0.37	0.47
Benzene	78.11	0.06	0.08
Cyclohexane	84.16	0.32	0.40
C7	96.00	2.05	2.25
M-C-Hexane	98.19	0.69	0.74
Toluene	92.14	0.28	0.31
C8	107.00	2.49	2.45
E-Benzene	106.17	0.09	0.09
M/P-Xylene	106.17	0.24	0.23
O-Xylene	106.17	0.16	0.16
C9	121.00	2.60	2.27
C10	134.00	3.06	2.41
C11	147.00	2.81	2.02
C12	161.00	2.45	1.61
C13	175.00	2.58	1.55
C14	190.00	2.50	1.39
C15	206.00	2.38	1.22
C16	222.00	2.19	1.04
C17	237.00	2.08	0.92
C18	251.00	2.08	0.87
C19	263.00	2.00	0.80
C20	275.00	1.77	0.68
C21	291.00	1.70	0.62
C22	300.00	1.58	0.56
C23	312.00	1.51	0.51
C24	324.00	1.43	0.47
C25	337.00	1.38	0.43
C26	349.00	1.34	0.41
C27	360.00	1.32	0.39
C28	372.00	1.30	0.37
C29	382.00	1.28	0.35
C30+	665.06	35.03	5.93
Total		100.00	100.00
MW			105.42

Table 3.11: Composition of synthetic sea water (SSW) and actual GOM sea water

Ion	Concentration	SSW (synthetic Sea water)	Actual GOM sea water (data provided by the operating company)
Chloride	mg/Kg	19300.8	19402.3
Bromide	mg/Kg	53.2	67.9
Sulfate	mg/Kg	2622.0	2600.8
Sodium	mg/Kg	11781.3	11099.7
Potassium	mg/Kg	376.4	377.7
Magnesium	mg/Kg	1637.2	1448.3
Calcium	mg/Kg	542.8	410.4
Carbonate	mg/Kg	1.7	1.1
Bicarbonate	mg/Kg	125.4	112.5
Boron	mg/Kg	3.9	4.5
Barium	mg/Kg	0.0	0.0
Silicon	mg/Kg	0.1	0.6
Strontium	mg/Kg	10.7	6.1

Tables 3.12-3.13 show the amount of each salt added to 3 liters of DIW (density = 0.9977 gm/cc at lab conditions) to prepare one 3-liter batch of each F-SRB and T-SRB in the lab for using it in ambient condition experiments. Certain properties of prepared F-SRB, T-SRB, and commercial SSW such as TDS, salinity and pH were measured at lab conditions. The same were measured by a service lab, where water samples were sent for detailed compositional analysis for quality check of prepared synthetic reservoir brines in the lab.

Table 3.12: Composition of F synthetic reservoir brine (F-SRB)

Salt	Chemical Name	Salt weight (g/Kg)	Salt weight (g/3 kg)	Salt weight g/3 liters (for DIW density of 0.9977 gm/cc)
NaCl	Sodium Chloride	22.1297	66.3890	70.5863* (66.2363+4.35)
KCl	Potassium Chloride	0.0926	0.2777	0.2771
KBr	Potassium Bromide	0.3028	0.9083	0.9062
$CaCl_2.2H_2O$	Calcium Chloride Dihydrate	1.6396	4.9189	4.9076
$MgCl_2.6H_2O$	Magnesium Chloride Hexahydrate	0.2635	0.7905	0.7886
H_3BO_3	Boric acid	0.0426	0.1278	0.1275
$SrCl_2.6H_2O$	Strontium Chloride Hexahydrate	0.0472	0.1415	0.1412
$Na_2SO4.10H_2O$	Sodium Sulfate Decahydrate	0.4411	1.3233	1.3202
$BaCl_2.2H_2O$	Barium Chloride Dihydrate	0.0329	0.0987	0.0985
$NaHCO_3$	Sodium Bicarbonate	1.1441	3.4323	3.4244
SiO_2	Silicon Dioxide	0.0380	0.1140	0.1137
HCOONa	Sodium Formate	0.0943	0.2828	0.2822
CH_3COONa	Sodium Acetate	2.0303	6.0909	6.0769
C_2H_5COONa	Sodium Propionate	0.3208	0.9625	0.9603
$CH_3C_2H_5COONa$	Sodium Butyrate	0.0389	0.1168	0.1165
TOTAL		28.6584	85.9751	85.7773

*Include the additional amount that was added to match up the TDS with actual reservoir brine

Table 3.13: Composition of T synthetic reservoir brine (T-SRB)

Salt	Chemical Name	Salt weight (g/Kg)	Salt weight (g/3 kg)	Salt weight g/3 liters (for DIW density of 0.9977 gm/cc)
NaCl	Sodium Chloride	10.8890	32.6669	35.5918 (32.5918+3.00)*
KCl	Potassium Chloride	0.0583	0.1750	0.1746
KBr	Potassium Bromide	0.1069	0.3208	0.3200
$CaCl_2.2H_2O$	Calcium Chloride Dihydrate	1.6837	5.0510	5.0393
$MgCl_2.6H_2O$	Magnesium Chloride Hexahydrate	0.0811	0.2434	0.2429
H_3BO_3	Boric acid	0.0041	0.0123	0.0123
$SrCl_2.6H_2O$	Strontium Chloride Hexahydrate	0.0222	0.0666	0.0665
$Na_2SO4.10H_2O$	Sodium Sulfate Decahydrate	0.6101	1.8304	1.8262
$BaCl_2.2H_2O$	Barium Chloride Dihydrate	0.0073	0.0219	0.0218
$NaHCO_3$	Sodium Bicarbonate	2.0349	6.1047	6.0906
SiO_2	Silicon Dioxide	0.0847	0.2541	0.2535
HCOONa	Sodium Formate	0.0478	0.1433	0.1429
CH_3COONa	Sodium Acetate	1.1729	3.5186	3.5105
C_2H_5COONa	Sodium Propionate	0.1381	0.4142	0.4133
$CH_3C_2H_5COONa$	Sodium Butyrate	0.0248	0.0743	0.0742
TOTAL		16.9658	50.8975	50.7804

*Include the additional amount that was added to match up the TDS with actual reservoir brine

These measured values were compared with the reported values for actual reservoir brines and actual sea water (data provided by the operating company) in the vicinity of the oil field and are given in Tables 3.14-3.16. As, evident from the water analysis data given in Tables 3.14-3.16, addition of extra NaCl into the synthetic reservoir brine solutions to match their TDS with the TDS of respective reservoir brines caused it to exceed the TDS of actual reservoir brine. Hence, a decision was made to not add extra NaCl in the new batch of F-SRB and T-SRB that were prepared for conducting the reservoir condition experiments with F and T reservoir fluids.

Table 3.14: Measured properties of F-SRB and actual F reservoir brine

Property	**Actual F Res. Brine (Data provided by operating company)**	**F Syn. Res. Brine (F-SRB) (before TDS adjustment)**	**F Syn. Res. Brine (F-SRB) (after TDS adjustment)**	**F Syn. Res. Brine (F-SRB) measured by service lab**
Density(gm/cc)	1.016	1.016	1.017	-
TDS(mg/l)	27,948	26,500	28,400	31,020 (Evaporated)
Conductivity (mS/cm)	35.5	42.5	45.7	42.90
Resistivity (Ohm-m)	0.282	0.235	0.222	0.233
Salinity (ppm)	24,734	27,600	29,600	27,620
pH	7.39	7.85	8.05	8.09
Remarks	1. All the ions, those have a concentration greater than 5 mg/kg in the actual reservoir brine were added to DIW 2. Additional NaCl was added to match the TDS of F-SRB with the TDS of actual F reservoir brine			

Table 3.15: Measured properties of T-SRB and actual T reservoir brine

Property	Actual T Res. Brine (Data provided by operating company)	T Syn. Res. Brine (T-SRB) (before TDS adjustment)	T Syn. Res. Brine (T-SRB) (after TDS adjustment)	T Syn. Res. Brine (T-SRB) measured by service lab
Density(gm/cc)	1.016	1.01	1.009	-
TDS(mg/l)	14,792	13,780	14,980	18,314 (Evaporated)
Conductivity (mS/cm)	21.59	22.6	24.3	25.30
Resistivity (Ohm-m)	0.463	0.443	0.411	0.395
Salinity (ppm)	12,181	14,200	15,600	14,429
pH	7.64	7.89	8.05	7.39
Remarks	1. All the ions, those have a concentration greater than 7 mg/kg in the actual reservoir brine, were added to DIW 2. Additional NaCl was added to match up the TDS of T-SRB with actual T reservoir brine			

Table 3.16: Measured properties of synthetic sea water (SSW) and actual sea water

Property	Actual GOM sea water (Data provided by the operating company) Mean Value	Measured for actual sea water (sample provided by the operating company)	Synthetic Sea Water (SSW) (Purchased from Cole-Parmer)	Synthetic Sea Water (SSW) (Purchased from Cole-Parmer) measured by service lab
Density(gm/cc)	1.025	1.024	1.024	-
TDS(mg/l)	43,434	35,800	35,600	48,911
Conductivity (mS/cm)	51.02	54.4	54.2	52.90
Resistivity (Ohm-m)	0.196	0.183	0.183	0.189
Salinity (ppm)	35,051	37,200	37,000	34,877
pH	7.64	could not be measured due to the small volume of the sample	8.18	8.15

3.3.3.1.4 Rock Mineral Surfaces

The GOM deepwater offshore oil field included in this study is a sandstone reservoir. According to the rock mineralogy analysis of F and T reservoir rock samples (data provided by the operating company), quartz is the dominant rock mineral (up to 97%) in both F and T reservoir rocks. Both reservoir rocks also have a small percentage of calcite (1-3%) and rest is clay. Both the quartz and the calcite mineral surfaces were chosen to conduct the contact angle experiments (the DDDC tests, and the sessile oil drop volume alteration tests), whereas the quartz mineral surfaces were used for conducting the majority of contact angle experiments at reservoir conditions. A few reservoir condition experiments were also conducted with the calcite mineral surfaces.

3.3.3.2 Details of Rock/fluids Systems Investigated in This Study (F and T Reservoirs)

Different combinations of the above mentioned fluids (sub-section 3.3.3.1) and the selected mineral crystals (quartz or calcite) were used for characterizing rock/fluids interactions in these reservoirs at both ambient and reservoir conditions. The details of rock/fluids systems investigated at ambient conditions are given in Tables 3.17-3.18.

Table 3.17: Rock/fluids systems investigated at ambient conditions, F reservoir

Oil/water IFT Experiment (3 systems)	Wettability (DDDC) test (6 systems)	Sessile oil drop volume alternation experiment (6 systems)
F-STO/DIW	Quartz/F-STO/DIW	Quartz/F-STO/DIW
F-STO/SSW	Quartz/F-STO/SSW	Quartz/F-STO/SSW
F-STO/F-SRB	Quartz/F-STO/F-SRB	Quartz/F-STO/F-SRB
	Calcite/F-STO/DIW	Calcite/F-STO/DIW
	Calcite/F-STO/SSW	Calcite/F-STO/SSW
	Calcite/F-STO/F-SRB	Calcite/F-STO/F-SRB

F-STO- Stock-tank oil (F reservoir), F-SRB- Synthetic reservoir brine (F reservoir), DIW- Deionized water
SSW- Synthetic Sea water

Table 3.18: Rock/fluids systems investigated at ambient conditions, T reservoir

Oil/water IFT Experiment (3 systems)	Wettability (DDDC) test (6 systems)	Sessile oil drop volume alternation experiment (6 systems)
T-STO/DIW	Quartz/T-STO/DIW	Quartz/T-STO/DIW
T-STO/SSW	Quartz/T-STO/SSW	Quartz/T-STO/SSW
T-STO/T-SRB	Quartz/T-STO/T-SRB	Quartz/T-STO/T-SRB
	Calcite/T-STO/DIW	Calcite/T-STO/DIW
	Calcite/T-STO/SSW	Calcite/T-STO/SSW
	Calcite/T-STO/T-SRB	Calcite/T-STO/T-SRB

T-STO- Stock-tank oil (T reservoir), T-SRB- Synthetic reservoir brine (T reservoir), DIW- Deionized water
SSW- Synthetic Sea water

In the case of the reservoir condition experiments for the F reservoir, the interfacial tension for various live oil/water systems at elevated pressures in the range from 8,000 to 13,454 psi and three different temperatures of 175°, 208° (reservoir temperature), and 250°F were measured. The reservoir condition pendant drop experiments involving stock-tank oil (F-STO) were also conducted in the pressure range from 8,000 to 13,454 psi and reservoir temperature of 208°F. The sessile oil drop volume alteration tests for both stock-tank and live oil (F-RLO and F-STO) and different rock/water systems were conducted at 10,000 psi and 208°F. The DDDC tests for F reservoir fluids (F-RLO and F-SRB) with the quartz and the calcite mineral surfaces were conducted at 10,000 psi and reservoir temperature of 208°F. A list of the oil/water IFT and the contact angle tests conducted at reservoir conditions in the case of F reservoir is given in Table 3.19.

In the case of the reservoir condition experiments for the T reservoir, the interfacial tension for various live oil/water systems at elevated pressures in the range from 8,000 to 14,400 psi and at reservoir temperature of 208°F were measured. The DDDC tests for the quartz/T-RLO systems and different aqueous phases (T-SRB, DIW and 35,000 ppm NaCl solution) were conducted at 12,000 psi and 208°F. The sessile oil drop volume alteration test for the quartz/T-RLO/T-SRB system was also conducted at 12,000 psi and 208°F. A list of the reservoir condition oil/water IFT and the contact angle tests conducted in the case of the T reservoir is given in Table 3.20.

Table 3.19: Rock/fluids systems investigated at reservoir conditions, F reservoir

Oil/water IFT Experiment (5 systems)	**Wettability (DDDC) test (4 systems) (P=10,000 psi, T=208°F)**	**Sessile oil drop volume alternation experiment (7 systems) (P=10,000 psi, T=208°F)**
F-RLO/DIW (P=8,000 to 13,454 psi and 208°F)	Quartz/F-RLO/DIW	Quartz/F-RLO/DIW
F-RLO/SSW (P=8,000 to 13,454 psi and 208°F)	Quartz/F-RLO/SSW	Quartz/F-RLO/SSW
F-RLO/F-SRB (P=8,000 to 13,454 psi and three different temperatures of 175°, 208°, and 250°F)	Quartz/F-RLO/F-SRB	Quartz/F-RLO/F-SRB
F-STO/F-SRB (P=8,000 to 13,454 psi and 208°F)	Calcite/F-RLO/F-SRB	Calcite/F-RLO/F-SRB
F-STO/SSW (P=8,000 to 13,454 psi and 208°F)	Calcite/F-RLO/DIW	Calcite/F-RLO/DIW
		Quartz/F-STO/F-SRB
		Quartz/F-STO/SSW

F-RLO- Recombined live oil (F reservoir), F-STO- Stock-tank oil (F reservoir),
F-SRB- Synthetic reservoir brine (F-SRB), DIW- Deionized water, SSW- Synthetic Sea water

Table 3.20: Rock/fluids systems investigated at reservoir conditions, T reservoir

Oil/water IFT Experiment (3 systems) (P=8,000 to 14,000 psi and 208°F)	Wettability (DDDC) test (3 systems) (P=12,000 psi, T=208°F)	Sessile oil drop volume alternation experiment (1 system) (P=12,000 psi, T=208°F)
T-RLO/T-SRB	Quartz/T-RLO/T-SRB	Quartz/T-RLO/T-SRB
T-RLO/DIW	Quartz/T-RLO/DIW	-
T-RLO/35K NaCl solution	Quartz/T-RLO/35K NaCl solution	-

T-RLO- Recombined live oil (T reservoir), T-SRB- Synthetic reservoir brine (T-SRB), DIW- Deionized water, 35 K NaCl- 35,000 ppm NaCl solution

3.3.4 Preparation of Mineral Crystal Surfaces

In this study, four different mineral crystals, namely quartz, dolomite, calcite, and glass were used as the solid phase. For preparing the mineral crystals, first, the raw mineral samples of quartz, dolomite, and calcite (purchased from Ward's Natural Science) were cut into an appropriate size of 0.90(L)×0.50(W)×0.20(T) in (2.25×1.25×0.5 cm) to use them in ambient condition experiments. In the case of reservoir condition experiments, the upper crystals were cut in the size of 0.40(L)×0.40(W)×0.20(T) in (1.01×1.01×0.51 cm) whereas the lower crystals were cut in the size of 0.40(L)×0.25(W)×0.10(T) in (1.01×0.64×0.25 cm). These mineral crystals were then prepared by grinding and polishing them in steps. In the first step of grinding, 200 grit (100 micron) silicon carbide abrasive sheets were used to grind crystal surfaces. In the next step, first 600 grit (50 micron) micro-finishing films followed by 1,200 grit (15 micron) polishing paper were used to achieve the desired smoothness. Finally, silk cloth was used to remove any rock particle remained attached to the surface during previous grinding and polishing steps. In the case of glass, pre-polished quartz glass slides purchased from Thermo Fisher Scientific Inc. were used after cutting them to a suitable size.

A rigorous cleaning procedure was followed to ensure the cleanliness of polished mineral crystal surfaces. Polished quartz crystals were soaked for approximately 30 minutes in hot sulphuric acid to which a few ammonium persulphate crystals were added to remove any insoluble impurity from the surface followed by a bath in boiling DIW for 2 hours to dissolve any traces of the acid. The same cleaning procedure was followed in the case of glass.

Polished dolomite crystals were soaked in a solution of 83% methyl alcohol+13% chloroform and refluxed for 30 minutes. After refluxing, they were kept in boiling DIW for 2 hours. In the case of calcite, polished crystals were washed by methylene chloride solution followed by DIW. Finally, crystals were dried carefully and were kept in air-tight glass containers to prevent any deposition of dust particles prior to experiment.

3.4 Experimental Procedures

Different combinations of oil/water and rock/oil/water systems were selected for conducting the oil/water IFT, the DDDC tests, and the sessile oil drop volume alteration experiments. All of the ambient condition experiments were performed at atmospheric pressure and room temperature (72 to 74°F).

The reservoir condition experiments for the B oil field were conducted at 1,500 psi and 238°F. In the case of the Y oil field, the reservoir condition experiments were conducted at 700 psi and 82°F. For the F and T reservoirs, all of the three types of experiments were conducted at various pressures and temperatures (Tables 3.19-3.20). A multi-step experimental procedure was followed to characterize rock/fluids interactions at both ambient and reservoir conditions in all of the four oil reservoirs included in the present study. These steps are discussed below in detail.

3.4.1 Oil/water Interfacial Tension (IFT) Measurements

The pendant drop experiments were conducted to determine the oil/water IFT for various oil/water systems at both ambient and reservoir conditions of elevated pressures and temperatures.

For this, a few drops of live oil/stock-tank oil were introduced into the aqueous phase through the injector tip located in the bottom of the optical cell (ambient or HPHT) after filling the optical cell with desired aqueous phase. The HPHT optical cell was heated up and pressurized to attain the desired pressure and temperature conditions and was left overnight at these conditions for attaining equilibrium between both phases before actual measurements. In the case of ambient condition experiments, the ambient condition optical cell was left overnight to attain the equilibrium between oil and aqueous phase.

After attaining equilibrium between both fluid phases, crude oil (live or stock-tank oil) was then introduced to form few pendant drops of oil hanging from the injector tip in the aqueous phase. The images of the pendant drops formed in that manner were digitally captured and were also recorded on video tape. Images captured at the particular moment when the pendant drop was about to detach from the injector tip were used to determine the oil/water IFT. Commercial drop shape analysis software (DSA) was used to analyze the images for obtaining the value of oil/water IFT.

3.4.2 The Sessile Oil Drop Volume Alteration Measurements

A linear relationship, as described by the modified Young's equation (Eq.11), between the sessile oil drop size and the water-advancing contact angle is often used to measure the line tension values in S/L/V systems. A similar approach was adopted for determining the value of line tension in S/L/L systems using Eq.12. The sessile oil drop volume alteration method discussed in sub-section 2.4.1.1.2 was used to investigate the effect of rock/oil adhesion interactions on the water-advancing contact angle by reducing the size of the sessile oil drop. This technique can easily be adapted to elevated pressure and temperature conditions.

In these tests, one carefully prepared and thoroughly cleaned mineral crystal was held horizontally by the side arm (ambient and moderate pressures) or by the upper arm of the optical cell in case of experiments conducted at high pressures and temperature (10,000 or 12,000 psi and

208°F). After filling the optical cell with aqueous phase, the HPHT optical cell was heated and pressurized to attain the desired pressure and temperature conditions. A few drops of crude oil (live or stock-tank oil) were then introduced into the aqueous phase through the injector tip located at the bottom of the optical cell and was left overnight at these conditions for attaining equilibrium between both the phases before actual measurements.

In the case of the ambient condition optical cell, after filling the optical cell with aqueous phase, a few drops of stock-tank oil were introduced into the aqueous phase through the injector tip located at the bottom of the optical cell and was left overnight for attaining equilibrium between different phases.

Then, a large sessile drop of crude oil (live or stock-tank oil) was formed on the bottom surface of the crystal by moving the injector tip near to the crystal surface or by moving the crystal surface held by the upper crystal arm near to the injector tip as per the procedure described in sub-section 2.4.1.1.2.

The system was then aged for 24 hours to attain equilibrium between all three phases, and the water-receding contact angle (θ_r) was measured. The water-receding contact angle showed a small variation within 2 to 5° from its initial value during the equilibration period. After measuring the water-receding contact angle, the size of the oil drop was reduced stepwise by withdrawing a small volume of oil back into the needle to determine the drop size dependence of the water-advancing contact angle. The size of the sessile oil drop was reduced in several steps by withdrawing small volumes of oil back into the needle at regular intervals of 15 minutes while monitoring the changes in contact radius, r, and the water-advancing contact angle (θ_a).

In all of the experiments, contact angles were measured manually using a goniometer (least count 1°) and were also calculated by analyzing the captured images of oil drop using the DSA software. Contact radius was measured using a simple digital ruler technique.

3.4.3 Determination of System Wettability

The Dual-Drop Dual-Crystal (DDDC) experiments were conducted to determine the wettability of various rock/oil/water systems at both ambient and reservoir conditions. In the DDDC test, the wettability state of rock/oil/water system is determined by measuring the water-advancing contact angle in dynamic condition. First, two carefully prepared and thoroughly cleaned mineral crystals were held parallel by the top and side arms of the DDDC optical cell.

In the case of ambient condition experiments, after filling the ambient condition DDDC optical cell with desired aqueous phase, a few drops of stock-tank oil (STO) were introduced into the aqueous phase through the injector tip located in the bottom of the optical cell and the cell was left overnight for attaining equilibrium between different phases. Then, sessile drops of STO were formed on the bottom surfaces of both crystals (upper and lower) by moving the injector tip near to the crystal surfaces.

For conducting the DDDC tests at elevated pressures and temperatures, the HPHT DDDC optical cell was filled with desired aqueous phase first and then it was heated and pressurized to attain the desired temperature and pressure conditions. When constant pressure and temperature conditions were achieved, a few drops of live oil were introduced into the aqueous phase through the injector tip located in the bottom of the optical cell. This was done to attain equilibrium between different phases, and the cell was left overnight for attaining equilibrium between different phases. Then, sessile drops of live oil were formed on the bottom surfaces of both crystals (upper and lower) by moving the injector tip near to the crystal surfaces.

The system was then aged for 24 hours to attain the equilibrium between all three phases, and the water-receding contact angle (θ_r) was measured. After that, the lower crystal was turned upside down by rotating the side arm of the optical cell. When the side arm was rotated to flip the lower crystal surface upside down, depending on the extent of rock/fluids interactions, the sessile oil drop either floated away completely from the crystal surface or stayed (partially/completely) on the

crystal surface. If the sessile oil drop stayed, it was allowed to mingle with the sessile drop placed on the upper crystal. After bringing the upper crystal near to the lower crystal, the lower crystal was moved laterally to observe the movement in the contact line. This gave the value of the water-advancing contact angle (θ_a) as water advanced to the area previously occupied by oil. The movement of the contact line was found to be reproducible as observed during the later shifting of lower crystal on second time after bringing the oil drop it to its original position.

The contact angles (θ_r) formed by the sessile oil drop with the lower crystal surface were either measured manually by using goniometer or by using the contact angle measurement capabilities of ADSA/DSA software by analyzing the captured image of sessile oil drop. A good agreement was found in the value of contact angle measured with both tools. In the case of the DDDC tests, the water-advancing contact angle, θ_a, (the contact angle observed during the movement of contact line on the previously oil occupied area of the crystal surface) was measured manually by using the available goniometer.

3.4.4 pH and Density Measurements

The pH of each aqueous phase was measured before and after each IFT and contact angle experiment. The aqueous phase samples collected after the experiments had traces of oil in it. All of the pH measurements were made at ambient conditions.

The density values of different oil and aqueous phase (needed for oil/water IFT measurements) at ambient conditions were measured using an Anton Paar 4500 density meter. In the case of elevated pressures and temperatures, densities of different oil and aqueous phases were measured using a newly purchased Anton Paar high-pressure high-temperature (HPHT) density meter.

3.4.4.1 Measurement of Fluid Densities at Reservoir Conditions

The densities of different oil and aqueous phases at elevated pressure and temperatures were measured using a newly purchased Anton Paar high-pressure high-temperature (HPHT) density meter capable of making such measurements up to 20,000 psi and 400°F. For this, HPHT density

meter was first calibrated in the pressure range from 1,000 psi to 17,000 psi and in the temperature range from 100°F to 300°F. Two standard fluids of known density, namely deionized water and toluene were used because density data for both fluids are readily available (NIST web book) in the pressure and temperature range used for the calibration. The experimental setup and schematic diagram of the HPHT density meter used in this study are shown in Figures 3.5 and 3.6, respectively.

In the calibration procedure, the oscillation period of the density meter was measured at given pressure and temperature step in a wide pressure and temperature range using two standard fluids. For this, temperature steps of 100, 150, 200, 250 and 300°F were selected to cover the temperature range, and at each temperature step, pressure was changed from 1,000 psi to 17,000 psi with incremental steps of 1,000 psi for measuring the oscillation period of the density meter for both the standard fluids (water and toluene). A high pressure floating piston transfer vessel (maximum working pressure=25,000 psia) containing one of the selected standard fluids at one side of the floating piston and the deionized water on the other side of the floating piston was connected to the external measuring cell of the HPHT density meter. The temperature of the external measuring cell was set at one of the selected temperatures and was kept constant within ±0.05°F of set temperature using an external bath heating thermostat. Then, the pressure was changed in the increment of 1,000 psi from 1,000 psi to 17,000 psi by generating the desired pressure at the water side of the floating piston transfer vessel using a high pressure generator and the corresponding oscillation period of the density meter was measured at each pressure and temperature point.

The same procedure was repeated with the second standard fluid. Each data point has four variables, i.e., pressure, temperature, oscillation period, and density of the standard fluid. Collected data comprising these four variables was fitted using a least square curve fit for obtaining the calibration coefficients of the HPHT density meter. These calibration coefficients were required before using the density meter to measure the density of any liquid at given pressure and

temperature in a wide pressure and temperature range. After feeding the values of density meter calibration coefficients into the evaluation unit of the HPHT density meter obtained from the procedure described above, accuracy of calibration was checked by measuring the density of another standard fluid (benzene) in the pressure range of 1,000 psia to 11,000 psia with 1,000 psia increments at 208°F. Measured density values of benzene are given in Table 3.21 along with their comparison with the published density values (NIST web book).

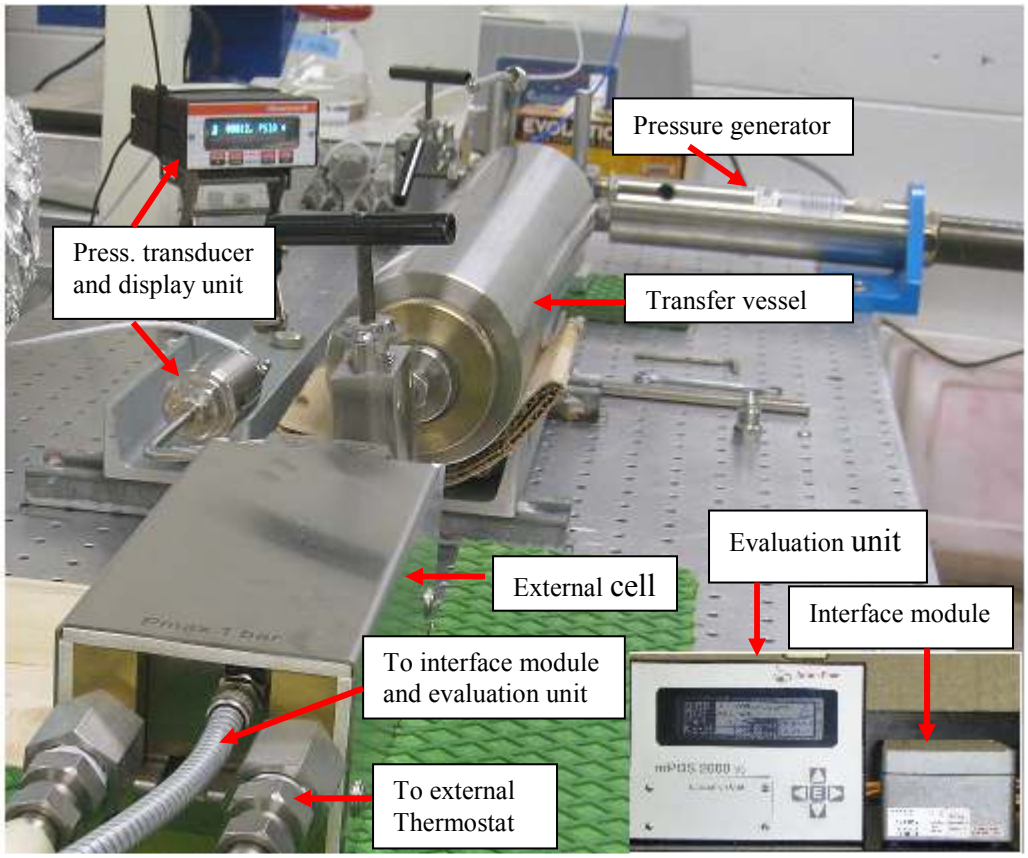

Figure 3.5: High-pressure high-temperature (HPHT) density measurement setup

The measured density data at different pressure steps and at 208°F was plotted along with the published density data and is shown in Figure 3.7. As evident from Figure 3.7, measured density data obtained after calibrating the HPHT density meter is in good agreement with the available

published values of density of benzene at given temperature and various pressure steps ranging from 1,000 psia to 11,000 psia.

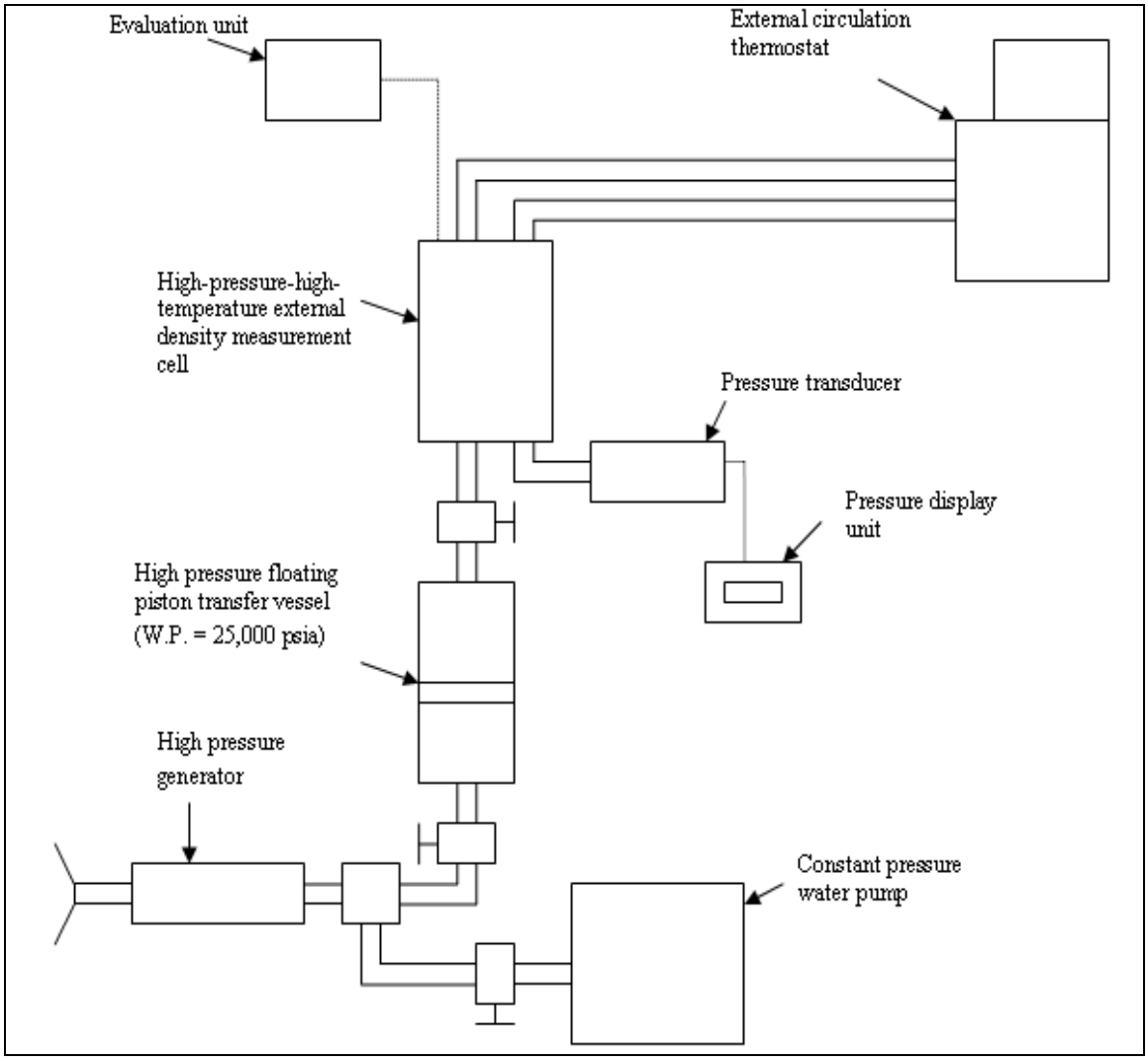

Figure 3.6: Schematic diagram of the HPHT density measurement experimental setup

After successful calibration of HPHT density meter, densities of different oil and aqueous phases were measured. These measured densities were used for determining the IFT of various oil/water systems.

Table 3.21: Measured density values for benzene at elevated pressures & 208°F

Pressure (psia)	Published (NIST web book)	Measured	Deviation	%Error	Phase
	Density (g/cc)	Density (g/cc)			
1,000	0.80263	0.8035	-0.00087	-0.11	liquid
2,000	0.81121	0.81275	-0.00154	-0.19	liquid
3,000	0.819	0.82143	-0.00243	-0.30	liquid
4,000	0.82617	0.8295	-0.00333	-0.40	liquid
5,000	0.83283	0.8364	-0.00357	-0.43	liquid
6,000	0.83906	0.8432	-0.00414	-0.49	liquid
7,000	0.84494	0.8497	-0.00476	-0.56	liquid
8,000	0.8505	0.8559	-0.0054	-0.63	liquid
9,000	0.85579	0.8621	-0.00631	-0.74	liquid
10,000	0.86084	0.8678	-0.00696	-0.81	liquid
11,000	0.86567	0.8783	-0.01263	-1.46	liquid

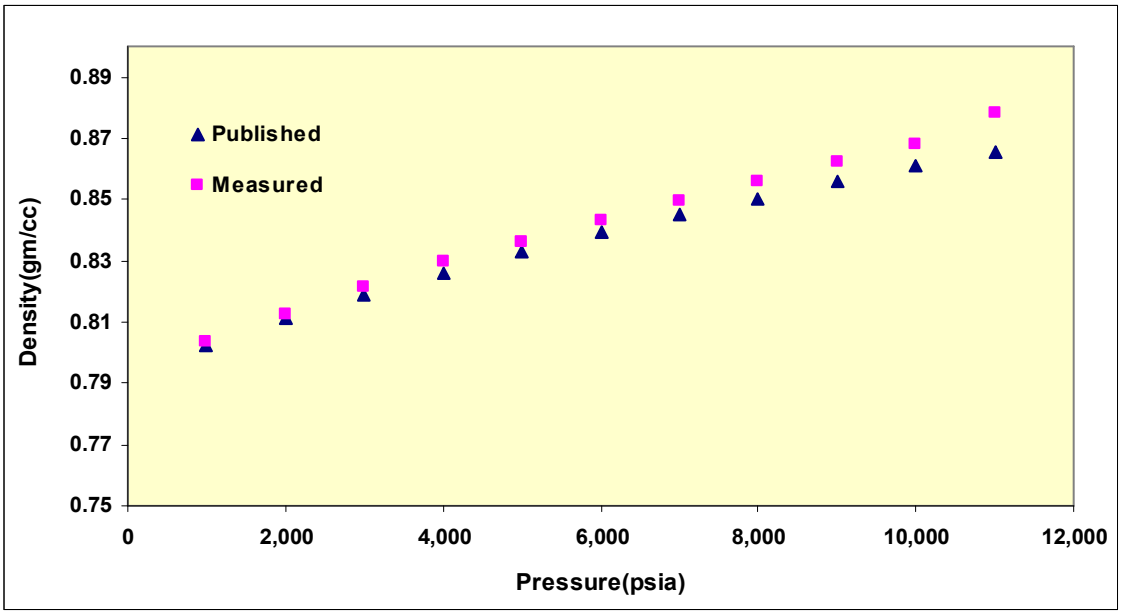

Figure 3.7: Measured and published density data for benzene at 208°F

In the case of the F reservoir, measured densities of live oil (F-RLO), stock-tank oil (F-STO), and different aqueous phases (F-SRB, SSW, and DIW) are plotted in Figure 3.8.

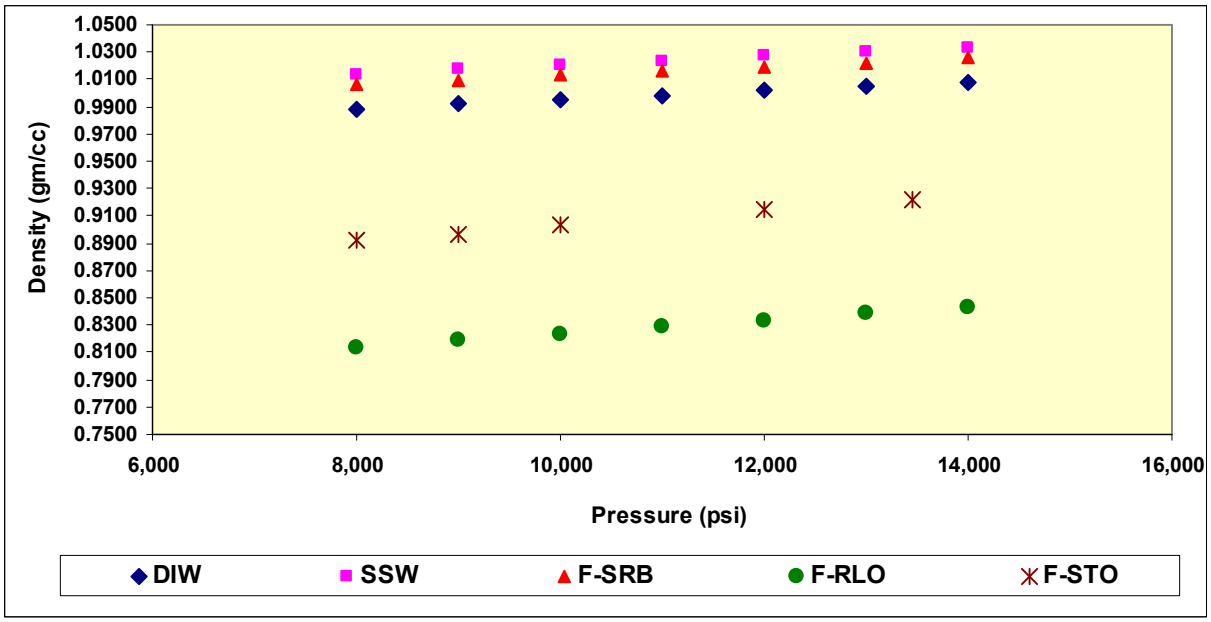

Figure 3.8: Measured densities of different fluid phases (F reservoir) at 208°F

A plot of measured densities of live oil (T-RLO) and different aqueous phases (T-RLO, T-SRB, DIW, and 35K NaCl) in the case of T reservoir is shown in Figure 3.9.

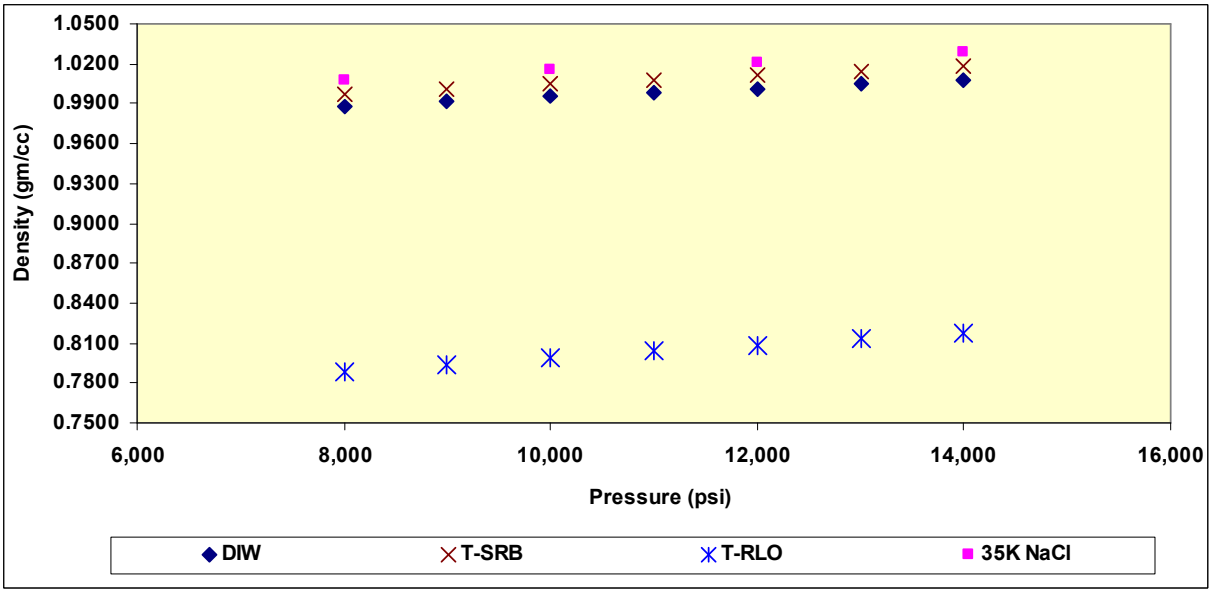

Figure 3.9: Measured densities of different fluid phases (T reservoir) at 208°F

4. RESULTS AND DISCUSSION

The results of both ambient and reservoir conditions oil/water IFT (the pendant drop method), dynamic contact angles (the DDDC tests), and the drop size dependence of dynamic contact angles (the sessile oil drop volume reduction method) experiments conducted for characterizing the rock/fluids interactions in four different (two onshore and two GOM deepwater offshore) oil reservoirs are presented in this chapter. The results are divided and discussed in the following six sections.

The first section (Section 4.1.) deals with the characterization of rock/fluids interactions in different rock/oil/water systems comprising the reservoir fluids of the B oil field. To experimentally determine the magnitude of different intermolecular surface forces in terms of contact angles for the complex rock/oil/water systems (B oil field), the applicability of the line tension-based modified Young's equation was evaluated at reservoir conditions of 1,500 psi and 238°F using both live oil (B-RLO) and stock-tank oil (B-STO), two different aqueous phases (synthetic reservoir brine (B-SRB) and deionized water (DIW)), and three common reservoir rock mineral surfaces (quartz, dolomite and calcite). The evaluation of the applicability of the modified Young's equation in complex rock/oil/water systems involves a three-step procedure that is discussed in detail in Section 4.1.

In Section 4.2, the efforts made to apply the knowledge gained in Section 4.1 for characterizing rock/fluids interactions for B oil field in terms of the work of adhesion (adhesion energy per unit area or interaction free energy per unit area) are discussed. A line-tension based modification to the conventional equation for determining the work of adhesion (the Young-Dupré equation) was introduced to experimentally investigate the effect of the extent of rock/oil adhesion interactions in complex rock/oil/water systems. The effects of the extent of rock/oil adhesion interactions to the

mobilization and saturation of residual oil in porous media were quantified using the line tension-based modified form of the equation for the work of adhesion.

Using the experimental methodology discussed in Sections 4.1 and 4.2, efforts were made to compute the magnitude of intermolecular forces in terms of change in adhesion energy per unit area (ΔW). These results are presented in Section 4.3. The experimental data and observations made during the sessile drop volume alteration experiments (discussed in sub-section 4.1.5) were then used to estimate the change in adhesion energy per unit area with change in distance as the pair of interfaces is brought from a large separation to a finite thickness. This process is equivalent to the measurement of a maximum disjoining pressure. The experimental observations and their interpretation, using the theoretical aspects of the presence and the stability of the thin aqueous wetting films, were used to derive a new equation to estimate the maximum disjoining pressure in complex rock/oil/water systems at reservoir conditions. This new equation was developed to quantify the strength of rock/fluids interactions in terms of measured adhesion energy per unit volume. The results of the estimated adhesion energy per unit volume for different rock/oil/water systems (B oil field) at reservoir conditions are presented in this section.

In Section 4.4, the results of sessile oil drop volume alteration experiments conducted on Y recombined live oil (Y-RLO) at 700 psi and 82° F are presented in order to estimate the extent of rock/fluids interactions. The strength of rock/fluids interactions was quantified in terms of the line tension, the work of adhesion, and the adhesion energy per unit volume. The two systems are a glass/Y-RLO/Y-SRB (pH=7.6) and a glass/Y-RLO/Y-SRB (pH=4.5) system. The published values of theoretically determined values of maximum disjoining pressure at reservoir conditions of 700 psi and 82° F (Busireddy and Rao, 2007) are compared with the experimental values obtained in this study. A film thickness of 6 Å was selected to compute the adhesion energy per unit volume in both of the above mentioned systems using Eq.21 because the theoretical disjoining isotherms exhibited a maximum value at this film thickness. This corresponds to a spontaneous change in the

wetting behavior or the collapse of the aqueous wetting film due to the presence of strong intermolecular surface forces in the system.

In Sections 4.5 and 4.6, the results of the experiments conducted at both ambient and reservoir conditions to characterize the rock/fluids interactions in the F and T reservoirs of a Gulf of Mexico (GOM) deepwater offshore oil field are presented and discussed.

In the case of the F reservoir, the oil/water IFT experiments were conducted in the pressure range of 8,000 psi to 13,454 psi and at temperatures of 175°, 208°, and 250°F. The contact angle (the DDDC and the sessile oil drop volume alteration tests) experiments were conducted at 10,000 psi and 208°F.

In the case of the T reservoir, the oil/water IFT experiments were conducted at pressure between 8,000 psi and 14,000 psi and at the reservoir temperature of 208°F. The contact angle (the DDDC and the sessile oil drop volume alteration tests) experiments were conducted at 12,000 psi and 208°F.

The effect of fluids composition, temperature, and pressure on the measured oil/water IFT was investigated in both reservoirs. The influence of rock mineralogy, oil composition, and effect of dissolved salts in brine on the wetting characteristics of various rock/oil/water systems was also investigated at these pressures and temperatures.

4.1 Characterization of Rock/fluids Interactions, B Oil Field

Rock/fluids interactions for the B oil field were characterized in terms of the measured oil/water IFT and dynamic contact angles. The bubble point pressure for B live oil (B-RLO) is around 1,150 psi. Hence, a pressure of 1,500 psi was selected for conducting the reservoir condition oil/water IFT and dynamic contact angle experiments.

4.1.1 Oil/water IFT Measurements

In the first step, the IFT for different oil/water systems was measured by conducting the pendant drop experiments at both ambient conditions (atmospheric pressure and 72°F) and at

reservoir conditions of 1,500 psi and 238°F. The captured images of pendant oil drops were analyzed using commercial image analysis software (DSA).

The measured average values of oil/water IFTs for stock-tank oil at ambient conditions are given in Table 4.1 and example images of pendant drops for these experiments are shown in Figure 4.1. As evident from the results, the absence of dissolved salts in the aqueous phase (DIW) resulted in a decrease in the measured IFT at ambient conditions.

Table 4.1: Measured oil/water IFT for B-STO at ambient conditions

Oil/water system	B-STO density (gm/cc)	Aqueous phase density (gm/cc)	Density difference (gm/cc)	Average equilibrium interfacial tension (mN/m)	Standard deviation (mN/m)
B-STO/DIW	0.8327	0.9982 (DIW)	0.1655	25.09	±0.98
B-STO/B-SRB	0.8327	1.0684 (B-SRB)	0.2356	27.42	±0.69

B-STO- Stock-tank oil (B oil field), B-SRB-Synthetic reservoir brine (B oil field), DIW- Deionized water

(B-STO/B-SRB system, IFT=27.42 mN/m)

(B-STO/DIW system, IFT= 25.09 mN/m)

Figure 4.1: Ambient condition pendant oil drop images, B-STO

Both recombined live oil (B-RLO) and stock-tank oil (B-STO) were used to conduct B-reservoir condition pendant drop experiments for studying the effect of oil composition on the

measured oil/water IFT. The measured average values of oil/water IFTs at reservoir conditions are given in Table 4.2 and representative images of reservoir condition pendant drops for different oil/water systems at are shown in Figure 4.2.

Table 4.2: Measured oil/water IFT for B-RLO and B-STO, 1,500 psi & 238°F

Oil/water system	Oil phase density (gm/cc)	Aqueous phase density (gm/cc)	Density difference (gm/cc)	Average equilibrium interfacial tension (mN/m)	Standard deviation (mN/m)
B-RLO/DIW	0.7466 (B-RLO)	0.9600 (DIW)	0.2134	21.12	±0.91
B-RLO/B-SRB	0.7466 (B-RLO)	1.0520 (B-SRB)	0.3054	23.58	±0.67
B-STO/DIW	0.7845 (B-STO)	0.9600 (DIW)	0.1755	17.28	±0.75
B-STO/B-SRB	0.7845 (B-STO)	1.0520 (B-SRB)	0.2675	18.40	±0.82

B-RLO- Recombined live oil (B oil field), B-STO- Stock-tank oil (B oil field)
B-SRB-Synthetic reservoir brine (B oil field), DIW- Deionized water

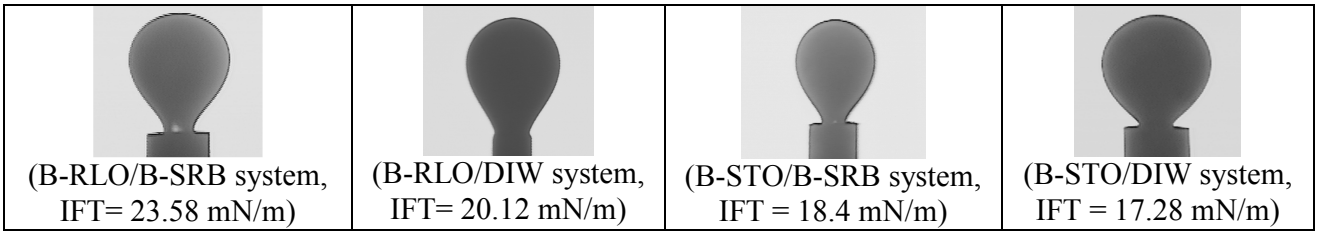

(B-RLO/B-SRB system, IFT= 23.58 mN/m) | (B-RLO/DIW system, IFT= 20.12 mN/m) | (B-STO/B-SRB system, IFT = 18.4 mN/m) | (B-STO/DIW system, IFT = 17.28 mN/m)

Figure 4.2: Reservoir condition pendant oil drop images, B-RLO and B-STO

To study the effect of brine composition on the reservoir condition oil/water IFT, deionized water was also used as another aqueous phase. The presence of dissolved salts in synthetic reservoir brine resulted in an increase in IFT as evident from higher IFT shown by the B-RLO/B-SRB system compared to the B-RLO/DIW system. Similar behavior was observed in the

case of stock-tank oil where the B-STO/B-SRB system showed higher IFT compared to the B-STO/DIW system. This is explained below.

4.1.1.1 Effect of Oil and Brine Composition on Oil/water IFT at Reservoir Conditions

The B-RLO/B-SRB system showed higher IFT compared to the B-STO/B-SRB system. This higher IFT value can be attributed to the compositional difference between recombined live oil and stock-tank oil (Figure 4.3). The presence of the lighter (gaseous) hydrocarbons in live oil (which generally have high IFTs with water) appeared to affect the oil/water IFT in this case.

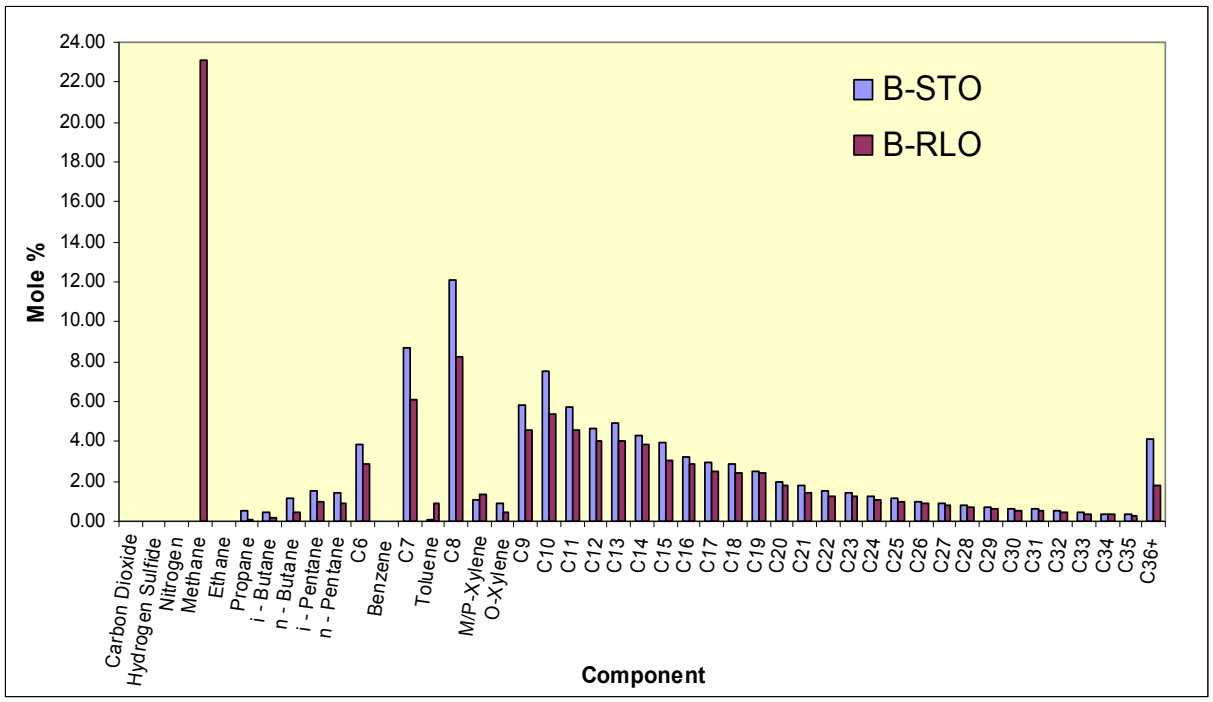

Figure 4.3: Comparison of the compositions of B-RLO and B-STO

The effect of oil composition on oil/water IFT was found to be more pronounced compared to the effect of brine composition. The B-STO/B-SRB and the B-STO/DIW systems showed lower IFT at reservoir conditions compared to ambient conditions. This reduction in oil/water IFT values at reservoir conditions appears to be caused by the high reservoir temperature of 238°F due to

higher density difference between the stock-tank oil and aqueous phase at reservoir conditions (Tables 4.1 and 4.2) than at ambient conditions.

4.1.2 The Sessile Oil Drop Volume Alteration Experiments

Next, the drop size dependence of dynamic contact angle for sessile oil drop was studied to evaluate the applicability of the modified Young's equation (Eq.12) for characterizing rock/fluids interactions at both ambient and reservoir conditions.

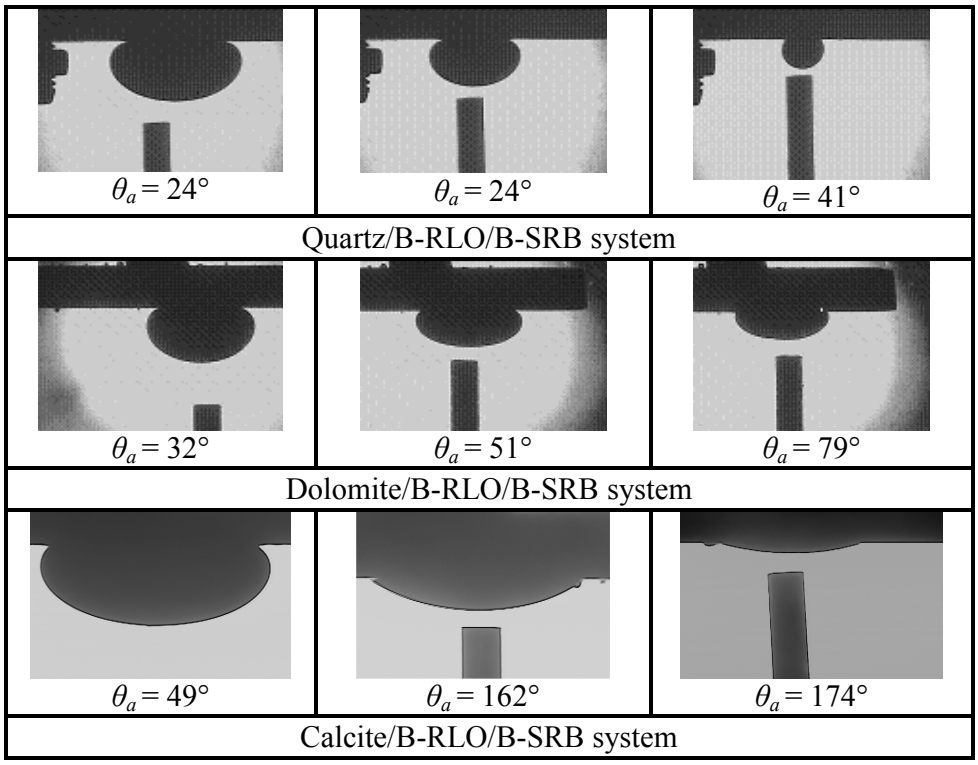

Figure 4.4: The sessile oil drop volume alteration experiments conducted for B-RLO at 1,500 psi & 238°F

The detailed experimental procedure to conduct sessile oil drop volume alteration experiments is discussed in Sub-Section 3.4.2. A series of captured images of varying drop size for different rock/oil/water systems at reservoir conditions are shown in Figure 4.4.

Captured images of sessile oil drops at each volume reduction step were analyzed using a computerized axisymmetric drop shape analysis (ADSA) technique for obtaining the water-advancing contact angle (θ_a) values. Actual and calculated sessile drop shape profiles of captured drop images analyzed by ADSA software are shown in Figure 4.5.

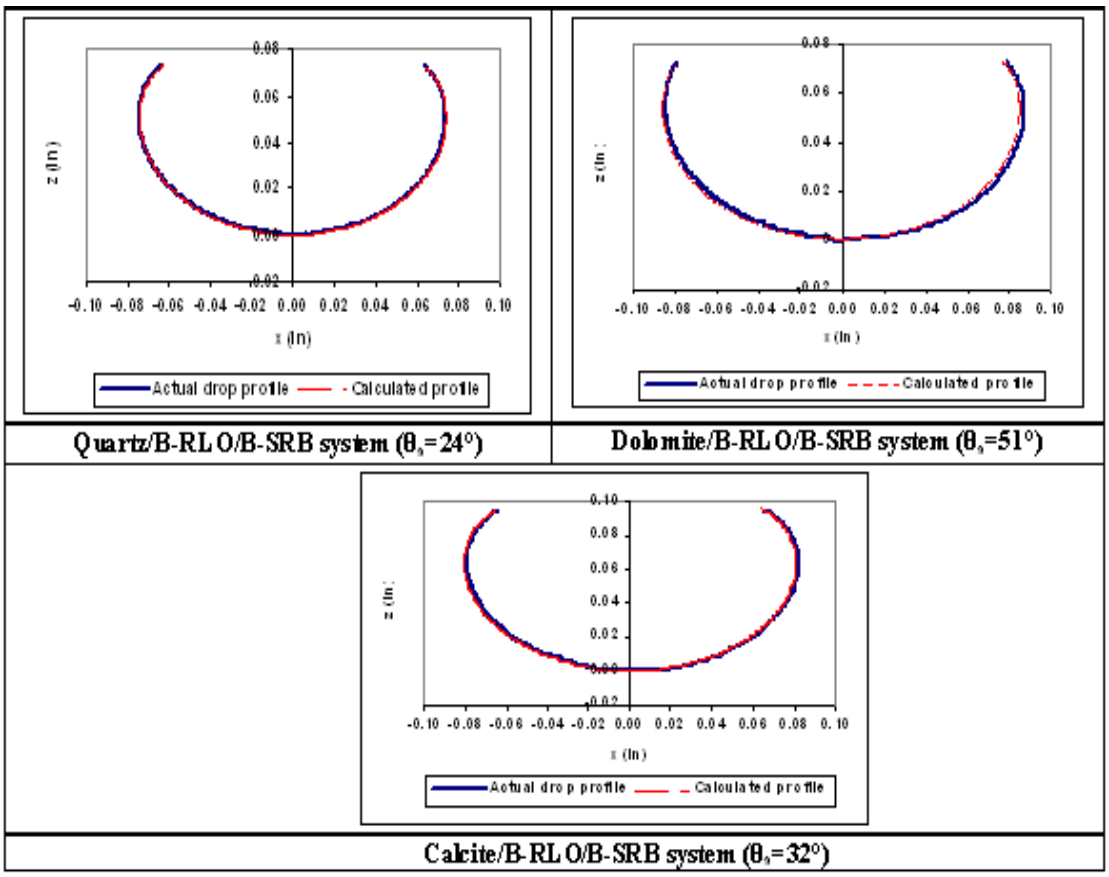

Figure 4.5: Profiles of sessile oil drop images generated by using ADSA software

4.1.3 Determination of the Line Tension

To explore the applicability of the modified Young's equation (Eq.12) in complex rock/oil/water systems, collected data of the oil/water IFT (γ_{ow}), the water advancing contact angle (θ_a) and contact radius (r) were used to determine the value of the line tension, σ, for those rock/oil/water systems that exhibited a movement of the contact line. $Cos\theta_a$ was plotted against $1/r$ values. The observed slopes of $Cos\theta_a$ versus $1/r$ relationship (i.e. σ/γ_{ow}) were used to estimate the line tension in various rock/oil/water systems.

4.1.3.1 Measured Line Tension at Reservoir Conditions

Graphs of the observed $Cos\theta_a$ versus *1/r* relationship for different rock/live oil/water systems at reservoir conditions are shown in Figure 4.6.

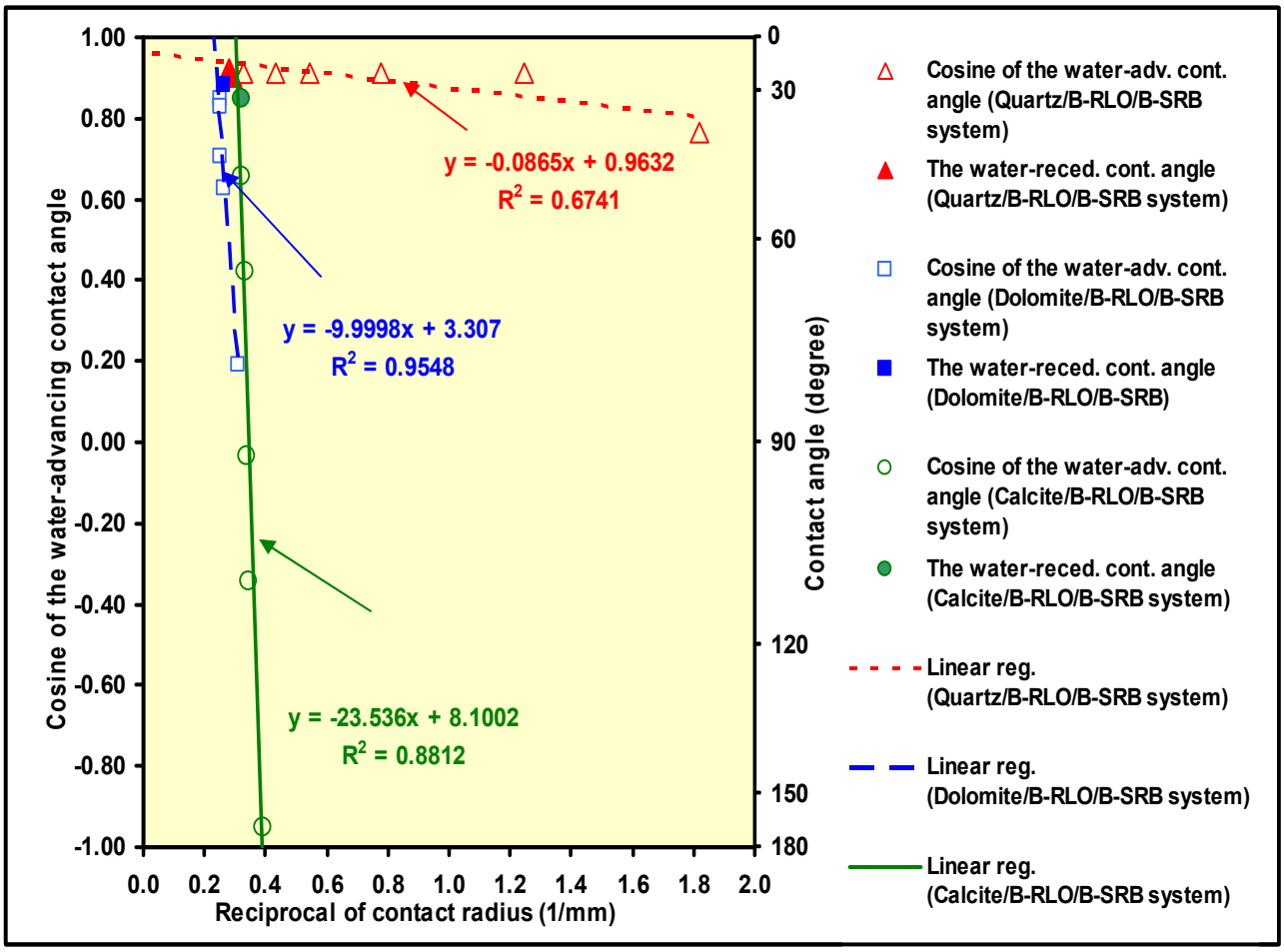

Figure 4.6: $Cos\theta_a$ versus *1/r* relationship for B-RLO at 1,500 psi & 238°F

The slopes of the data in these graphs were then used to determine the line tension for each system. The measured line tension values for different rock/oil/water systems at reservoir conditions are given in Table 4.3. The quartz/B-RLO/B-SRB system has a low value of the line tension, while both the dolomite/B-RLO/B-SRB and the calcite/B-RLO/B-SRB systems had high

line tension values. The calcite and dolomite systems exceed the quartz system by two orders of magnitude. The line tension value in the calcite system was almost twice that of the dolomite system.

4.1.3.1.1 Effect of Oil Composition on Measured Line Tension

To study the effect of oil composition on line tension, recombined live oil was replaced with stock-tank oil. The observed $Cos\theta_a$ versus $1/r$ relationship for different rock/stock-oil/water systems at reservoir conditions is shown in Figure 4.7.

Table 4.3: Measured line tension for B-RLO and B-STO at 1,500 psi & 238°F

Rock/oil/water system	Variation in contact radius (mm)	Slope of $Cos\theta_a$ versus $1/r$ (1/mm) plot	Line tension, σ (mN)
Quartz/B-RLO/B-SRB	3.02 to 0.55	-0.087	0.0022
Dolomite/B-RLO/B-SRB	3.97 to 3.20	-9.999	0.2360
Calcite/B-RLO/B-SRB	3.08 to 2.56	-23.536	0.5550
Quartz/B-RLO/DIW	No change	Infinite	Pinning of contact line
Dolomite/B-RLO/DIW	No change	Infinite	Pinning of contact line
Calcite/B-RLO/DIW	No change	Infinite	Pinning of contact line
Quartz/B-STO/B-SRB	1.66-0.80	-1.65	0.0304
Dolomite/B-STO/B-SRB	2.61-2.24	-18.610	0.3420
Calcite/B-STO/B-SRB	No change	Infinite	Pinning of contact line
Quartz/B-STO/DIW	2.66-2.47	-46.338	0.8000
Dolomite/B-STO/DIW	No change	Infinite	Pinning of contact line
Calcite/B-STO/DIW	No change	Infinite	Pinning of contact line

B-RLO- Recombined live oil (B oil field), B-STO- Stock-tank oil (B oil field)
B-SRB- Synthetic reservoir brine (B oil field), DIW- Deionized water

The magnitude of the line tension value for the quartz/B-STO/B-SRB system was found to be 13.7 times higher compared to the observed line tension in the live oil system. The value for the dolomite system was 1.45 times higher than the live oil system and the calcite system exhibited a "pinning" of the contact line when using stock-tank oil. The line tension could not be calculated in this case. The steep slope the calcite/live oil system compared to the pinning of the contact line

(infinite slope or vertical $Cos\theta_a$ versus $1/r$ line) observed in the calcite/stock-tank oil system suggests that a change in oil composition had only a small effect on the line tension in the case of the calcite surface.

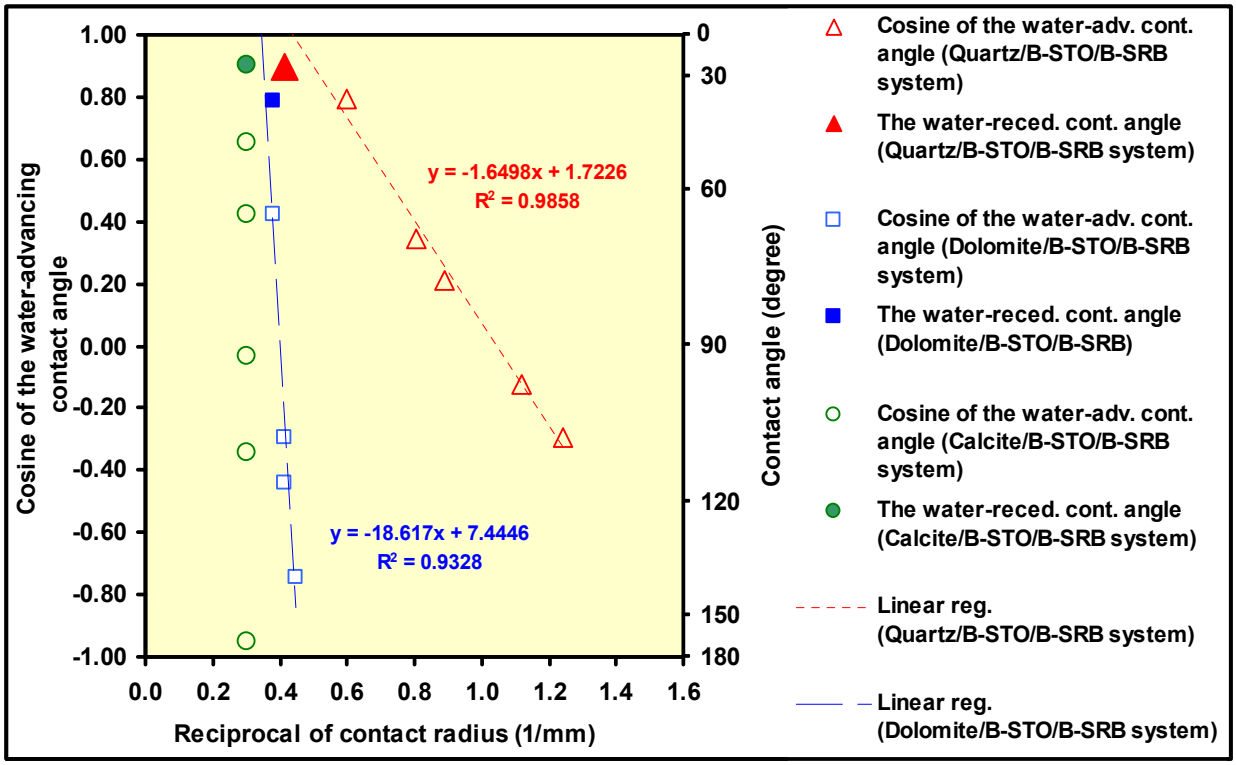

Figure 4.7: $Cos\theta_a$ versus $1/r$ relationship for B-STO at 1,500 psi & 238°F

4.1.3.1.2 Effect of Brine Composition on Measured Line Tension

Deionized water was used as another aqueous phase to study the effect of brine composition on line tension. A pinning of the contact line was observed in all of the three cases studied: the quartz/B-RLO/DIW, the dolomite/B-RLO/DIW, and the calcite/B-RLO/DIW system. This behavior indicates that dissolved salts play a role in the stabilization of the aqueous wetting film trapped between the bulk oil phase and the rock surface. The effect of a change in brine composition on the measured line tension values at reservoir conditions for reservoir B was found to be more pronounced than a change in the oil composition.

4.1.3.2 Measured Line tension at Ambient Conditions

Cosθ_a versus *1/r* relationship shown by different rock/oil/water systems at ambient conditions is plotted in Figure 4.8. All of the three systems showed steep slopes in this relationship. When B-SRB was replaced with DIW as an aqueous phase, all of the three systems showed almost vertical slopes.

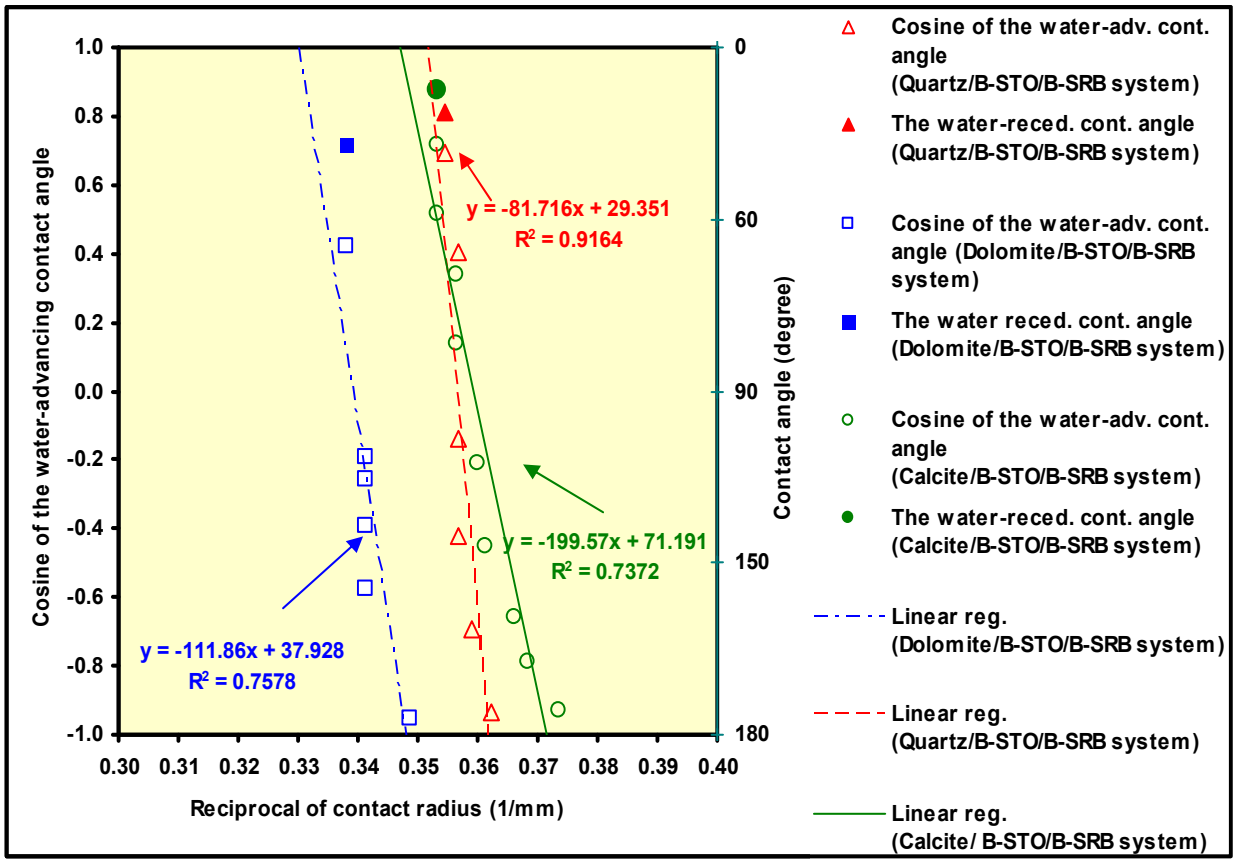

Figure 4.8: *Cos*θ_a versus *1/r* relationship for B-STO at ambient conditions

The measured line tension values for these systems are given in Table 4.4. The quartz system showed lower line tension value compared to both dolomite and calcite systems with synthetic reservoir brine as the aqueous phase. The line tension values could not be calculated for these three systems when DIW was the aqueous phase due to the vertical (infinite slope) *Cos*θ_a versus *1/r* lines shown by these systems.

Table 4.4: Measured line tension for B-STO at ambient conditions

Rock/oil/water system	Variation in contact radius (mm)	Slope of $Cos\theta_a$ versus $1/r$ (1/mm) plot	Line tension, σ (mN)
Quartz/B-STO/B-SRB	2.82 to 2.75	-199.520	5.470
Dolomite/B-STO/B-SRB	2.95 to 2,86	-111.860	3.070
Calcite/B-STO/B-SRB	2.79 to 2.67	-81.716	2.530
Quartz/B-STO/DIW	No change	-	Pinning of contact line
Dolomite/B-STO/DIW	No change	-	Pinning of contact line
Calcite/B-STO/DIW	No change	-	Pinning of contact line

B-STO- Stock-tank oil (B oil field), B-SRB- Synthetic reservoir brine (B oil field),
DIW- Deionized water

4.1.3.3 Effect of Experimental Conditions on Measured Line Tension

As evident from the results given in Tables 4.3 and 4.4, a change in the experimental conditions of pressure and temperature resulted in a significant change in the measured line tension values in different rock/oil/water systems. Both the quartz/B-STO/B-SRB and the dolomite/B-STO/B-SRB systems showed lower line tension at reservoir conditions compared to ambient conditions. However, in the case of the calcite/B-STO/B-SRB system, an opposite trend was observed where the system showed a pinning of the contact line at reservoir conditions compared to a finite (2.53 mN) line tension value at ambient conditions.

In the case of the quartz/B-STO/DIW system, a finite line tension (0.8 mN) was observed at reservoir conditions compared to a pinning of the contact line at ambient conditions. However, in the case of the dolomite/B-STO/DIW system and the calcite/B-STO/DIW system, no significant effect of experimental conditions can be inferred because a pinning of the contact line was observed at both reservoir and ambient conditions in these systems.

4.1.4 Determination of the Wettability of the B oil Field

In third step, to determine the wettability of the B oil field, the DDDC tests were conducted at reservoir conditions of 1,500 psi and 238°F using recombined live oil (B-RLO) and synthetic reservoir brine (B-SRB) with three different reservoir rock mineral surfaces (quartz, dolomite, and calcite). The results of the DDDC tests are given in Table 4.5.

Table 4.5: Results of the DDDC tests conducted for the B oil field at 1,500 psi & 238°F

Rock/oil/water system	Water-receding contact angle, θ_r		Water-advancing contact angle, θ_a	Wettability	Normalized TPCL movement
	Upper crystal	Lower crystal			
Quartz/B-RLO/B-SRB	25°	24°	28°	Strongly water-wet	1.40 to 1.23
Dolomite/B-RLO/B-SRB	32°	28°	82°	Intermediate-wet	1.43 to 1.33
Calcite/B-RLO/B-SRB	30°	32°	154°	Strongly oil-wet	1.53 to 1.44

The quartz surface showed a strongly water-wet behavior at reservoir conditions by exhibiting low water-advancing contact angle (<70°). It indicates the presence of a relatively stable aqueous wetting film on the quartz surface which results in weak adhesion between live oil and the quartz surface. The water-advancing contact angle of 82° for the dolomite system at reservoir conditions shows its intermediate-wet nature. The water-advancing contact angles between 70 to 115° are thought to represent an intermediate wettability state of the system in which it is assumed that all the portions of the rock surface have a slight but nearly equal preference to being wetted by water or oil (Anderson, 1986). The calcite surface showed a strongly oil-wet behavior by yielding a water-advancing contact angle of 154° at reservoir conditions. A large water-advancing contact angle (>115°) indicates the presence of much stronger adhesion between the oil and rock surface and the oil-wet nature of the rock surface. The oil drop images taken during these experiments are shown in Figure 4.9.

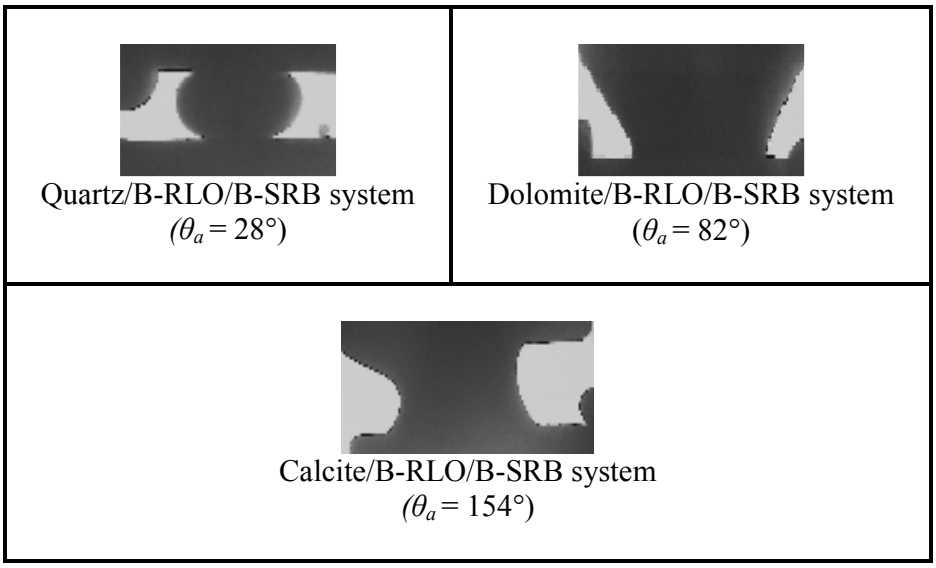

Figure 4.9: Reservoir condition DDDC tests images, B-RLO

The dynamic nature of the water-advancing contact angle in these tests was ensured by observing the movement of the three phase contact line (TPCL) on the lower crystal. It was measured in terms of a normalized TPCL movement which is defined as the relative position of the oil drop at a given time step to its initial position during the lateral movement of the lower crystal. A TPCL value greater than unity signifies that the crude oil drop is still moving within the initially oil-exposed area of the lower surface, thereby satisfying the definition of the water-advancing contact angle.

The measured normalized TPCL movements for all of the three systems are shown in Figures 4.10-4.12. The reproducibility of the measured water-advancing contact angle was ensured by bring the oil drop back to its initial position and moving the lower crystal (laterally) again. The measured water-advancing contact angles showed a small deviation (2-3°) in subsequent lateral movement of the lower crystal.

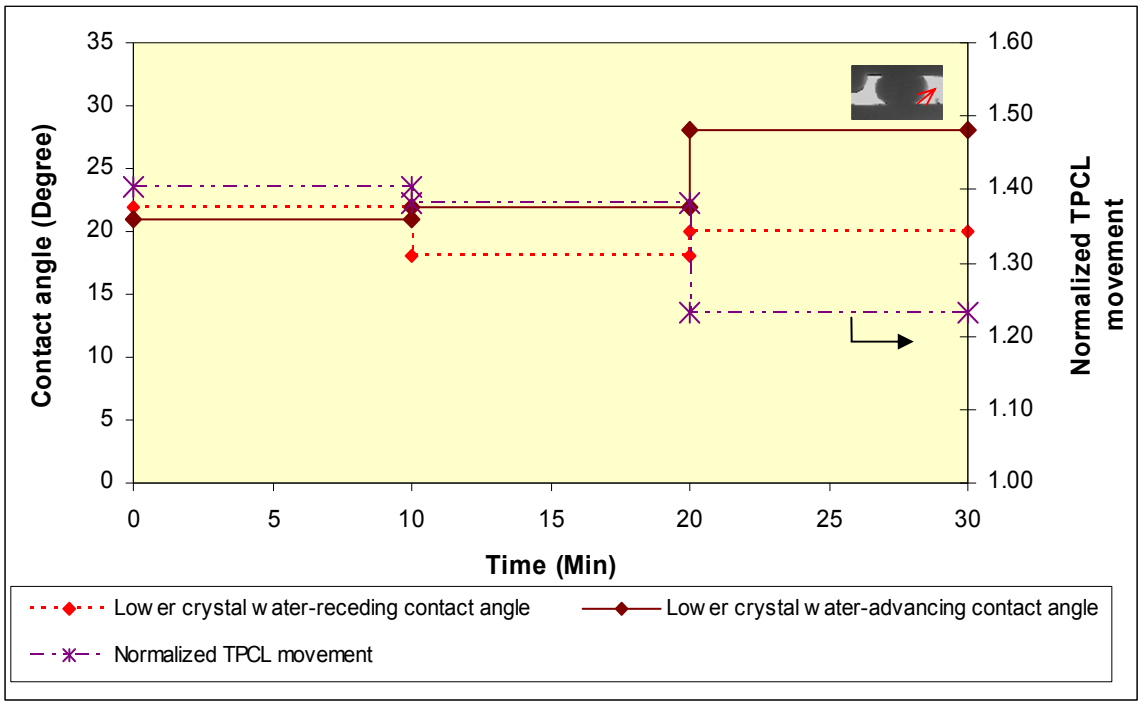

Figure 4.10: TPCL movement in the quartz/B-RLO/B-SRB system at 1,500 psi & 238°F

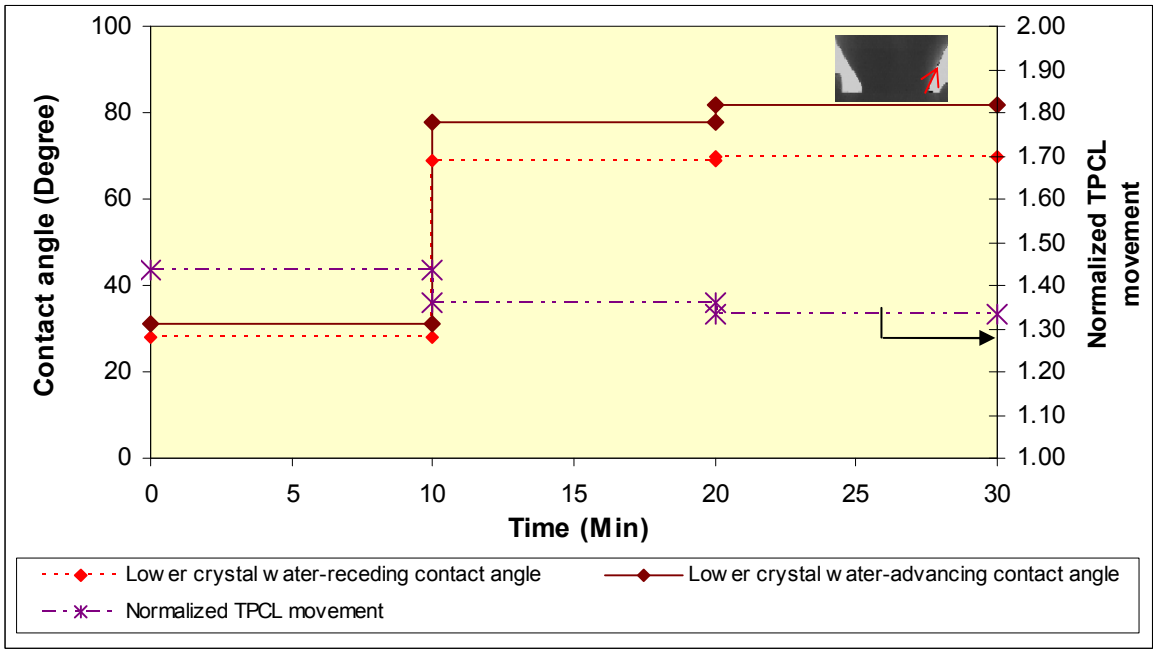

Figure 4.11: TPCL movement in the dolomite/B-RLO/B-SRB system at 1,500 psi & 238°F

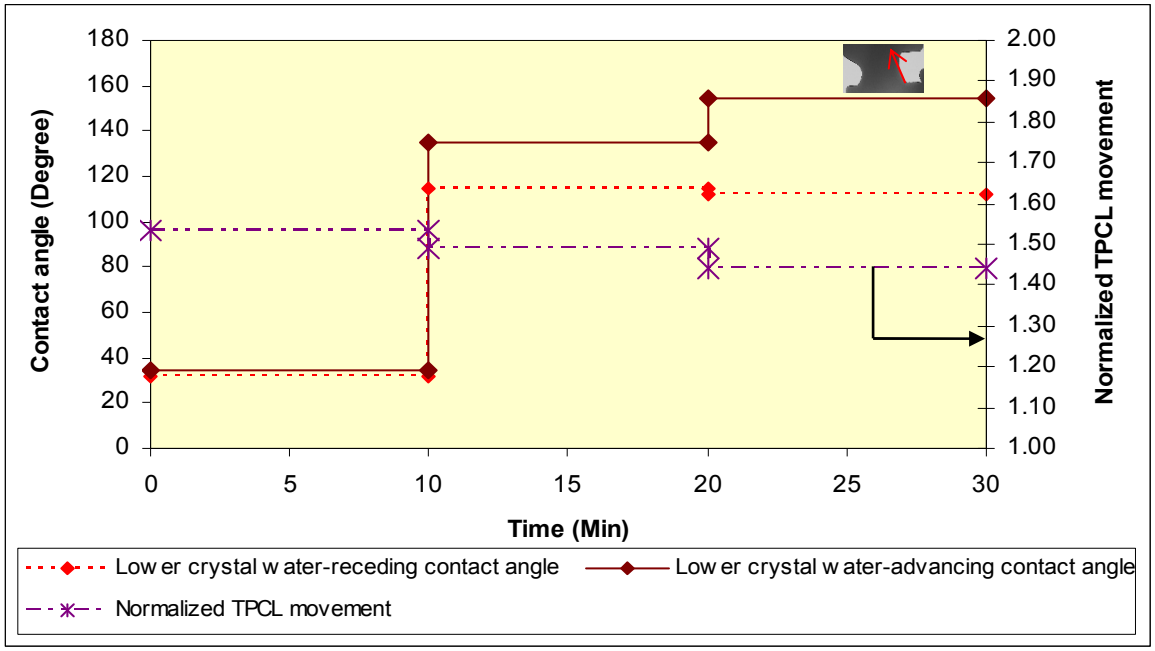

Figure 4.12: TPCL movement in the calcite/B-RLO/B-SRB system at 1,500 psi & 238°F

4.1.5 Effect of Rock/oil Adhesion Interactions on $Cos\theta_a$ versus $1/r$ Relationship

While conducting the sessile oil drop volume alteration experiments, the size of the sessile oil drop was gradually increased to form a big sessile oil drop. At each step of drop size increase, dynamic contact angle was measured which corresponds to the water receding contact angle (θ_r) in this situation. Then the system was aged (16 to 24 hr) to attain the equilibrium between all three phases. A small variation was observed in the equilibrium contact angle, θ_∞ (Young's contact angle) and θ_r values. In the next step, the sessile oil drop size was decreased to determine the magnitude of the line tension in different rock/oil/water systems. In this situation, the measured dynamic contact angle corresponds to the water-advancing contact angle (θ_a).

Plots of sessile oil drop size (in terms of contact radius, r) versus measured dynamic contact angles (θ_r and θ_a) for different rock/recombined live oil/synthetic reservoir brine systems are shown in Figures 4.13-4.15.

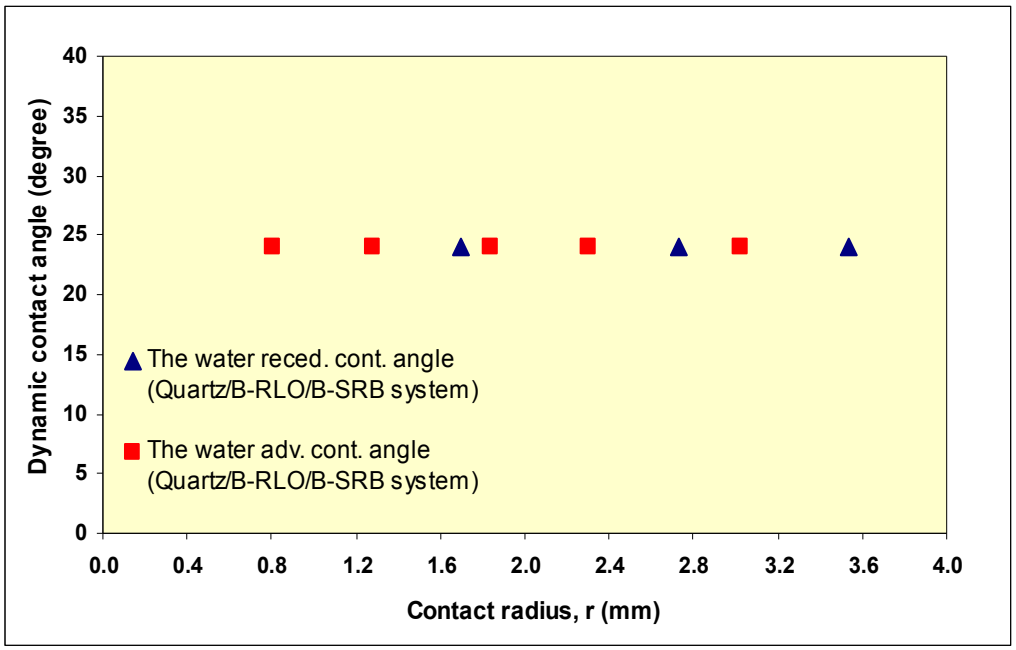

Figure 4.13: The Effect of drop size variation on the water-receding and the water-advancing contact angle values for the quartz/B-RLO/B-SRB system at 1,500 psi & 238°F

As evident from Figure 4.13, the quartz/B-RLO/B-SRB system showed negligible contact angle hysteresis (θ_a-θ_r) in the sessile oil drop volume alteration experiment. The dolomite/B-RLO/B-SRB system showed moderate contact angle hysteresis (Figure 4.14), whereas significant contact hysteresis was shown by the calcite/B-RLO/B-SRB system (Figure 4.15). All three systems showed similar, low values of θ_r irrespective of their distinct wetting characteristics determined by measuring θ_a in the DDDC tests. The low values of θ_r shown by all of the three systems irrespective of their wettability behavior observed in the DDDC tests clearly demonstrate the presence of the stable aqueous wetting film between the sessile oil drop and the mineral crystal surface when the sessile oil drop is formed initially with the mineral surface in such experiments.

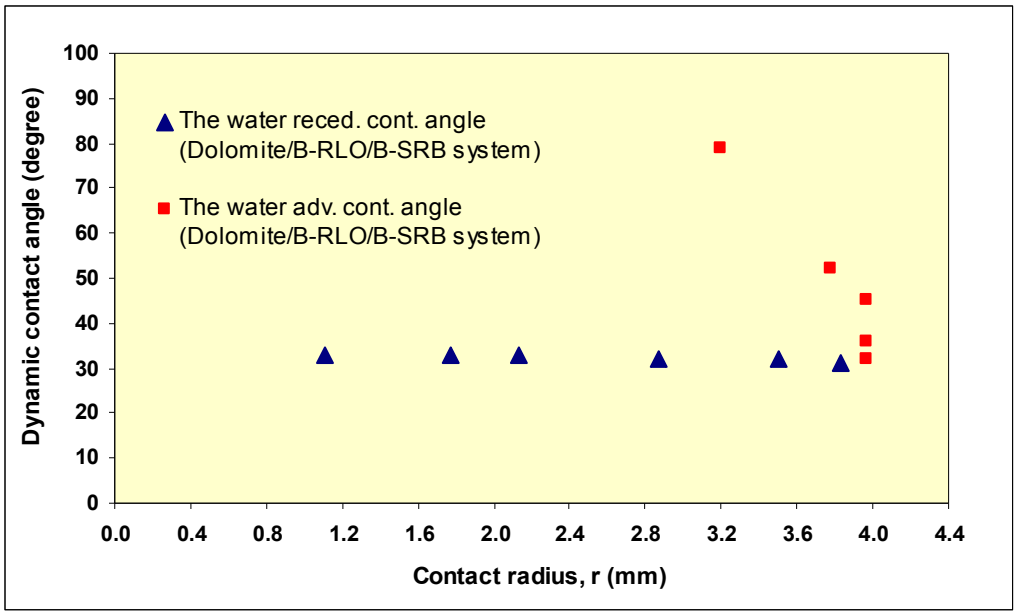

Figure 4.14: The Effect of drop size variation on the water-receding and the water-advancing contact angle values for the dolomite/B-RLO/B-SRB system at 1,500 psi & 238°F

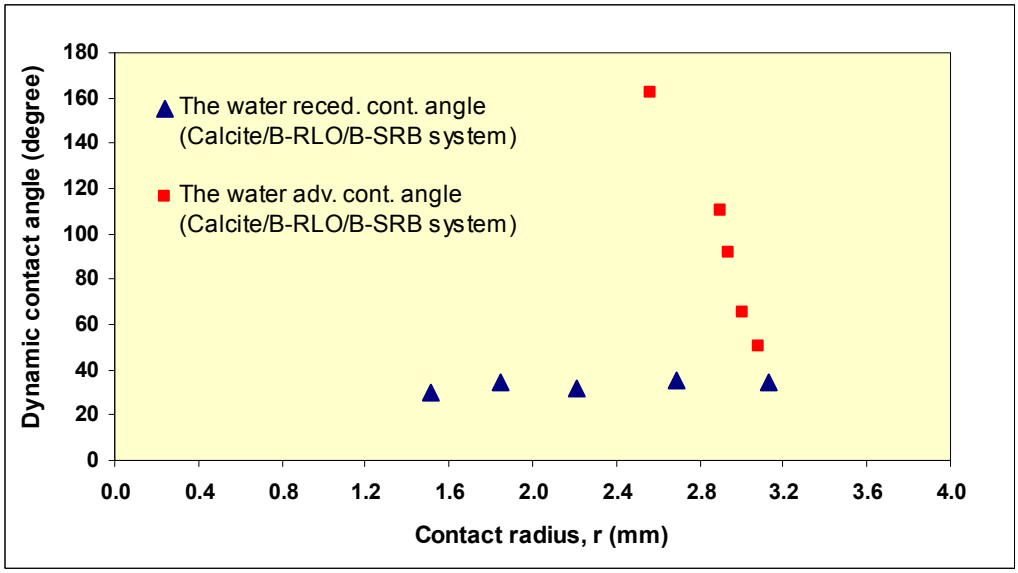

Figure 4.15: The Effect of drop size variation on the water-receding and the water-advancing contact angle values for the calcite/B-RLO/B-SRB system at 1,500 psi & 238°F

However, a significant contact angle hysteresis shown by two other rock/recombined live oil/water systems, especially by the calcite/B-RLO/B-SRB system during the stepwise reduction in the drop volume indicates the that there has been complete drainage of the aqueous wetting film squeezed between the sessile oil drop and the mineral crystal surface or that the film has been reduced to a thinner, likely only a few molecules thick, film that allowed interaction between the oil and the rock surface. This results in the development of a strong adhesion between the rock surface and the oil phase.

According to the modified Young's equation (Eq.12), the y-intercept of the $Cos\theta_a$ versus $1/r$ line corresponds to the equilibrium contact angle, θ_∞. However, all $Cos\theta_a$ versus $1/r$ lines except one (quartz/B-RLO/B-SRB system) yielded an intercept >1. This behavior is not physically possible. To resolve this inconsistency, the $Cos\theta_a$ versus $1/r$ line was shifted towards the Y-axis in such a manner that it could yield an intercept equal to the cosine of the initial θ_r value on the Y-axis. This operation is shown in Figure 4.16.

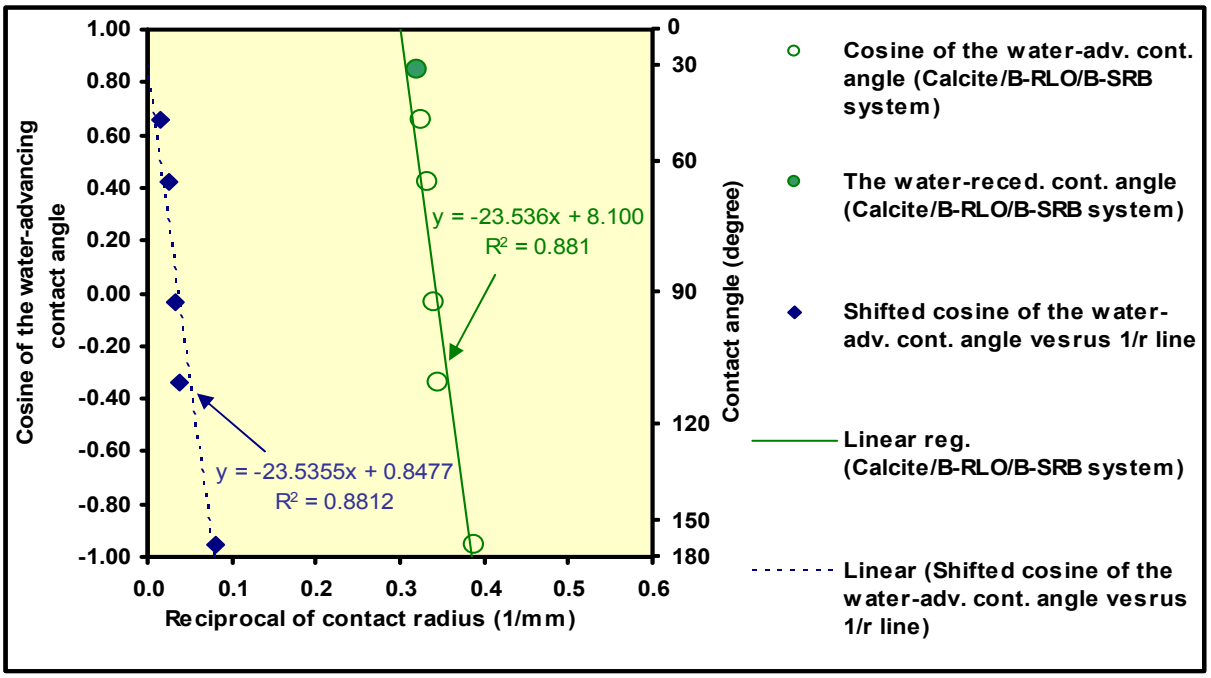

Figure 4.16: Schematic depiction of the shifting of $Cos\theta_a$ versus $1/r$ line towards the Y axis

However, as evident from Figure 4.16, this new $Cos\theta_a$ versus *1/r* line corresponds to large value of *r* ($r \rightarrow \infty$). As $r \rightarrow \infty$, Eq.12 is reduced to $Cos\theta_a = Cos\theta_\infty$. Physically, when $r \rightarrow \infty$, then oil has spread on the mineral surface, thus exhibiting significant contact angle hysteresis.

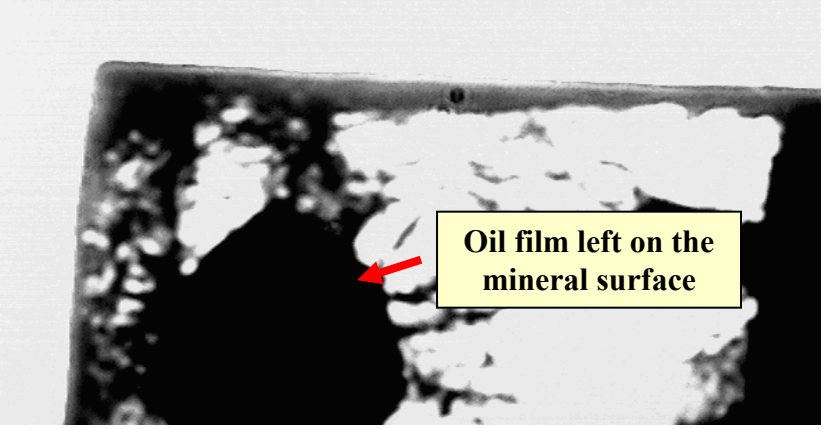

Figure 4.17: Oil film left on the mineral surface during the sessile oil drop volume alteration experiment

This behavior is evident from the thin oil film left on the rock surface after the final drop size reduction step during the sessile oil drop volume experiment when almost all the oil had been removed by withdrawing it back into the injector tip available at the bottom of the optical cell (Figure 4.17). A similar behavior was also observed during the independently conducted DDDC tests (Figure 4.18).

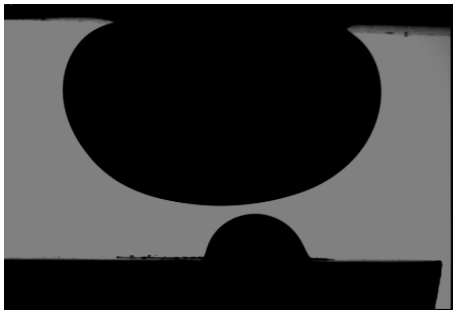

Figure 4.18: Fraction of sessile oil drop left on the lower mineral surface in the DDDC test

The oil film left on the mineral surface also means that θ_a (θ_∞) has attained a value very close to 180° in such cases. Hence, the steep slopes in the $Cos\theta_a$ versus *1/r* graphs experimentally

demonstrate that the water-advancing contact angle, θ_a, actually corresponds to the equilibrium contact angle, θ_∞ in oil-wet systems. Similar conclusions, i.e. $\theta_a=\theta_\infty$, have been reported by Neumann and Good (1972) for S/L/V systems with heterogeneous surfaces. They used a simple model and concluded that for the heterogeneous surfaces, the advancing contact angle was equal to the equilibrium contact angle that would be observed on the smooth homogeneous surfaces of a low energy component.

In S/L/V systems, the lighter vapor phase may not be able to eliminate the effect of surface roughness completely in the presence of a heavier liquid phase. However the presence of the heavier phase filling the crevices of the rough surface could render the crystal surface fairly smooth in S/L/L systems, thus making the effect of roughness on contact angles negligible as evident in the image (Figure 4.19[12]) taken by an environmental scanning electron microscope (ESEM).

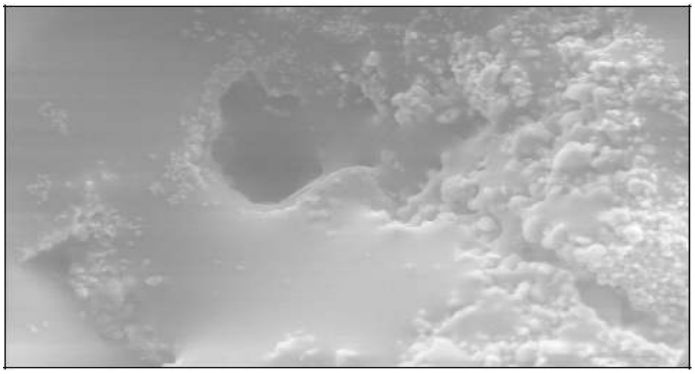

Figure 4.19: The development of sheet-like cover of water on calcite grains (Al-Shafei and Okasha, 2009)

The observed steepness in the slopes in the $Cos\theta_a$ versus $1/r$ graphs indicates the extent of deviation of the system from the Young's equation. This deviation from the Young's equation, which appears to be mainly caused by rock/oil adhesion interactions, was responsible for the high line tension values in oil-wet system. In extreme cases, where a pinning of the contact line was observed, the sessile oil drop just snapped leaving a fraction of oil drop attached to the rock surface

[12] © SPE 2009, reproduced with permission

during the drop size reduction steps of the sessile oil drop volume alteration experiments. This clearly indicates the presence of strong rock/oil adhesion interactions in the system.

Hence, an effort was made to correlate the line tension with the extent of rock/oil adhesion interactions in complex rock/oil/water systems. A careful comparison of the adhesion number with the line tension-based modified Young's equation (Eq.12) reveals that both describe the extent of rock/fluids interactions in terms of different measurable parameters hence a proportional relationship between line tension and adhesion number can be expected.

Table 4.6: Measured line tension and adhesion number for B-RLO and B-STO at 1,500 psi & 238°F

Rock/oil/water system	Water-receding contact angle θ_r, (°)	Water-advancing contact angle θ_a, (°)	Adhesion No ($Cos\theta_r$ - $Cos\theta_a$)	Line tension, σ (mN)
Quartz/B-RLO/B-SRB	24*	28*	0.0310	0.0022
Dolomite/B-RLO/B-SRB	28*	82*	0.7430	0.2360
Calcite/B-RLO/B-SRB	32*	154*	1.746	0.5500
Quartz/B-RLO/DIW	23	~180	1.920	pinning of contact line
Dolomite/B-RLO/DIW	35	~180	1.819	pinning of contact line
Calcite/B-RLO/DIW	41	~180	1.754	pinning of contact line
Quartz/B-STO/B-SRB	26	107	1.190	0.0304
Dolomite/B-STO/B-SRB	38	138	1.531	0.3420
Calcite/B-STO/B-SRB	25	~180	1.906	pinning of contact line
Quartz/B-STO/DIW	26	133	1.580	0.8000
Dolomite/B-STO/DIW	48	~180	1.669	pinning of contact line
Calcite/B-STO/DIW	41	~180	1.754	pinning of contact line

* Measured in the DDDC tests, B-RLO- Recombined live oil (B oil field), B-STO- Stock-tank oil (B oil field) B-SRB- Synthetic reservoir brine (B oil field), DIW- Deionized water

For this, the measured line tension values were plotted against the adhesion number. The adhesion number (Rao, 2003) was calculated by using the measured values of θ_r and θ_a obtained in the DDDC tests conducted for selected rock/oil/water systems. In other cases, the adhesion number was calculated using measured θ_r and the maximum value of θ_a obtained in the sessile oil drop volume alteration experiments. In the cases, where a pinning of the contact line was observed, the adhesion number was calculated by assuming the water-advancing contact angle (θ_a) of 180°. The adhesion number and the line tension values measured at reservoir conditions for different rock/oil/water systems are given in Table 4.6.

A plot between the measured line tension and adhesion number values for different rock/recombined live oil/synthetic reservoir brine systems is shown in Figure 4.20.

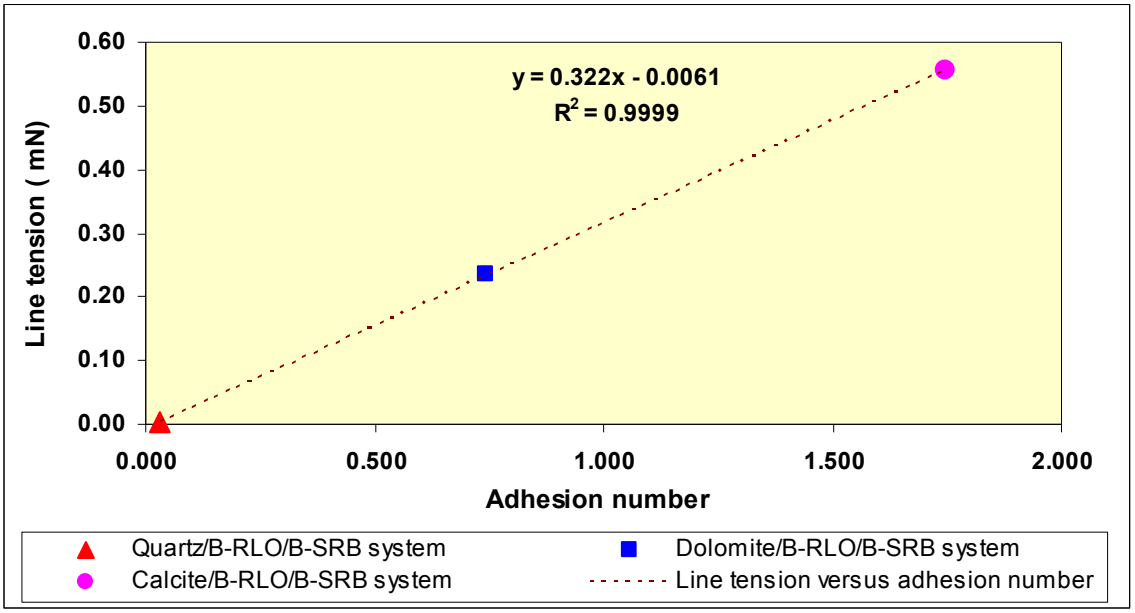

Figure 4.20: Line tension versus adhesion number relationship for B-RLO at 1,500 psi & 238°F

As can be seen in Figure 4.20, the B-RLO/B-SRB system with different mineral surfaces (quartz, dolomite, and calcite) showed a proportional relationship between the adhesion number and the line tension. The oil-wet calcite system (high adhesion number) exhibited significantly

higher line tension value than water-wet quartz system (low adhesion number). Hence, the measured line tension may be used as an experimental means to quantitatively estimate the extent of rock/oil adhesion interactions.

At ambient conditions, all of the three rock/B-STO/B-SRB systems exhibited high adhesion number and correspondingly high line tension values were observed in them. In the case of the rock/B-STO/DIW systems, a pinning of the contact line was observed in all of the three systems. The ambient condition line tension and adhesion numbers values for different rock/stock-tank oil/systems are given in Table 4.7.

Table 4.7: Measured line tension and adhesion number for B-STO at ambient conditions

Rock/oil/water system	Water-receding contact angle θ_r, (°)	Water-advancing contact angle θ_a (°)	Adhesion No ($Cos\theta_r$ - $Cos\theta_a$)	Line tension, σ (mN)
Quartz/B-STO/B-SRB	33	159	1.772	5.470
Dolomite/B-STO/B-SRB	22	160	1.860	3.070
Calcite/B-STO/B-SRB	21	158	1.860	2.530
Quartz/B-STO/DIW	17	~180	~1.956	Pinning of contact line
Dolomite/B-STO/DIW	43	~180	~1.731	Pinning of contact line
Calcite/B-STO/DIW	25	~180	~1.906	Pinning of contact line

B-STO- Stock-tank oil (B oil field), B-SRB- Synthetic reservoir brine (B oil field), DIW- Deionized water

The extent of rock/oil adhesion interactions in different rock/stock-tank oil/synthetic reservoir brine systems at ambient conditions was found to be much higher than rock/recombined live oil/synthetic reservoir brine systems at reservoir conditions due to the compositional difference between live oil (B-RLO) and stock-tank oil (B-STO) (Figure 4.3) along with a significant difference in the experimental conditions of elevated pressure and temperature. This suggests that ambient condition experiments conducted with stock-tank oil could yield

misleading results by not capturing the cumulative effect of rock/fluids interactions that are present in the case of live oil at elevated pressure and temperature.

The successful application of the line tension-based modified Young's equation for characterizing rock/fluids interactions suggests that the measurement of the line tension in complex rock/oil/water systems could serve as an experimental means to quantify the extent of rock/oil adhesion interactions in such systems.

4.1.6 Observed pH Behavior of Different Aqueous Phases, B Oil Field

The measured changes in the pH of the aqueous phase before and after each contact angle experiment are given in Table 4.8. All of the pH measurements were conducted at ambient conditions.

Table 4.8: Measured pH data for different aqueous phases, B oil field

Oil/water system	Experimental pressure and temperature conditions	Sample collection pressure and temperature conditions	pH before Exp.	pH after Exp.	Change in measured pH (Δ pH)
B-RLO/DIW	1500 psi, 238°F	Atm. Press, 72°F	6.95	6.53	0.42
B-RLO/B-SRB	1500 psi, 238°F	Atm. Press, 72°F	6.61	6.16	0.45
B-STO/B-DIW	1500 psi, 238°F	Atm. Press, 72°F	6.95	6.45	0.50
B-STO/B-SRB	1500 psi, 238°F	Atm. Press, 72°F	6.61	6.16	0.45
B-STO/B-DIW	Atm. Press, 72°F	Atm. Press, 72°F	6.95	6.68	0.27
B-STO/B-SRB	Atm. Press, 72°F	Atm. Press, 72°F	6.61	6.33	0.28

The aqueous phase samples collected after the experiments had traces of crude oil in them. In the reservoir conditions experiments, the change in pH ranged from 0.42 (live oil/DIW) to 0.50 (live oil/brine) while ambient conditions experiments showed a change of 0.28. These minor changes in pH are attributed to the interactions between oil and brine at the experimental conditions and duration of each experiment. No particular trend in pH behavior was observed for different mineral crystals.

4.2 Estimation of the Extent of Rock/oil Adhesion Interactions in Terms of the Work of Adhesion

The interpretations of the sessile oil drop volume alteration experiments in conjunction with the DDDC test results discussed in Section 4.1 are of practical importance in studying the dynamic situation present in the reservoir. In the dynamic situation, a certain amount of work needs to be exerted on the system to overcome the rock/oil adhesion interactions and mobilize residual oil depending on the extent of these interactions present in the system. Understanding of the extent of rock/oil adhesion interactions is then of practical importance in the success of any EOR process because it enables the development of means to overcome these rock/oil adhesion interactions in order to achieve substantial increase in oil recoveries.

The concept of the work of adhesion is commonly used to experimentally determine the extent of rock/oil adhesion interactions in complex rock/oil/water systems. For this, two different experimental approaches are used. The first approach uses adhesion tests in various forms (the conventional adhesion test and the sessile drop volume alteration method). The second approach consists of experimental measurement of intermolecular surface forces in terms of the adhesion energy per unit area (Atomic force microscopy technique (AFM) and Surface force apparatus (SFA)). An overview of both the approaches was given in Sub-Section 2.4.1.2.

Displacement of oil though the pore space of a rock matrix is analogous to the separation of an oil drop formed with a solid surface in the presence of an aqueous phase. In this situation, two new unit interfaces i.e. oil/water and solid/water are formed and solid/oil interface is eliminated. The necessary work required to attain this interfacial separation is expressed by the work of adhesion. For rock/oil/water systems, the work of adhesion, W_{sow} is expressed as (Rao and Maini, 1993):

$$W_{sow} = (\gamma_{sw} + \gamma_{ow}) - \gamma_{so}$$

Or

$$W_{sow} = \gamma_{ow} - (\gamma_{so} - \gamma_{sw}) \quad \text{(13)}$$

Where, γ_{ow}, γ_{so}, and γ_{sw} are the interfacial tensions of the oil/water interface, the solid/oil interface, and the solid/water interface. Using the Young's equation, Eq.13 for W_{sow} can easily be expressed using the Young-Dupré equation (Eq.6). The Young-Dupré equation provides a basic equation for experimentally estimating the work of adhesion in complex rock/oil/water systems. It involves the measurement of oil/water IFT (γ_{ow}) and the equilibrium contact angle (θ_{∞}). These quantities can be measured at elevated pressure and temperature conditions using the HPHT optical cell apparatus (Figure 3.3).

In the case of rock/oil/water systems with weak or no rock/oil adhesion interactions, an oil drop can be completely detached from a rock surface without leaving any oil behind on that rock surface in a conventional adhesion test. However, in other cases where strong rock/oil interactions are present, detachment of the oil drop results in leaving a fraction of that oil drop on the rock surface. Similar behavior was observed in the sessile oil drop volume alteration experiments discussed in Section 4.1. Stepwise withdrawal of the oil drop using the injector needle available at the bottom of the optical cell left a fraction of the original oil drop adhered to the rock surface. This observed behavior was characterized in terms of line tension using the modified Young's equation (Eq.12). The step slopes of $Cos\theta_a$ versus $1/r$ lines obtained in oil-wet systems clearly demonstrates that θ_a corresponds to the equilibrium contact angle, θ_{∞} (described by the Young's equation) in such systems.

In view of these experimental observations, a line tension-based modification to the Young-Dupré equation of the work of adhesion (Eq.6) using the relationship between θ_{∞} and θ_a described by the modified Young's equation (Eq.12) is proposed. This modification is sought to derive a functional relationship between θ_a and the work of adhesion, as θ_a is directly correlated to the reservoir wettability.

From the Young's equation (Eq.2) for S/L/L (rock/oil/water) systems, we have:

$$Cos\theta_{\infty} = \frac{(\gamma_{so} - \gamma_{sw})}{\gamma_{ow}} \quad \text{(14)}$$

Replacing $Cos\theta_{\infty}$ in the line tension-based modified Young's equation (Eq.12) with the right hand-side term in Eq.12 means that Eq.1 can be rewritten as:

$$Cos\,\theta_a = \frac{(\gamma_{so} - \gamma_{sw})}{\gamma_{ow}} - \frac{\sigma}{\gamma_{ow}}(1/r) \quad \text{(15)}$$

Using Eq.13 and Eq.15, a line tension-based modified equation for the work of adhesion can now be written as:

$$W_{sow} = \gamma_{ow}(1 - Cos\,\theta_a) - \frac{\sigma}{r} \quad \text{(16)}$$

Where σ is the line tension, r is the radius of contact line in the plane of solid surface, and W_{sow} is the work of adhesion or "adhesion energy per unit area" of the oil phase interacting with the solid surface in the presence of an aqueous phase. However, the steep slopes of the $Cos\theta_a$ versus $1/r$ graphs exhibited by non water-wet system clearly demonstrated the development of an oil film on the rock surface due to the presence of strong rock/oil adhesion interactions or in other words, oil had spread on the rock surface. In this situation, $r \rightarrow \infty$, hence a zero value is assigned to the term containing r in Eq.16 for estimating the extent of rock/oil adhesion interactions in terms of work of adhesion. Equation 16 can then be rewritten as:

$$W_{sow} = \gamma_{ow}(1 - Cos\,\theta_a) \quad \text{(17)}$$

Equation 17 provides a way to compute the adhesion energy per unit area, W_{sow}, in terms of the water-advancing contact angle after accounting for the effect of strong rock/oil adhesion interactions present in the system.

The conventional approach (Eq.6) which uses the measured oil/water IFT (γ_{ow}) and the equilibrium contact angle (θ_{∞}) data to estimate the work of adhesion in rock/oil/water systems is

particularly valid in strongly water-wet systems. In strongly water-wet systems, when the sessile oil drop formed to the mineral crystal surface is detached, it does not leave any oil on the rock surface. Also in rock/oil/water systems, the equilibrium contact angle (θ_∞) formed by a sessile oil drop with the rock surface corresponds to the water-receding contact angle (θ_r) unless the equilibrium is disturbed by some means. However, the extent of rock/oil adhesion interactions can only be estimated by disturbing this equilibrium. When equilibrium is disturbed, depending on the extent of rock/oil adhesion interactions, θ_∞ can take any value ranging from θ_r to θ_a. Hence, Eq.17 rather than Eq.6 should be used to reliably estimate the extent of rock/fluids interactions in terms of the work of adhesion in complex rock/oil/water systems of petroleum engineering interest.

The use of Eq.17 to estimate the extent of rock/oil adhesion interactions is of practical importance, because in dynamic situations, a certain amount of work needs to be exerted on the system to overcome the rock/oil adhesion interactions depending on the extent of rock/oil adhesion interactions present in the system. Equation 17 takes this into account and hence, provides a realistic estimate of the necessary work required to overcome the rock/oil adhesion interactions present in the system during the mobilization of residual oil.

In the next sub-section, the results of the estimated work of adhesion for different rock/oil/water systems at reservoir conditions of 1,500 psi and 238°F using the recombined live oil and synthetic reservoir brine are presented. The data collected during the sessile oil drop volume alteration experiments in conjunction with the measured oil/water IFT and the DDDC test results were used to correlate the effect of the work of adhesion to the mobilization of residual oil. The residual oil saturation was inferred in terms of the sessile oil drop volume ratio, which is the ratio of the volume of the sessile oil drop which remained attached to the mineral crystal surface at a given drop size reduction step to the volume of initial sessile oil drop.

4.2.1 Estimation of the Work of Adhesion for B-RLO at Reservoir Conditions

Equation 17 was used to estimate the work of adhesion, W_{sow}, in the quartz/B-RLO/B-SRB, the dolomite/B-RLO/B-SRB, and the calcite/B-RLO/B-SRB systems at 1,500 psi and 238°F. The measured oil/water IFT (Table 4.2) data and the DDDC tests results (Table 4.5) along with the drop size dependence of sessile drop dynamic contact angle data given in Tables 4.9-4.11 were used to estimate W_{sow}. Computed W_{sow} for each system (Table 4.9-4.11) were plotted against sessile oil drop volume ratio. A plot of W_{sow} versus sessile oil drop volume ratio relationships for these systems is shown in Figure 4.21. The varying slope observed in the work of adhesion versus drop volume ratio relationships for the quartz, dolomite and calcite surfaces indicates that more work is required to remove oil from an oil-wet system due to the formation of oil film on the rock surface compared to a water-wet system where no such oil film is formed due to the presence of weak rock/oil adhesion interactions.

Table 4.9: Estimated W_{sow} for the quartz/B-RLO/B-SRB system at 1,500 psi & 238°F

Quartz/B-RLO/B-SRB system (measured σ = 0.00221 mN) γ_{ow} = 23.58 mN/m (θ_r = 24°, initial aging time of large sessile drop = 24 h)							
Vol. red. step No.	**Water-advancing contact angle, θ_a (°)**	**Cos θ_a**	**Contact radius, r (in)**	**Contact radius, r (m)**	**Drop volume ratio***	**Work of adhesion/area W_{sow}, (J/m^2) Eq.(17)**	**Work of adhesion/area W_{sow}, (mJ/m^2) Eq.(17)**
1	24	0.9135	0.119	3.03E-03	0.85	2.04E-03	2.04
2	24	0.9135	0.091	2.31E-03	0.73	2.04E-03	2.04
3	24	0.9135	0.072	1.84E-03	0.48	2.04E-03	2.04
4	24	0.9135	0.050	1.28E-03	0.36	2.04E-03	2.04
5	24	0.9135	0.032	8.02E-04	0.24	2.04E-03	2.04
6	40	0.766	0.022	5.51E-04	0.15	5.52E-03	5.52

*Drop volume ratio =Volume of sessile oil drop at a given drop size red. step / Volume of initial sessile oil drop

Table 4.10: Estimated W_{sow} for the dolomite/B-RLO/B-SRB system at 1,500 psi & 238°F

Dolomite/B-RLO/B-SRB system, (measured σ = 0.236 mN) γ_{ow} = 23.58 mN/m (θ_r = 28°, initial aging time of large sessile drop = 24 hr)							
Vol. red. step No.	**Water-advancing contact angle, θ_a,(°)**	**Cos θ_a**	**Contact radius, r (in)**	**Contact radius, r (m)**	**Drop volume ratio***	**Work of adhesion/area W_{sow}, (J/m^2) Eq.(17)**	**Work of adhesion/area W_{sow}, (mJ/m^2) Eq.(17)**
1	32	0.848	0.1563	3.97E-03	0.89	3.58E-03	3.58
2	34	0.829	0.1563	3.97E-03	0.81	4.03E-03	4.03
3	45	0.7071	0.1563	3.97E-03	0.39	6.91E-03	6.91
4	51	0.6293	0.1488	3.78E-03	0.18	8.74E-03	8.74
5	79	0.1908	0.1260	3.20E-03	0.11	1.91E-02	19.08

*Drop volume ratio =Volume of sessile oil drop at a given drop size red. step / Volume of initial sessile oil drop

Table 4.11: Estimated W_{sow} for the calcite/B-RLO/B-SRB system at 1,500 psi & 238°F

Calcite/B-RLO/B-SRB system, (measured σ = 0.555 mN) γ_{ow} = 23.58 mN/m (θ_r = 32° initial aging time of large sessile drop = 24 hr)							
Vol. red. step No.	**Water-advancing contact angle, θ_a,(°)**	**Cos θ_a**	**Contact radius, r (in)**	**Contact radius, r (m)**	**Drop volume ratio***	**Work of adhesion/area W_{sow}, (J/m^2) Eq.(17)**	**Work of adhesion/area W_{sow}, (mJ/m^2) Eq.(17)**
1	49	0.6561	0.121	3.08E-03	0.92	8.11E-03	8.11
2	65	0.4226	0.118	3.00E-03	0.83	1.36E-02	13.62
3	92	-0.0349	0.116	2.94E-03	0.55	2.44E-02	24.40
4	110	-0.342	0.114	2.90E-03	0.35	3.16E-02	31.64
5	162	-0.9511	0.101	2.57E-03	0.08	4.60E-02	46.01

*Drop volume ratio =Volume of sessile oil drop at a given drop size red. step / Volume of initial sessile oil drop

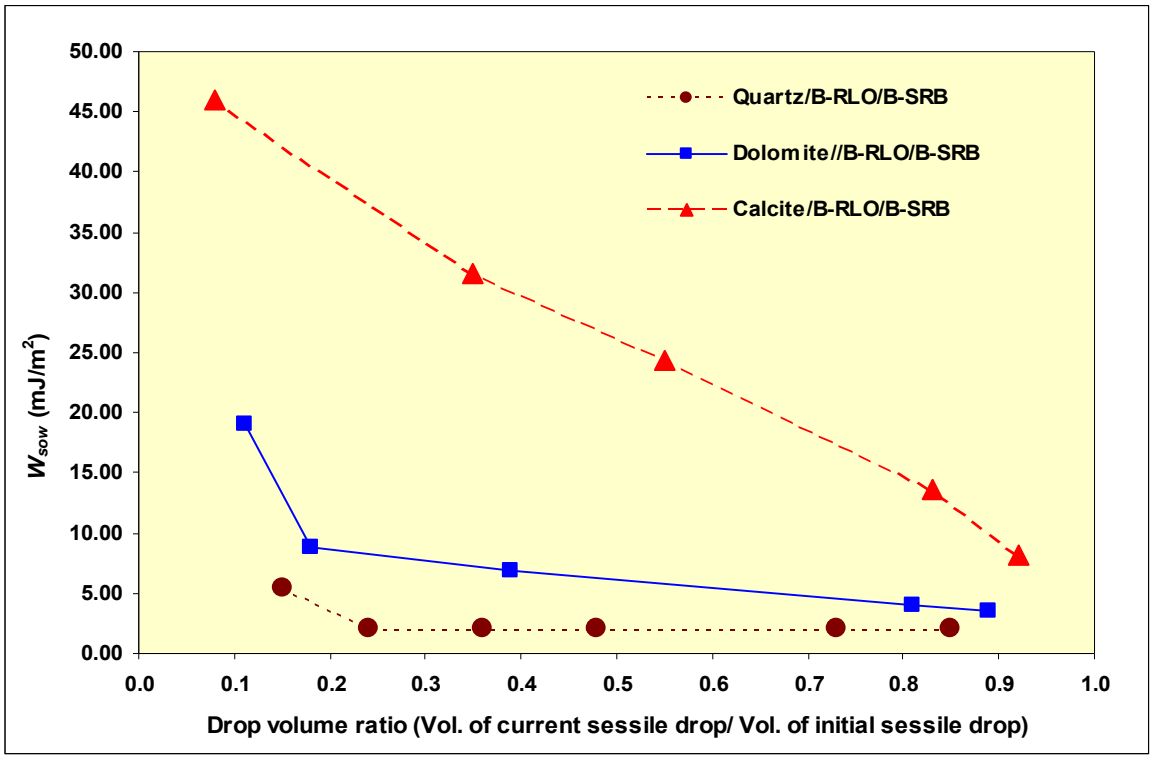

Figure 4.21: W_{sow} versus sessile oil drop volume ratio relationship for B-RLO at 1,500 psi & 238°F

Higher values of the work of adhesion at lower drop volume ratio (Figure 4.21) for the calcite system indicate that more and more work needs to be exerted in order to displace the residual oil in the oil-wet system as oil saturation decreases.

Table 4.12: Computed W_{sow} for B-RLO at 1,500 psi & 238°F using Eq.17 and Eq.6

Rock/oil/water system	The work of adhesion $W_{sow,}$ (mJ/m^2), Eq.(17)	The work of adhesion $W_{sow,}$ (mJ/m^2), Eq.(6)	Ratio = W_{sow} (Eq.17)/ W_{sow} (Eq.6)
Quartz/B-RLO/B-SRB	5.51	2.04	3
Dolomite/B-RLO/B-SRB	19.08	2.76	7
Calcite/B-RLO/B-SRB	46.01	3.58	13

These results demonstrate the usefulness of Eq.17 in the experimental evaluation of the effect of the extent of rock/oil adhesion interactions on the mobilization of residual oil.

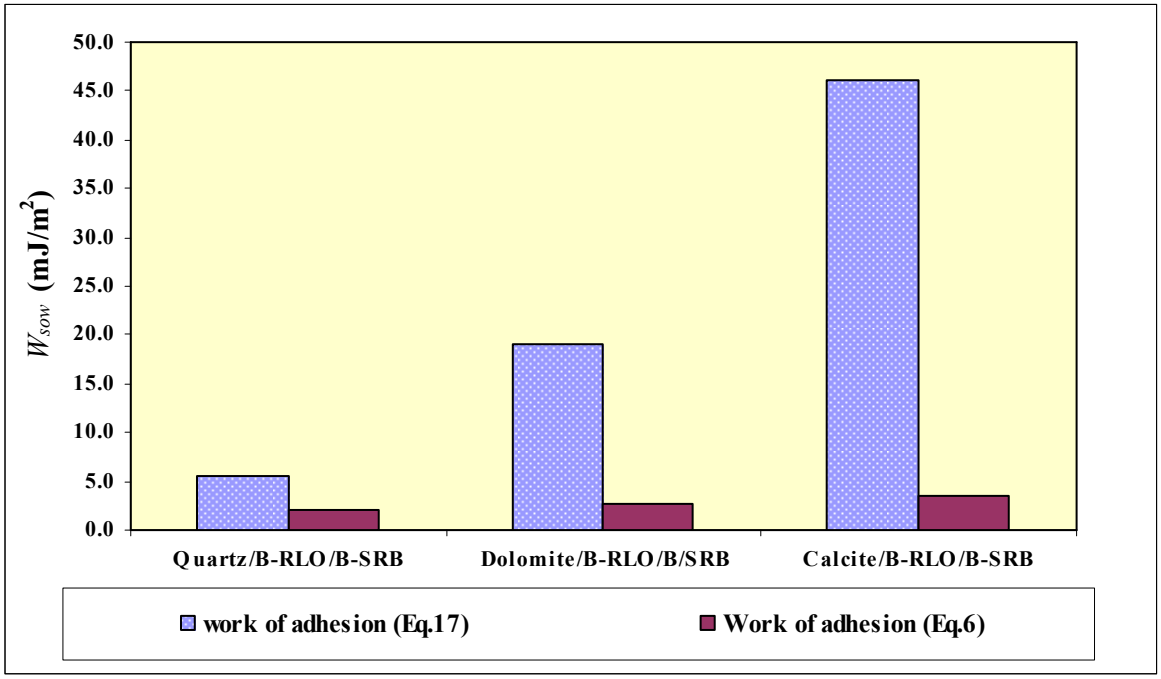

Figure 4.22: Computed W_{sow} for B-RLO at 1,500 psi & 238°F using Eq.17 and Eq.6

For each rock/oil/water system, a W_{sow} value corresponding to θ_a (measured in the DDDC test) was also computed using Eq.17. These values then were compared with the estimated W_{sow} values computed by using Eq.6 ($\theta_\infty = \theta_r$). The comparison results are given in Table 4.12 and are plotted in Figure 4.22. In the case of the calcite (oil-wet) system, the work of adhesion is significantly higher (13 times at 0.1 drop volume ratio) when accounting for the extent of the rock/oil adhesion interactions (Eq.17) as compared to when these adhesion interactions are not considered (Eq.6).

In the next section, the use of the line tension-based modified form of the equation for the work of adhesion (Eq.17) to derive a new equation for estimating the magnitude of intermolecular surface forces in terms of the maximum change in the adhesion energy per unit area are discussed. This maximum change in the adhesion energy per unit area is estimated for a change in distance as

the pair of interfaces is brought from a large separation to a finite thickness. This process is equivalent to the measurement of a maximum disjoining pressure. This equation was derived on the basis of experimental results discussed in Sections 4.1 and 4.2.

4.3 A New Approach for Determining the Magnitude of Maximum Disjoining Pressure at Reservoir Conditions

4.3.1 Determination of Intermolecular Surface Forces in Terms of Adhesion Energy per Unit Area

The different experimental techniques discussed in the Sub-Section 2.4.1.2 for measuring the magnitude of intermolecular surface forces provide an experimental means to quantify the rock/fluids interactions either in terms of the disjoining pressure or the adhesion energy per unit area by considering the presence and stability of thin aqueous wetting films. The experimental results are generally correlated with the equilibrium (Young's) contact angle, θ_∞ (Basu and Sharma, 1996; Drummond and Israelachvili, 2002). Good agreement is observed in the measured and computed intermolecular forces either in terms of disjoining pressure or the work of adhesion and the observed behavior is explained in terms of the presence and the stability of the thin aqueous wetting films. However, these experimental approaches are of limited use for characterizing rock/fluids interactions in complex rock/oil/water systems at reservoir conditions. The use of these techniques has only been reported in the literature in conducting such studies at ambient conditions using either pure hydrocarbons or stock-tank oil as the fluid phase.

It appears that the experimental results presented in Sections 4.1 and 4.2, and their interpretations can be used to measure the magnitude of different intermolecular surface forces present in rock/oil/water systems at reservoir conditions. As discussed in Sections 4.1 and 4.2, θ_a corresponds to θ_∞ in non water-wet systems where strong rock/oil adhesion interactions are present. This can also be explained in terms of the presence and the stability of the thin aqueous wetting films. In the presence of the stable aqueous wetting films in the system, it is observed that

$\theta_a=\theta_\infty=\theta_r$, and water-wet behavior is exhibited by the system. When the strong rock/oil adhesion interactions are present in the system, then we find that $\theta_a=\theta_\infty\neq\theta_r$. This situation is normally explained in terms of complete drainage of a thin aqueous wetting film squeezed between the bulk oil phase and the rock surface or the reduction of this thickness to a few molecules that results in the development of strong rock/oil adhesion interactions in the system and a wetting behavior ranging from weakly water-wet to oil-wet behavior is observed

On the basis of the experimental results that are discussed in Sections 4.1 and 4.2, a new equation based on the experimental estimation of the work of adhesion (the adhesion energy per unit area) using the DDDC technique and the sessile oil drop volume alteration method for computing the maximum disjoining pressure (i.e. the maximum change in the energy per unit area with change in distance at the pair of interfaces is brought from a large separation to a finite thickness) was proposed. While conducting the DDDC tests and the sessile oil drop volume alteration experiments, irrespective of its wetting characteristics, each rock/oil/water system showed a low value of θ_r (Tables 4.6 and 4.7). This clearly demonstrates the presence of a stable aqueous wetting film between the mineral surface and the sessile oil drop during the formation of the sessile drop. The moment, when the bulk oil phase first comes into contact with the mineral surface, the contact angle formed by the sessile oil drop with the mineral surface corresponds to the water receding contact angle (θ_r). After some time, when the equilibrium is disturbed, depending on the extent of rock/oil adhesion interactions, the measured contact angle (θ_a) may be significantly different from the initial contact angle (θ_r) value.

As evident from the results discussed in the Section 4.1 and 4.2, water-wet systems exhibited small deviation between the measured contact angles (θ_a and θ_r) on disturbing initial equilibrium in the DDDC or the sessile drop volume alteration experiments. However, non-water wet systems showed significant contact angle hysteresis (θ_a-θ_r) on disturbing initial equilibrium. Hence, Eq.17 and Eq.6 can be used to compute the change in the adhesion energy per

unit area after attaining equilibrium in the system and the moment oil comes in contact with the mineral surface, respectively. This situation actually mimics the pristine drainage process that occurred over the long geological time in petroleum reservoirs. Hence, the difference in the computed adhesion energy per unit area at these two times can be used to estimate the magnitude of intermolecular surface forces experienced by the system due to rock/fluids interactions manifested by the observed contact angle hysteresis.

Mathematically, the adhesion energy per unit area at time t=0 (when the stable wetting aqueous film is present in the system) can be expressed using Eq.6:

$$(W)_{t=0} = (W_{sow})_{t=0} = \gamma_{ow}(1 - Cos\theta_{\infty}) = \gamma_{ow}(1 - Cos\theta_r) \quad \text{(18)}$$

The adhesion energy per unit area at equilibrium time can be expressed using Eq.17:

$$(W)_t = (W_{sow})_t = \gamma_{ow}(1 - Cos\theta_a) \quad \text{(19)}$$

Subtracting Eq.18 from Eq.19 yields:

$$\Delta W = (W_{sow})_t - (W_{sow})_{t=0} = \gamma_{ow}(1 - Cos\theta_a) - \gamma_{ow}(1 - Cos\theta_r)$$

Or

$$\Delta W = (W_{sow})_t - (W_{sow})_{t=0} = \gamma_{ow}(Cos\theta_r - Cos\theta_a) \quad \text{(20)}$$

Equation 20 provides a way to experimentally estimate the magnitude of intermolecular surface forces present in rock/oil/water systems in terms of the measureable quantities of the oil/water IFT, the water-receding contact angle (θ_r) and the water-advancing contact angle (θ_a). Also, θ_a and θ_r measured in the DDDC test are the extreme values of these contact angles shown by the system. Hence, Eq.20 corresponds to the maximum change in the adhesion energy per unit area shown by the particular rock/oil/water systems. These quantities can be measured at reservoir conditions using representative reservoir fluids with the help of the pendant drop method and the DDDC contact angle measurement technique, respectively using the HPHT DDDC optical cell.

4.3.1.1 Estimation of ΔW for B-RLO at Reservoir Conditions

Using the methodology discussed in Sub-Section 4.3.1, an effort was made to estimate the magnitude of intermolecular surface forces in different rock/oil/water systems at reservoir conditions using Eq.20. Computed ΔW for these systems is given in Table 4.13.

Table 4.13: Estimated ΔW for B-RLO at 1,500 psi & 238°F

Rock/oil/water system	Work of adhesion W_{sow}, (mJ/m^2), Eq.(17)	Work of adhesion W_{sow}, (mJ/m^2), Eq.(6)	ΔW (mJ/m^2) Eq.(20)
Quartz/B-RLO/B-SRB	5.51	2.04	3.47
Dolomite/B-RLO/B-SRB	19.08	2.76	16.32
Calcite/B-RLO/B-SRB	46.01	3.58	42.43

The change in the adhesion energy per unit area (ΔW) was significantly higher in the calcite (oil-wet) system compared to the quartz (water-wet) system. Ideally in a perfectly water-wet system, the ΔW value should be zero (no contact angle hysteresis). However, a low value of ΔW in a water-wet system indicates the presence of weak rock/oil adhesion interactions in systems. Similar observations were made by Rao and Maini (1993) while reporting the results of the adhesion test conducted with live oil at reservoir conditions for a water-wet system. They concluded that the rupture of the thin aqueous wetting films may not be the necessary condition for the development of adhesion between the rock surface and the oil phase even in a water-wet system.

4.3.2 Determination of Adhesion Energy per Unit Volume (Correlatable to Maximum Disjoining Pressure) at Reservoir Conditions

Equation 20 provides a way to experimentally determine the magnitude of intermolecular surface forces present in a rock/oil/water system in terms of the maximum change in the adhesion energy per unit area. This equation can be conveniently converted into the maximum change in the

adhesion energy per unit area with the change in distance as the pair of interfaces is brought from a large separation to a finite thickness (i.e. maximum disjoining pressure) as it happens in both the DDDC and the sessile oil drop volume alteration experiments. If an appropriate thickness of the aqueous wetting film squeezed between the sessile oil drop and the mineral surface is used, the relationship between the disjoining pressure and the adhesion energy per unit area (Eq.4) can be used to derive an expression to estimate the magnitude of a maximum disjoining pressure by dividing ΔW (Eq.20) by appropriate thickness value, h.

An expression for the change in the adhesion energy per unit area with respect to the thickness of the aqueous wetting film, h, or the adhesion energy per unit volume can be written as:

$$E_{adhesion} = \frac{\gamma_{ow}(Cos\theta_r - Cos\theta_a)}{h} \quad \text{.....} \quad (21)$$

An appropriate value for the thickness of the aqueous wetting films appears to be of the order of 10 Å as found in the published literature (Figure 4.23[13]).

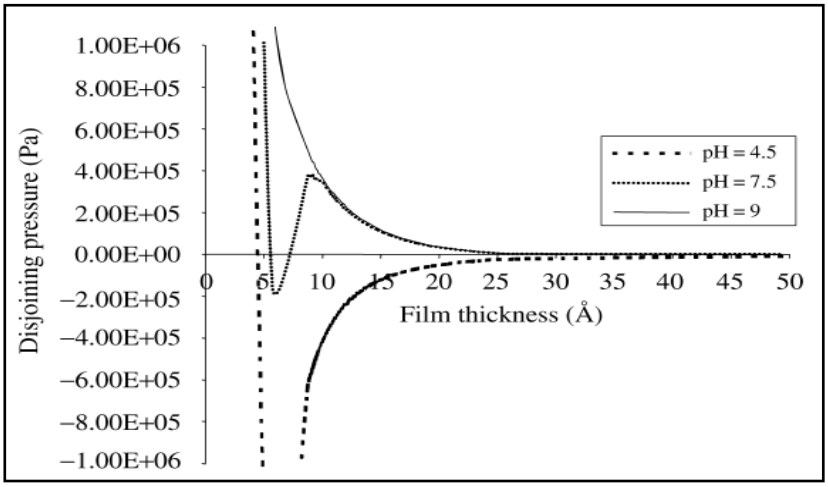

Figure 4.23: Reservoir condition disjoining pressure isotherms for Berea/Yates crude oil/Yates brine system (Busireddy and Rao, 2007)

[13] © ELSEVIER 2007, reproduced with permission

Similar values of the thickness of the aqueous wetting films have been suggested in other published studies (Hirasaki, 1991; Melrose, 1982).

During the DDDC and the drop volume alteration experiments, the aqueous wetting film trapped between the mineral surface and the sessile oil drop is reduced to such an extent that the maximum effect of these intermolecular surface forces can be felt easily by the system as manifested by a significant contact angle hysteresis (θ_a-θ_r) observed in non water-wet rock/oil/water systems. Hence, using an assumed appropriate value of the aqueous wetting films, the adhesion energy per unit volume can be obtained using Eq 21. Equation 21 is of practical importance as it provides an experimental means for estimating the magnitude of different intermolecular surface forces present in the complex rock/oil/water systems which corresponds to a spontaneous change in the wetting behavior.

4.3.2.1 Determination of Adhesion Energy per Unit Volume at Reservoir Conditions, B-RLO

Using the methodology discussed in Sub-Section 4.3.2, an attempt was made to estimate the adhesion energy per unit volume ($E_{adhesion}$) at reservoir conditions for different rock/oil/water systems using the ΔW data (Table 4.13) and various assumed thicknesses values for the aqueous wetting films. The reservoir condition disjoining pressure isotherms curves reported in the literature (Busireddy and Rao, 2007) showed a value of around 6 Å (Figure 4.23). The results from these calculations can be seen in Table 4.14 and Figure 4.24.

Table 4.14: Estimated $E_{adhesion}$ (from Eq.21) for B-RLO at 1,500 psi & 238°F

Rock/oil/water system	$E_{adhesion}$ (Pa) (Eq.21)			
	h = 6 Å	h = 50 Å	h = 100 Å	h = 500 Å
Quartz/B-RLO/B-SRB	1.20E+06	1.44E+05	7.21E+04	1.44E+04
Dolomite/B-RLO/B-SRB	2.92E+07	3.51E+06	1.75E+06	3.51E+05
Calcite/B-RLO/B-SRB	6.87E+07	8.24E+06	4.12E+06	8.24E+05

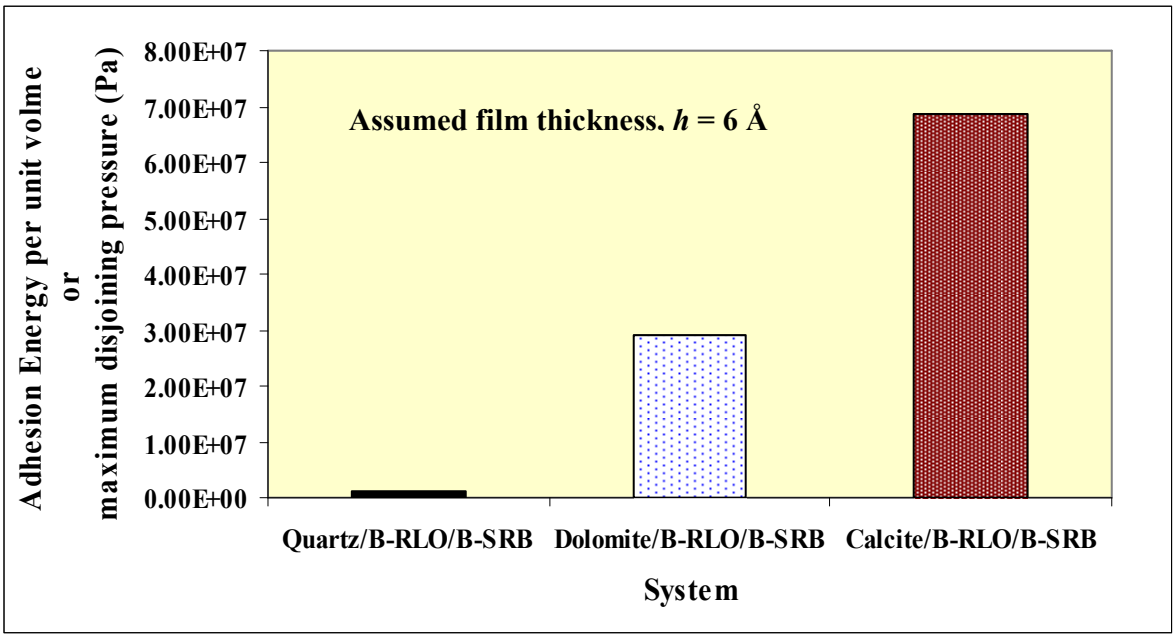

Figure 4.24: Estimated $E_{adhesion}$ (Eq.21) for B-RLO at 1,500 psi & 238°F

All three systems exhibited a positive value for the adhesion energy per unit volume due to the attractive nature of intermolecular surface forces present in the system. The disjoining pressure was largest for the calcite system. At the 6 Å thickness film, the maximum disjoining pressure value was one order of magnitude higher for oil-wet (calcite/B-RLO/B-SRB) compared to water-wet (quartz/B-RLO/B-SRB) system.

This appears to be the first time that an estimate has been made for maximum disjoining pressure for a complex rock/oil/water system at reservoir conditions. The results presented in the Table 4.14 are of practical importance because they can be used to predict the wetting behavior at the pore level. The results suggest that if a capillary pressure of $1.20x10^{+06}$ Pa (174 psi) in a water-wet system such as the quartz/B-RLO/B-SRB system is imposed then a spontaneous change in the wetting behavior may be observed. On the other hand, a significantly high capillary pressure ($8.24x10^{+06}$ Pa (~1200 psi) at 50 A°) must be applied in the oil-wet system such as the calcite/B-RLO/B-SRB system to move any residual oil in oil-wet pores.

In the next section, experimental results for two glass/Y-RLO/Y-SRB systems at reservoir conditions of 700 psi and 82°F are presented. The published results (Busireddy and Rao, 2007) of theoretically determined disjoining pressure isotherms at these conditions (Figure 2.19) are compared with the experimentally estimated adhesion energy per unit volume values (Eq.21).

4.4 Characterization of Rock/fluids Interactions, Y Oil Field

4.4.1 Oil/water IFT Measurements

In the first step, the IFT for two live oil/water systems were measured at 700 psi and 82°F using the pendant drop method. Images of live oil pendant drops captured during these experiments are shown in Figure 4.25. The measured average values of the equilibrium oil/water IFT at reservoir conditions are given in Table 4.15.

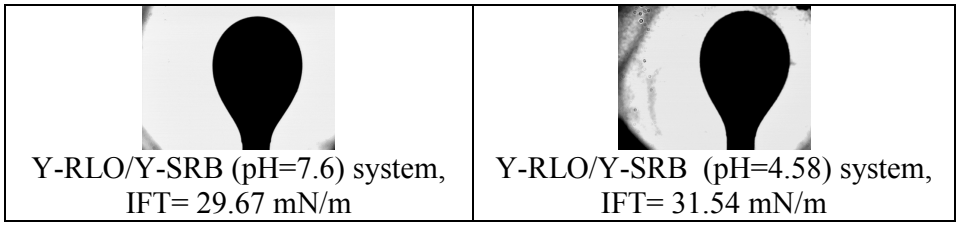

Y-RLO/Y-SRB (pH=7.6) system, IFT= 29.67 mN/m

Y-RLO/Y-SRB (pH=4.58) system, IFT= 31.54 mN/m

Figure 4.25: Reservoir condition pendant drop images, Y-RLO

Table 4.15: Measured oil/water IFTs for Y-RLO at 700 psi & 82°F

Oil/water system	Pressure and temperature Conditions	No. of pendant drops	Average equilibrium interfacial tension (mN/m)	Standard deviation (mN/m)
Y-RLO/Y-SRB(pH=7.6)	700 psi, 82°F	5	29.67	±0.48
Y-RLO/Y-SRB(pH=4.58)	700 psi, 82°F	5	31.54	±0.76

Y-RLO-Y recombined live oil, Y-SRB-Y synthetic reservoir brine

4.4.2 The Sessile Oil Drop Volume Alteration Experiments

In the second step, the sessile oil drop volume alteration experiments were conducted. A series of captured images of varying drop size during the experiments are shown in Figure 4.26. Both systems, i.e. glass/Y-RLO/Y-SRB (pH=7.6) and glass/Y-RLO/Y-SRB (pH=4.58), showed low values of θ_r (29° and 45° respectively) on gradually increasing the drop size in order to obtain a sufficiently large sessile oil drop. A small variation of 2-3° was observed in θ_r values during this step. Low values of θ_r clearly indicate the presence of an aqueous wetting film trapped between the sessile oil drop and the glass surface. A change in the pH from 7.6 to 4.58 was done by adding a few drops of HCl to synthetic reservoir brine.

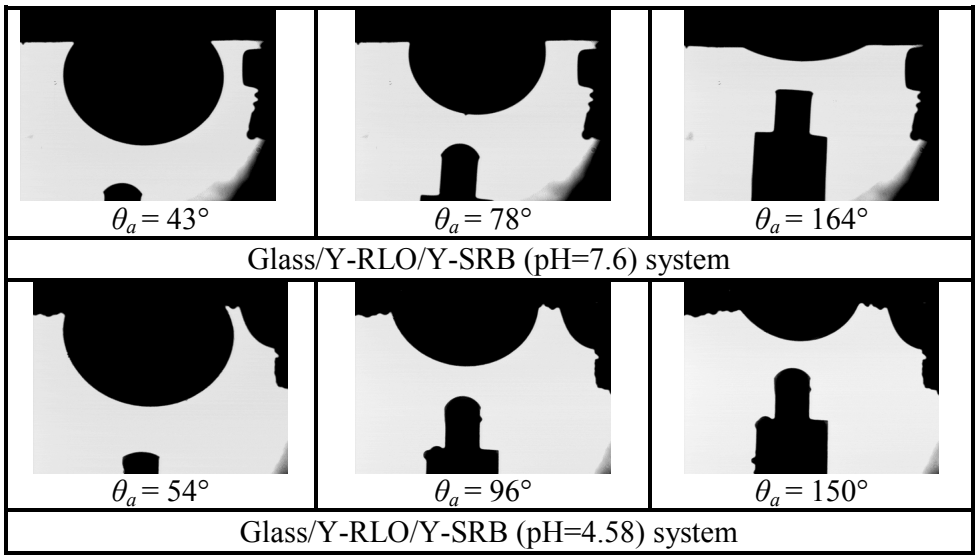

Figure 4.26: The sessile oil drop volume alteration experiments for Y-RLO conducted at 700 psi & 82°F

A higher water-receding contact angle (45°) value was exhibited by low pH (4.58) system compared to high pH (7.6) system where a water-receding contact value of 29° was observed. Thus, lower brine pH resulted in an increased spreading of an oil drop on the glass surface in the presence of the aqueous wetting film. All of the pH values mentioned here are ambient condition values.

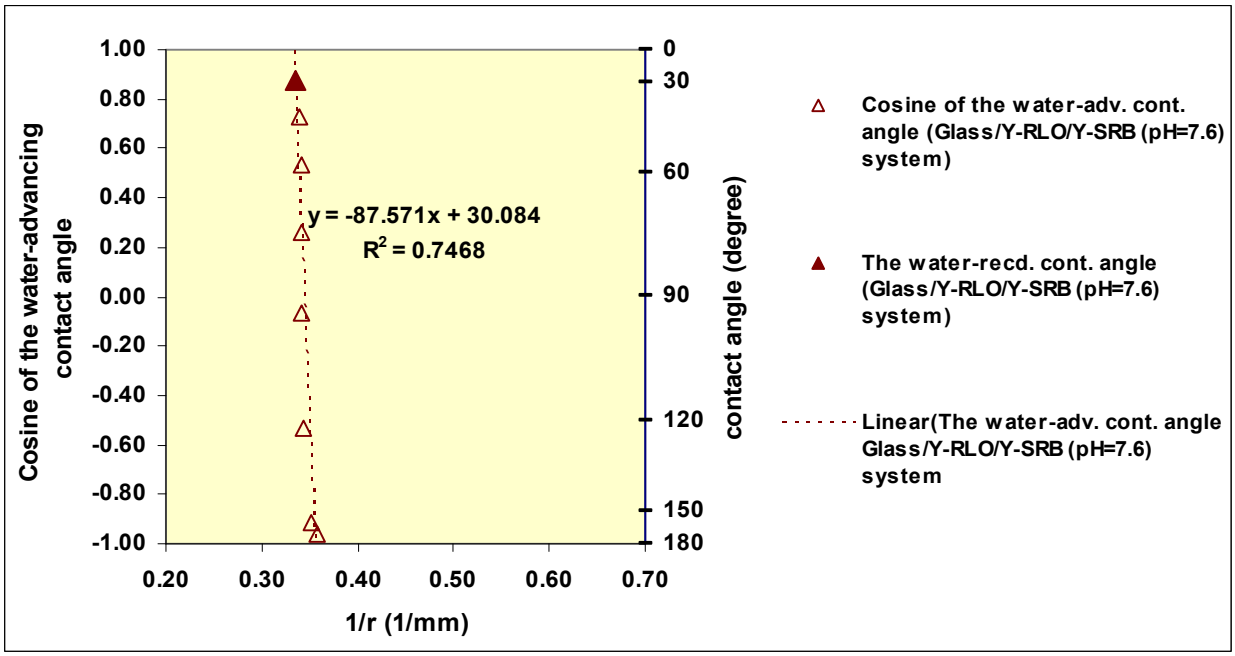

Figure 4.27: *Cosθ_a* versus *1/r* relationship for the glass/Y-RLO/Y-SRB (pH=7.6) system at 700 psi & 82°F

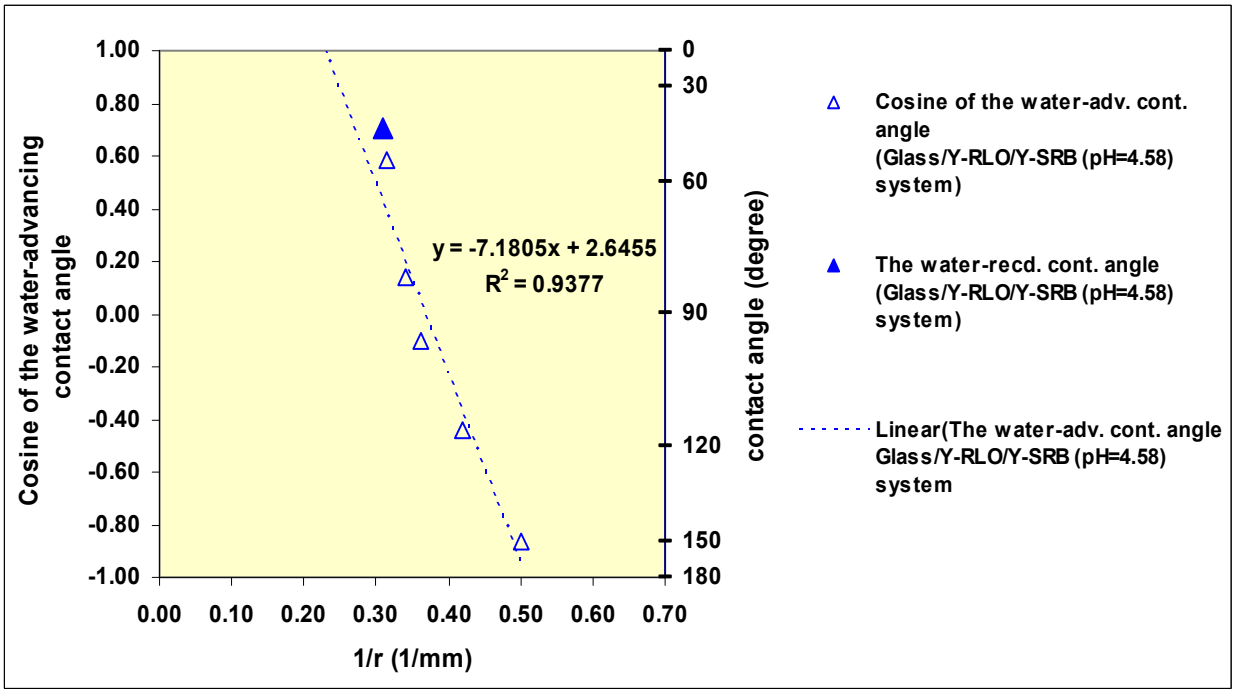

Figure 4.28: *Cosθ_a* versus *1/r* relationship for the glass/Y-RLO/Y-SRB (pH=4.58) system at 700 psi & 82°F

The line tension values for both the systems were estimated using the measured oil/water IFT and the observed slopes in the $Cos\theta_a$ versus *1/r* relationships exhibited by them. These graphs are shown in Figures 4.27-4.28. The measured line tension values are given in Table 4.16. The high pH system showed a limited movement of the contact line (steep slope in the $Cos\theta_a$ versus *1/r* graph), thus indicating the presence of relatively stronger adhesion interactions (high line tension value of 2.60 mN) between the live oil and the glass surface. A low line tension value of 0.23 mN was observed in the case of low pH system. The increased spreading behavior and corresponding lower line tension value appears to be affected only by the lower pH.

Table 4.16: Measured line tension for Y-RLO at 700 psi & 82°F

Rock/oil/water system	Variation in contact radius (mm)	Slope of $Cos\theta_a$ versus *1/r* (1/mm) plot	Line tension, σ (mN)
Glass/Y-RLO/Y-SRB (pH=7.6) system	2.98 to 2.79	-87.57	2.60
Glass/Y-RLO/Y-SRB (pH=4.58) system	3.24 to 1.99	-7.18	0.23

Y-RLO- Y recombined live oil, Y-SRB-Y synthetic reservoir brine

4.4.3 Estimation of the Work of Adhesion at Reservoir Conditions, Y-RLO

Equation 17 was used to estimate the work of adhesion, $W_{sow,}$ for both high and low pH systems. The measured oil/water IFT (Table 4.15) data along with the drop size dependence of the sessile oil drop dynamic contact angle data given in Tables 4.17-4.18 were used to estimate W_{sow} for these systems. The estimated W_{sow} for both systems were plotted against sessile oil drop volume ratio and are shown in Figure 4.29. The W_{sow} versus drop volume ratio plots for both systems are

similar to the W_{sow} versus drop volume ratio plot obtained for the calcite (oil-wet) system (Figure 4.21). This clearly indicates the presence of strong rock/oil adhesion interactions in both systems.

Table 4.17: W_{sow} for the glass/Y-RLO/Y-SRB (pH=7.6) system at 700 psi & 82°F

Glass/Y-RLO/Y-SRB(pH=7.6) system, (measured σ = 2.60 mN) γ_{ow} = 29.67 mN/m (θ_r = 29°, initial aging time of large sessile drop = 24 h)							
Vol. red. Step No.	**Water-advancing contact angle, θ_a, (°)**	**$Cos\theta_a$**	**Contact radius, *r* (in)**	**Contact radius, *r* (mm)**	**Drop volume ratio***	**Work of adhesion/area W_{sow}, (J/m^2) Eq.(17)**	**Work of adhesion/area W_{sow}, (mJ/m^2) Eq.(17)**
1	43	0.7314	0.1160	2.9473	0.5496	7.97E-03	7.97
2	58	0.5299	0.1153	2.9298	0.4029	1.39E-02	13.95
3	75	0.2588	0.1153	2.9298	0.2801	2.20E-02	21.99
4	94	-0.0698	0.1153	2.9298	0.1357	3.17E-02	31.74
5	122	-0.5299	0.1147	2.9124	0.0702	4.54E-02	45.39
6	156	-0.9135	0.1119	2.8426	0.0543	5.68E-02	56.77
7	164	-0.9613	0.1102	2.7990	0.0363	5.82E-02	58.19

*Drop volume ratio =Volume of sessile oil drop at a given drop size red. step/Volume of initial sessile oil drop

Table 4.18: W_{sow} for the glass/Y-RLO/Y-SRB (pH=4.58) system at 700 psi & 82°F

Glass/Y-RLO/Y-SRB(pH=4.58) system, (measured σ = 0.23 mN) γ_{ow} = 31.54 mN/m (θ_r = 45°, initial aging time of large sessile drop = 24 h)							
Vol. red. Step No.	**Water-advancing contact angle, θ_a, (°)**	**$Cos\theta_a$**	**Contact radius, r (in)**	**Contact radius, r (mm)**	**Drop volume ratio***	**Work of adhesion/area W_{sow}, (J/m^2) Eq.(17)**	**Work of adhesion/area W_{sow}, (mJ/m^2) Eq.(17)**
1	54	0.5878	0.1256	3.1900	0.8034	1.30E-02	13.00
2	82	0.1392	0.1155	2.9335	0.4896	2.72E-02	27.15
3	96	-0.1045	0.1089	2.7652	0.3162	3.48E-02	34.84
4	116	-0.4384	0.0937	2.3805	0.1193	4.54E-02	45.37
5	150	-0.8660	0.0786	1.9958	0.0599	5.89E-02	58.85

*Drop volume ratio =Volume of sessile oil drop at a given drop size red. step/Volume of initial sessile oil drop

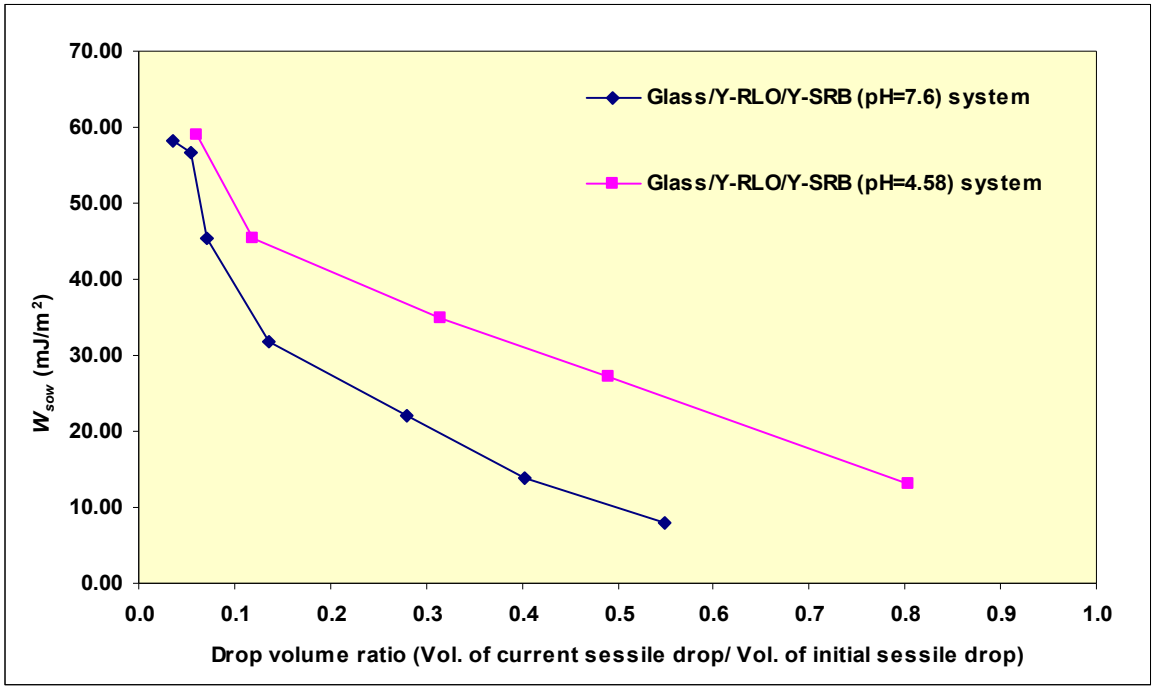

Figure 4.29: W_{sow} versus sessile oil drop volume ratio relationship for Y-RLO at 700 psi & 82°F

As can be seen in Figure 4.29, low pH system showed a higher W_{sow} value at a given drop volume ratio than high pH system despite the measured line tension value for low pH system being significantly smaller (0.23 mN) than high pH system (2.60 mN). This observed behavior may be attributed to the facilitation of the formation of two new oil/water interfaces (remaining sessile oil drop and the fraction of sessile oil drop withdrawn into the injector tip) during the volume reduction process due to the presence of relatively stronger rock/oil adhesion interactions in the high pH system compared to low pH system.

4.4.4 Estimation of Adhesion Energy per Unit Volume at Reservoir Conditions, Y-RLO

Using the methodology discussed in Sub-Section 4.3.2, values for the adhesion energy per unit volume (correlatable to maximum disjoining pressure) for both high and low pH systems were estimated at reservoir conditions using Eq.21. The measured oil/water IFT (Table 4.15), the water-receding contact angle (θ_r), and the maximum value of the water-advancing contact angle (θ_a) (Tables 4.17-4.18) were used to compute the $E_{adhesion}$ using Eq.21 at an assumed aqueous wetting film thicknesses of 6 Å. The film thickness was chosen to correspond to the value found for the theoretically determined maximum disjoining pressure values at 6 Å (Figure 2.19). A comparison of the $E_{adhesion}$ values and the maximum disjoining pressure value derived from Figure 2.19 is given in Table 4.19.

Table 4.19 shows that the theoretically determined reservoir condition maximum disjoining pressure values for the glass/oil/brine systems are about an order of magnitude lower than the value of the adhesion energy per unit volume estimated using Eq.21. These values do not appear to be affected significantly by a change in the pH of the aqueous phase. However, the theoretically determined maximum disjoining pressure (Figure 4.19) shows a significantly increase at low pH. The published theoretical model (Busireddy and Rao, 2007) is only valid for the water-wet case. It appears that this conclusion was derived on the basis of low values of the water-receding contact angles measured for a sessile oil drop that correspond to the equilibrium (Young's) contact angles

in complex rock/oil/water systems. However, the results of the sessile oil drop volume alteration experiments conducted for the glass/oil/water systems clearly demonstrate the presence of strong rock/oil adhesion interactions in these systems. Thus, the results found make sense as similar behavior was observed in the theoretically determined disjoining pressure curves shown in Figure 2.19 when the thickness of the aqueous wetting film was of the order of 6 Å.

Table 4.19: Comparison of the estimated $E_{adhesion}$ (Eq.21) for Y-RLO with the theoretically determined maximum disjoining pressure values derived from Fig 2.19

Rock/oil/water system	$E_{adhesion}$, (Pa) at h = 6 Å, (Eq.21)	Theoretically determined maximum disjoining pressure, (Pa) derived from Fig. 2.19, (Busireddy and Rao, 2007)	Ratio (Column 2/Column 3)
Glass/Y-RLO/Y-SRB (pH=7.6) system	9.08E+07	1.10E+06 (attractive)	82.5
Glass/Y-RLO/Y-SRB (pH=4.58) system	8.27E+07	> 1.50E+06 (attractive)	55.1 (assuming a value of 1.50E+06 in column 3)

The proposed equation (Eq.21) to compute adhesion energy per unit volume appears to provide an experimental means for estimating the maximum disjoining pressure value in complex rock/oil/water systems at reservoir conditions using representative reservoir fluids and common reservoir rock mineral surfaces. This value corresponds to a spontaneous change in wetting behavior or the collapse of the aqueous wetting film as manifested by the observed large contact angle hysteresis in the contact angle experiments and the maximum negative disjoining pressure value on the theoretical disjoining pressure curves.

In the next section, the results of experiments conducted for characterizing rock/fluids interactions at reservoir conditions of elevated pressures (up to 13,454 psi) and temperatures (up to 250°F) are presented and discussed for the F reservoir, a Gulf of Mexico (GOM) deepwater offshore oil reservoir.

4.5 Characterization of Rock/fluids Interactions, F Reservoir

In deepwater offshore reservoirs, the temperatures and pressures often exceed 200°F and 10,000 psi. They present a unique challenge to confidently characterize rock/fluids interactions in such reservoirs. The two Gulf of Mexico (GOM) deepwater offshore oil reservoirs included in this study are designated as F reservoir and T reservoir, respectively.

The F reservoir has an initial pressure of 13,454 psi and reservoir temperature of 208°F. The reported bubble point pressure for the F reservoir is 2,420 psi @ 208°F and the onset pressure for asphaltene precipitation is in the range of 4,500 psi to 5,000 psi. In this study, the oil/water IFTs for different oil/water systems comprising F reservoir fluids were measured using the pendant drop method at pressures ranging from 8,000 psi to 13,454 psi and at temperatures of 175°, 208° and 250°F. The DDDC tests and the sessile oil drop volume alteration experiments were conducted at 10,000 psi and 208°F.

To investigate the effect of oil composition on rock/fluids interactions, both recombined live oil (F-RLO) and stock-tank oil (F-STO) were used to conduct the IFT and contact angle experiments at reservoir conditions. Three different aqueous phases, namely synthetic reservoir brine (F-SRB), synthetic sea water (SSW), and deionized water (DIW) were used to investigate the effect of aqueous phase composition on rock/fluids interactions. SSW was chosen to characterize rock/fluids interactions in the presence of a potential injection fluid in deepwater offshore environment.

Because quartz is the dominant (up to 97%) mineral of the F reservoir rock, polished quartz mineral crystals were used as the solid phase in the contact angle experiments. A few tests were also conducted with the calcite mineral crystals to study the effect of rock mineralogy on the

rock/fluids interactions. Stock-tank oil was used as the oil phase to conduct the ambient condition (atmospheric pressure and 74°F) oil/water IFT and contact angle experiments.

4.5.1 Oil/water IFT Measurements

The IFTs for different oil/water systems were measured by conducting pendant drop experiments at both ambient and reservoir conditions.

4.5.1.1 Ambient Condition Oil/water IFT Results

The results of ambient condition pendant drop experiments are given in Table 4.20. For this, 10-15 pendant drops of stock-tank oil (STO) were formed by injecting STO at a slow rate (~1 drop/90 sec) into the ambient condition optical cell filled with oil equilibrated aqueous phase. The measured oil/water IFT in this situation corresponds to the equilibrium IFT. However, variations were observed in the IFTs measured for individual pendant drops. The average equilibrium IFT values for different oil/water systems are given in Table 4.20. Example images of pendant oil drops captured during these experiments are shown in Figure 4.30. A comparison of the measured oil/water IFT for different oil/water systems is shown in Figure 4.31.

Table 4.20: Measured oil/water IFT at ambient conditions, F reservoir

Oil/water system	F-STO density (gm/cc)	Aqueous phase density (gm/cc)	Density difference (gm/cc)	No. of pendant drops	Average equilibrium interfacial tension (mN/m)	Std. dev. (mN/m)
F-STO/DIW	0.9065	0.9974 (DIW)	0.0909	12	32.69	±0.45
F-STO/SSW	0.9065	1.024 (SSW)	0.1175	10	30.86	±0.53
F-STO/F-SRB	0.9065	1.0172 (F-SRB)	0.1107	13	29.74	±0.74

F-STO- Stock-tank oil (F reservoir), F-SRB- Synthetic reservoir brine (F reservoir), DIW- Deionized water, SSW- Synthetic sea water

Only a small variation in the measured oil/water IFT was observed for a significant variation in the aqueous phase composition. These results suggest that the ambient condition oil/water IFT was not affected significantly by a variation in the aqueous phase composition.

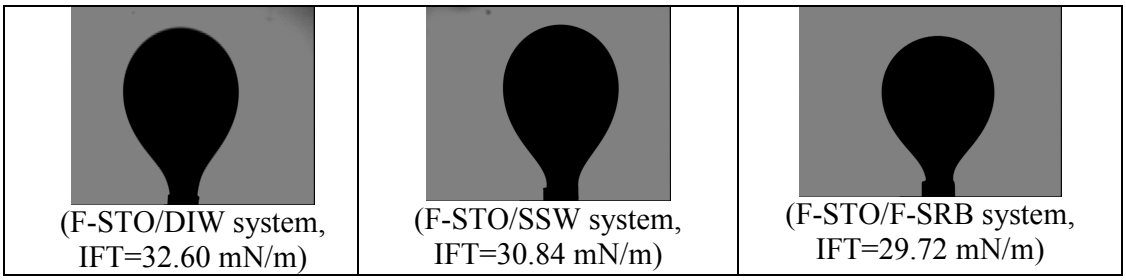

Figure 4.30: Ambient condition pendant drop images, F reservoir

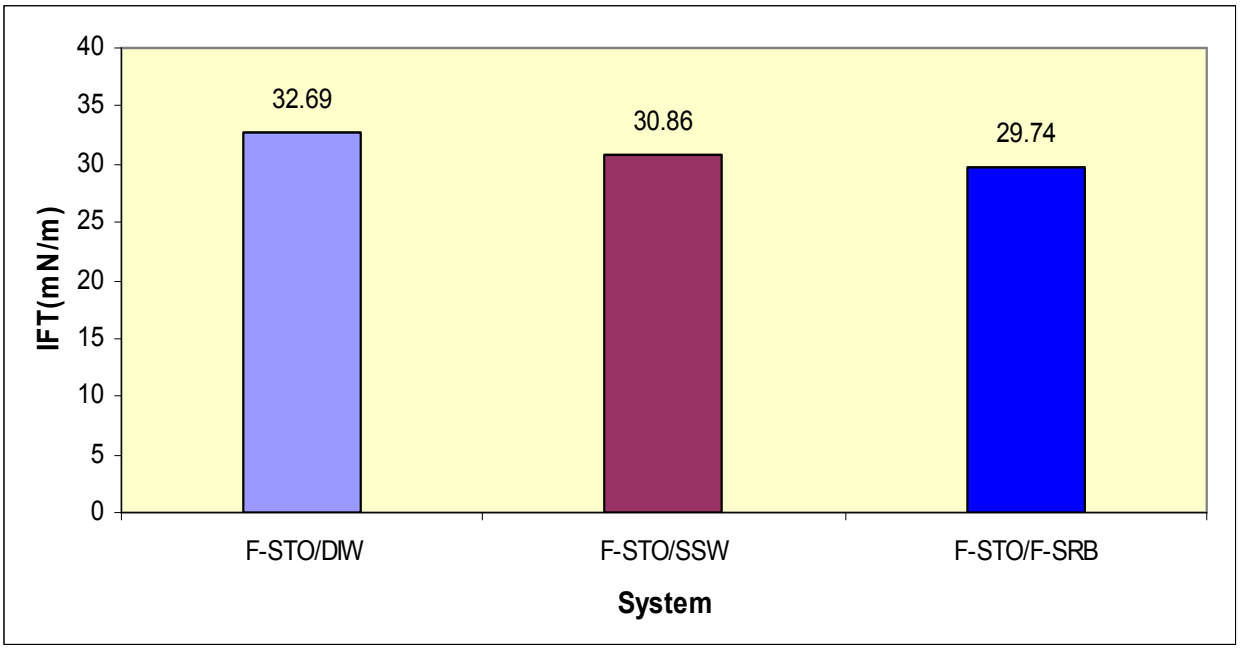

Figure 4.31: Measured oil/water IFT at ambient conditions, F reservoir

4.5.1.2 Reservoir Condition Oil/water IFT Results

In the case of the F reservoir, the oil/water IFT at reservoir conditions was measured by conducting the pendant drop experiments with recombined live oil (F-RLO) and three different aqueous phases (F-SRB, SSW, and DIW) in the pressure range from 8,000 psi to 13,454 psi and at the reservoir temperature of 208°F. To ensure the accuracy of the measured oil/water IFT data, experiments were also repeated at a few pressure steps. The measured IFT data are given in Tables 4.21-4.23. Representative images of pendant drops captured during these experiments are shown in Figures 4.32-4.34.

Table 4.21: Measured oil/water IFT for the F-RLO/F-SRB system at elevated press. & 208°F

F-RLO/F-SRB system								
						IFT values obtained in repeat experiment		
Press.	**F-RLO density**	**F-SRB density**	**Number of pendant drops**	**Average equilibrium interfacial tension**	**Std. dev.**	**Number of pendant drops**	**Average equilibrium interfacial tension**	**Std. dev.**
psi	**gm/cc**	**gm/cc**		**mN/m**	**mN/m**		**mN/m**	**mN/m**
8,000	0.81325	1.0060	10	32.50	±0.70	10	32.04	±0.57
9,000	0.8186	1.0093	10	33.26	±0.93	10	32.44	±0.27
10,000	0.8238	1.0127	10	33.51	±0.78	10	33.03	±0.61
11,000	0.8288	1.0160	10	32.06	±0.41	10	32.32	±0.32
12,000	0.8336	1.0193	10	32.07	±0.18	-	-	-
13,454	0.8414	1.0241	10	32.33	±0.45	-	-	-

Table 4.22: Measured oil/water IFT for the F-RLO/SSW system at elevated press. & 208°F

F-RLO/SSW system								
						IFT values obtained in repeat experiment		
Press.	F-RLO density	SSW density	Number of pendant drops	Average equilibrium interfacial tension	Std. dev.	Number of pendant drops	Average equilibrium interfacial tension	Std. dev.
psi	gm/cc	gm/cc		mN/m	mN/m		mN/m	mN/m
8,000	0.81325	1.0140	7	30.87	±1.11	5	29.89	±0.72
9,000	0.8186	1.0175	12	31.81	±0.37	-	-	-
10,000	0.8238	1.0205	13	31.76	±0.49	5	31.48	±0.30
11,000	0.8288	1.0239	14	32.01	±0.32	-	-	-
12,000	0.8336	1.0271	10	31.87	±0.50	5	32.01	±0.65
13,454	0.8414	1.0276	10	31.61	±0.38	-	-	-

Table 4.23: Measured oil/water IFT for the F-RLO/DIW system at elevated press. & 208°F

F-RLO/DIW system								
						IFT values obtained in repeat experiment		
Press.	F-RLO density	DIW density	Number of pendant drops	Average equilibrium interfacial tension	Std. dev.	Number of pendant drops	Average equilibrium interfacial tension	Std. dev.
psi	gm/cc	gm/cc		mN/m	mN/m		mN/m	mN/m
8,000	0.81325	0.9883	8	28.42	±0.80	-	-	-
9,000	0.8186	0.9917	10	28.75	±0.41	6	29.10	±0.96
10,000	0.8238	0.9952	10	29.70	±0.27	5	29.85	±0.50
11,000	0.8288	0.9985	9	29.48	±0.74	5	29.48	±0.49
12,000	0.8336	1.0017	8	29.44	±0.22	-	-	-
13,454	0.8418	1.0067	9	29.07	±0.49	-	-	-

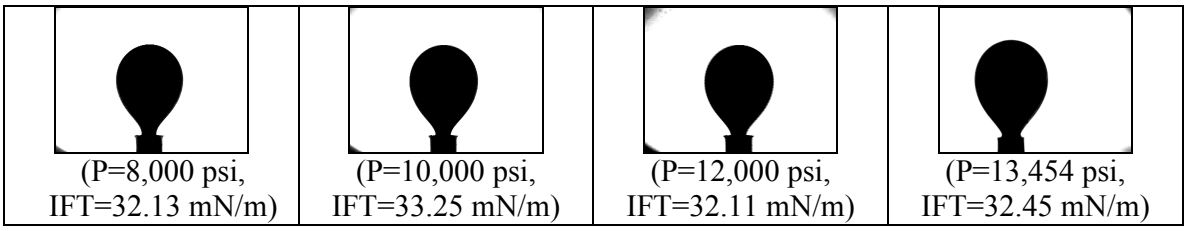

Figure 4.32: Pendant drop images for the F-RLO/F-SRB system at elevated press. & 208°F

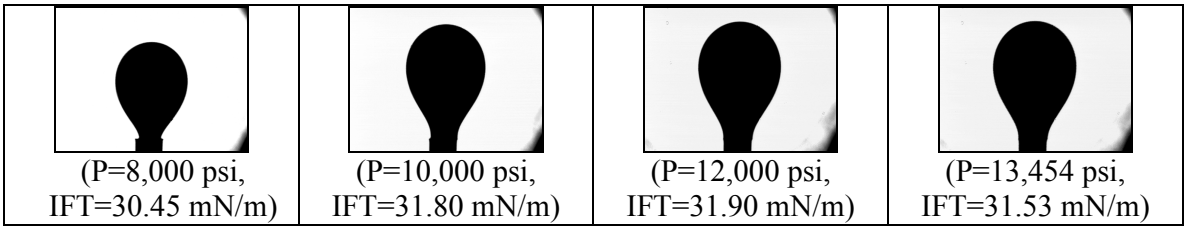

Figure 4.33: Pendant drop images for the F-RLO/SSW system at elevated press. & 208°F

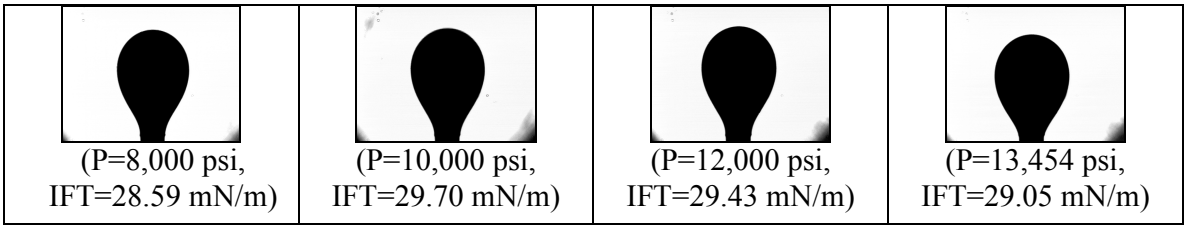

Figure 4.34: Pendant drop images for the F-RLO/DIW system at elevated press. & 208°F

A plot of the measured IFT data for different oil/water systems is shown in Figure 4.35. An increase in the measured oil/water IFT was observed in the pressure range from 8,000 to 10,000 psi in all of the cases. However, at pressures above 10,000 psi, a decrease in IFT was observed. The absence of dissolved salt in the aqueous phase (DIW) resulted in a significant decrease in the observed measured live oil/water IFT. The observed IFT values for the F-RLO/SSW system were found to be comparable with the F-RLO/F-SRB system at pressures above 10,000 psi. However, a small deviation was observed in the IFT values in these two systems at pressures below 10,000 psi. These results suggest that the presence of specific ions and variation in their concentrations (Figure 4.36) had a negligible on the measured IFT.

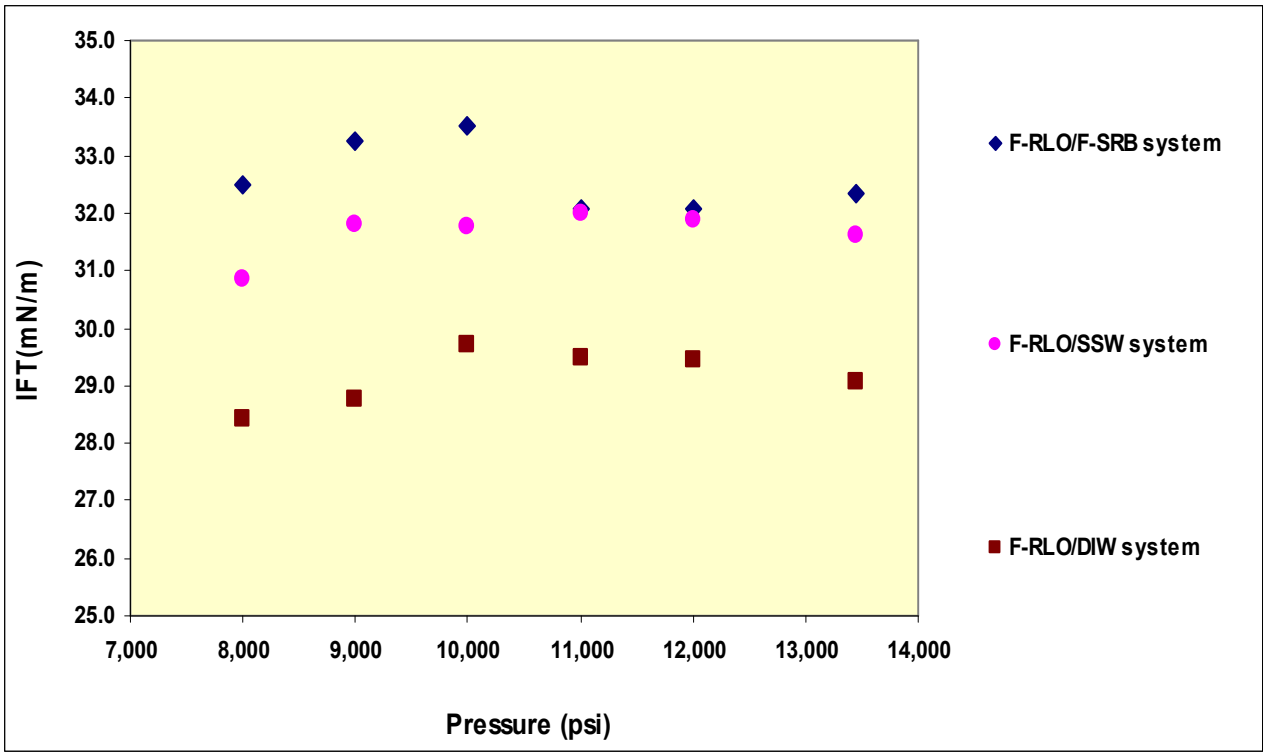

Figure 4.35: Measured oil/water IFT for the F reservoir at elevated pressures & 208°F

This appears to be the first time when IFTs for different live oil/water systems are measured at pressure exceeding 10,000 psi and elevated temperature using representative reservoir fluids.

These measurements are of practical importance as they attempt to eliminate the uncertainty associated with the IFT values for live reservoir oil/water systems at HPHT conditions. According to Shafer and Fate (2007), in the absence of any experimental IFT data, the uncertainty in the IFT of any live reservoir oil at HPHT conditions may be nearly an order of magnitude. They mentioned that a linear extrapolation of IFT data from Hocott (1939) from 4,000 psi to 20,000 psi resulted in a decrease in IFT from about 30 dyne/cm to 10 dyne/cm.

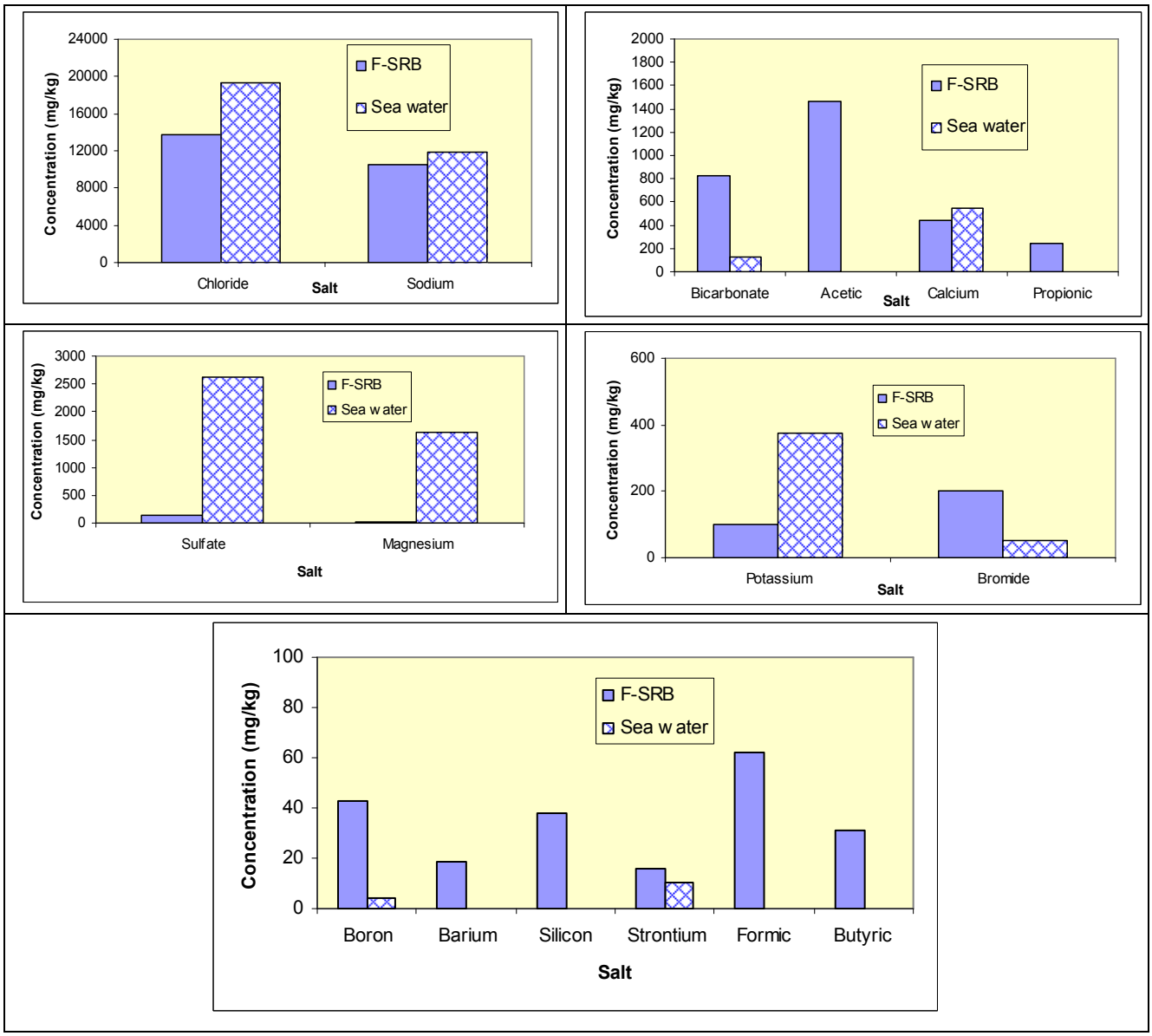

Figure 4.36: Comparison of the compositions of F-SRB and SSW

4.5.1.2.1 Effect of Temperature on Live Oil/water IFT

To investigate the effect of temperature on the measured IFT in the case of live oil/synthetic reservoir brine systems, experiments were also conducted for the F-RLO/F-SRB system at two different temperatures of 175° and 250°F and elevated pressures in the range from 8,000 to 13,454 psi. The measured IFT data are given in Tables 4.24-4.25. Example images of pendant oil drops taken during the experiments are shown in Figures 4.37-4.38.

Table 4.24: Measured oil/water IFT for the F-RLO/F-SRB system at elevated press. & 175°F

Pressure	F-RLO density	F-SRB density	Number of pendant drops	Average equilibrium interfacial tension	Std. dev.
psi	gm/cc	gm/cc		mN/m	mN/m
8,000	0.8196	1.0177	8	31.57	±0.88
10,000	0.8317	1.0243	6	32.27	±0.17
12,000	0.8411	1.0308	6	30.91	±0.26
13,454	0.8476	1.0353	7	30.64	±0.83

Table 4.25: Measured oil/water IFT for the F-RLO/F-SRB system at elevated press. & 250°F

Pressure	F-RLO density	F-SRB density	Number of pendant drops	Average equilibrium interfacial tension	Std. dev.
psi	gm/cc	gm/cc		mN/m	mN/m
8,000	0.7943	0.9893	8	32.61	±0.40
10,000	0.8067	0.9967	7	32.20	±0.40
12,000	0.8181	1.0038	8	30.80	±0.28
13,454	0.8254	1.0089	10	30.82	±0.43

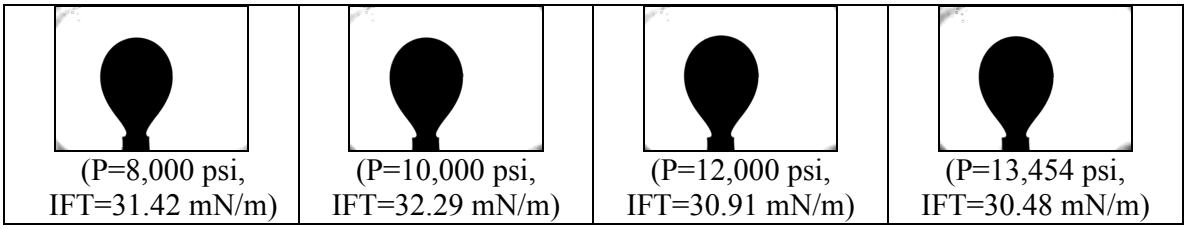

Figure 4.37: Pendant drop images for the F-RLO/F-SRB system at elevated press. & 175°F

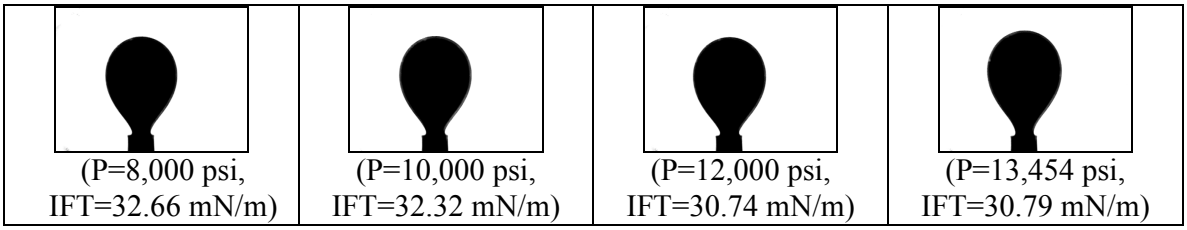

Figure 4.38: Pendant drop images for the F-RLO/F-SRB system at elevated press. & 250°F

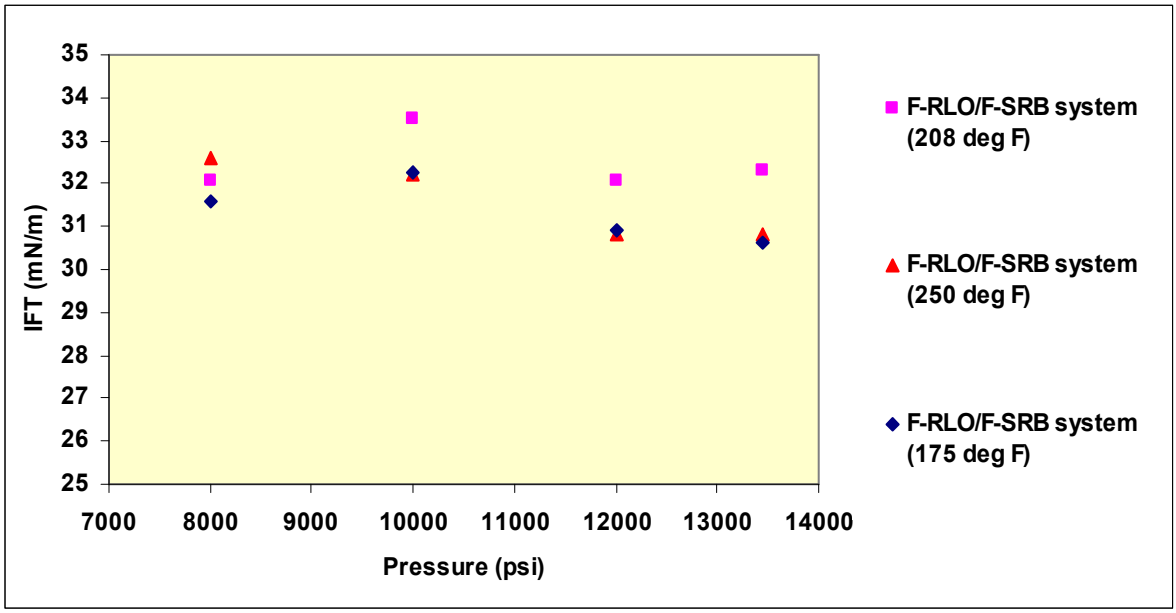

Figure 4.39: Effect of temperature on the measured IFT for the F-RLO/F-SRB system at elevated pressures

A comparison of the measured oil/water IFT data for the F-RLO/F-SRB system measured at elevated pressures and the three different temperatures of 175°, 208°, and 250°F is shown in

Figure 4.39. The measured IFT showed a decrease with an increase in the pressure at 250°F. An increase in the IFT at pressures up to 10,000 psi and a decrease at pressures above 10,000 psi were observed at 175°F. The measured IFT at pressures above 8,000 psi was found to be slightly higher at 208°F compared to the IFT measured at 175° and 250°F. The results suggest that variation in the temperature had a small effect on the measured oil/water IFT in the case of the F-RLO/F-SRB system.

4.5.1.2.2 Effect of Oil Composition on Oil/water IFT

To investigate the effect of oil composition (Figure 4.40) on the crude oil/water IFT, pendant drop experiments were also conducted with stock-tank oil (F-STO). The measured IFT data are given in Tables 4.26-4.27 and representative images of pendant oil drops are shown in Figures 4.41-4.42.

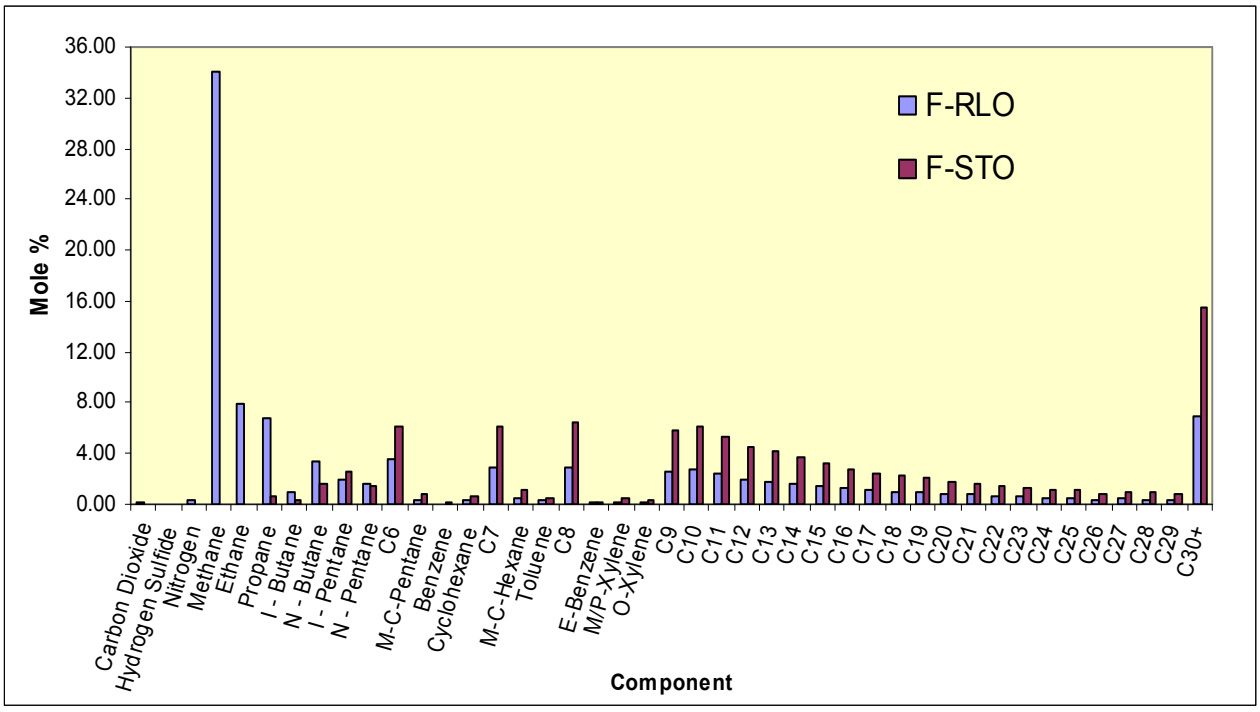

Figure 4.40: Comparison of the compositions of F-RLO and F-STO

Table 4.26: Measured oil/water IFT for the F-STO/F-SRB system at elevated press. & 208°F

Pressure	F-STO density	F-SRB density	Number of pendant drops	Average equilibrium interfacial tension	Std. dev.
psi	gm/cc	gm/cc		mN/m	mN/m
8,000	0.89194	1.0060	5	32.00	±0.36
10,000	0.90345	1.0127	5	32.08	±0.35
12,000	0.91445	1.0193	5	31.48	±0.49
13,454	0.92245	1.0241	5	31.09	±0.11

Table 4.27: Measured oil/water IFT for the F-STO/SSW system at elevated press. & 208°F

Pressure	F-STO density	SSW density	Number of pendant drops	Average equilibrium interfacial tension	Std. dev.
psi	gm/cc	gm/cc		mN/m	mN/m
8,000	0.89194	1.0140	5	33.26	±0.33
10,000	0.90345	1.0205	7	32.76	±0.53
12,000	0.91445	1.0271	6	32.99	±0.30
13,454	0.92245	1.0276	6	32.73	±0.43

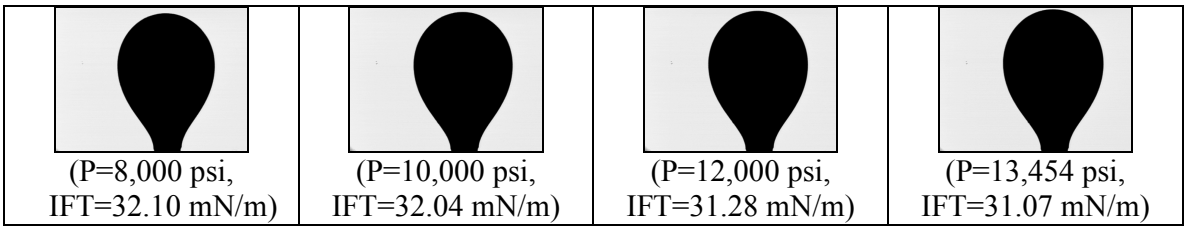

(P=8,000 psi, IFT=32.10 mN/m) (P=10,000 psi, IFT=32.04 mN/m) (P=12,000 psi, IFT=31.28 mN/m) (P=13,454 psi, IFT=31.07 mN/m)

Figure 4.41: Pendant drop images for the F-STO/F-SRB system at elevated press. & 208°F

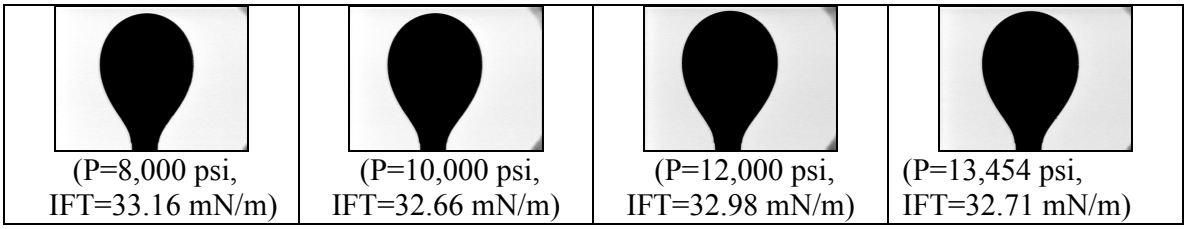

Figure 4.42: Pendant drop images for the F-STO/SSW system at elevated press. & 208°F

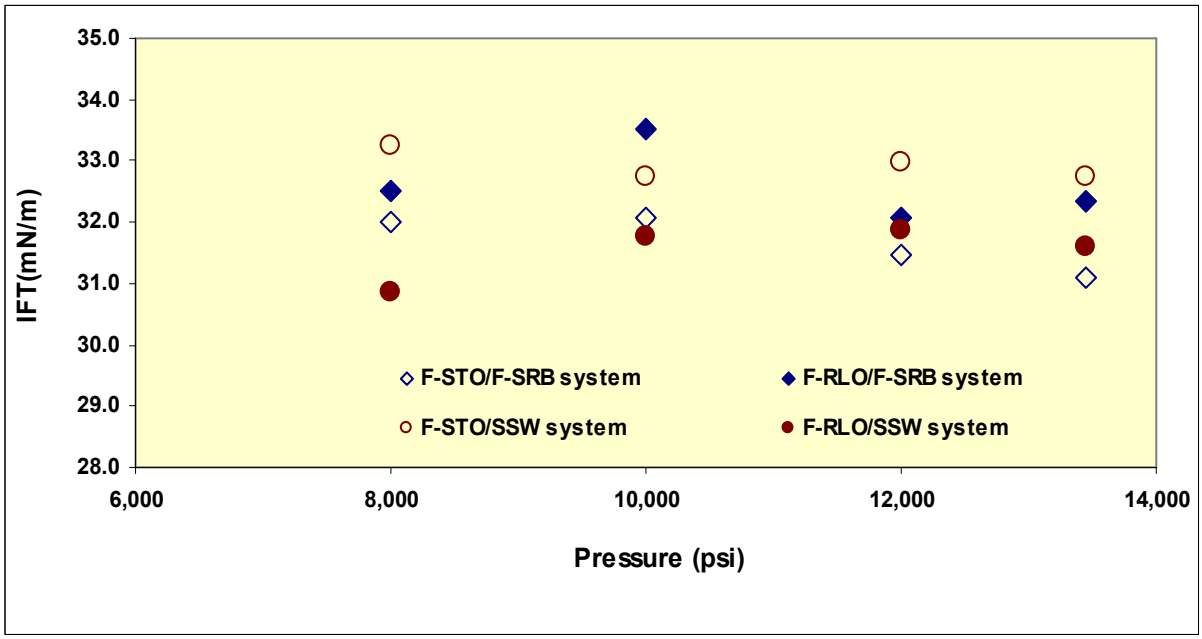

Figure 4.43: Measured oil/water IFT at elevated pressures & 208°F, F-STO and F-RLO

The measured IFT data for stock-tank oil and different aqueous phases along with its comparison with IFT values obtained in the case of live oil are shown in Figure 4.43. The measured IFT values obtained in the case of the F-STO/F-SRB system were comparable to the IFT values obtained in the case of the F-RLO/F-SRB system. However, in the case of synthetic sea water, stock-tank oil exhibited higher IFT than live oil. At elevated pressure and temperature, the F-STO/SSW system exhibited higher IFT than the F-STO/F-SRB system. This is similar to measured IFT values at ambient conditions for both systems. In the case of F-STO, there was a

slight increase in the measured reservoir condition IFT values compared to ambient condition values.

4.5.2 The Sessile Oil Drop Volume Alteration Experiments

Sessile oil drop volume alteration experiments at both ambient and reservoir conditions were conducted for selected rock/oil/water systems to quantify the extent of rock/oil adhesion interactions in the F reservoir. The extent of rock/oil adhesion interactions was quantified in terms of the line tension (Eq.12) and the line tension-based modified equation for the work of adhesion (Eq.17).

4.5.2.1 Reservoir Condition Experiments, 10,000 psi & 208°F

Both recombined live oil (F-RLO) and stock-tank oil (F-STO) were used as the oil phase in the reservoir condition experiments. Three different aqueous phases, namely F-SRB, SSW, and DIW were used.

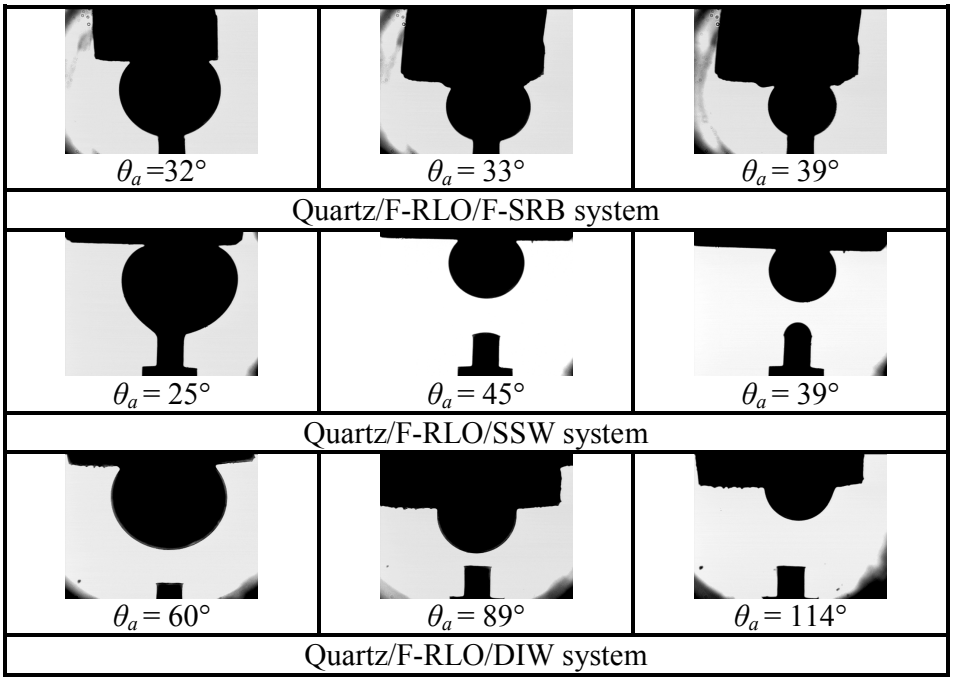

Figure 4.44: The sessile oil drop volume alteration experiments conducted for the quartz/F-RLO system at 10,000 psi & 208°F

The quartz surface was used as the solid phase since it is the main constituent of the F reservoir rock (97%). To evaluate the effect of mineralogy on the extent of rock/oil adhesion interactions in the F reservoir, experiments were also conducted with the calcite surface for selected oil/water systems. A series of captured images of various drops during the drop volume reduction steps are shown in Figures 4.44-4.45.

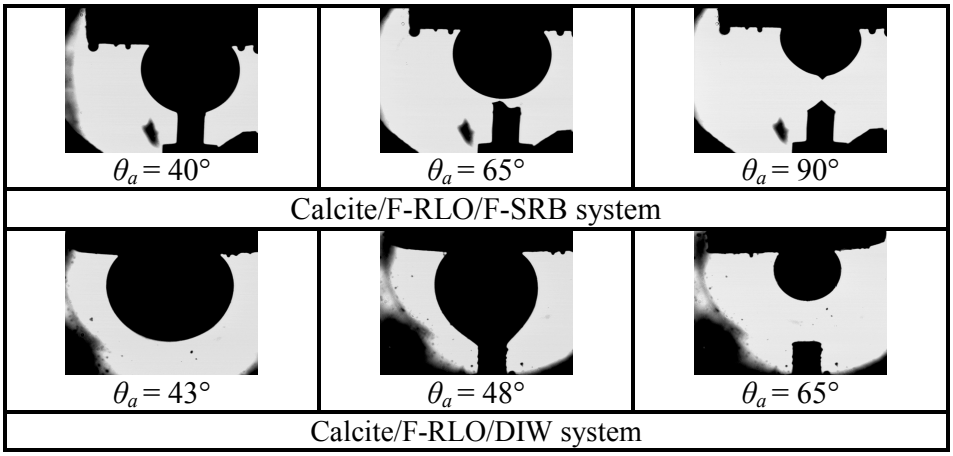

Figure 4.45: The sessile oil drop volume alteration experiments conducted for the calcite/F-RLO system at 10,000 psi & 208°F

The water-advancing contact angle (θ_a) measured at each volume reduction step and corresponding change in the contact radius, *r*, was plotted as $Cos\theta_a$ versus *1/r* to determine the magnitude of the line tension at reservoir conditions. Graphs of the observed $Cos\theta_a$ versus *1/r* relationship for different rock/live oil/water systems are shown in Figures 4.46-4.47.

Both the quartz/F-RLO/F-SRB and the quartz/F-RLO/F-SSW systems showed low slopes. However, the quartz/F-RLO/DIW system had a high slope. The calcite/F-RLO/F-SRB system showed higher slope than the quartz/F-RLO/F-SRB system whereas, the calcite/F-RLO/DIW system showed a lower slope compared to both the calcite/F-RLO/F-SRB and the

quartz/F-RLO/DIW systems. The measured water-receding contact angles (θ_r) for all of the systems are also shown in Figures 4.46-4.47. All of the systems exhibited lower values of θ_r in the range from 23° to 33°. Thus there are stable aqueous wetting films squeezed between the sessile oil drop and the mineral crystal surface during the formation of the big sessile oil drop on the mineral crystal surface.

The computed line tension values at reservoir conditions for the F reservoir are shown in Table 4.28. The effect of individual variables (fluids composition and rock mineralogy) on the measured line tension in the case of the F reservoir is discussed next.

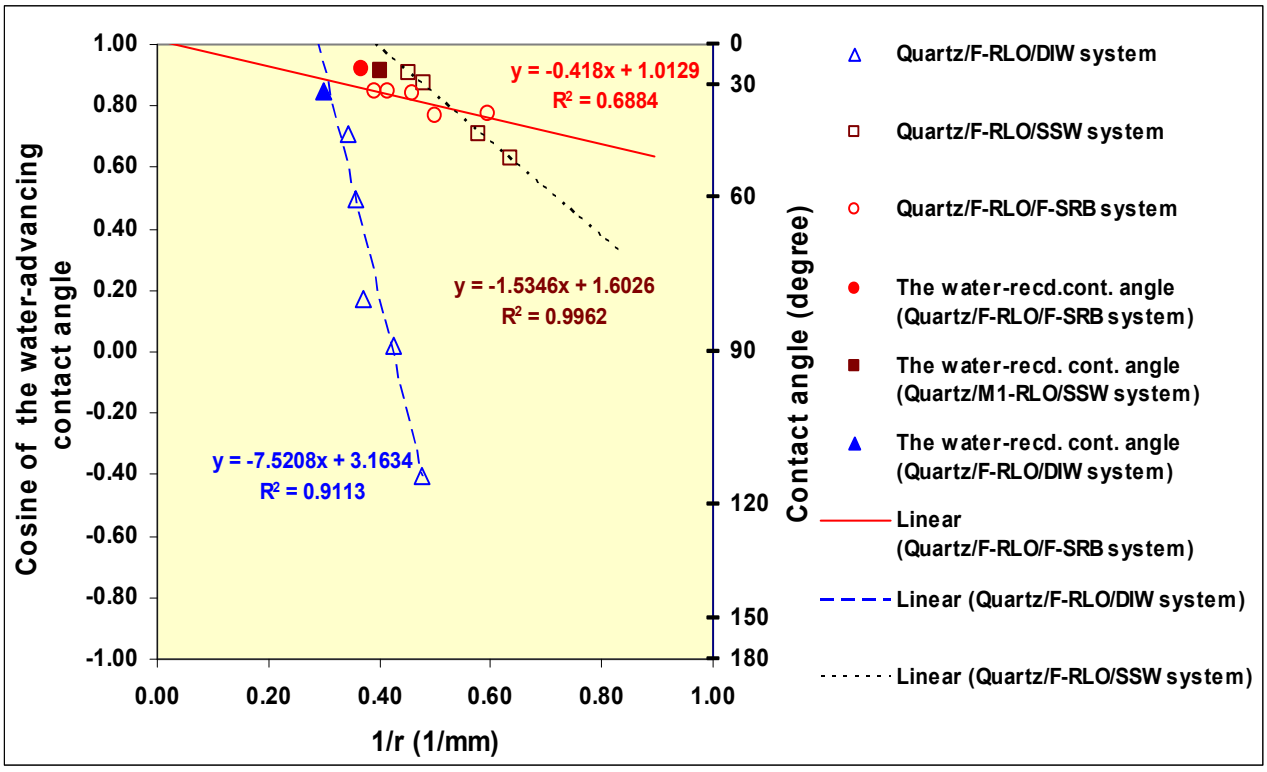

Figure 4.46: *Cos*θ_a versus *1/r* relationship for the quartz/F-RLO system at 10,000 psi & 208°F

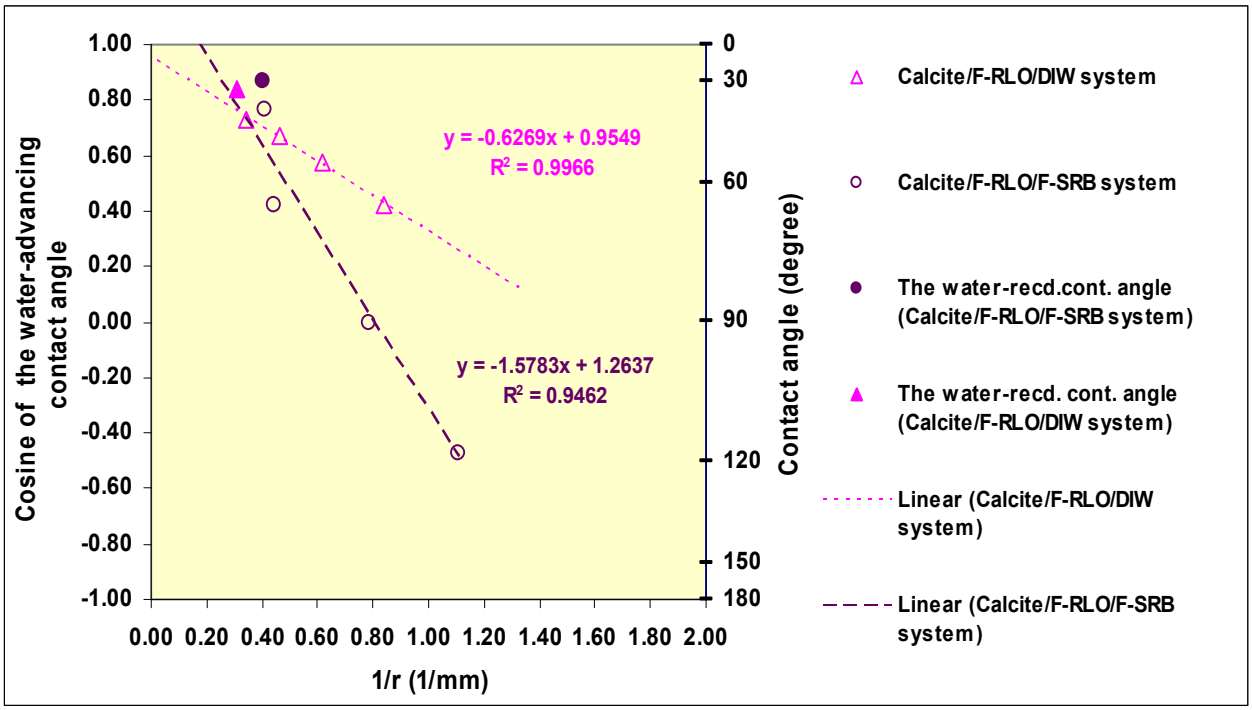

Figure 4.47: $Cos\theta_a$ versus *1/r* relationship for the calcite/F-RLO system at 10,000 psi & 208°F

Table 4.28: Measured line tension for F-RLO at 10,000 psi & 208°F

Rock/oil/water system	Variation in contact line radius (mm)	Slope of $Cos\theta_a$ versus *1/r* (1/mm) plot	Line tension σ (mN)
Quartz/F-RLO/DIW	2.90 to 2.10	-7.520	0.2239
Quartz/F-RLO/F-SRB	2.55 to 1.67	-0.418	0.0134
Quartz/F-RLO/SSW	2.21 to 1.56	-1.535	0.0476
Calcite/F-RLO/DIW	2.90 to 1.19	-0.626	0.0179
Calcite/F-RLO/F-SRB	2.42 to 0.90	-1.578	0.0529

F-RLO- Recombined live oil (F reservoir), F-SRB- Synthetic reservoir brine (F reservoir),
DIW- Deionized water, SSW- Synthetic sea water

4.5.2.1.1 Effect of Brine Composition on Measured Line Tension

In the case of the quartz surface, both the F-RLO/F-SRB and the F-RLO/SSW systems showed low line tension values thus indicated the presence of weak rock/oil adhesion interactions. However, a lower line tension value exhibited by the F-RLO/F-SRB system than the F-RLO/SSW system clearly indicates the presence of weaker rock/oil adhesion interactions in the presence of F-SRB compared to SSW. The observed variation in the extent of rock/oil adhesion interactions at reservoir conditions in these systems may be attributed to the presence of specific ions and differences in their concentrations (Figure 4.36). The DIW results show that the absence of dissolved salts in the aqueous phase resulted in strong rock/oil adhesion interactions.

4.5.2.1.2 Effect of Rock Mineralogy on Measured Line Tension

The effect of rock mineralogy was investigated by conducting the experiments with the calcite surface and selected live oil/water systems. The calcite system showed almost four times higher line tension value compared to the quartz system when F-SRB was used as aqueous phase. This clearly indicates the presence of stronger rock/oil adhesion interactions in the system when calcite is the mineral surface and reservoir fluids are used. When DIW is used instead of F-SRB, the measured line tension was found to be significantly than the quartz system. These results indicate that the calcite surface has more affinity to brine compared to the quartz surface but is not affected by the absence of dissolved salts in the aqueous phase. The results obtained for the calcite surface reinforces the need to conduct the experiments using representative reservoir fluids at actual reservoir conditions because the ambient condition experiments or experiments conducted using non-representative fluids may yield misleading results.

4.5.2.1.3 Effect of Oil Composition on Measured Line Tension

To investigate the effect of oil composition on the extent of rock/oil adhesion interactions, the sessile oil drop volume alteration experiments were also conducted for the quartz/F-STO/F-SRB

and the quartz/F-STO/SSW systems. The observed $Cos\theta_a$ versus $1/r$ relationships for these two systems are shown in Figure 4.48.

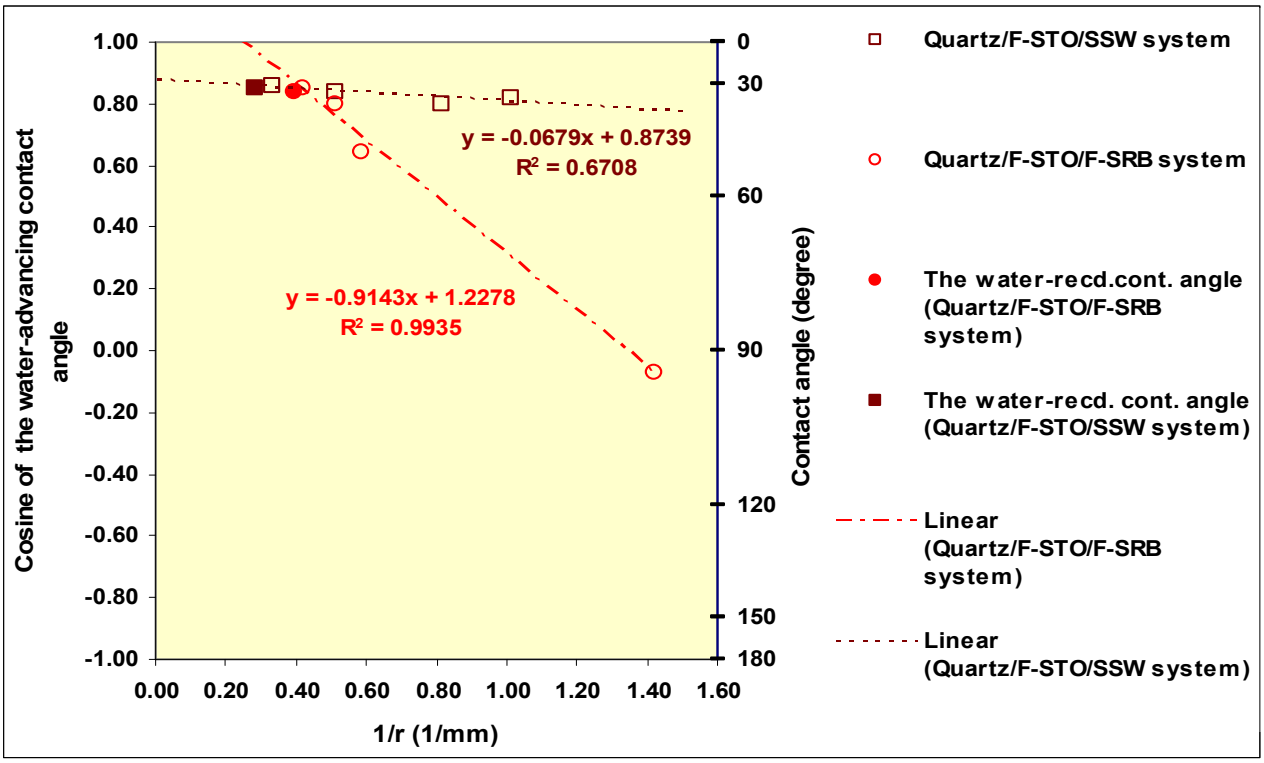

Figure 4.48: $Cos\theta_a$ versus $1/r$ relationship for the quartz/F-STO system at 10,000 psi & 208°F

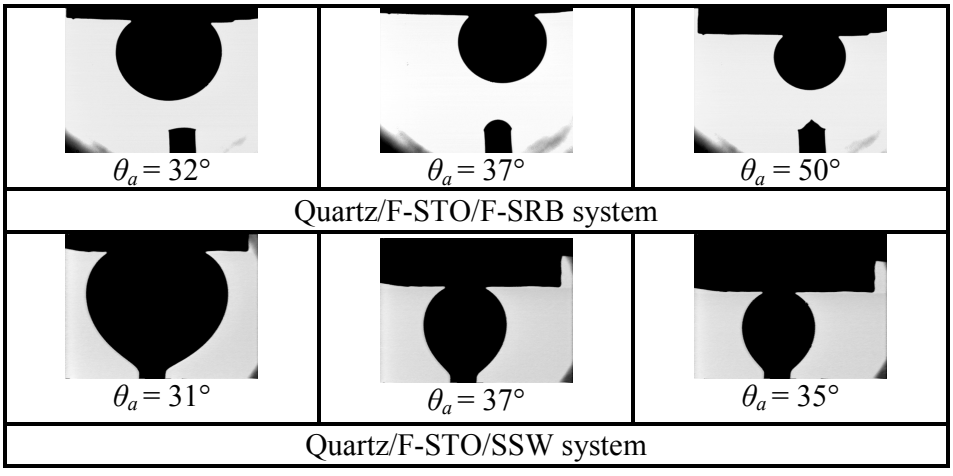

Figure 4.49: The sessile oil drop volume alteration experiments conducted for the quartz/F-STO systems at 10,000 psi & 208°F

Images of various drops captured during the drop volume reduction steps of the experiments conducted for stock-tank oil are shown in Figure 4.49. The measured line tension results are given in Table 4.29.

Table 4.29: Measured line tension for F-STO at 10,000 psi & 208°F

Rock/oil/water system	Variation in contact line radius, *r* (mm)	Slope of $Cos\theta_a$ versus *1/r* (1/mm) plot	Line tension σ (mN)
Quartz/F-STO/SSW	2.97 to 0.98	-0.0678	0.0022
Quartz/F-STO/F-SRB	2.38 to 0.70	-0.9143	0.0293

A comparison of the measured line tension values for the quartz/F-RLO/F-SRB and the quartz/F-STO/F-SRB systems indicates the presence of stronger rock/oil adhesion interactions in the system when stock-tank oil was used in place of live oil. However, the effect of oil composition was more pronounced in the case of SSW, where the quartz/F-STO system showed a significantly lower line tension values than the quartz/F-RLO system. The sessile oil drop volume alteration experiment was not conducted for the quartz/F-STO/DIW system since the use of DIW in the F-RLO experiment showed the presence of strong rock/oil adhesion interactions.

4.5.2.2 Ambient Condition Experiments

Sessile oil drop volume experiments were also conducted for selected rock/oil/water systems at ambient conditions using stock-tank oil and the three aqueous phases. The quartz and the calcite mineral surfaces were used as the solid phase. All of the rock/oil/water systems exhibited a low and comparable value of θ_r in the range from 11° to 15° at ambient conditions. Images of various drops captured during these experiments shown in Figure 4.50. Graphs of $Cos\theta_a$ versus *1/r* relationships for the quartz/F-STO/F-SRB and the calcite/F-STO/F-SRB systems are

shown in Figure 4.51. The measured line tension values for these systems are shown in Table 4.30. For the quartz/F-STO/SSW, the quartz/F-STO/DIW, the calcite/F-STO/SSW, and the calcite/F-STO/DIW systems, a pinning of the contact line resulted in a monotonic increase in the contact angle values during the volume reduction step of the experiment, thus exhibiting vertical (infinite slope) $Cos\theta_a$ versus *1/r* lines. Hence, the line tension values could not be obtained for these systems. However, this behavior was an evidence of the presence of strong rock/oil adhesion interactions in these systems.

A low line tension value was exhibited by the quartz/F-STO/F-SRB system indicates the presence of weak rock/oil adhesion interactions in the system. The absence of dissolved salts, the presence of additional ions and/or, a variation in the concentration of the ions present in the aqueous phase (Figure 4.36) significantly affected the extent of rock/oil adhesion interactions at ambient conditions.

The use of the calcite surface resulted in an increase of two orders of magnitude in the line tension compared to the quartz surface.

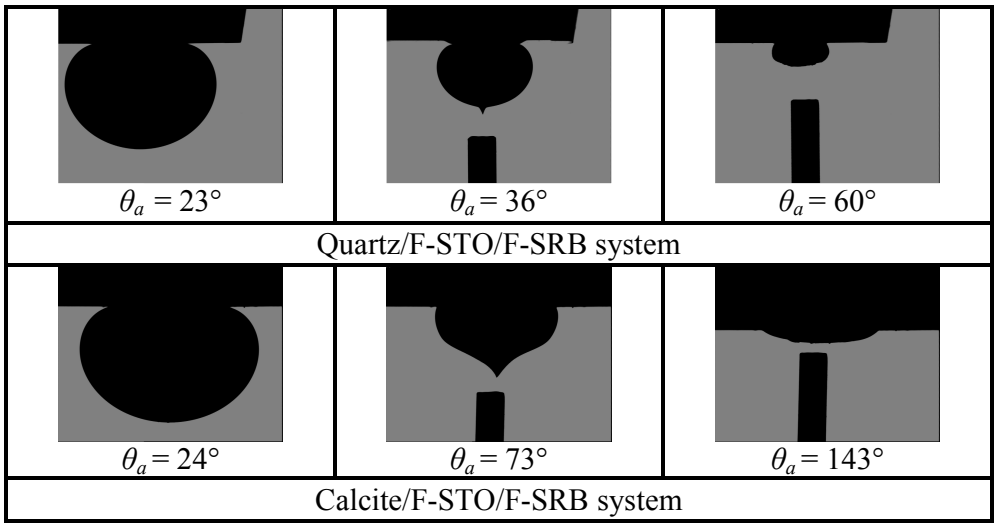

Figure 4.50: The sessile oil drop volume alteration experiments conducted for the quartz/F-STO and the calcite/F-STO systems at ambient conditions

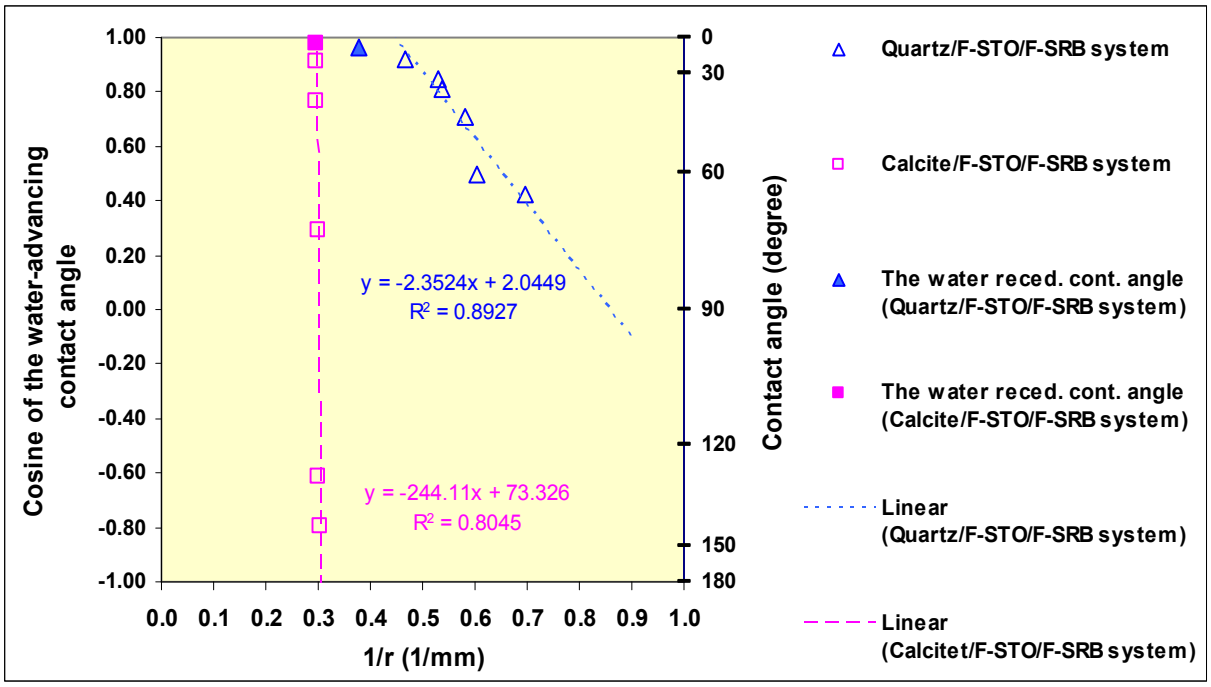

Figure 4.51: *Cos*θ_a versus *1/r* relationship for F-STO at ambient conditions

Table 4.30: Measured line tension for F-STO at ambient conditions

Rock/oil/water system	Variation in contact line radius (mm)	Slope of *Cos*θ_a versus *1/r* (1/mm) plot	Line tension σ (mN)
Quartz/F-STO/DIW	No change	infinite	Pinning of contact line
Quartz/F-STO/SSW	No change	infinite	Pinning of contact line
Quartz/F-STO/F-SRB	2.14 to 1.42	-2.3524	0.072
Calcite/F-STO/DIW	No change	infinite	Pinning of contact line
Calcite/F-STO/SSW	No change	infinite	Pinning of contact line
Calcite/F-STO/F-SRB	2.14 to 1.42	-244.11	7.26

4.5.2.3 Effect of Experimental Conditions on Measured Line Tension

The measured line tension for the quartz/F-STO/F-SRB system was found to be 2.76 times higher at ambient conditions compared to the measured line tension value at 10,000 psi and 208°F. It indicates the presence of weaker rock/oil adhesion interactions at elevated pressure and temperature compared to ambient conditions. Similar behavior was observed in the case of quartz/F-STO/SSW system. This also indicates that the presence of weaker rock/oil adhesion interactions in a particular rock/stock-tank oil/water system at reservoir conditions compared to ambient conditions.

4.5.3 Determination of the Wettability of the F Reservoir

In the third step, the wetting characteristics of different rock/oil/water systems involving the F reservoir fluids (F-RLO, F-SRB) were determined by conducting the DDDC tests at reservoir conditions of 10,000 psi and 208°F. At ambient conditions, stock-tank oil (F-STO) was used at the oil phase. The effect of brine composition was investigated by using SSW and DIW as an aqueous phase. The quartz and the calcite surfaces were used as the solid phase to study the effect of rock mineralogy. The results are presented and discussed next.

4.5.3.1 Ambient Condition DDDC Tests

The results of the DDDC tests conducted at ambient conditions (atmospheric pressure and 74°F) are given in Table 4.31. The water-receding and advancing contact angles obtained in the ambient condition DDDC tests conducted for the quartz and the calcite systems are shown in Figure 4.52 and 4.53, respectively. The quartz system showed weakly water-wet behavior (θ_a=62°) with F-SRB. However, an oil-wet behavior ($\theta_a \geq$142°) was observed for both the F-STO/SSW and the F-STO/DIW systems. This observed change in the wetting behavior in the case of quartz surface may be attributed to the presence of certain additional ions in F-SRB compared to SSW and to the difference in the concentration of common ions in them (Figure 4.36). This clearly points out the significant role of the dissolved salts, the presence of specific ions, and their varying

concentrations in the aqueous phase on the ambient condition wetting characteristics of the quartz surface. However, the effect of aqueous phase composition on the ambient condition wetting behavior was less pronounced in the case of the calcite surface.

Table 4.31: Results of the DDDC tests conducted for the F reservoir at ambient conditions

Rock/oil/water system	Water-receding contact angle, θ_r		Water-advancing contact angle, θ_a	Wettability
	Upper crystal	Lower crystal		
Quartz/F-STO/DIW	27°	24°	159°	Oil-wet
Quartz/F-STO/SSW	24°	23°	142°	Oil-wet
Quartz/F-STO/F-SRB	15°	16°	62°	Weakly water-wet
Calcite/F-STO/DIW	16°	14°	155°	Oil-wet
Calcite/F-STO/SSW	15°	14°	139°	Oil-wet
Calcite/F-STO/F-SRB	11°	13°	118°	Weakly oil-wet

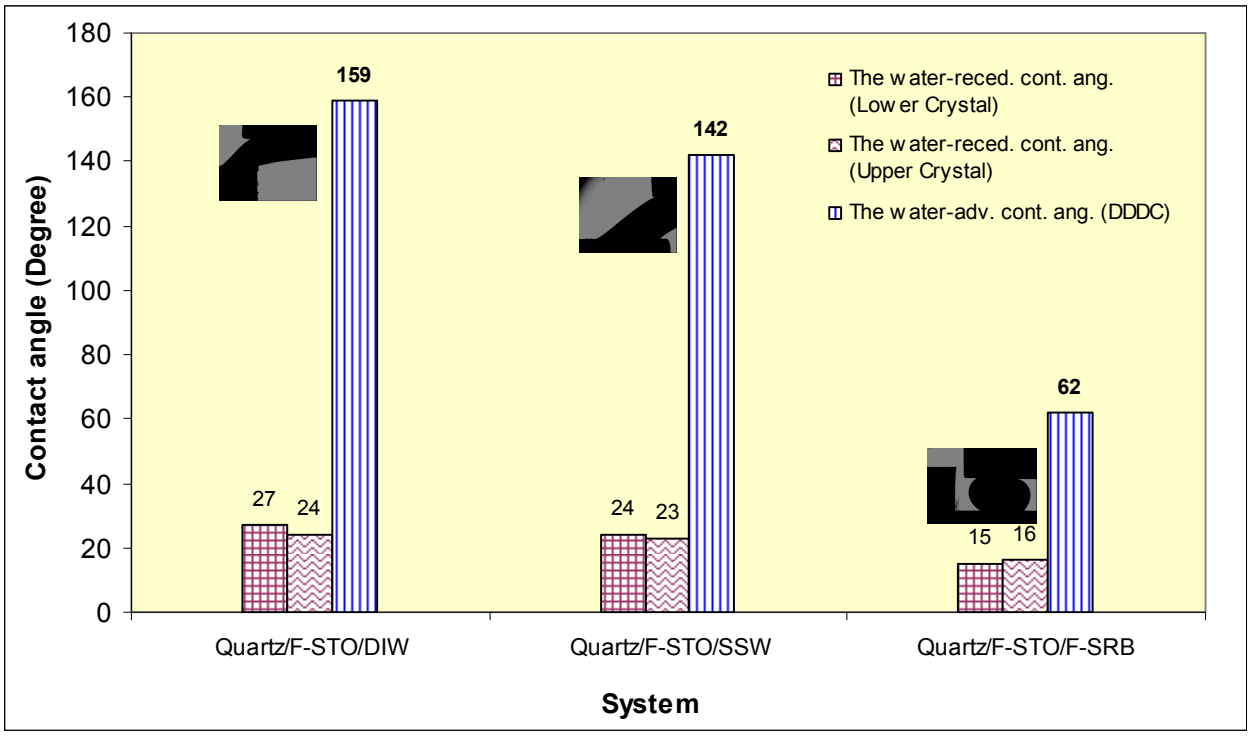

Figure 4.52: Ambient condition DDDC test results for the quartz/F-STO systems

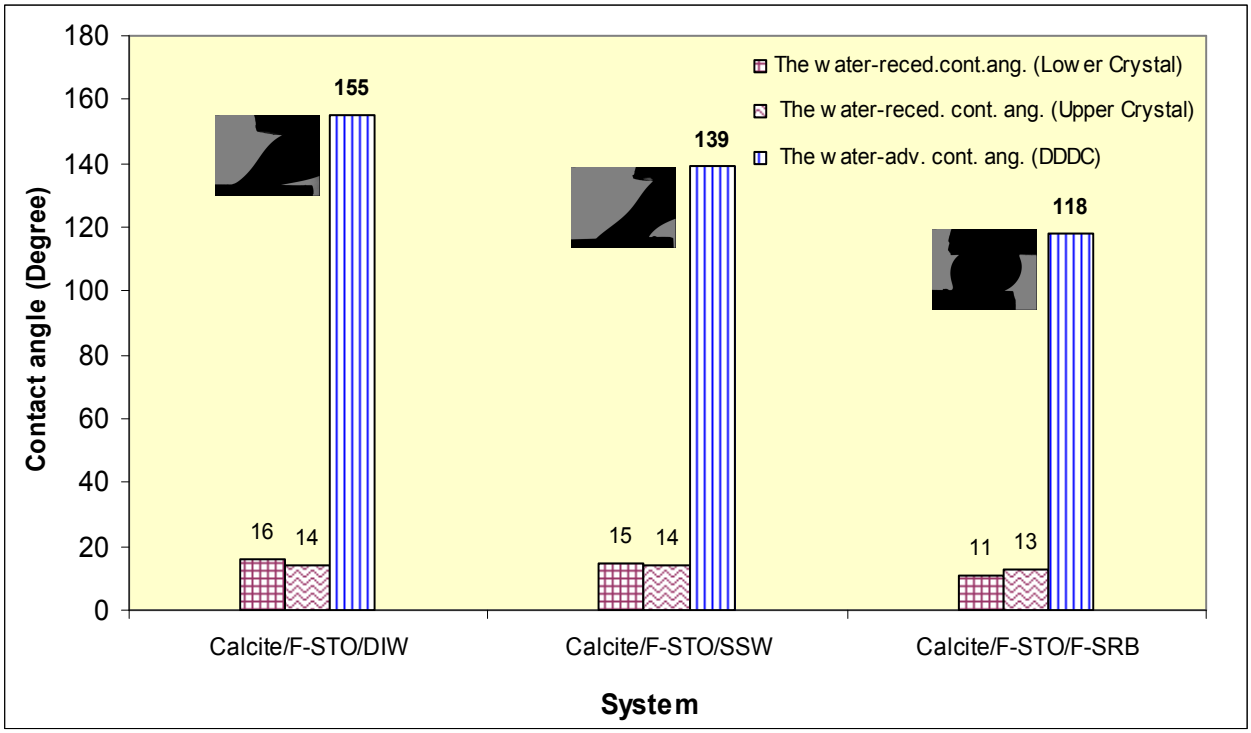

Figure 4.53: Ambient condition DDDC test results for the calcite/F-STO systems

4.5.3.2 Reservoir Condition DDDC Tests

The reservoir condition wetting behavior of the F reservoir was determined by conducting the DDDC tests with the quartz and the calcite surfaces at 10,000 psi and 208°F using recombined live oil (F-RLO). In the case of the quartz system, synthetic reservoir brine (F-SRB), synthetic sea water (SSW), and deionized water (DIW) were used as the aqueous phase. In the case of calcite system, the DDDC tests were conducted with F-SRB and DIW.

The results of the reservoir condition DDDC tests conducted with live oil are given in Table 4.32. The dynamic nature of the water-advancing contact angle in the DDDC tests was ensured by observing the movement of the three phase contact line (TPCL) and measured as a

normalized TPCL movement. The measured normalized TPCL movements along with the corresponding water-receding and the water-advancing contact angles (lower crystal) for different rock/recombined live oil/water systems are shown in Figures 4.54-4.58.

Table 4.32: The DDDC test results for the F reservoir conducted at 10,000 psi & 208°F

Rock/oil/water system	Water-receding contact angle, θ_r		Water-advancing contact angle, θ_a	Wettability	Normalized TPCL movement
	Upper crystal	Lower crystal			
Quartz/F-RLO/F-SRB	22°	23°	28°	Strongly water-wet	2.10 to 1.88
Quartz/F-RLO/SSW	26°	24°	29°	Strongly water-wet	2.80 to 2.24
Quartz/F-RLO/DIW	35°	32°	128°	Oil-wet	4.35 to 4.12
Calcite/F-RLO/F-SRB	36°	29°	66°	Weakly water-wet	2.62 to 2.42
Calcite/F-RLO/DIW	32°	29°	24°	Strongly water-wet	2.41 to 1.97

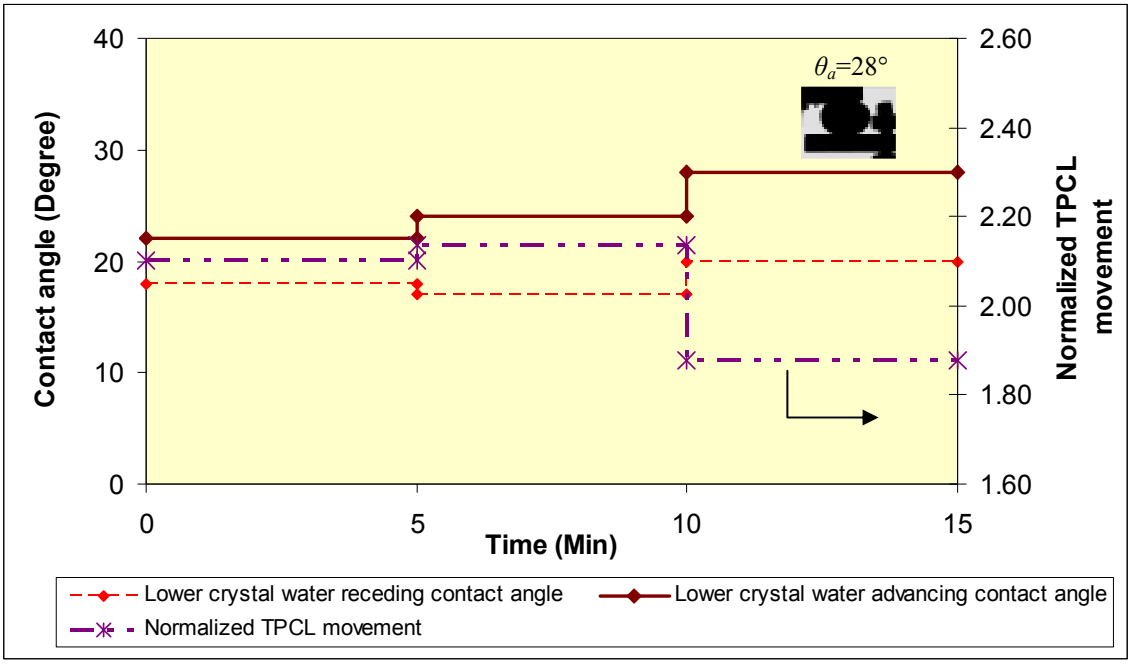

Figure 4.54: TPCL movement in the quartz/F-RLO/F-SRB system at 10,000 psi & 208°F

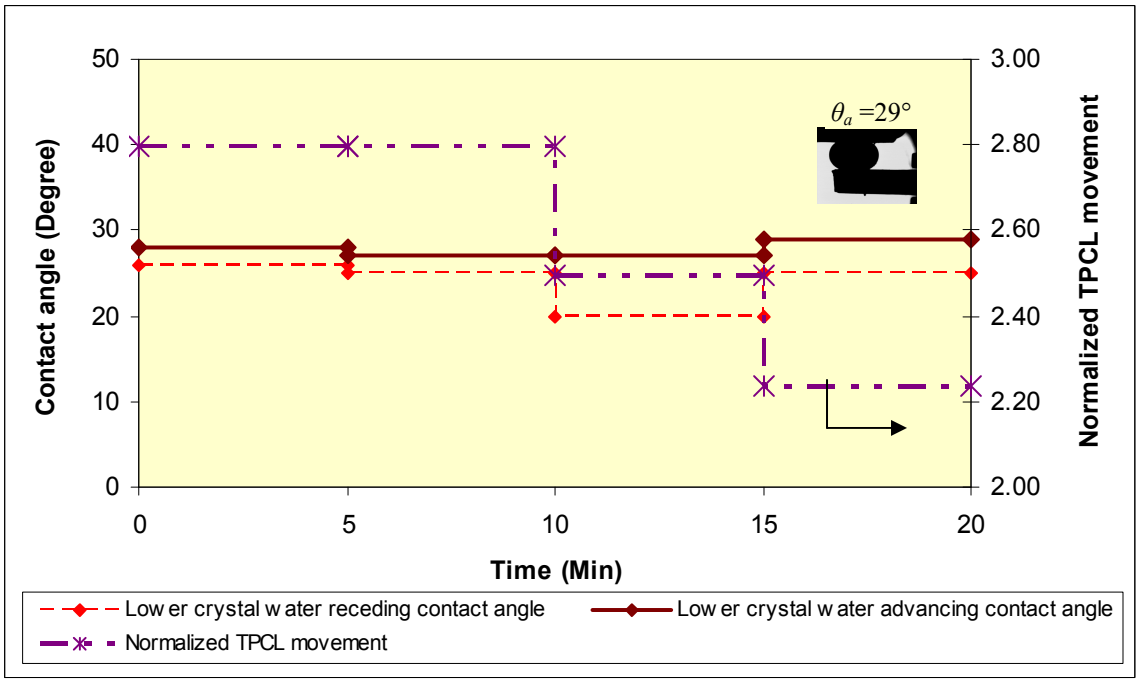

Figure 4.55: TPCL movement in the quartz/F-RLO/SSW system at 10,000 psi & 208°F

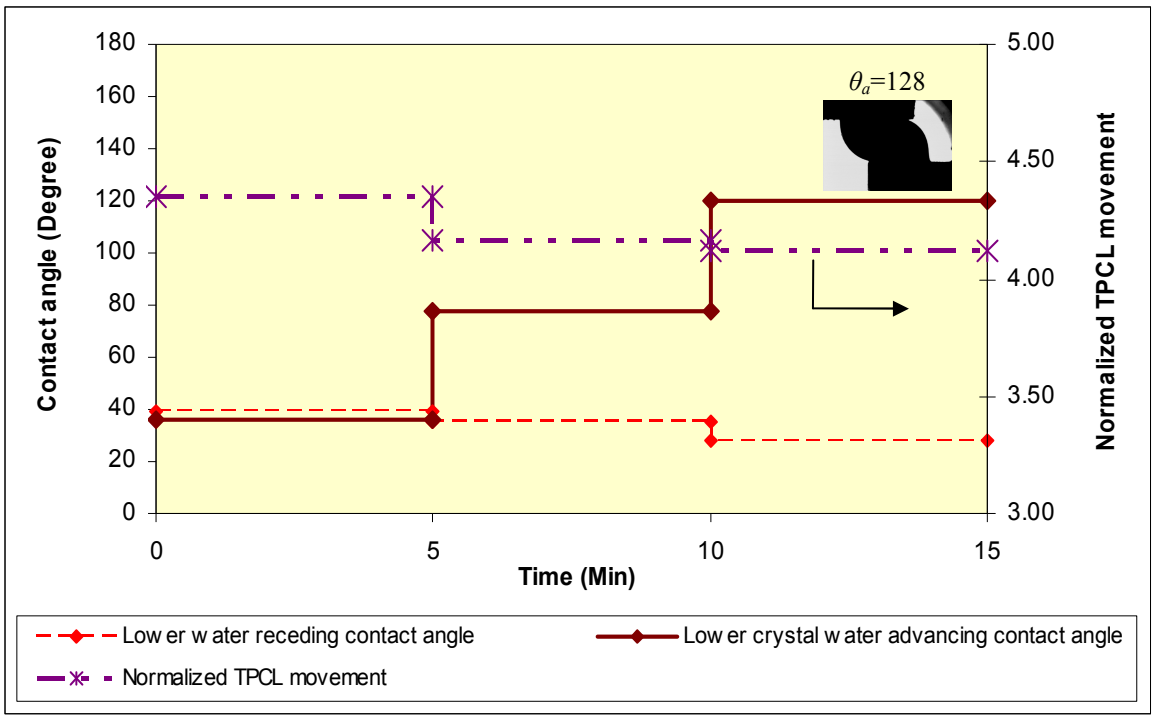

Figure 4.56: TPCL movement in the quartz/F-RLO/DIW system at 10,000 psi & 208°F

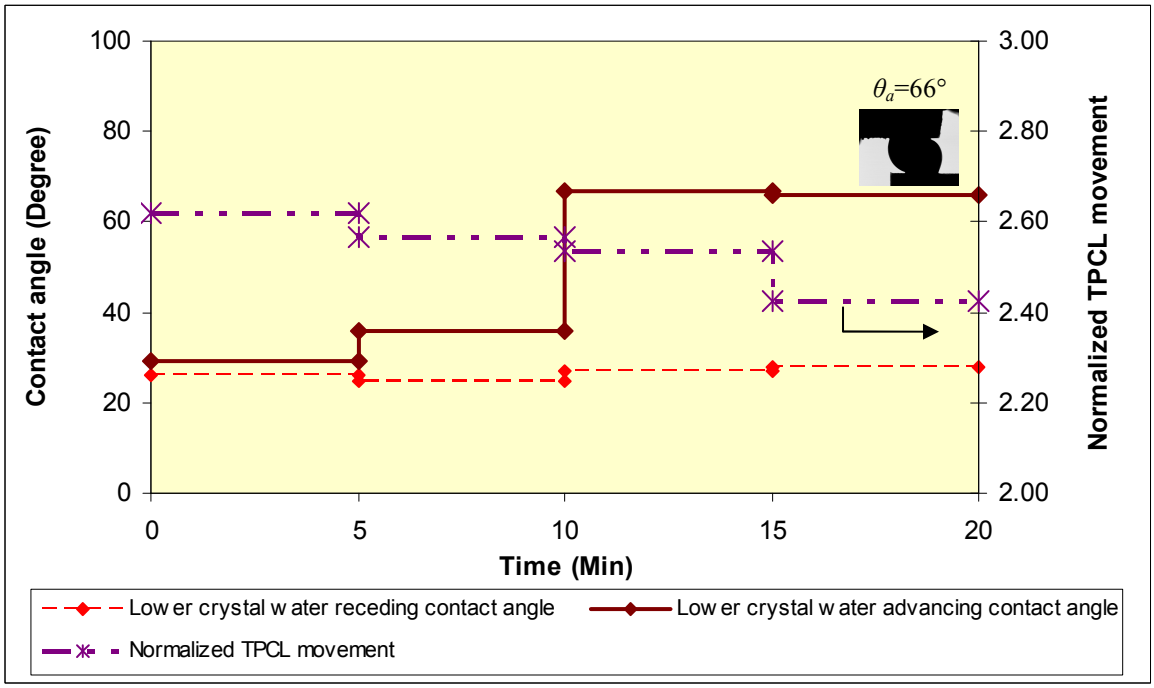

Figure 4.57: TPCL movement in the calcite/F-RLO/F-SRB system at 10,000 psi & 208°F

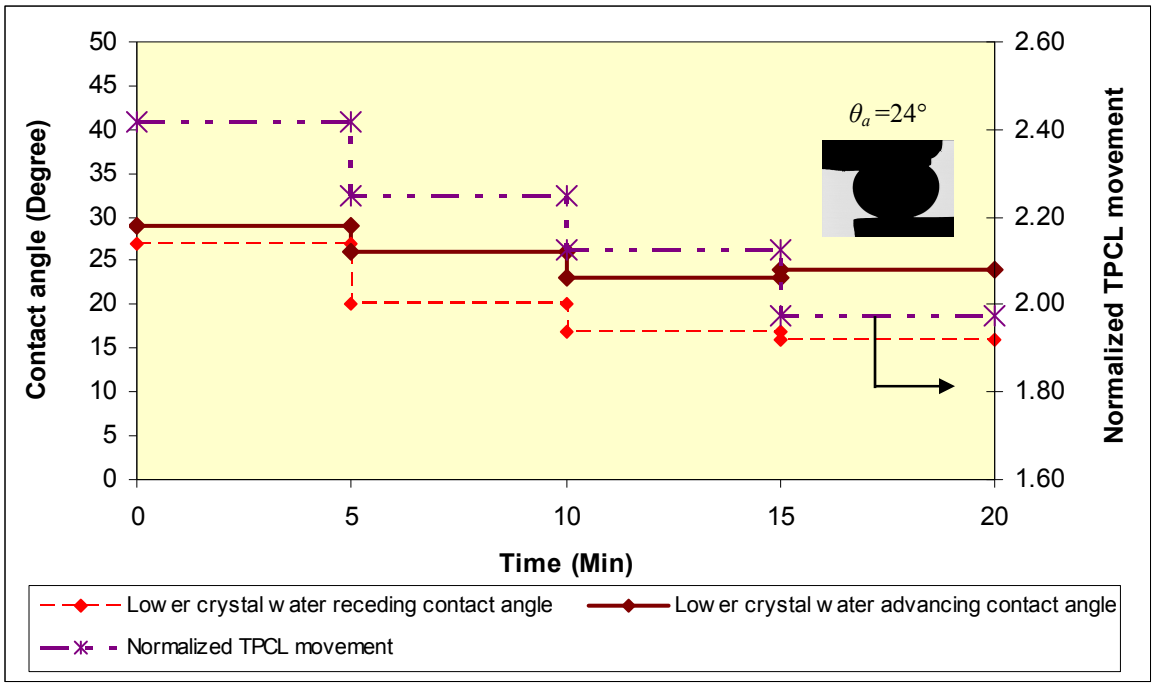

Figure 4.58: TPCL movement in the calcite/F-RLO/DIW system at 10,000 psi & 208°F

The effect of different variables (brine composition and rock mineralogy) on the wetting behavior is discussed next.

4.5.3.2.1 Effect of Brine Composition and Rock Mineralogy on the Wetting Behavior

The quartz system showed the strongly water-wet behavior at reservoir conditions with both F-SRB (θ_a=28°) and SSW (θ_a=29°). The use of synthetic sea water in place of synthetic reservoir brine did not result in any significant change in the wetting behavior. However, the extent of rock/oil adhesion interactions was slightly higher in the quartz/F-RLO/SSW system than the quartz/F-RLO/F-SRB system as indicated by the measured line tension values. The absence of the dissolved salts in the aqueous phase (DIW) resulted in oil-wet behavior (θ_a=128°).

The use of calcite surface in place of the quartz surface resulted in weakly water-wet behavior (θ_a=66°) when tested with the F-RLO/F-SRB system. This behavior may be attributed to a low concentration of calcium ion (~440 ppm) in F-SRB. An increase in water-wetness (θ_a=24°) was observed in the absence of dissolved salts in the aqueous phase (DIW) where calcite system exhibited the water-advancing contact angle of 24°. These results suggest that there were stable aqueous wetting films present in these systems at these conditions of pressure and temperature that prevented the development of strong rock/oil adhesion interactions between the sessile live oil drop and the calcite surface. Generally, the calcite surface exhibits oil-wet behavior, however the DDDC test results obtained for these systems does not agree with this notion.

4.5.4 Estimation of the Work of Adhesion, W_{sow}, F Reservoir

To evaluate the impact of the extent of rock/oil adhesion interactions on the dynamic behavior of reservoir fluids, the work of adhesion, W_{sow}, was estimated using the Eq.17 at both reservoir and ambient conditions in selected rock/oil/water systems. The collected oil/water IFT data and the drop size dependence of sessile oil drop (θ_a and r data) observed in the drop volume alteration experiments were used to compute W_{sow} for different rock/oil/water systems.

4.5.4.1 Estimation of W_{sow} at Reservoir Conditions

The results for the quartz systems are shown in Tables 4.33-4.35.

Table 4.33: Measured W_{sow} for the quartz/F-RLO/F-SRB system at 10,000 psi & 208°F

Quartz/F-RLO/F-SRB system (measured σ = 0.0134 mN), γ_{ow} = 33.51 mN/m, θ_r = 23°, Eq. time = 18 h					
Vol. red. step No.	**Water-advancing contact angle, θ_a, (°)**	**$Cos\theta_a$**	**Contact radius, r (mm)**	**Drop volume ratio***	**Work of adhesion/area $W_{sow,}$ (mN/m or mJ/m^2) Eq.17**
1	32	0.8480	2.5538	0.67	5.09
2	32	0.8480	2.4079	0.64	5.09
3	33	0.8387	2.1798	0.54	5.41
4	40	0.7660	2.0066	0.21	7.84
5	39	0.7771	1.6782	0.16	7.47

*Drop volume ratio =Volume of sessile oil drop at a given drop size red. step/Volume of initial sessile oil drop

Table 4.34: Measured W_{sow} for the quartz/F-RLO/SSW system at 10,000 psi & 208°F

Quartz/F-RLO/SSW system (measured σ = 0.04764 mN), γ_{ow} = 31.76 mN/m, θ_r = 24°, Eq. time = 18 h					
Vol. red. step No.	**Water-advancing contact angle, θ_a, (°)**	**$Cos\theta_a$**	**Contact radius, r (mm)**	**Drop volume ratio***	**Work of adhesion/area $W_{sow,}$ (mN/m or mJ/m^2) Eq.17**
1	25	0.9063	2.2182	0.76	2.98
2	29	0.8746	2.0829	0.63	3.98
3	45	0.7071	1.7313	0.28	9.30
4	51	0.6293	1.5690	0.21	11.77

*Drop volume ratio =Volume of sessile oil drop at a given drop size red. step/Volume of initial sessile oil drop

Table 4.35: Measured W_{sow} for the quartz/F-RLO/DIW system at 10,000 psi & 208°F

Quartz/F-RLO/DIW system (measured σ = 0.2239 mN), γ_{ow} = 29.85 mN/m, θ_r = 32°, Eq. time = 18 h					
Vol. red. step No.	**Water-advancing contact angle, θ_a, (°)**	**$Cos\theta_a$**	**Contact radius, r (mm)**	**Drop volume ratio***	**Work of adhesion/area W_{sow}, (mN/m or mJ/m^2) Eq.17**
1	45	0.7071	2.9095	0.58	8.74
2	60	0.5000	2.8001	0.46	14.93
3	80	0.1736	2.7088	0.28	24.67
4	89	0.0175	2.3440	0.16	29.33
5	114	-0.4067	2.1069	0.08	41.99

*Drop volume ratio =Volume of sessile oil drop at a given drop size red. step/Volume of initial sessile oil drop

A plot of W_{sow} versus sessile drop volume ratio relationship for the quartz systems is shown in Figure 4.59. In the case of F-SRB and SSW, the variation in W_{sow} with drop volume ratio was comparable. However, a significant large amount of work was needed in the case of DIW to displace oil as drop volume ratio decreased.

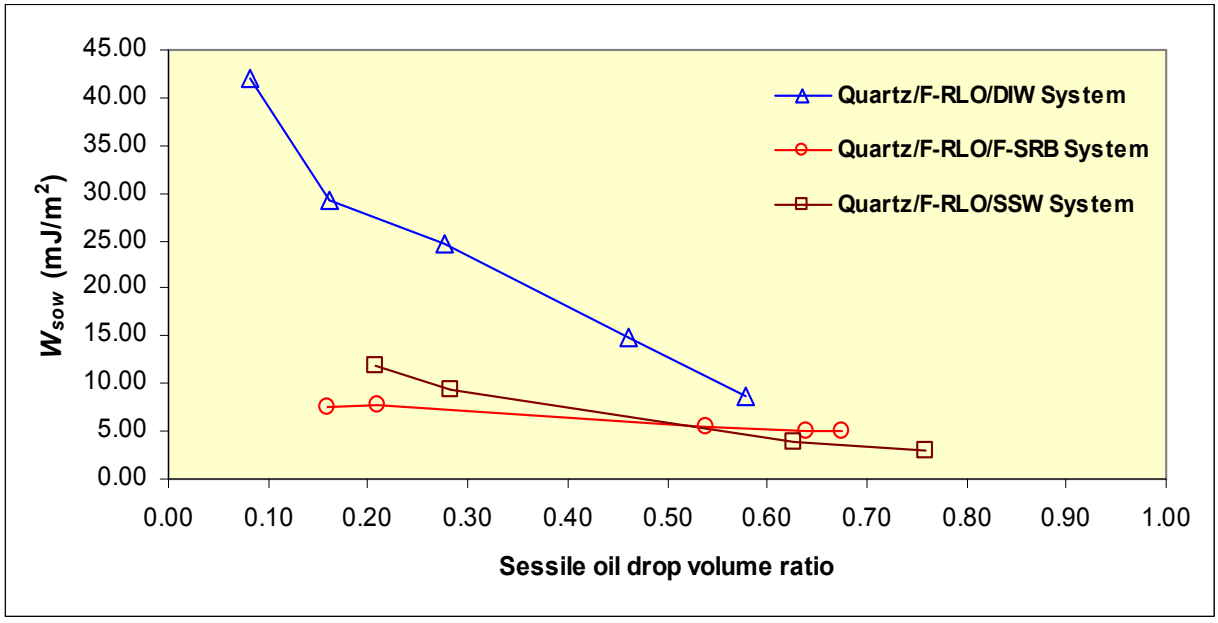

Figure 4.59: Effect of brine composition on oil mobilization at reservoir conditions

4.5.4.1.1 Effect of Oil Composition on Oil Mobilization

To study the effect of oil composition on oil mobilization in the case of quartz systems, the variation in W_{sow} with sessile oil drop volume ratio was also determined in the cases of the F-STO/F-SRB and the F-STO/SSW systems. The results are given in Tables 4.36-4.37 and are plotted in Figure 4.60.

Table 4.36: Measured W_{sow} for the quartz/F-STO/F-SRB system at 10,000 psi & 208°F

Quartz/F-STO/F-SRB system (measured σ = 0.0293 mN), γ_{ow} = 32.08 mN/m, θ_r = 33°, Eq. time = 18 h					
Vol. red. step No.	**Water-advancing contact angle, θ_a, (°)**	**$Cos\theta_a$**	**Contact radius, r (mm)**	**Drop volume ratio***	**Work of adhesion/area W_{sow}, (mN/m or mJ/m^2) Eq.17**
1	32	0.8480	2.3805	0.79	4.87
2	37	0.7986	1.9609	0.48	6.46
3	50	0.6428	1.6964	0.27	11.46
4	94	-0.0698	0.7023	0.01	34.32

*Drop volume ratio =Volume of sessile oil drop at a given drop size red. step/Volume of initial sessile oil drop

Table 4.37: Measured W_{sow} for the quartz/F-STO/SSW system at 10,000 psi & 208°F

Quartz/F-STO/SSW system (measured σ = 0.0022 mN), γ_{ow} = 32.76 mN/m, θ_r = 32°, Eq. time = 18 h					
Vol. red. step No.	**Water-advancing contact angle, θ_a, (°)**	**$Cos\theta_a$**	**Contact radius, r (mm)**	**Drop volume ratio***	**Work of adhesion/area W_{sow}, (mN/m or mJ/m^2) Eq.17**
1	31	0.8572	2.9733	0.78	4.68
2	33	0.8387	1.9518	0.46	5.29
3	37	0.7986	1.2222	0.21	6.60
4	35	0.8192	0.9850	0.12	5.92

*Drop volume ratio =Volume of sessile oil drop at a given drop size red. step/Volume of initial sessile oil drop

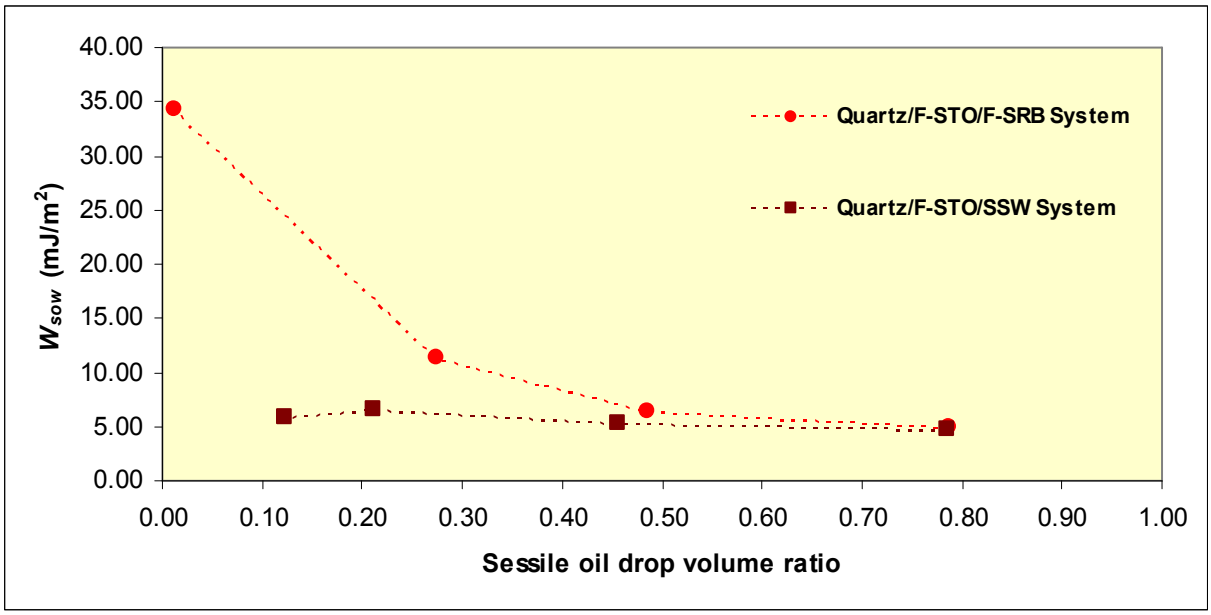

Figure 4.60: W_{sow} versus sessile oil drop volume ratio relationship for the quartz/F-STO systems at 10,000 psi & 208°F

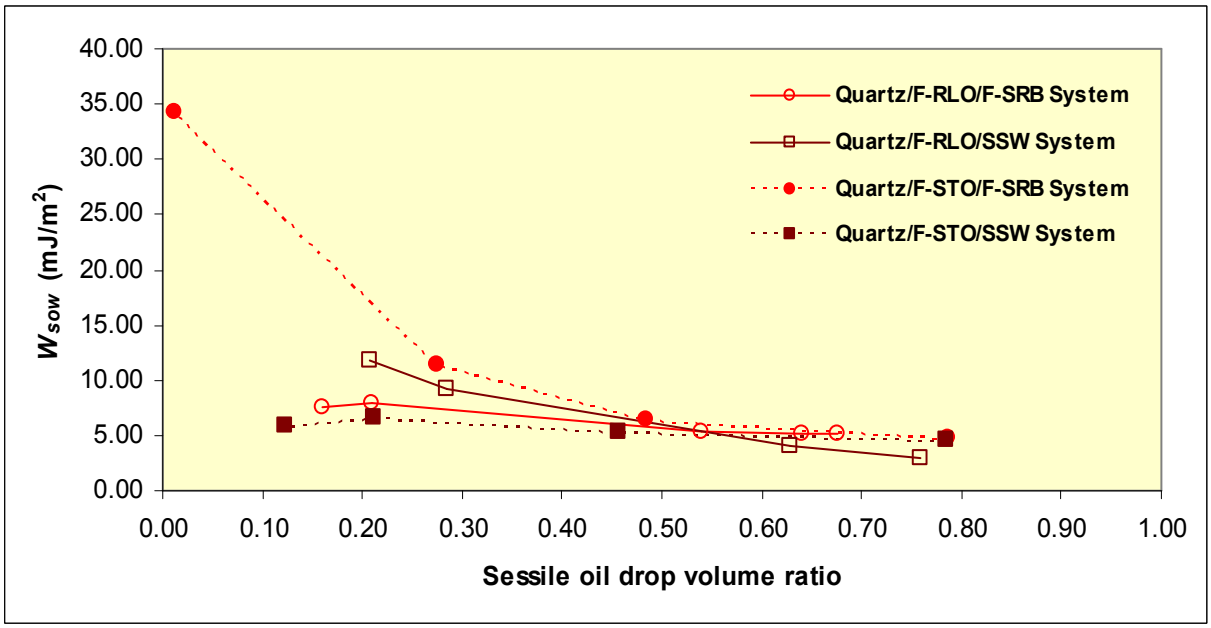

Figure 4.61: Effect of oil composition on oil mobilization at reservoir conditions

As can be seen in Figure 4.60, the results are comparable for both the systems at high drop volume ratios (i.e. from 0.80 to 0.45). However, a significant deviation is observed at small drop volume ratios (i.e. from 0.45 to 0.15).

The effect of the oil composition on oil mobilization for the quartz systems is shown in Figure 4.61. For the quartz surface, the use of stock-tank oil rather than live oil resulted in an increase in W_{sow} values at low drop volume ratios. This suggests that more work needs to be exerted at low oil saturations to move the residual oil in the case of stock-tank oil compared to live oil.

4.5.4.1.2 Effect of Rock Mineralogy on Oil Mobilization

The effect of rock mineralogy on oil mobilization was investigated by using the calcite surface and two oil/water systems, namely the F-RLO/F-SRB and the F-RLO/DIW system. The results are given in Tables 4.38-4.39 and are plotted in Figure 4.62.

Table 4.38: Measured W_{sow} for the calcite/F-RLO/F-SRB system at 10,000 psi & 208°F

Calcite/F-RLO/F-SRB system (measured σ = 0.05295 mN), γ_{ow} = 33.51 mN/m, θ_r = 29°, Eq. time = 18 h					
Vol. red. step No.	**Water-advancing contact angle, θ_a, (°)**	**$Cos\theta_a$**	**Contact radius, r (mm)**	**Drop volume ratio***	**Work of adhesion/area W_{sow}, (mN/m or mJ/m^2) Eq.17**
1	40	0.7660	2.4251	0.89	7.84
2	65	0.4226	2.2735	0.43	19.35
3	90	0.0000	1.2749	0.08	33.51
4	118	-0.4695	0.9005	0.03	49.24

*Drop volume ratio =Volume of sessile oil drop at a given drop size red. step/Volume of initial sessile oil drop

Table 4.39: Measured W_{sow} for the calcite/F-RLO/DIW system at 10,000 psi & 208°F

Calcite/F-RLO/DIW system (measured σ = 0.0179 mN), γ_{ow} = 29.85 mN/m, θ_r = 33°, Eq. time = 18 h					
Vol. red. step No.	**Water-advancing contact angle, θ_a, (°)**	**$Cos\theta_a$**	**Contact radius, r (mm)**	**Drop volume ratio***	**Work of adhesion/area W_{sow}, (mN/m or mJ/m^2) Eq.17**
1	43	0.7314	2.9066	0.74	8.02
2	48	0.6691	2.1476	0.44	9.88
3	55	0.5736	1.6129	0.13	12.73
4	65	0.4226	1.1903	0.03	17.23

*Drop volume ratio =Volume of sessile oil drop at a given drop size red. step/Volume of initial sessile oil drop

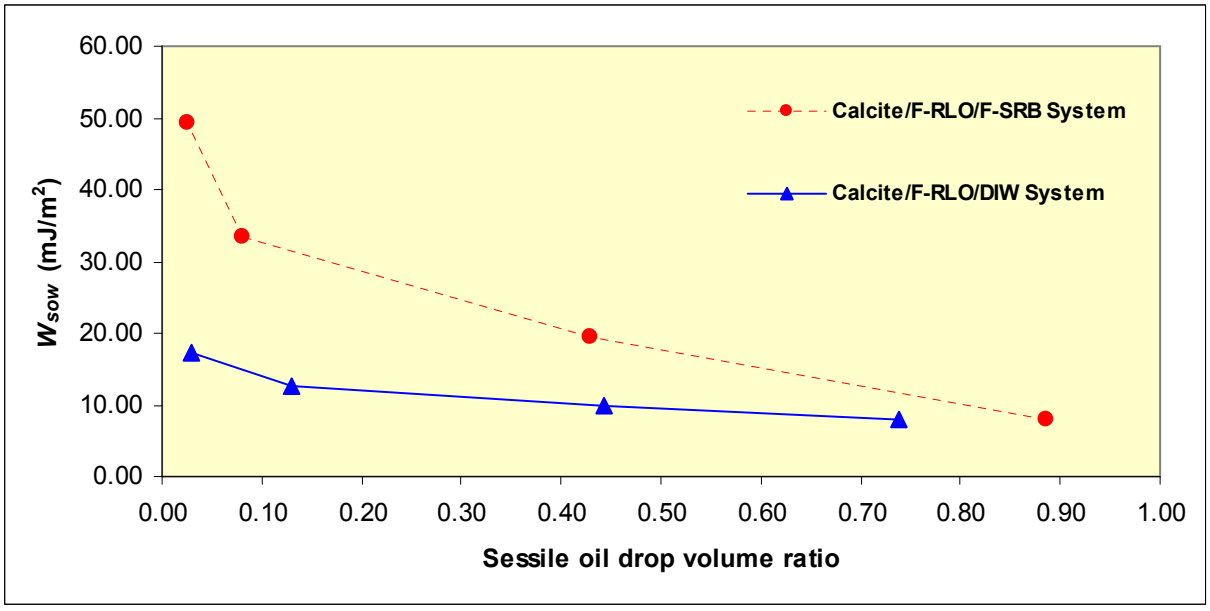

Figure 4.62: W_{sow} versus sessile oil drop volume ratio relationship for the calcite/F-RLO system at 10,000 psi & 208°F

To deduce the effect of rock mineralogy on the magnitude of the work of adhesion in the case of live oil, the results obtained for the calcite systems were compared with the results obtained for the quartz systems and are shown in Figure 4.63.

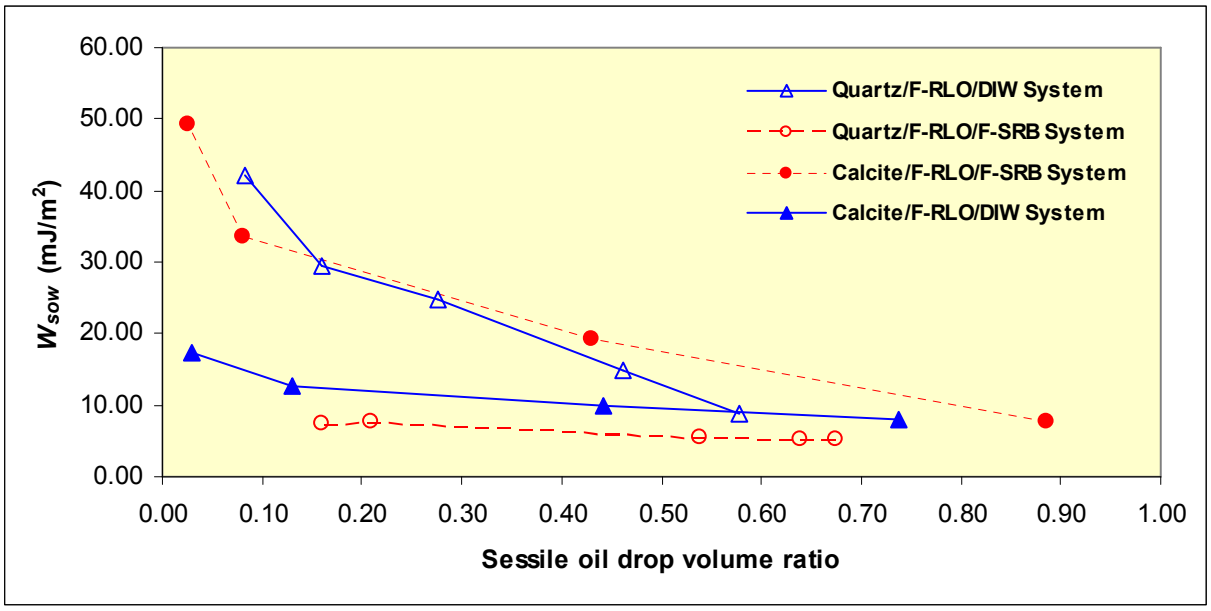

Figure 4.63: Effect of rock mineralogy on oil mobilization at reservoir conditions

The calcite system showed significantly higher W_{sow} values than quartz system at low drop volume ratios (<0.50) when F-SRB was the aqueous phase. This indicates that more work needs to be exerted at low oil saturations to move the oil in the calcite system compared to the quartz system. However, in the case of DIW, the calcite system showed significantly lower W_{sow} values compared to the quartz system at low drop volume ratios. In the absence of dissolved salts in the aqueous phase that resulted in the weak rock/oil adhesion interactions, less work needs to be done to move live oil in the case of the calcite system compared to the quartz system.

4.5.4.2 Estimation of W_{sow} at Ambient Conditions

The variation in W_{sow} with decreasing drop volume ratio was also determined at ambient conditions using stock-tank oil. The data is given in Table 4.40 and 4.41.

Table 4.40: Measured W_{sow} for the quartz/F-STO/F-SRB system at ambient conditions

Quartz/F-STO/F-SRB system (measured σ = 0.072 mN), γ_{ow} = 29.74 mN/m, θ_r = 15°, Eq. time = 24 h					
Vol. red. step No.	**Water-advancing contact angle, θ_a, (°)**	**$Cos\theta_a$**	**Contact radius, r (mm)**	**Drop volume ratio***	**Work of adhesion/area W_{sow}, (mN/m or mJ/m^2) Eq.17**
1	23	0.9205	2.1357	0.56	2.36
2	32	0.8480	1.8825	0.30	4.52
3	36	0.8090	1.8571	0.23	5.68
4	45	0.7071	1.7221	0.16	8.71
5	60	0.5000	1.6545	0.10	14.87
6	65	0.4226	1.4351	0.05	17.17

*Drop volume ratio =Volume of sessile oil drop at a given drop size red. step/Volume of initial sessile oil drop

Table 4.41: Measured W_{sow} for the calcite/F-STO/F-SRB system at ambient conditions

Calcite/F-STO/F-SRB system (measured σ = 7.26 mN), γ_{ow} = 29.74 mN/m, θ_r = 11°, Eq. time = 24 h						
Vol. red. step No.	**Water-advancing contact angle, θ_a, (°)**	**$Cos\theta_a$**	**Contact radius, r (mm)**	**Drop volume ratio***	**Work of adhesion/area W_{sow} (mN/m) Eq.17**	**W_{sow} (mJ/m^2)**
1	24	0.9135	3.3766	0.75	2.57	2.57
2	40	0.7660	3.3597	0.47	6.96	6.96
3	73	0.2924	3.3175	0.21	21.04	21.04
4	128	-0.6157	3.3175	0.07	48.05	48.05
5	143	-0.7986	3.3006	0.04	53.49	53.49

*Drop volume ratio =Volume of sessile oil drop at a given drop size red. step/Volume of initial sessile oil drop

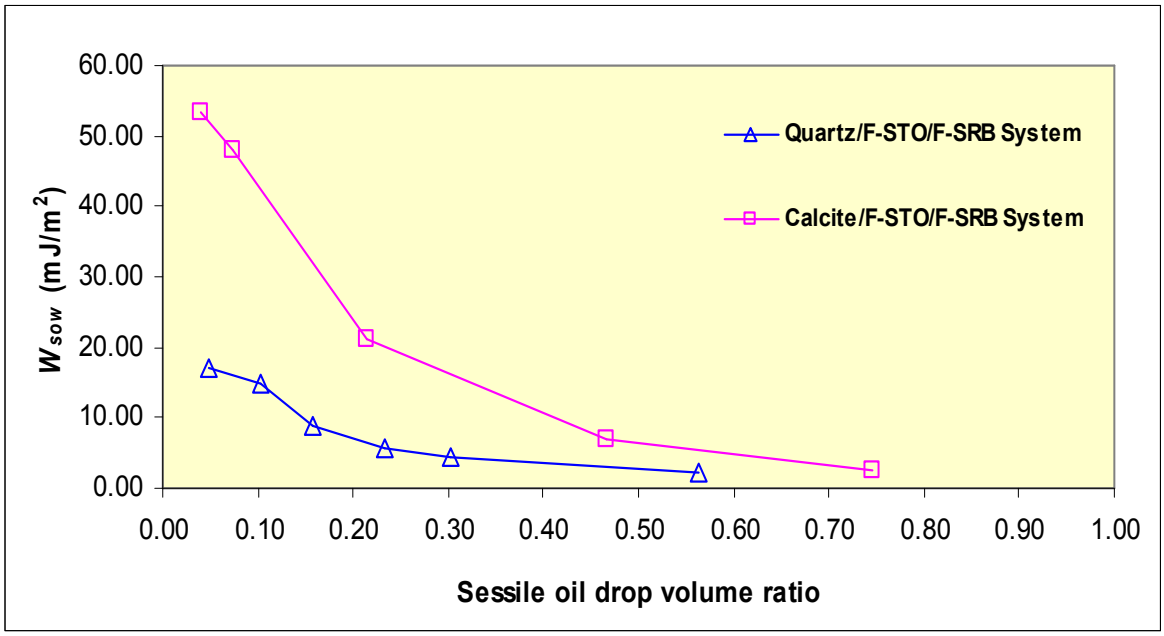

Figure 4.64: W_{sow} versus sessile oil drop volume ratio relationships for the quartz and the calcite systems at ambient conditions

A comparison of the computed W_{sow} versus drop volume ratio relationships exhibited by the quartz and the calcite systems is shown in Figure 4.64. At ambient conditions, a significantly higher work needs to be exerted to move the oil in the case of the calcite system compared to the quartz system.

4.5.4.3 Effect of Experimental Conditions on Oil Mobilization

A comparison of the variation in W_{sow} with drop volume ratio for the quartz/F-SRB systems with live oil and stock-tank oil at both reservoir and ambient conditions is shown in Figure 4.65. The results indicate that in the case of stock-tank oil, more work needs to be exerted to move the oil at reservoir conditions compared to ambient conditions as saturation decreases. Also, at reservoir conditions, a significantly higher amount of work is to be done to move the residual oil in the case of stock-tank oil compared to live oil. This suggests that in

the presence of lighter (gaseous) hydrocarbon components in the oil phase (live oil), significantly less amount of work needs to be exerted to move the oil, especially at low drop volume ratios.

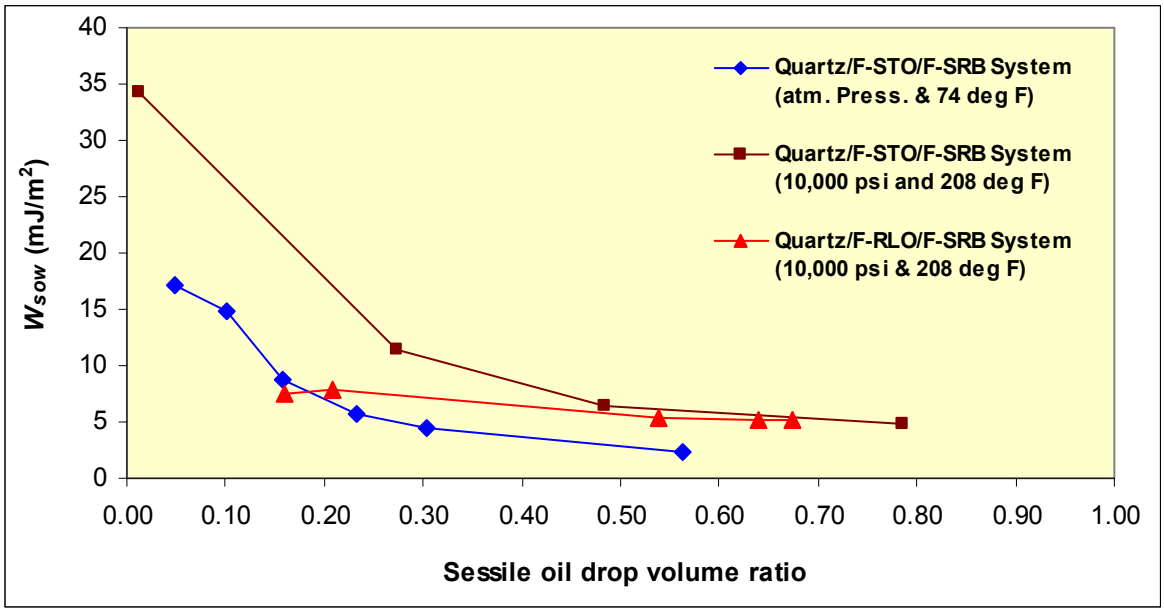

Figure 4.65: Effect of experimental conditions on W_{sow} versus sessile oil drop volume ratio relationship for the quartz/F-RLO and the quartz/F-STO systems

4.5.5 Estimation of Adhesion Energy per Unit Volume at Reservoir Conditions, F-RLO

In the last step, the magnitude of the adhesion energy per unit volume was determined for selected rock/oil/water systems using Eq.21. The measured water-receding (θ_r) and advancing (θ_a) contact data obtained in the DDDC tests (Table 4.32), the measured oil/water IFTs (Tables 4.21-4.23), and an assumed thickness of the aqueous wetting films (10 Å) were used to estimate the magnitude of the adhesion energy per unit volume. The results are given in Table 4.42 and are plotted in Figure 4.66. Figure 4.66 shows that the magnitudes of the maximum disjoining pressure (adhesion energy per unit volume) were comparable in the quartz/F-RLO/F-SRB and the quartz/F-RLO/SSW systems. However, a significantly higher value was observed when DIW was used as an aqueous phase which again signifies the role dissolved salts play on the presence and the stability of the aqueous wetting films in rock/oil/water systems.

Table 4.42: Estimated $E_{adhesion}$ (Eq.21) for F-RLO at 10,000 psi & 208°F

Rock/oil/water system	Oil/water IFT (mN/m)	θ_r, (°) from the DDDC test	$Cos\theta_r$	θ_a, (°) from the DDDC test	$Cos\theta_a$	$E_{adhesion}$, (Pa) @ h = 10 Å, (Eq.21)
Quartz/F-RLO/F-SRB	33.51	23	0.9205	28	0.8829	1.259E+06
Calcite/F-RLO/F-SRB	33.51	29	0.8746	66	0.4067	1.568E+07
Quartz/F-RLO/SSW	31.76	24	0.9135	29	0.8746	1.236E+06
Quartz/F-RLO/DIW	29.85	32	0.8480	128	-0.6157	4.369E+07
Calcite/F-RLO/DIW	29.85	29	0.8746	24	0.9135	-1.162E+06

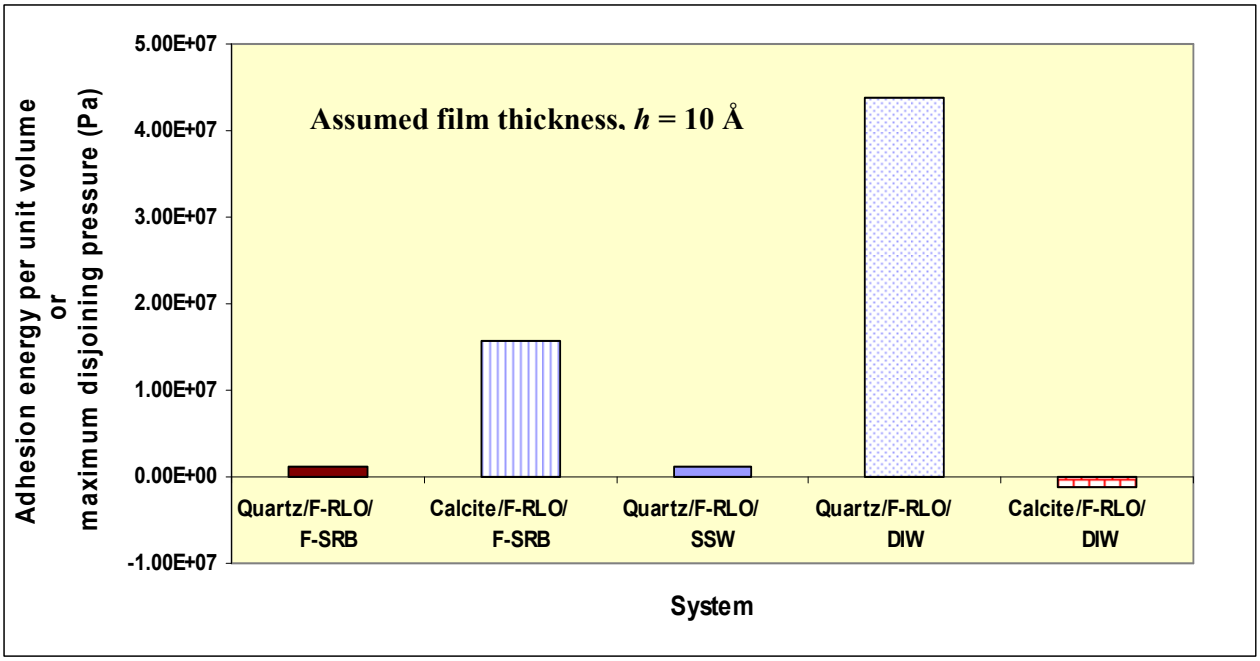

Figure 4.66: Estimated $E_{adhesion}$ (Pa) for F-RLO at 10,000 psi & 208°F

Positive (attractive) values of the adhesion energy per unit volume exhibited by the quartz system in the presence of F-SRB and SSW indicate the presence of rock/oil adhesion interactions even in these water-wet systems. These quantitative results substantiate the conclusions derived by Rao and Maini (1993) while explaining the exhibited behavior of the water-wet systems in

reservoir condition adhesion tests that the collapse of the aqueous wetting films is not the necessary condition for the development of rock/oil adhesion interactions.

The calcite system exhibited one order of magnitude higher of the adhesion energy per unit volume compared to the quartz system when F-SRB was the aqueous phase, thus suggesting the presence of stronger adhesion interactions between the bulk oil phase and the calcite surface compared to the quartz surface. However, a negative (repulsive) value of the adhesion energy per unit volume was observed in the calcite/F-RLO/DIW system. This result suggests the absence of dissolved salts in the aqueous phase allowed the aqueous wetting film to squeeze between the bulk oil phase and the calcite mineral surface and prevented the development of strong rock/oil adhesion interactions at these conditions of pressure and temperature.

4.5.6 Observed pH Behavior of Different Aqueous Phases, F Reservoir

The measured changes in the pH of the aqueous phase before and after the contact angle experiments are given in Table 4.43.

Table 4.43: Measured pH data for different aqueous phases, F reservoir

Oil/water system	Experimental conditions	Sample collection conditions	pH before Exp.	pH after Exp.	Change in measured pH (Δ pH)
F-STO/DIW	Atm. Press, 74°F	Atm. Press, 74°F	7.10	6.88	0.22
F-STO/SSW	Atm. Press, 74°F	Atm. Press, 74°F	8.18	8.06	0.12
F-STO/F-SRB	Atm. Press, 74°F	Atm. Press, 74°F	8.03	7.83	0.20
F-STO/F-SRB	8,000-13, 454 psi, 208°F	Atm. Press, 74°F	8.10	7.72	0.38
F-RLO/F-SRB	8,000-13, 454 psi, 208°F	Atm. Press, 74°F	7.85	7.74	0.11
F-RLO/SSW	8,000-13, 454 psi, 208°F	Atm. Press, 74°F	8.25	7.42	0.83
F-RLO/DIW	8,000-13, 454 psi, 208°F	Atm. Press, 74°F	7.35	7.54	-0.19

F-STO- Stock-tank oil (F reservoir), F-SRB- Synthetic reservoir brine (F reservoir), DIW- Deionized water, SSW- Synthetic sea water

All of the pH measurements were made at ambient conditions. The aqueous phase samples collected after the experiments had traces of crude oil in them. In the reservoir condition experiments, the change in pH ranged from -0.19 (F-RLO/DIW) to 0.83 (F-RLO/SSW) while in the ambient condition experiments the pH ranged from 0.12 (F-STO/SSW) to 0.22 (F-STO/DIW). These minor changes in pH are attributed to the interactions between oil and brine and the duration of each experiment. No particular trend in pH behavior was observed for different mineral surfaces.

4.6 Characterization of Rock/fluids Interactions, T Reservoir

In this section, the results of the oil/water IFT and the contact angle experiments conducted at both ambient and reservoir conditions for characterizing the rock/fluids interactions in the case of the T reservoir are presented.

The T reservoir is a deepwater GOM oil reservoir and has an initial pressure of 15,769 psi and reservoir temperature of 208°F. The reported bubble point pressure for the T reservoir is 4,000 psi @ 208°F and onset pressure for asphaltene precipitation is 5,500 psi. In this study, the oil/water IFT for different oil/water systems comprising T reservoir fluids was measured using the pendant drop method at pressures between 8,000 psi and 14,000 psi and at the reservoir temperature of 208°F. The DDDC and the sessile oil drop volume alteration experiments were conducted at 12,000 psi and 208°F. Three different aqueous phases, namely synthetic reservoir brine (T-SRB), deionized water (DIW), and 35,000 ppm NaCl solution (35K NaCl) were used in the reservoir condition experiments. In the case of the ambient condition experiments, stock-tank oil (T-STO) was used as the oil phase. T-SRB, SSW and DIW were used as the aqueous phase. Because quartz is the dominant (up to 97%) mineral of the T reservoir rock, polished quartz mineral crystals were used as the solid phase in the reservoir condition contact angle experiments. In the case of the ambient condition contact angle experiments, both the quartz and the calcite mineral surfaces were used as the solid phase.

4.6.1 Oil/water IFT Measurements

The IFT for different oil/water systems was measured by conducting pendant drop experiments at both reservoir and ambient conditions. The results are presented and discussed next.

Table 4.44: Measured oil/water IFT at ambient conditions, T reservoir

Oil/water system	T-STO density (gm/cc)	Aqueous phase density (gm/cc)	Density difference (gm/cc)	No. of pendant drops	Average equilibrium interfacial tension (mN/m)	Std. dev. (mN/m)
T-STO/DIW	0.8877	0.9976 (DIW)	0.1099	10	33.18	±0.90
T-STO/SSW	0.8877	1.024 (SSW)	0.1363	10	28.56	±0.56
T-STO/T-SRB	0.8877	1.008 (T-SRB)	0.1203	15	24.43	±0.83

T-STO- Stock-tank oil (T reservoir), T-SRB- Synthetic reservoir brine (T reservoir), DIW- Deionized water, SSW- Synthetic sea water

4.6.1.1 Ambient Condition Oil/water IFT Results

The results of ambient condition pendant drop experiments are given in Table 4.44. Higher oil/water IFT value was obtained in the case of DIW than SSW and T-SRB. These results suggest that the absence of dissolved salts in the aqueous phase significantly affected the IFT. A variation in the concentration of various ions and the presence of specific ions in the aqueous phase (Figure 4.67) also affected the IFT as evident from the lower IFT exhibited when SSW was used as the aqueous phase in place of T-SRB.

4.6.1.2 Reservoir Condition Oil/water IFT Results

The IFT for different oil/water systems comprising recombined live oil (T-RLO) and three different aqueous phases (T-SRB, DIW, and 35K NaCl soluition) were measured by conducting the

pendant drop experiments in the pressure range from 8,000 psi to 14,000 psi and at the reservoir temperature of 208°F.

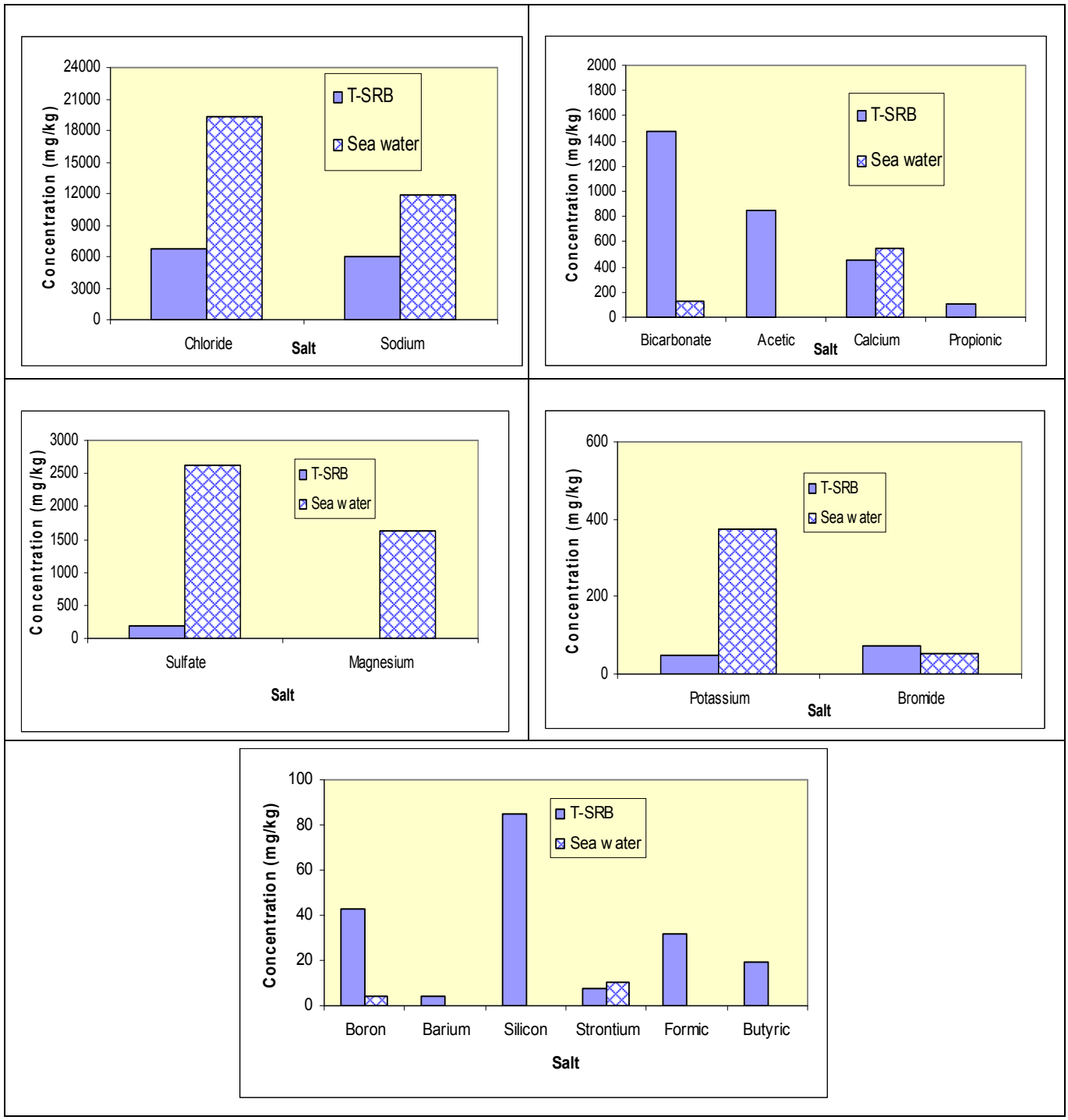

Figure 4.67: Comparison of the compositions of T-SRB and SSW

To ensure the accuracy of the measured oil/water IFT data, experiments were also repeated at a few pressure steps in the case of selected oil/water systems. The measured IFT data are given in Tables 4.45-4.47.

Table 4.45: Measured oil/water IFT for the T-RLO/T-SRB system at elevated press. & 208°F

T-RLO/T-SRB system								
						IFT values obtained in repeat experiment		
Pressure	**T-RLO density**	**T-SRB density**	**Number of pendant drops**	**Average Equilibrium Interfacial Tension**	**Std. Dev.**	**Number of pendant drops**	**Average Equilibrium Interfacial Tension**	**Std. Dev.**
psi	**gm/cc**	**gm/cc**		**mN/m**	**mN/m**		**mN/m**	**mN/m**
8,000	0.7888	0.9976	10	31.74	±0.24	6	31.08	±0.58
10,000	0.7989	1.0044	10	31.66	±0.72	6	30.99	±0.53
12,000	0.8085	1.0110	10	31.80	±0.28	6	31.65	±0.21
14,000	0.8177	1.0177	10	32.10	±0.28	7	31.97	±0.37

Table 4.46: Measured oil/water IFT for the T-RLO/DIW system at elevated press. & 208°F

T-RLO/DIW system					
Pressure	**T-RLO density**	**DIW density**	**Number of pendant drops**	**Average Equilibrium Interfacial Tension**	**Std. Dev.**
psi	**gm/cc**	**gm/cc**		**mN/m**	**mN/m**
8,000	0.7888	0.9883	8	30.22	±0.20
10,000	0.7989	0.9952	8	30.79	±0.33
12,000	0.8085	1.0017	8	30.98	±0.26
14,000	0.8177	1.0082	8	31.4	±0.39

Table 4.47: Measured oil/water IFT for the T-RLO/35K NaCl system at elevated press. & 208°F

T-RLO/35K NaCl system					
Pressure	**T-RLO density**	**35K NaCl density**	**Number of pendant drops**	**Average Equilibrium Interfacial Tension**	**Std. Dev.**
psi	**gm/cc**	**gm/cc**		**mN/m**	**mN/m**
8,000	0.7888	1.0082	6	25.03	±0.49
10,000	0.7989	1.0151	6	25.42	±0.29
12,000	0.8085	1.0215	7	26.16	±0.63
14,000	0.8177	1.0285	7	26.34	±0.56

Representative images of live oil drops captured during these experiments are shown in Figures 4.68-4.70.

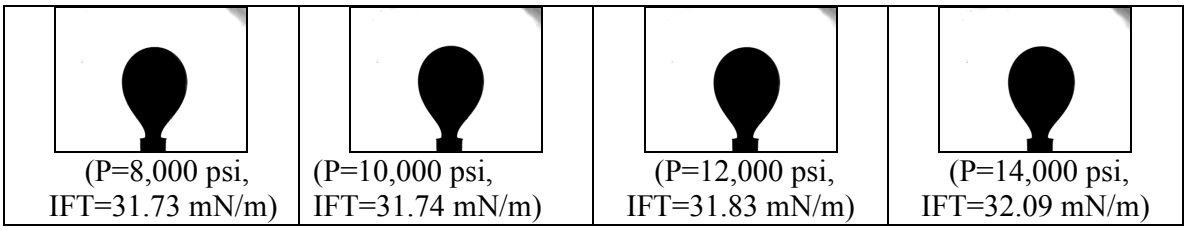

(P=8,000 psi, IFT=31.73 mN/m) (P=10,000 psi, IFT=31.74 mN/m) (P=12,000 psi, IFT=31.83 mN/m) (P=14,000 psi, IFT=32.09 mN/m)

Figure 4.68: Pendant drop images for the T-RLO/T-SRB system at elevated press. & 208°F

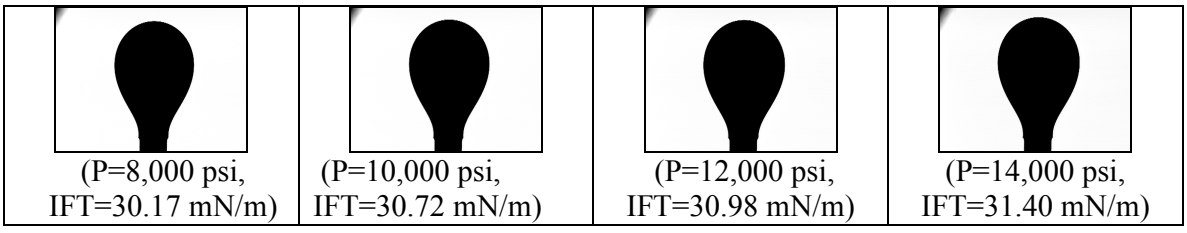

(P=8,000 psi, IFT=30.17 mN/m) (P=10,000 psi, IFT=30.72 mN/m) (P=12,000 psi, IFT=30.98 mN/m) (P=14,000 psi, IFT=31.40 mN/m)

Figure 4.69: Pendant drop images for the T-RLO/DIW system at elevated press. & 208°F

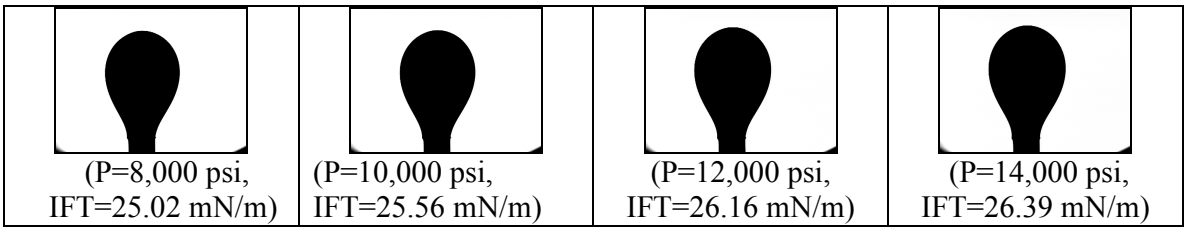

Figure 4.70: Pendant drop images for the T-RLO/35K NaCl system at elevated press. & 208°F

A plot of the measured IFT data for different live oil/water systems is shown in Figure 4.71.

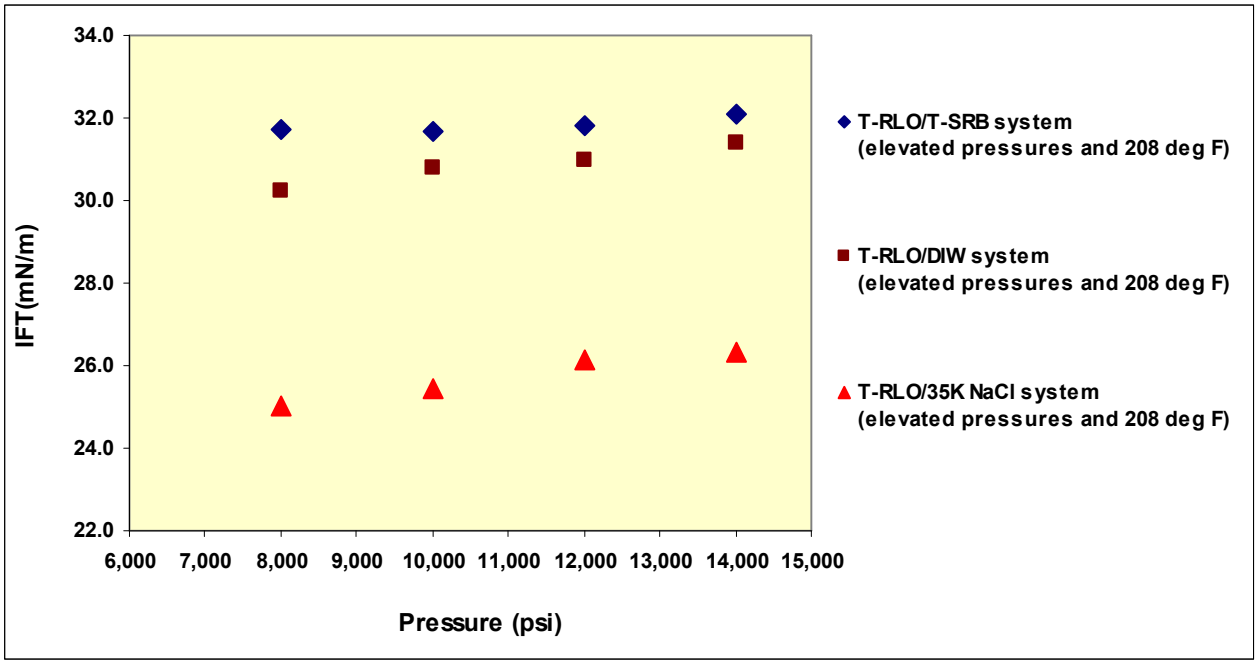

Figure 4.71: Measured oil/water IFT for the T reservoir at elevated press. & 208°F

The effect of pressure on the measured IFT was negligible in the case of the T-RLO/T-SRB system. However, an increase in the IFT was observed with pressure in the case of the T-RLO/DIW system. These results also suggest that the measured IFT was not affected significantly by complete absence of dissolved salts in the aqueous phase. However, in the case of

35,000 ppm NaCl solution, the measured IFT was found to be significantly lower than T-SRB. This indicates that the presence of additional ions in the aqueous phase (T-SRB) resulted in an increase in the measured IFT values (Figure 4.72).

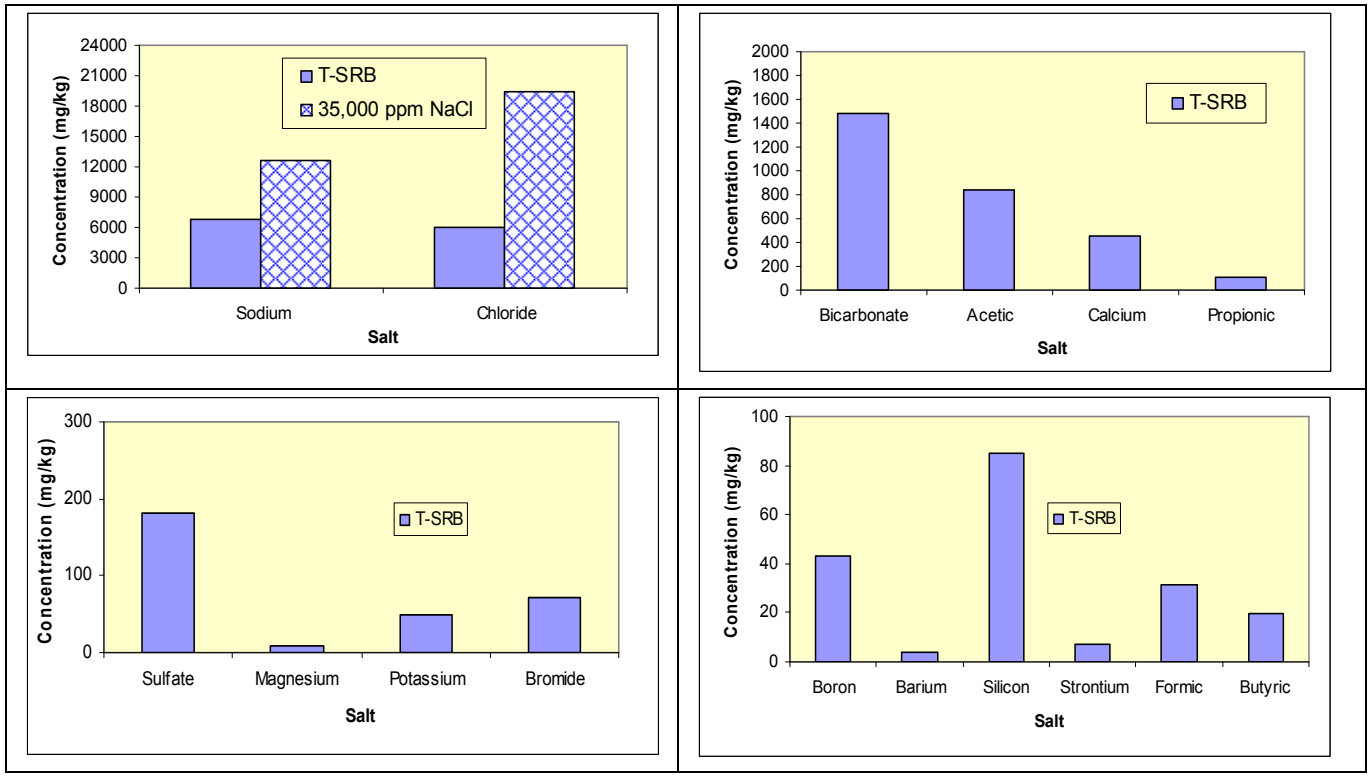

Figure 4.72: Comparison of the compositions of T-SRB and 35K NaCl

4.6.2 Determination of the Wettability of the T Reservoir

In the next step, the wetting characteristics of different rock/oil/water systems were determined by conducting the DDDC tests at both ambient and reservoir conditions.

4.6.2.1 Ambient Condition DDDC Tests

The ambient condition DDDC tests were conducted using stock-tank oil (T-STO). T-SRB and DIW were used as the aqueous phase. The quartz and the calcite mineral crystals were used as the solid phase in these tests. The results are given in Table 4.48. The water-receding and the

water-advancing contact angles obtained in the ambient condition DDDC tests are plotted in Figures 4.73-4.74.

Table 4.48: Results of the DDDC tests conducted for the T reservoir at ambient conditions

System	Experimental pressure and temperature conditions	Water-receding contact angle θ_r		Water-advancing contact angle θ_a	Wettability
		Upper crystal	Lower crystal		
Quartz/T-STO/DIW	Atm. Press, 74°F	15°	13°	143°	Strongly oil-wet
Quartz/T-STO/SSW	Atm. Press, 74°F	15°	14°	135°	Strongly oil-wet
Quartz/T-STO/T-SRB	Atm. Press, 74°F	14°	13°	147°	Strongly oil-wet
Calcite/T-STO/DIW	Atm. Press, 74°F	14°	13°	123°	Weakly oil-wet
Calcite/T-STO/SSW	Atm. Press, 74°F	15°	14°	118°	Weakly oil-wet
Calcite/T-STO/T-SRB	Atm. Press, 74°F	14°	13°	145°	Strongly oil-wet

T-STO- Stock-tank oil (T reservoir), T-SRB- Synthetic reservoir brine (T reservoir), DIW- Deionized water, SSW- Synthetic sea water

In the case of the quartz surface, all of the three systems showed strongly oil-wet behavior by exhibiting $\theta_a \geq 135°$. The calcite systems with DIW and SSW showed weakly oil-wet behavior ($118° \leq \theta_a \leq 123°$). However, strongly oil-wet behavior ($\theta_a = 145°$) was observed in the case of T-SRB. This behavior indicates that the effect of the presence of specific ions and a variation in the concentration of different ions in the aqueous phase on the ambient condition wetting behavior was more pronounced in the calcite systems than the quartz systems when T-SRB and SSW were the aqueous phase. However, the wetting behavior was not affected significantly when the dissolved salts in the aqueous phase were absent. Both the quartz and the calcite systems showed strongly oil-wet behavior ($\theta_a \geq 143°$) when tested with DIW.

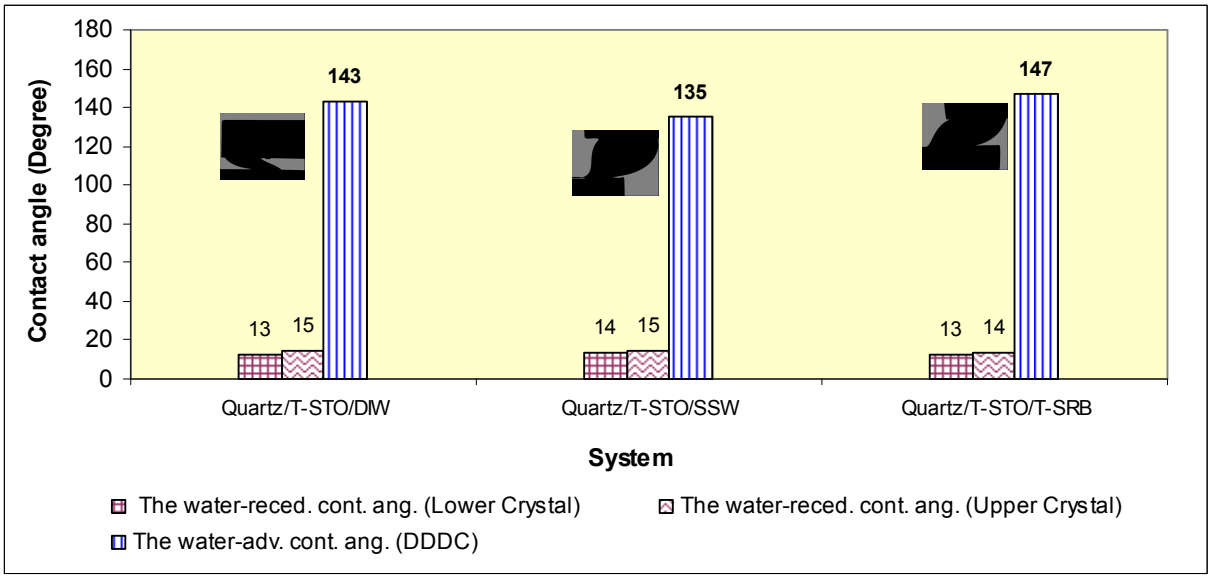

Figure 4.73: Ambient condition DDDC test results for the quartz/F-STO systems

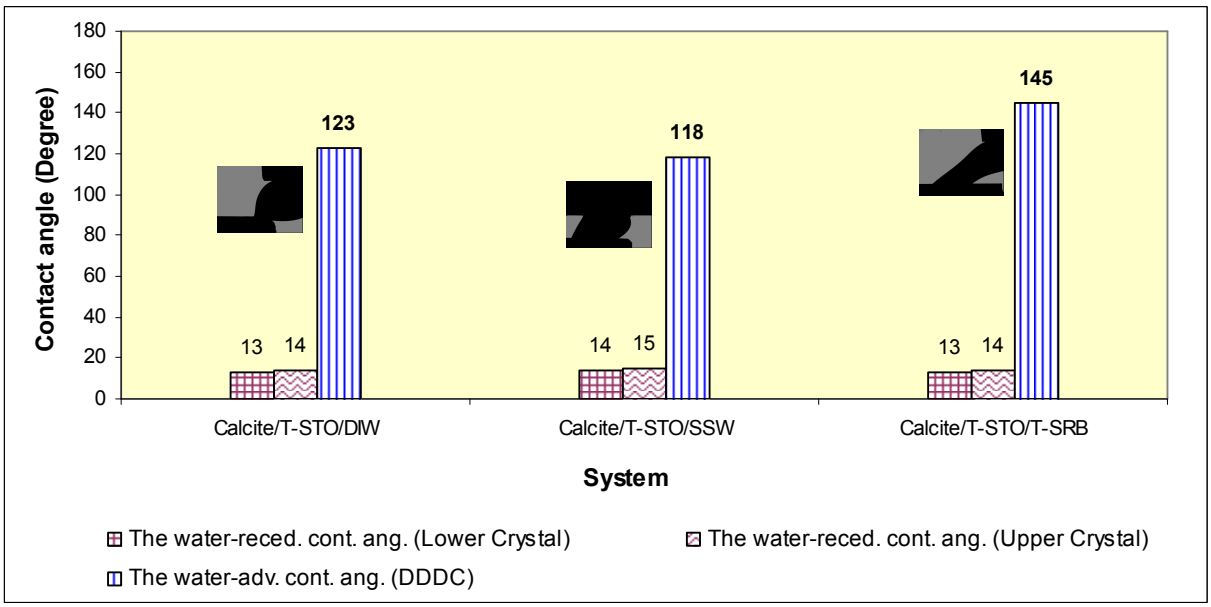

Figure 4.74: Ambient condition DDDC test results for the calcite/F-STO systems

4.6.2.2 Reservoir Condition DDDC Tests

The initial wettability state of the T reservoir was determined by conducting the DDDC tests for the quartz/T-RLO/T-SRB system at 12,000 psi and 208°F. The effect of brine composition on

the wetting behavior was investigated by using DIW and 35,000 ppm NaCl solution as other aqueous phase. The results are given in Table 4.49.

Table 4.49: Results of the DDDC tests conducted for the T reservoir at 12,000 psi & 208°F

System	Water-receding contact angle θ_r		Water - advancing contact angle θ_a	Wettability	Normalized TPCL movement
	Upper crystal	Lower crystal			
Quartz/T-RLO/T-SRB	24°	22°	30°	Strongly Water-Wet	3.59 to 2.98
Quartz/T-RLO/ DIW	28°	28°	33°	Strongly Water-Wet	6.36 to 4.36
Quartz/T-RLO/35K NaCl	40°	17°	22°	Strongly Water-Wet	1.91 to 1.69

The observed TPCL movements for different systems along with the corresponding water-receding and the water-advancing contact angles measured during the lateral movement of the lower crystal in the DDDC tests are shown in Figures 4.75-4.77.

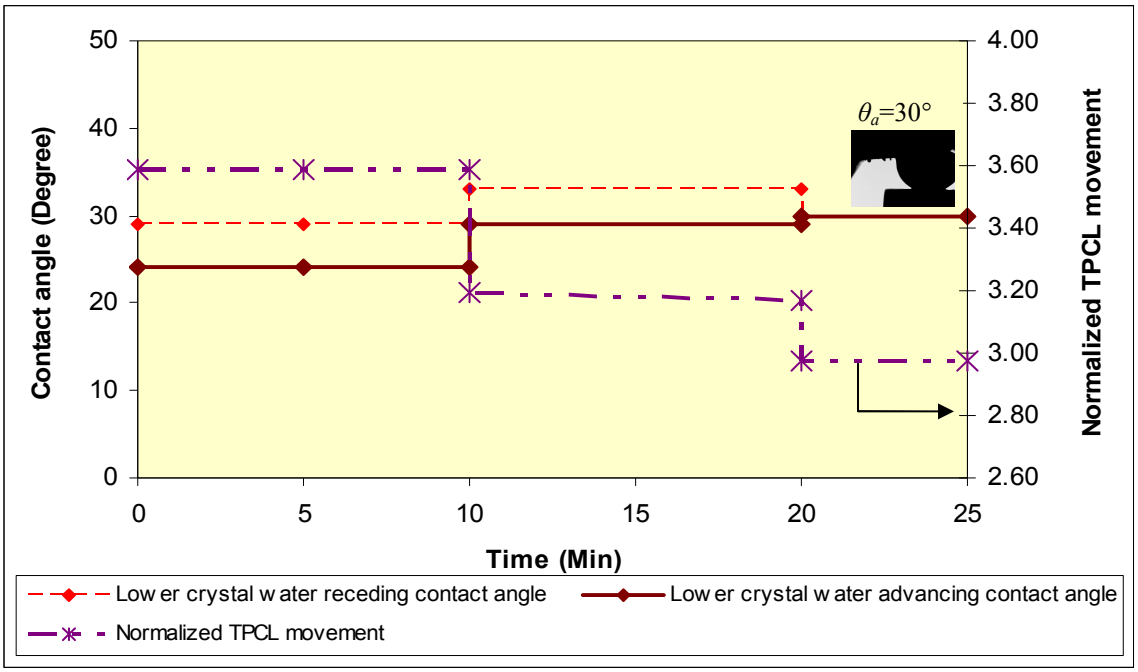

Figure 4.75: TPCL movement in the quartz/T-RLO/T-SRB system at 12,000 psi & 208°F

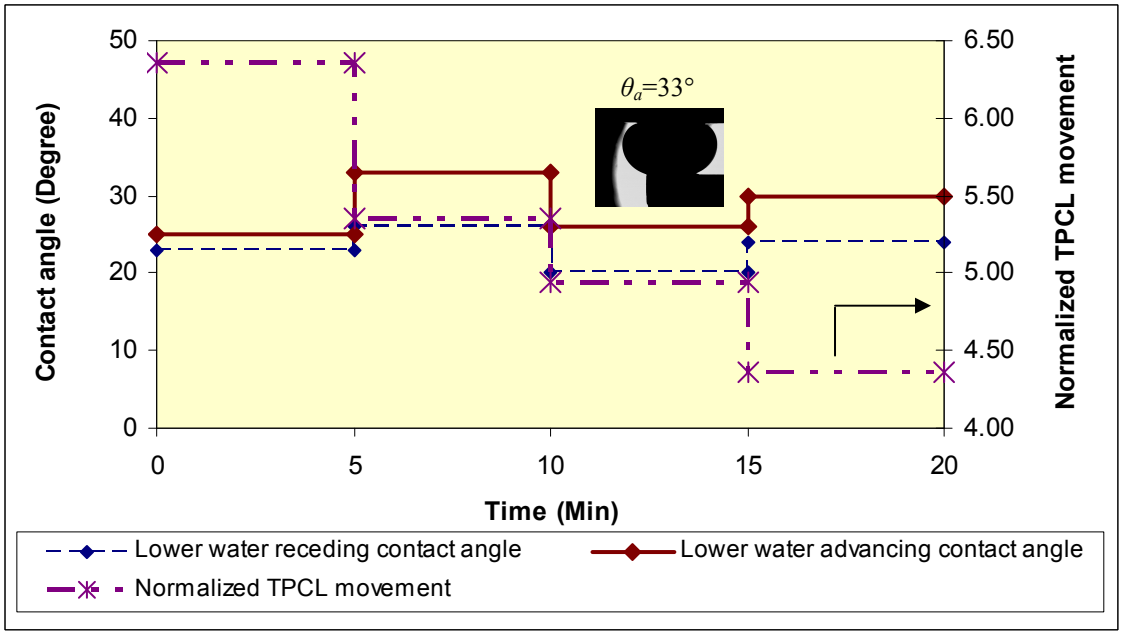

Figure 4.76: TPCL movement in the quartz/T-RLO/DIW system at 12,000 psi & 208°F

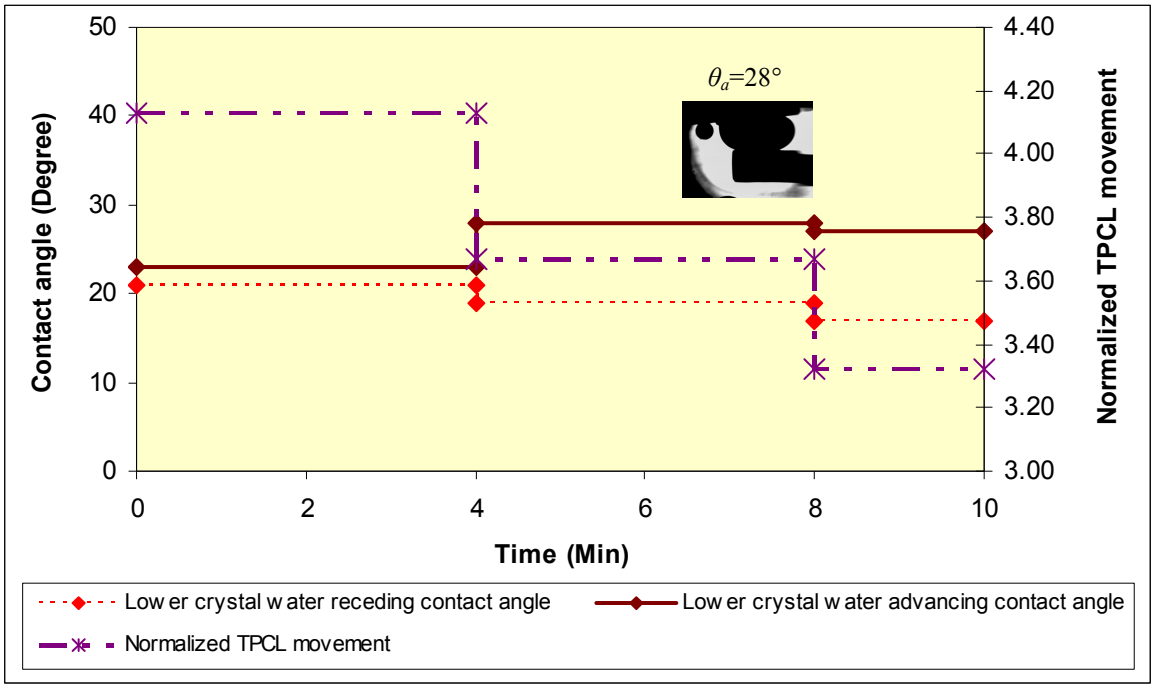

Figure 4.77: TPCL movement in the quartz/T-RLO/35K NaCl system at 12,000 psi & 208°F

All of the three systems showed the strongly water-wet behavior at reservoir conditions by exhibiting the water-advancing contact angle in the range from 22° to 33°. These results indicate that the wetting behavior of the quartz systems was neither affected by the absence of dissolved salts in the aqueous phase nor by the absence of all other ions except sodium and chloride ions (Figure 4.72).

4.6.3 The Sessile Oil Drop Volume Alteration Experiments

The extent of rock/oil adhesion interactions in the T reservoir was determined by conducting the sessile oil drop volume alteration experiments at both ambient and reservoir conditions. The extent of rock/oil adhesion interactions was quantified in terms of the line tension (Eq.12) and the line tension-based modified equation for the work of adhesion (Eq.17).

4.6.3.1 Ambient Condition Experiments

First, the sessile oil drop volume experiments were conducted for different rock/oil/water systems using stock-tank oil and three different aqueous phases (T-SRB, SSW, and DIW). The quartz and the calcite mineral crystals were used as the solid phase. Images of various sessile oil drops captured during these experiments are shown in Figure 4.78.

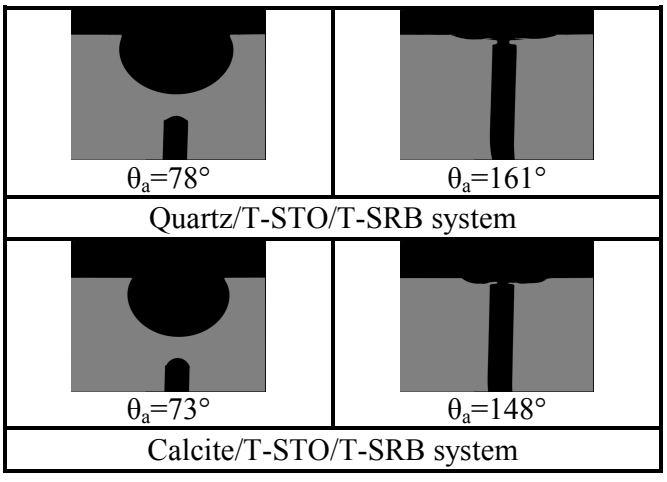

Figure 4.78: The sessile oil drop volume alteration experiments conducted for the quartz and the calcite systems at ambient conditions

All of the rock/oil/water systems exhibited low and comparable values of θ_r (13-14°). Both the quartz and the calcite surfaces showed a large variation in the measured θ_a for a small change in the contact radius with synthetic reservoir brine. Similar behavior was exhibited by the calcite systems when DIW and SSW were used as the aqueous phase. In view of the DDDC test results (Table 4.48), the sessile oil drop volume alteration experiments were not conducted for the quartz/T-STO/DIW and the quartz/T-STO/DIW systems because both systems exhibited strongly oil-wet behavior in the DDDC tests.

Graphs of observed $Cos\theta_a$ versus $1/r$ relationships for the quartz and the calcite systems are shown in Figures 4.79 and 4.80, respectively. The line tension values obtained from the observed slopes of the $Cos\theta_a$ versus $1/r$ relationships for both the quartz and the calcite systems are given in Table 4.50.

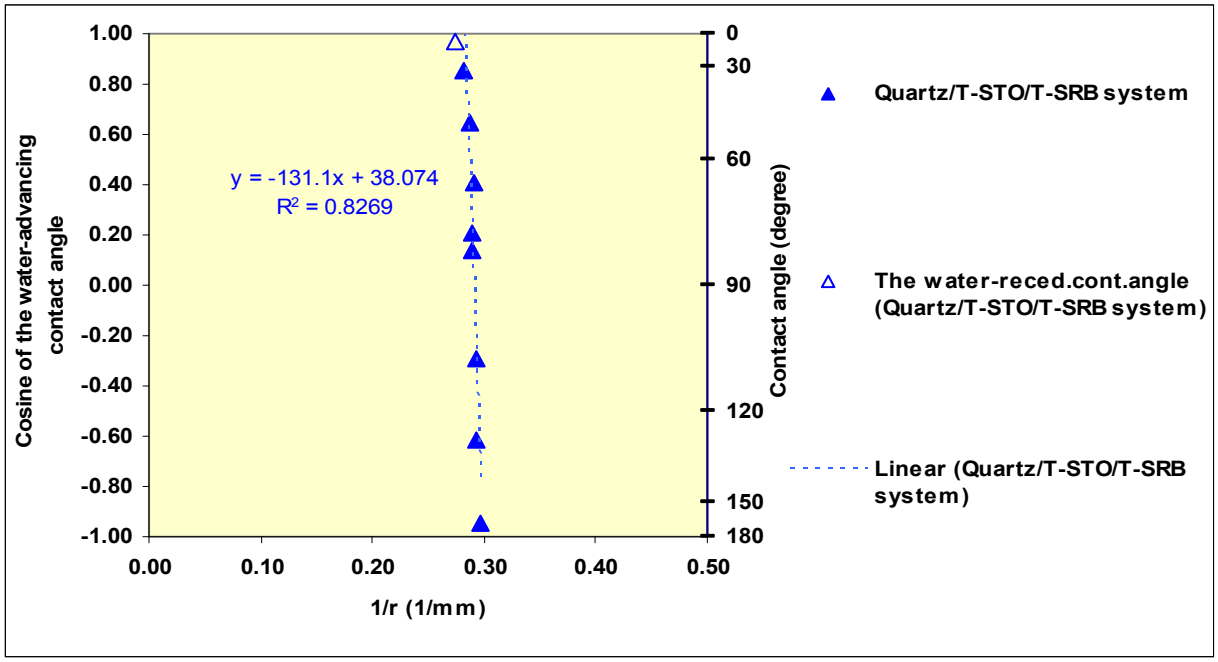

Figure 4.79: $Cos\theta_a$ versus $1/r$ relationship for the quartz/T-STO system at ambient conditions

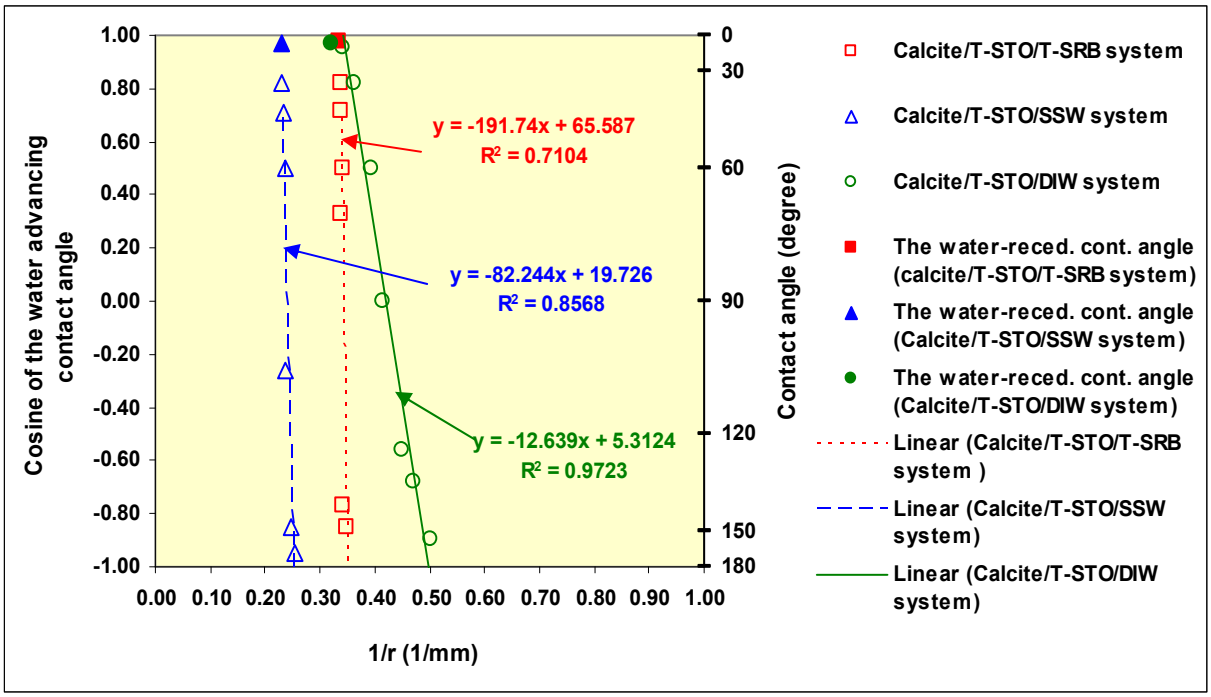

Figure 4.80: *Cos*θ_a versus *1/r* relationship for the calcite/T-STO system at ambient conditions

Table 4.50: Measured line tension for T-STO at ambient conditions

System	Variation in contact line radius (mm)	Slope of *Cos*θ_a versus *1/r* (1/mm) plot	Line tension σ (mN)
Quartz/T-STO/T-SRB	3.55 to 3.38	-131.1	3.203
Calcite/T-STO/T-SRB	2.94 to 2.87	-191.74	4.683
Calcite/T-STO/DIW	2.94 to 1.99	-12.639	0.418
Calcite/T-STO/SSW	4.32 to 3.92	-82.244	2.339

The calcite system showed higher line tension than the quartz system when T-SRB was the aqueous phase. This clearly indicates the presence of stronger rock/oil adhesion interactions the calcite system than the quartz system. The calcite system with DIW showed lower line tension values than SSW and T-SRB. It suggests that the presence of weaker rock/oil adhesion interactions in the calcite system when the dissolved salts in the aqueous phase were absent.

4.6.3.2 Reservoir Condition Experiments

The extent of rock/oil adhesion interactions in the T reservoir at reservoir conditions was quantified in terms of the line tension by conducting the sessile oil drop volume alteration experiment at 12,000 psi and 208°F for the quartz/T-RLO/T-SRB system. Representative images of various sessile oil drops captured during this experiment are shown in Figure 4.81. Graph of the observed $Cos\theta_a$ versus *1/r* relationship is shown in Figure 4.82.

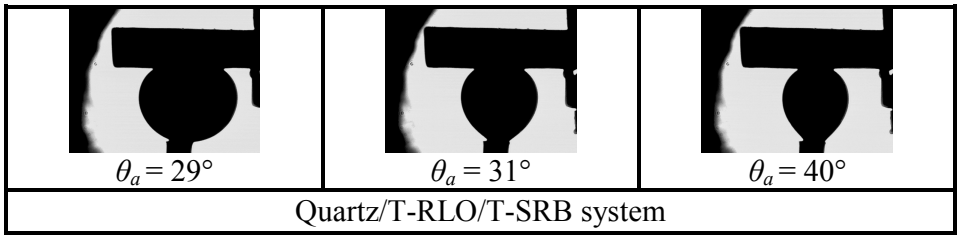

Figure 4.81: The sessile oil drop volume alteration experiment conducted for the quartz/T-RLO/T-SRB system at 12,000 psi & 208°F

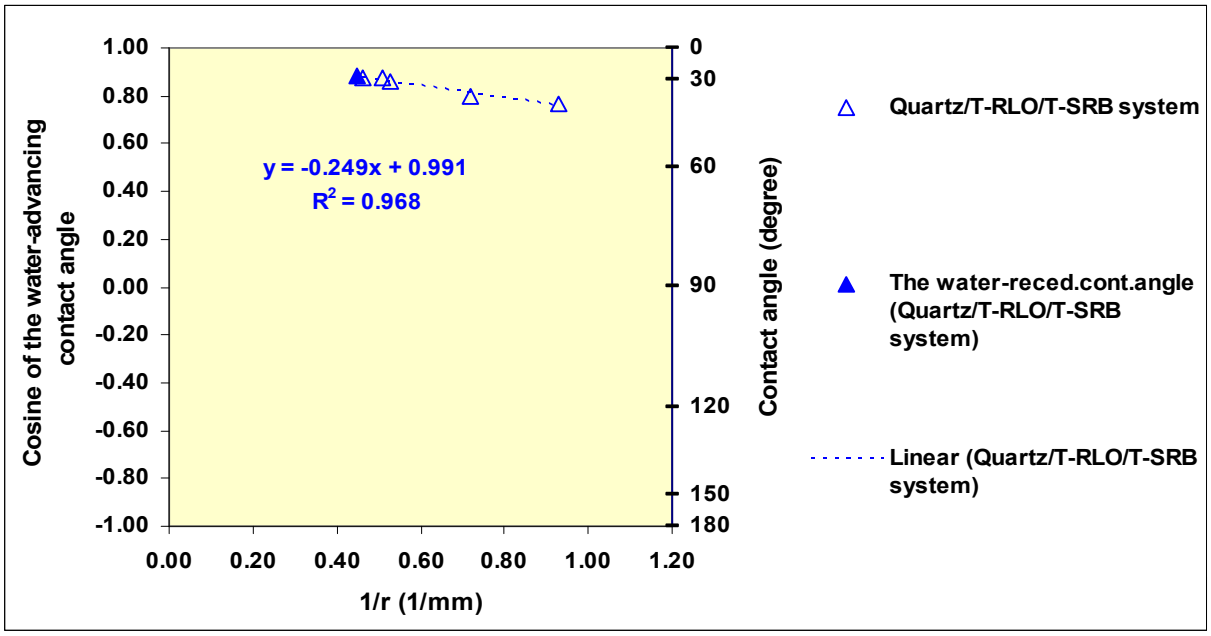

Figure 4.82: $Cos\theta_a$ versus *1/r* relationship for the quartz/T-RLO/T-SRB system at 12,000 psi & 208°F

The quartz system exhibited a low slope (-0.249) of $Cos\theta_a$ versus *1/r* line, thus exhibited a low line tension value (0.008 mN). This behavior clearly indicates the presence of weak rock/oil adhesion interactions in the system. Similar behavior was observed in the DDDC test. In view of the DDDC test results, the sessile drop volume alteration experiments were not conducted for the quartz/T-RLO/DIW and the quartz/T-RLO/35K NaCl systems.

4.6.4 Estimation of the Work of Adhesion, W_{sow}, T Reservoir

The extent of rock/oil adhesion interactions was also quantified in terms of the work of adhesion, $W_{sow,}$ (Eq.17) at both reservoir and ambient conditions. The collected oil/water IFT data and the drop size dependence of sessile oil drop (θ_a and r data) observed in drop volume alteration experiments were used to compute W_{sow} in the case of selected rock/oil/water systems.

4.6.4.1 Estimation of W_{sow} at Ambient Conditions

The computed W_{sow} values for the selected rock/stock-tank oil/water systems are given in Tables 4.51-4.52.

Table 4.51: Measured W_{sow} for the quartz/T-STO/T-SRB system at ambient conditions

Quartz/T-STO/T-SRB system (measured σ = 3.203 mN), γ_{ow} = 24.43 mN/m, θ_r = 14°, Eq. time = 24 h					
Vol. red. Step No.	**Water-advancing contact angle, θ_a, (°)**	**$Cos\theta_a$**	**Contact radius, r (mm)**	**Drop volume ratio***	**Work of adhesion/area $W_{sow,}$ (mN/m or mJ/m^2) Eq.17**
1	31	0.8572	3.5454	0.73	3.49
2	50	0.6428	3.4863	0.52	8.73
3	66	0.4067	3.4357	0.38	14.49
4	78	0.2079	3.4526	0.28	19.35
5	82	0.1392	3.4610	0.20	21.03
6	107	-0.2924	3.4162	0.10	31.57
7	128	-0.6157	3.4162	0.05	39.47
8	161	-0.9455	3.3745	0.02	47.53

*Drop volume ratio =Volume of sessile oil drop at a given drop size red. step/Volume of initial sessile oil drop

Table 4.52: Measured W_{sow} for the calcite/T-STO/T-SRB system at ambient conditions

Calcite/T-STO/T-SRB system (measured σ = 4.683 mN), γ_{ow} =24.43 mN/m, θ_r = 13°, Eq. time = 24 h					
Vol. red. Step No.	**Water-advancing contact angle, θ_a, (°)**	**$Cos\theta_a$**	**Contact radius, r (mm)**	**Drop volume ratio***	**Work of adhesion/area W_{sow}, (mN/m or mJ/m^2) Eq.17**
1	35	0.8192	2.9461	0.77	4.42
2	44	0.7193	2.9545	0.62	6.86
3	60	0.5000	2.9292	0.42	12.22
4	71	0.3256	2.9461	0.25	16.48
5	140	-0.7660	2.9208	0.09	43.14
6	148	-0.8480	2.8785	0.03	45.15

*Drop volume ratio =Volume of sessile oil drop at a given drop size red. step/Volume of initial sessile oil drop

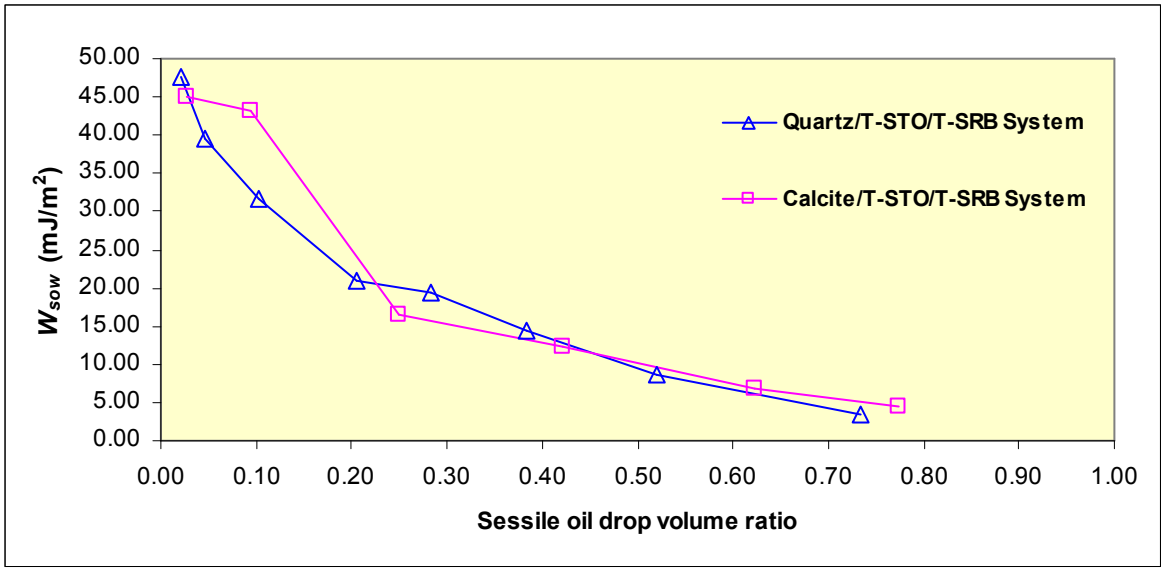

Figure 4.83: Effect of brine composition on oil mobilization at ambient conditions, T reservoir

The effect of the extent of rock/oil adhesion interactions on oil mobilization was evaluated by plotting the computed W_{sow} values against drop volume ratios. A plot of W_{sow} versus sessile oil drop volume ratio relationship for these systems is shown in Figure 4.83. A significantly higher work

needs to be exerted to move the oil in both oil-wet (the quartz/T-STO/T-SRB and the calcite/T-STO/T-SRB) systems, especially at lower drop volume ratios.

4.6.4.2 Estimation of W_{sow} at Reservoir Conditions

In the case of the quartz/T-RLO/T-SRB system, the collected oil/water IFT, θ_a, and r data were used to compute the magnitude of W_{ows} at reservoir conditions. The results are given in Table 4.52.

Table 4.53: Measured W_{sow} for the quartz/T-RLO/T-SRB system at 12,000 psi & 208°F

Quartz/T-RLO/T-SRB system (measured σ = 0.008 mN), γ_{ow} = 31.8 mN/m, θ_r = 24°, Eq. time = 24 h					
Vol. red. Step No.	**Water-advancing contact angle, θ_a, (°)**	**$Cos\theta_a$**	**Contact radius, r (mm)**	**Drop volume ratio***	**Work of adhesion/area W_{sow}, (mN/m or mJ/m^2) Eq.17**
1	29	0.8746	2.1707	0.91	3.99
2	29	0.8746	1.9701	0.80	3.99
3	31	0.8572	1.8880	0.68	4.54
4	37	0.7986	1.3863	0.47	6.40
5	40	0.7660	1.0762	0.30	7.44

*Drop volume ratio =Volume of sessile oil drop at a given drop size red. step / Volume of initial sessile oil drop

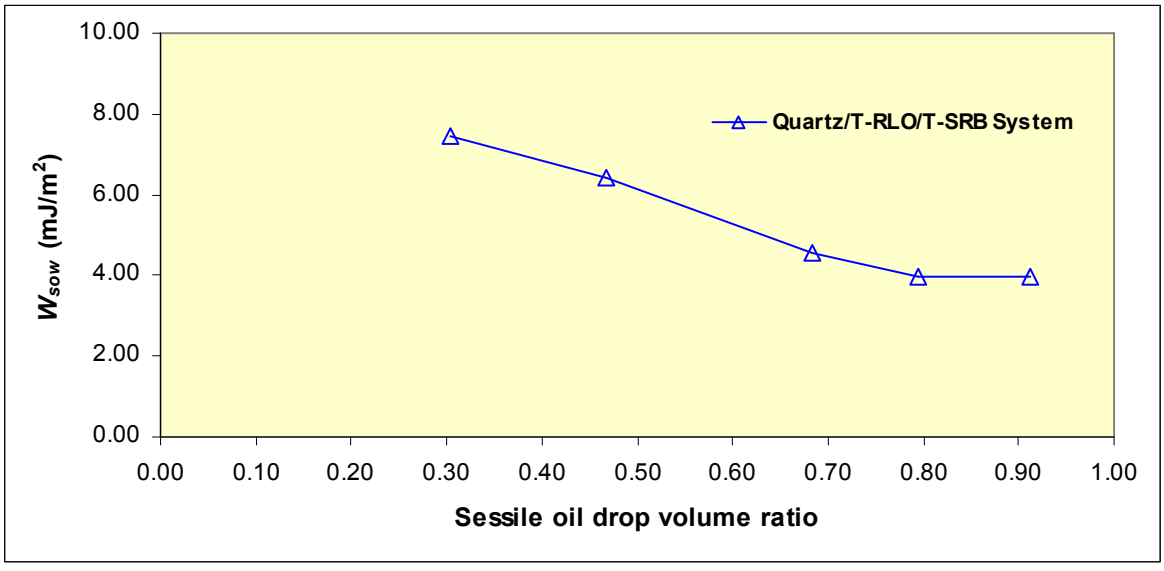

Figure 4.84: W_{sow} versus sessile oil drop volume ratio relationship for the quartz/T-RLO/T-SRB system at 12,000 psi & 208°F

Graph of W_{sow} versus sessile drop volume ratio relationship for this system is shown in Figure 4.84. As can be seen in Figure 4.84, in the presence of weak rock/oil adhesion interactions, the amount of work that needs to be exerted to mobilize the oil did not change significantly even for a significant decrease in its saturation (a decrease in drop volume ratio).

4.6.5 Estimation of Adhesion Energy per Unit Volume at Reservoir Conditions, T-RLO

In the last step, the magnitude of the adhesion energy per unit volume for different rock/oil/water systems was estimated using Eq.21. The measured water-receding contact angle (θ_r) and the water-advancing contact angle (θ_a) data obtained in the DDDC test (Table 4.49), the measured oil/water IFT (Tables 4.45-4.47), and an assumed thickness of the aqueous wetting films (10 Å) was used to estimate the adhesion energy per unit volume. The results are given in Table 4.54 and are shown in Figure 4.85. A positive (attractive) and low value of the adhesion energy per unit volume exhibited by all of three cases indicate the presence of some but weak rock/oil adhesion interactions in these systems even though water-wet behavior was exhibited by them in the DDDC tests. These results suggest that the magnitude of the adhesion energy per unit volume in the case of the T reservoir was not affected by a variation in the composition of the aqueous phase.

Table 4.54: Estimated $E_{adhesion}$ (Eq.21) for T-RLO at 12,000 psi & 208°F

System	Oil/water IFT (mN/m)	θ_r, (°) from the DDDC test	$Cos\theta_r$	θ_a, (°) from the DDDC test	$Cos\theta_a$	$E_{adhesion}$, (Pa) @ h = 10 Å, (Eq.21)
Quartz/T-RLO/ T-SRB	31.80	24	0.9135	30	0.8660	1.511E+06
Quartz/T-RLO/ DIW	30.98	28	0.8829	33	0.8387	1.372E+06
Quartz/T-RLO/ 35K NaCl	26.16	17	0.9563	22	0.9272	7.618E+05

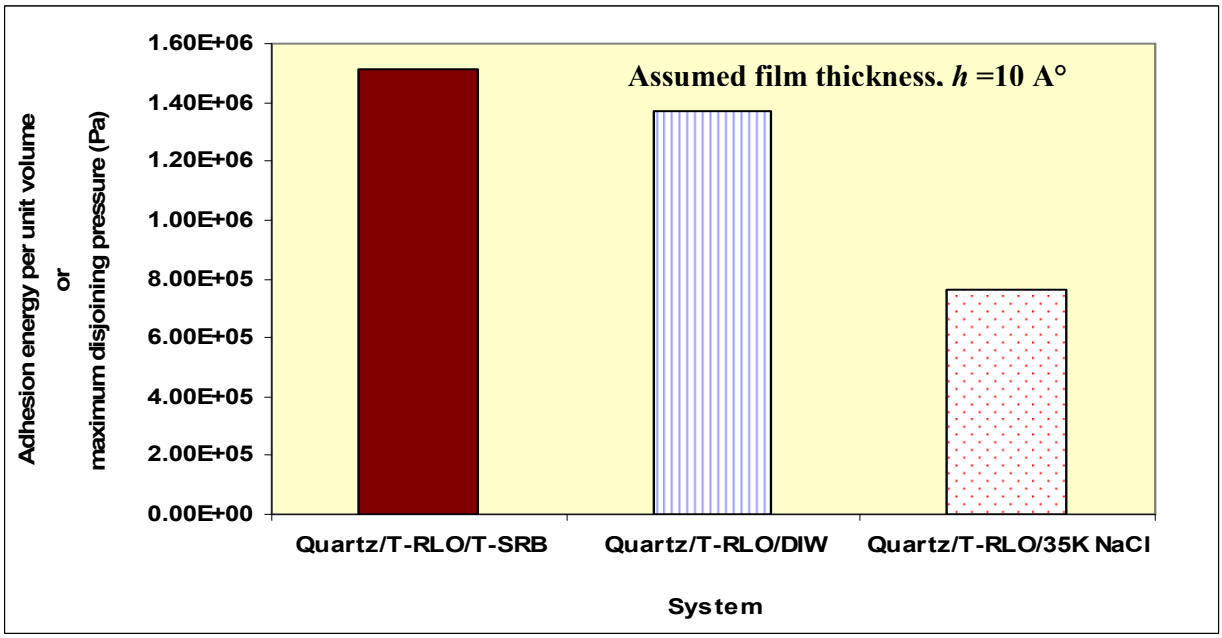

Figure 4.85: Estimated $E_{adhesion}$ (Pa) for T-RLO at 12,000 psi & 208°F

4.6.6 Observed pH Behavior of Different Aqueous Phases, T Reservoir

The measured changes in the pH of aqueous phase before and after the contact angle experiments are given in Table 4.55.

Table 4.55: Measured pH data for different aqueous phases, T reservoir

Oil/water system	Experimental conditions	Sample collection conditions	pH before Exp.	pH after Exp.	Change in measured pH (Δ pH)
T-STO/DIW	Atm. Press, 74°F	Atm. Press, 74°F	6.56	7.65	-1.09
T-STO/SSW	Atm. Press, 74°F	Atm. Press, 74°F	8.14	8.04	0.10
T-STO/T-SRB	Atm. Press, 74°F	Atm. Press, 74°F	7.89	7.76	0.13
T-RLO/T-SRB	8,000-14,000 psi, 208°F	Atm. Press, 74°F	7.91	7.40	0.51
T-RLO/DIW	8,000-14,000 psi, 208°F	Atm. Press, 74°F	6.98	6.68	0.30
T-RLO/35K NaCl	8,000-14,000 psi, 208°F	Atm. Press, 74°F	7.25	7.10	0.15

T-STO- Stock-tank oil (T reservoir), T-SRB- Synthetic reservoir brine (T reservoir), DIW- Deionized water, SSW- Synthetic sea water, 35K NaCl -35,000 ppm NaCl solution

All of the pH measurements were made at ambient conditions. The aqueous phase samples collected after the experiments had traces of crude oil in them. In the reservoir condition experiments, the change in pH ranged from 0.30 (T-RLO/DIW) to 0.51 (T-RLO/T-SRB) while in the ambient condition experiments, pH ranged from 0.13 (T-STO/T-SRB) to -1.09 (T-STO/DIW). No particular trend in pH behavior was observed for different mineral surfaces.

5. CONCLUSIONS AND RECOMMENDATIONS

In this study, the pendant drop method, the dual-drop dual-crystal (DDDC) technique, and the sessile oil drop volume alteration method were successfully used to characterize the interfacial phenomena of the oil/water interfacial tension, spreading, wettability, and the extent of rock/oil adhesion interactions in various rock/live oil/synthetic reservoir brine systems at pressures up to 14,000 psi and temperatures up to 250°F.

This appears to be first time when the applicability of line tension based-modified Young's equation in complex rock/oil/water systems at reservoir conditions was evaluated to overcome the inadequacy of the Young's equation in taking account of the presence of strong intermolecular surface forces present in the system. The measured line tension values in different rock/oil/water systems were correlated with adhesion number which is defined as ($Cos\theta_r$-$Cos\theta_a$) in complex rock/oil/water systems. The results suggest that the extent of deviation from the Young's equation exhibited by rock/oil/brine systems may be directly related to the rock/oil adhesion interactions. This provides an experimental means to quantify the adhesion aspect of the wettability in terms of the line tension. Earlier such quantification of rock/oil adhesion interactions was available only through water-advancing contact angles. The measured line tension results were also used to experimentally demonstrate that the measured water-advancing contact angle (θ_a) is a good estimate of the equilibrium contact angle (the Young's contact angle) in complex rock/oil/water systems.

The successful applicability of modified Young's equation in describing the observed behavior of drop size dependence of dynamic contact angle in complex rock/oil/water systems led to a new line tension-based modification of the Young-Dupré equation. This modification suitably incorporates the effect of rock/oil adhesion interactions on the work of adhesion. The work of adhesion values measured using the new line tension-based modified form of the Young-Dupré

equation were correlated to a change in the sessile oil drop volume observed during the drop volume alteration experiments. The observed relationship between the measured work of adhesion and the sessile oil drop volume ratio was successfully used to study the effect of rock/oil adhesion interactions on residual oil saturation (manifested by the decreasing sessile oil drop volume ratio in the experiment). The effect of fluids composition on the oil/water interfacial tension and the effect of rock mineralogy and fluids composition on the wetting characteristics of complex rock/oil/water systems at elevated pressures and temperatures were also successfully evaluated in this study.

A new equation was developed to estimate the adhesion energy per unit volume (correlatable to maximum disjoining pressure) in complex rock/oil/water systems at representative reservoir conditions using actual reservoir fluids and common reservoir rock mineral surfaces. This equation uses the measured oil/water interfacial tension and dynamic contact angles along with an assumed thickness of the aqueous wetting films similar to the value found in the reservoir condition theoretical disjoining pressure isotherms at which a spontaneous change in wetting behavior is exhibited by the system. Such estimates of the maximum disjoining pressure in the form of the adhesion energy per unit volume in conjunction with pore size distribution data and values of connate water saturation are expected to provide better predictions of in-situ wettability at the pore level.

A comparison of the reported values of the theoretically determined maximum disjoining pressures with the estimated values of the adhesion energy per unit volume using the equation developed in this study suggests that the experimental techniques used in this study overcome the difficulty associated with the existing theoretical models. The theoretical models use certain parameters that are not easily measureable in the case of complex rock/oil/water systems, especially at reservoir conditions. However the equation developed in this study uses the measureable quantities of the oil/water interfacial tension and dynamic contact angles along with

an assumed thickness of the aqueous wetting films for estimating the maximum disjoining pressure in the form of the adhesion energy per unit volume.

The estimated values of the adhesion energy per unit volume for complex rock/oil/water systems at reservoir conditions obtained in this study provide a threshold value of the imposed capillary pressure beyond that a spontaneous change in the wetting behavior may occur for an initially water-wet system. The adhesion energy per unit volume values in the range from $1.44x10^{+05}$ Pa (20 psi) at 50 Å to $1.20x10^{+06}$ Pa (174 psi) at 6 Å for the water-wet systems such as the quartz/B-RLO/B-SRB system suggests that a spontaneous change in the wetting behavior may be observed in a given pore, if there exist the conditions of connate water saturation that lead to the thickness of the aqueous wetting films in the order of 5 Å and the imposed capillary pressure value exceeds 174 psi. Also the significantly high adhesion energy per unit volume values ($8.24x10^{+06}$ Pa (~1200 psi) at 50 Å) for oil-wet systems such as the calcite/B-RLO/B-SRB system suggests that significantly high capillary pressure (manifested by the high value of the work of adhesion in oil-wet systems) must be applied to move any residual oil in oil-wet pores.

The results of ambient and reservoir condition experiments conducted using stock-tank oils and different aqueous phases (deionized water, synthetic reservoir brines, and synthetic sea water) reinforces the need to conduct the experiments at reservoir conditions using representative reservoir fluids (live oil and brine) to confidently characterize the interfacial interactions of the oil/water IFT, spreading, wettability, and the rock/oil adhesion in complex rock/oil/water systems.

5.1 Recommendations for Future Work

The experimental results presented in this study suggest that the role of specific ions present in brine, especially magnesium and sulfate ions, on the extent of rock/oil adhesion interactions in the case of quartz systems need to be explored further at representative reservoir conditions using live oils as the ambient condition experiments conducted with stock-tank oil may yield misleading results. The role of the presence and variation of the concentration of calcium ion on the extent of

rock/oil adhesion interactions in the case of the calcite systems also deserves further investigation to understand its role on the wetting behavior of the system for devising means to overcome strong rock/oil adhesion forces present in the system.

The effect of oil composition and especially the role of gaseous/lighter components on the extent of rock/oil adhesion interactions need to be explored by conducting experiments at various pressures below the bubble point pressure and the reservoir temperature using live oil mixtures with low to high gas oil ratios because the condition of stock-tank oil may never be achieved in the life of a reservoir.

The estimation of the maximum disjoining pressure in the form of the adhesion energy per unit volume obtained in this study needs to be explored further to establish a direct relationship between these two quantities.

The effects of different variables on the extent of rock/fluids interactions observed in this study need to be explored further by conducting the reservoir condition core-flooding experiments to evaluate their implications to oil recovery.

REFERENCES

1. "Facing the hard truths about energy" Report prepared by Advanced Resources International of Arlington, VA for U.S. Department of Energy (DOE), 2007

2. Richardson, G.Ed, Nixon, L.D., Bohannon, C.M., Montgomery, T.M., and Gravois, M.P.: "Deepwater Gulf of Mexico 2008: America's offshore energy future", OCS report, MMS 2008-13

3. Sarian, S. and Gibson, A.: "Wireline evaluation technology in HPHT wells" SPE 97571, 2005, Paper presented at SPE High Pressure/High Temperature Sour Well Design Applied Technology Workshop, 17-19 May 2005, The Woodlands, Texas

4. Craig, Jr., F.F.: The reservoir engineering aspects of waterflooding, SPE monograph, Vol-3, 1971, pp-12-28

5. Tiab, D. and Donaldson, E.C.: Petrophysics – The theory and practice of measuring reservoir rock and fluid transport properties, Gulf Publishing Company, Houston, USA, 1996

6. Nutting, P.G.: "Some physical and chemical properties of reservoir rocks bearing on the accumulation and discharge of oil", Problems of Petroleum Geology, AAPG, Tulsa, 1934

7. Katz, D.L.: "Possibilities of secondary recovery for the Oklahoma city Wilcox Sand" , Trans., AIME, 146(1942), pp-28-43

8. Treiber, L.E. , Archer, D.L. and Owens, W.W.: "A laboratory evaluation of the wettability of fifty oil-producing reservoirs", SPE 3526-PA, 1972

9. Amott, E.: "Observations relating to the wettability of porous rock", Trans., AIME, 216(1959), pp-156-162

10. Donaldson, E.C., Kendall, R.F., Thomas, R.D. and Lorenz, P.B.: "Wettability determination and its effect on recovery efficiency", SPE 2238, SPE Journal, March-1969, pp-13-20

11. Salathiel, R.A.: "Oil recovery by surface film drainage in mixed-wettability rocks", SPE 4104, JPT, Oct-1973, pp-1216-1224

12. Anderson, W.G.: "Wettability literature survey-part 1: Rock/Oil/Brine interactions and the effects of core handling on wettability", SPE 13932-PA, JPT, Oct- 1986

13. Anderson, W.G.: "Wettability literature survey-part 2: Wettability measurement. SPE 13933-PA, JPT,Nov-1986

14. Anderson, W.G.: "Wettability literature survey-part 3: The effect of wettability on the electrical properties of porous media", SPE 13934-PA, JPT, Dec-1986

15. Anderson, W.G.: “Wettability literature survey-part 4: The effects of wettability on capillary pressure”, SPE 15271-PA, JPT, Oct-1987

16. Anderson, W.G.: “Wettability literature Survey-part 5: “The effects of wettability on relative permeability”, SPE 16323-PA, JPT, Nov-1987

17. Anderson, W.G.: “Wettability literature Survey-part 6: “The effects of wettability on waterflooding”, SPE 16471-PA, JPT, Dec-1987

18. Morrow, N.R.: “Wettability and its effects on oil recovery”, SPE 21621, SPE Distinguished Author Series, JPT, Dec-1990

19. Rao, D.N., Girard, M.G., and Sayegh, S.G.: “Impact of miscible flooding on wettability, relative permeability, and oil recovery”, SPE Reservoir Engineering, May-1992, pp-204-212

20. Vizika, O. and Lombard, J.M.: “Wettability and Spreading: Two key parameters in oil recovery with three-phase gravity drainage”, SPE 28613-PA, SPE Reservoir Engineering, Feb-1996,54-60

21. Christensen, J.R., Stenby, E.H., and Skauge, A.: “Review of the WAG field experience”, SPE 71203-PA, SPE Reservoir Evaluation and Engineering, Apr-2001, 97-106

22. Agbalaka, C., Dandekar, A.Y., Patil, S.L., Khataniar, S., and Hemsath, J.R.: “The effect of wettability on oil recovery: a review”, SPE 114496, 2008

23. Young, T.: In ‘Miscelleneous Work’ (G. Pecock, ed.) vol. 1. Murray, London, 1855

24. Wenzel, R.N.: J. Phys. Chem. 53,1466(1949)

25. Bobek, J.E., Mattax, C.C., and Denekas, M.O.: “Reservoir rock wettability-its significance and evaluation” Trans., AIME, 213(1958): 155-160

26. Neumann, A.W. and Good, R.J.: “Thermodynamics of contact angle, I. Heterogeneous solid surfaces”, Journal of Colloid and Interface Science, Vol. 38, No. 2, February 1972

27. Rao, D.N.: “The concept, characterization, concerns and consequences of contact angles in solid-liquid-liquid systems”, Contact Angle, Wettability and Adhesion, 3 (2003), pp-191-210, Ed. K.L. Mittal, VSP, Utrecht

28. Wagner, O.R. and Leach, R.O.: Improving oil displacement efficiency by wettability adjustment” 1101G, Trans. AIME, 216,1956

29. Leach, R.O., Wagner, O.R., Wood, H.W., and Harpke, C.F.: “A laboratory and field study of wettability adjustment in water flooding,” Journal of Petroleum Technology, p. 206, February 1962; Trans, AIME, 225

30. McCaffery, F.G.: “Measurement of interfacial tension and contact angles at high temperature and pressure,” Journal of Canadian Petroleum Technology, Jul-Sep 1972: 26-32

31. Hjelmeland, O.S.: Thesis, The Norwegian Institute of Technolgy, The University of Trondheim, Trondheim, Norway, 1984

32. Hjelmeland, O.S. and Larrando, L.E.: "Experimental investigation of the effects of temperature, pressure and crude oil composition on interfacial properties", SPE 12124-PA, 1986

33. Teeters, D., Wilson, J.F., Andersen, M.A., and Thomas, D.C., "A Dynamic Wilhelmy Plate Technique Used for Wettability Evaluation of Crude Oils", Journal of Colloid and Interface Science (1988) Vol. 126, pp-641-644.

34. Wang, W. and Gupta, A.: " Investigation of the effect of temperature and pressure on wettability using modified pendant drop method," SPE 30544, Paper presented at the SPE Annual Technical Conference and Exhibition, Dallas, TX, 22-25 October, 1995

35. Rao, D.N. and Girard, M.G.: "A new technique for reservoir wettability characterization", Journal of Canadian Petroleum Technology, Jan-1996, pp-31-39

36. Rao, D.N.: "Is there a correlation between wettability from corefloods and contact angles," SPE 37234, Paper presented at the SPE International Symposium on Oil Field Chemistry held in Houston, TX, 18-21 Feburary,1997

37. Rao, D.N.: "Fluid-fluid and solid-fluid interfacial interactions in petroleum reservoirs," Petroleum Science and Technology, 19(1&2), 2001, 157-188

38. Rao, D.N. and Karyampudi, R.S.: "Application of the dual-drop dual crystal contact angle technique to characterize heavy oil reservoir wettability," J. Adhesion Sci. Technol., Vol. 16, No. 5, 2002, pp-581-598

39. Xu, W., Ayirala, S.C., and Rao, D.N.: "Compositional dependence of wetting and contact angles in solid-liquid-liquid systems under realistic environments," The Canadian Journal of Chemical Engineering, Vol. 84, February 2006, 44-51

40. Buckley, J.S., Liu, Y., and Monsterleet, S.: " Mechanisms of wetting alteration by crude oils" SPE Journal, March 1998, 54-61

41. Buckley, J.S., Takamura, K., and Morrow, N.R.: "Influence of electrical surface charges on the wetting properties of crude oils," SPE 16964-PA, SPE Reservoir Engineering, Aug-1989, pp-332-340

42. Buckley, J.S. and Morrow, N.R.: "Characterization of crude oil wetting behavior by adhesion tests," SPE/DOE 20263, Paper presented at the SPE/DOE Seventh Symposium on Enhance Oil Recovery held in Tulsa, Oklahoma, 22-25 April,1990

43. Valat, M., Bertin, H., and Robin, M.: "Two-Phase flow in porous media: Influence of PH on wettability", Advances in Core Evaluation III: Reservoir Management, Worthington, P.F. and C. Chardaire-Rivière, C. (Eds), 1993, Taylor & Francis, pp-387-409

44. Rao, D.N. and Maini, B.B.: " Impact of adhesion on reservoir mechanics", CIM-93-65, Paper presented at the 44th Annual Technical Meeting of the Petroleum Society of CIM held in Calgary, Alberta, 10-12 May 1993

45. Liu, Y. and Buckley, J.S.: "Evolution of wetting alteration by adsorption from crude oil", SPE 328970-PA, SPE Formation Evaluation, March-1997, pp-5-11

46. Basu, S. and Sharma, M.M.: "Measurement of critical disjoining pressure for dewetting of solid surfaces", Journal of Colloid and Interface Science, 181(1996), pp-443-455

47. Drummond, C. and Israelachvili, J.: "Surface forces and wettability", Journal of Petroleum Science and Engineering 33 (2002), pp-123-133

48. Ward, A.D., Ottewill, R.H., and Hazlett, R.D.: "An investigation into the stability of aqueous films separating hydrocarbon drop from quartz surfaces", Journal of Petroleum Science and Engineering 24 (1999), pp-213-220

49. Derjaguin, B.V. and Landau, L.: Acta Physicochim. URSS 14, 633–622 (1941).

50. Verwey, E.J.W. and Overbeek, J.Th.G.: "Theory of the Stability of Lyophobic Colloids", Elsevier, Amsterdam (1948)

51. Israelachvili, J.: "Intermolecular & surface forces", Second addition (2006), Academic Press, London

52. Derjaguin, B.V. and Churaev, N.V.: J. Colloid Interface Sci. 49, 249–255 (1974)

53. Derjaguin, B.V.: colloid Zeits. 69, 155(1934)

54. Christenson, H.K., and Israelachvili, J.: "Direct measurement of interactions and viscosity of crude oils in thin films between model clay surfaces," Journal of Colloid and Interface Science, 119 (1987), pp-194-202

55. Gregory, J.: J. Colloid Interface Sci. 83, 138–145 (1981)

56. Mohanty, K.K., Davis, H.T., and Scriven, L. E.: "Role of Thin Film in Fluid Distributions in Porous Media," Published in 'Surface Phenomena in Enhanced Oil Recovery', Ed- Shah, D.O., Plenum Press, New York (1981)

57. Hirasaki, G.J.: "Thermodynamics of thin films and three-phase contact regions", Interfacial Phenomena in Petroleum Recovery, (1991): 23-75, Ed: N.R. Morrow, Marcel Dekker Inc., New-York

58. Radke, C.J., Kovscek, A.R., and Wong, H.: "A pore-level scenario for the development of mixed wettability in oil reservoirs", SPE 24880, 1992

59. Melrose, J.C.: Proc. 57th Annual Fall Technical Conference and Exhibition of Society of Petroleum Engineers, New Orleans, LA, Paper No. SPE 10971 (1982)

60. Martynov, G.A. and Derjaguin, B.V.: Colloid J. 24, 411 (1962)

61. Busireddy, C. and Rao, D.N: “Development of a model for thin-film stability and spreading in solid–liquid–liquid systems”, J. Adhesion Sci. Technol., Vol. 21, No. 3–4, 2007, pp-243–265

62. Freer, E.M., Svitova, T., and Radke, C.J.: “The role of interfacial rheology in reservoir mixed wettability”, Journal of Petroleum Science and Engineering 39 (2003), pp-137-158

63. Amirfazli, A. and Neumann, A.W.: “Status of the three-phase line tension”, Advances in Colloid and Interface Science, 110 (2004), pp-121-141

64. Gibbs, J.W.: “The scientific papers of JW Gibbs”, Dover, New York, 1(1961): 288

65. Toshev, B.V., Platikanov, D., and Scheludko, A.: “Line tension in three-phase equilibrium systems”, Langmuir, 4 (1988), pp-489-499

66. Drelich, J.: “The significance and magnitude of the line tension in three-phase (solid-liquid-fluid) systems”, Colloids and Surfaces A: Physicochemical and Engineering Aspects, 116 (1996), pp-43-54

67. Boruvka, L. and Neumann, A.W.: “Generalization of the classical theory of capillarity”, J.Chem. Phys., 66 (1977), pp-5464-5476

68. Li, D. and Neumann, A.W.: “Determination of line tension from the drop size dependence of contact angles”, Colloids and Surfaces, 43 (1990), pp-195-206

69. Drelich, J. and Miller, J.D.: “The line/pseudo-line tension in three-phase systems”, Particulate Science and Technology, 10 (1992), pp-1-20

70. Marmur, A: “ Line tension and the intrinsic contact angle in solid-liquid-fluid systems”, J. Colloid Interface Sci., 186, 462-466 (1997)

71. Rao, D.N., Finot, M.O., Fisher D.B., and Girard, M.G.: “Evaluation of interfacial phenomena at reservoir conditions”, Report 1994/95-9, Petroleum Recovery Institute, Calgary, Alberta, Canada, March 1995

72. Hocott, C.R.: “ Interfacial tension between water and oil under reservoir conditions”, Trans. AIME,1939,132, pp-184-190

73. Jennings, Jr., H.Y.: “ The effect of temperature and pressure on the interfacial tension of Benzene-water and normal decane-water”, J. of Colloid and Interface science, 24(3) 1967, pp-323-329

74. Jennings, Jr., H.Y. and Newman, G.H.: “ The effect of temperature and pressure on interfacial tension of water against methane-normal decane mixtures,” SPE 3071-PA,1971

75. Amin, R. and Smith, T.N.: “Interfacial tension and spreading coefficient under reservoir conditions,” Fluid Phase Equilibria, 142 (1998), pp-231-241

76. Buckley, J.S. and Fan, T.: “Crude oil/brine interfacial tensions”, SCA2005-01, International Symposium of the Society of Core Analysts held in Toronto, Canada, -2121-25 Aug, 2005

77. Xu, W., Ayirala, S.C., and Rao, D.N.: “Measurement of Surfactant-Induced Interfacial Interactions at Reservoir Conditions,” SPE Reservoir Evaluation and Engineering, Feb-2008, pp-83-94

78. Saini, D. and Rao, D.N.: “Line tension-based modification of Young's equation for rock/oil/brine systems,” SPE 113321-PA, SPE Reservoir Evaluation and Engineering Journal, Oct 2009, pp-702-712

79. Shafer, J. and Fate, T.: “ Coring and core analysis: Challenges of offshore ultra deep water reservoirs,” SCA 2007-21, International Symposium of the Society of Core Analysts held in Calgary, Canada, 10-12 Sep., 2007

80. Sequeira, D.S.: “Compositional effects on gas-oil interfacial tension and miscibility at reservoir conditions”, MS Thesis, Louisiana State University, December 2006

81. NIST Web book (http://webbook.nist.gov/chemistry/fluid)

82. Al-Shafei, M.A. and Okasha, T.M.: “ Wettability studies at the pore level of Saudi Aramco reservoirs,” SPE 126088, Paper presented at the SPE Saudi Arabia Section Technical Symposium and Exhibition, Alkhobar, Saudi Arabia, 9-11 May 2009

83. Saada, A., Siffert, B., and Papirer, E: “Comparison of the hydrophilicity/ hydrophobicity of illites and kaolinites,” Journal of Colloid and Interface Science, 174, 185-190, 1995

84. Hamon, G: “Field wide variations of wettability,” SPE 63144, Paper presented at the SPE Annual Technical Conference and Exhibition, Dallas, TX, 1-4 October 2000

85. Saini, D. and Rao, D.N.: “Effect of line tension on the work of adhesion for rock/oil/brine Systems”, Contact Angle, Wettability and Adhesion, 6 (2009), Ed. K.L. Mittal, VSP, Utrecht, pp-95-111

APPENDIX: PERMISSIONS

Society of Petroleum Engineers
Calgary • Dallas • Dubai • Houston • Kuala Lumpur • London • Moscow
www.spe.org

June 14, 2010

Dayanand Saini
PHD Graduate Student
Louisiana State U.
3516 Patrick F. Taylor Hall
Baton Rouge LA 70803

Permission to use SPE Copyrighted Material

Dear Dayanand,

Thank you for your request to clear material copyrighted to the Society of Petroleum Engineers. Please take note that under the 'Author-Retained Rights' you already have permission to include material from

> Saini D., Rao, D.N. 2009. Line-Tension Based Modification of Young's Equation for Rock-Oil-Brine Systems. *SPE Res Eval & Eng* **12** (5): 702-712. SPE-113321-PA. DOI: 10.2118/113321-PA.

The relevant applicable paragraph states:

> "Authors/employers may incorporate all or part of the paper in future writings or presentations. If the entire paper or a portion thereof is used in substantially unchanged form, proper acknowledgement of SPE copyright must be made."

This is to further grant one-time permission to reproduce in your doctoral thesis

> **Fig. 7**
>
> Al-Shafei, M.A., Okasha, T.M. 2009. Wettability Studies at the Pore Level of Saudi Aramco Reservoirs. Paper SPE-126088-MS, presented at the SPE Saudi Arabia Section Technical Symposium, Al-Khobar, Saudi Arabia, 9-11 May.

These permissions are granted with these further conditions:

Proper notice of SPE copyright ownership is required and consists of the word "Copyright" or the copyright symbol, the year, and the words "Society of Petroleum Engineers" or "SPE". This acknowledgement must appear legibly on each copy of the work or portion thereof. Please add to it the words: "Reproduced with permission".

Americas Office
222 Palisades Creek Drive • Richardson, Texas 75080-2040 USA • Tel: +1.972.952.9393 • Fax: +1.972.952.9435 • Email: spedal@spe.org

Society of Petroleum Engineers
Calgary • Dallas • Dubai • Houston • Kuala Lumpur • London • Moscow
www.spe.org

In addition, SPE requires that each acknowledgment include the title, the authors and either (1) the date of publication of the book or journal in which published or (2) the name, location, and dates of the meeting where first presented (see above paper references).

The Society's copyright position encourages the broadest possible distribution of technical material to which it holds copyright, as is consistent with our copyright agreements with authors. Thank you for your cooperation in this matter, which is essential to protect the rights of the many authors who make technical material generally available through the Society.

Sincerely,

Ursula Blum
Copyright Coordinator
SPE Technical Publications

Tel: 972.952.9453
Fax: 972.952.1150
ublum@spe.org

Americas Office
222 Palisades Creek Drive • Richardson, Texas 75080-2040 USA • Tel: +1.972.952.9393 • Fax: +1.972.952.9435 • Email: spedal@spe.org

VITA

Dayanand Saini, the son of Shivlal Saini and Chameli Devi, was born in 1977 in Shahbajpur, a small village in the northern part of India. After completing his high school education, he obtained a Bachelor of Science (B.Sc.) degree in mathematics in June 1996 and Bachelor of Engineering (B.E.) degree in chemical engineering in December 2000 both from Choudhary Charan Singh University, Meerut, India. He worked as reservoir engineer for Oil and Natural Gas Corporation Limited (ONGC), India, from March 2001 to July 2006.

In August 2006, he joined the Craft & Hawkins Department of Petroleum Engineering at Louisiana State University to pursue the degree of Master of Science in Petroleum Engineering. Beginning fall 2007 term, he entered into the doctoral program on an economic development assistantship (EDA) awarded to his supervising professor by the Board of Regents and Louisiana State University. He won the prestigious SPE Nico Van Wingen Graduate Fellowship in 2009. His research paper titled “Line tension-based modification of Young's equation for rock/oil/brine systems” (SPE 113321-PA) was considered for 2010 SPE Cedric K. Ferguson Medal. The doctoral degree in petroleum engineering will be conferred in May 2011.